Dissertation zur Erlangung des Doktorgrades
der Fakultät für Chemie und Pharmazie
der Ludwig-Maximilians-Universität München

Structural basis of co-translational protein modification by Map1, NatA and NatB

Alexandra Gabriele Knorr
aus
Dachau, Deutschland

2020

Dissertation zur Erlangung des Doktorgrades
der Fakultät für Chemie und Pharmazie
der Ludwig-Maximilians-Universität München

Structural basis of co-translational protein modification by Map1, NatA and NatB

Alexandra Gabriele Knorr
aus
Dachau, Deutschland

2020

Erklärung

Diese Dissertation wurde im Sinne von § 7 der Promotionsordnung vom 28. November 2011 von Herrn Prof. Dr. Roland Beckmann betreut.

Eidesstattliche Versicherung

Diese Dissertation wurde eigenständig und ohne unerlaubte Hilfe erarbeitet.

München, 10.09.2020

Alexandra Gabriele Knorr

Dissertation eingereicht am 10.09.2020

1. Gutachter: Prof. Dr. Roland Beckmann

2. Gutachter: Prof. Dr. Karl-Peter Hopfner

Mündliche Prüfung am 30.10.2020

Summary

Protein synthesis is a highly regulated process executed by the ribosome. During translation, the nascent polypeptide chain (NC) gets synthesized in a sequential process and moves through the ribosomal exit tunnel to the tunnel exit site (TE) at surface of the ribosome. This exit site functions as a binding hub for many ribosome-associated protein biogenesis factors. This includes chaperones that assist in folding (e.g. RAC), proteins that are performing subcellular targeting (e.g. SRP) or enzymes responsible for early co-translational modifications (methionine cleavage, acetylation). Even though studied a lot in the past, the spatial and temporal organization of these exit site factors is still not fully understood.

The focus of this work was on early processing enzymes that have been studied biochemically but structures of the protein complexes were only solved in isolation and not in context with the ribosome.
One of the first modifying enzymes at the ribosome exit site are methionine aminopeptidases (MetAPs) that cleave off the starter methionine. This modification is conserved among the kingdoms of life and happens in up to 80% of all proteins. The major isoform in *S. cerevisiae*, Map1, was purified in complex with the ribosome using a native pull out approach. Subsequent cryo-EM analysis allowed for the first time the positioning of a eukaryotic aminopeptidase on the 80S ribosome. It is located below the TE interacting with ribosomal RNA (rRNA) and ribosomal proteins. Its binding involve the highly flexible eukaryotic specific expansion segment (ES) ES27a that is placed close to the TE in the so called exit position. Biochemical assays revealed ES27a as the major contributor in Map1-ribsome binding.

Another very common protein modification is the N-terminal acetylation, notably occurring in 90% of all human proteins. An acetyl moiety is transferred by N-terminal acetyl transferases (NATs) from acetyl-CoA to the α-amino group of the NC. NatA, the major NAT, is a heterotrimeric complex (consisting of Naa15, Naa10 and Naa50) and acetylates NCs with mainly Ser or Ala N-termini after the starter methionine has been removed by MetAPs. Therefore, MetAPs and NatA need to be coordinated

at the ribosome exit site. A similar native pull out approach as for Map1 and cryo-EM analysis revealed surprisingly that in NatA-ribosome interactions only rRNA is involved. Here, we verify that the large auxiliary subunit (Naa15) functions as the anchor for the catalytic subunit (Naa10) to the ribosome. In addition, the third subunit in yeast, Naa50, which function remained enigmatic so far, was shown to serve as a second ribosome binding subunit for the NatA complex. Furthermore, three of the observed binding sites involve eukaryotic specific expansion segments (again ES27a as well as ES7a and ES39a) which are crucial for binding as we could prove with binding assays. The triangular geometry of the expansion segments localize NatA underneath the peptide exit in a flexible manner, allowing NatA to adopt slightly different positions for sufficient acetylation of different NCs. A minimum length of the NC of approximately 50 aa is required until it reaches the catalytic center of NatA. However, an *in vitro* reconstitution of purified components gives evidence that the NC does not take the direct way. Instead, it seems to get guided along tetratricopeptide repeat (TPR) motifs that are part of the auxiliary subunit before it enters the catalytic center and allows a later acetylation event. These new insights include the idea of a sequential handover of the NC from Map1 to NatA but also give hints to concomitant binding of these two enzymes to the ribosome.

The second most common NAT, NatB, transfers the acetyl group directly on the starter methionine. The dimeric complex with Naa20 as the catalytic and Naa25 as the auxiliary subunit comprises a similar architecture as the NatA complex, suggesting a similar binding mode to the ribosome. However, *in vitro* studies and cryo-EM analysis show that its position on the ribosome differs from that of NatA. The binding does not include any expansion segments but other rRNA helices as well as a ribosomal protein. In addition, the NC needs a minimal length of 55 aa to enter the catalytic center for acetylation by NatB, therefore being in the same range as the minimum length for NatA acetylation. Nevertheless, NatA and NatB concomitant binding can be excluded on a structural basis.

Taken together, this data provide first insights on how these three early interactors, Map1, NatA and NatB are coordinated on the ribosome in order to correctly modify the NC. Especially the role of ES27a as the global coordinator for these exit factors came increasingly clear throughout the study as it can adopt specific sub-conformations

depend of the factor bound to it. Moreover, flexible binding and a dynamic nature seems to be one of the major characteristics of factors associated at the ribosomal peptide exit site. These results are included into a greater picture of the coordination of different exit site factors and provides further information about the spatial and temporal organization of various nascent chain interacting factors assembling at the at the ribosomal tunnel exit.

Contents

List of Figures

List of Tables

1 Introduction

Proteins are complex molecules of various sizes that fulfill a wide range of important functions in the cell. Their roles range from catalyzing reactions as enzymes, acting as antibodies in immune response, propagating chemical signals, to functioning as enzymes in DNA replication or as transporting molecules amongst others. Proteins are synthesized by ribosomes, large molecular machines that add amino acid by amino acid to form a growing polypeptide chain. This polypeptide can be chemically modified or processed by specific enzymes during protein maturation and gets folded at the end into a fully functional protein adopting its unique 3D structure. The highly regulated process of protein synthesis catalyzed by ribosomes is called translation. Here, messenger RNAs (mRNAs), synthesized from a DNA template by RNA polymerases during transcription, serve as a construction plan for proteins (Crick 1970). Via specific interactions of the mRNA with transfer RNAs (tRNAs), the necessary amino acids (aa) get delivered to the ribosome that in turn builds up newly snythesized proteins.

1.1 Structural architecture of ribosomes

Ribosomes are large macromolecular complexes consisting of ribosomal RNA (rRNA) and ribosomal proteins (r-proteins) and their function and structural core is conserved throughout the kingdoms of life. Ribosomes are composed of two subunits each of which has defined functional sites (fig. 1.1).
The small ribosomal subunit (SSU) comprises the mRNA channel and the decoding center (DC) where the mRNA gets decoded by tRNAs loaded with appropriate amino acids (aminoacyl-tRNA) (Berg and Offengand, 1958; Crick et al., 1961). Specific codon-anticodon interactions between mRNA and tRNA ensures a correct incorporation of the amino acids. The large ribosomal subunit (LSU) contains the peptidyl transferase center (PTC) where peptide bond formation is catalyzed and amino acids get connected to each other, therefore building up the growing nascent polypeptide chain (NC). In addition, the LSU accommodates the peptide exit tunnel, a 100 Å long

and 10-20 Å wide large cavity starting at the PTC and extending towards the solvent-exposed site of the LSU (summarized in Kramer et al., 2009). It directs the NC out of the ribosome where it leaves the 60S SU at the tunnel exit (TE) (fig. 1.1). The exposed NC can then interact immediately with modifying enzymes, chaperones or other protein factors (see chap. 1.3). The intersubunit space between the two subunits constitutes three binding sites for tRNAs: aminoacyl (A-), peptidyl (P-) and exit (E-) site. The new incoming aminoacyl-tRNA is accommodated at the A-site, the P-site holds the NC that is attached to the peptidyl-tRNA and in the E-site the deacylated tRNA is placed. During translation, tRNAs sequentially translocate from A- over P- to the E-site (summarized in Melnikov et al., 2012; Weisser and Ban, 2019).
According to their Svedberg coefficients (S) which describes the sedimentation rate during differential centrifugation, prokaryotic and eukaryotic SSU (30S, 40S) and LSU (50S, 60S) assemble to a fully functional 70S or 80S ribosome, respectively (Taylor et al. 1967).

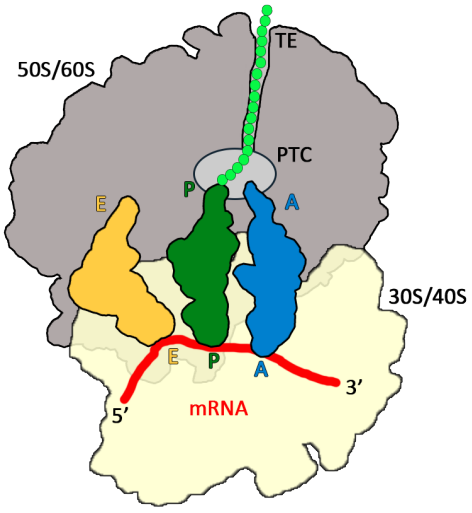

Figure 1.1: Schematic representation of a translating ribosome. Shown is the LSU (gray), SSU (light yellow), A-tRNA (blue), P-tRNA with NC (green), E-tRNA (yellow), NC (light green), PTC (circle within LSU) and mRNA (red). TE, tunnel exit.

Despite the conservation of the overall architecture and function of the ribosome, differences between pro- and eukaryotic ribosomes have been encountered. On the one hand, pro- and eukaryotes have their individual sets of specific proteins. On the other hand, eukaryotic ribosomes exhibit extension and insertions of conserved proteins and especially rRNA that increase their size compared to prokaryotes (Lecompte et

al., 2002; Gerbi 1986). This is also reflected in the molecular weight of ribosomes that varies from 2.3 MDa to 4.3 MDa for bacteria to higher eukaryotes respectively (fig. 1.2).

Notably, more mass accounts for the additional rRNA than r-proteins. Eukaryotes harbor an extra rRNA molecule (5.8S rRNA) on top of the other three (5/18/28S rRNA). The latter are present in prokaryotes as well but at lower mass (5/16/23S rRNA). Furthermore, eukaryotes comprise so called eukaryotic specific expansion segments (ES). ESs are long, often α-helical rRNA extensions localized at the solvent-exposed side of the large and small SU and pointing like long tentacles away from the ribosomal core. These tentacles increase in length progressively in higher eukaryotes. For example, ES27 in yeast has about 160 nucleotides in total but it reaches a size of ~ 700 nucleotides in humans (fig. 1.2, red). Therefore, it is not surprising that ESs contribute to the majority of the 40% mass increase of the ribosome size from pro- to eukaryotes (Gerbi 1996; Jenner et al. 2012). According to their position and length, ESs tend to be very flexible. This dynamic nature explains, why these ESs are often not entirely resolved in X-ray crystallography or cryo-EM structures.

The function of ESs has not yet been fully elucidated. Yet, some have been shown to play a role in factor binding. Expansion segments of the SSU for example function as docking sites for initiation factors or viral internal ribosome entry sites (IRES) (Hashem et al., 2013; Yamamoto et al., 2015). On the LSU, ES7 has been shown to have a similar role in being the interaction partner for various proteins (Gómez Ramos et al., 2016). ES27, which is also located on the LSU, seems to be the most flexible ES in yeast. It consists of ES27a, ES27b and H63 (previously ES27c) (http://apollo.chemistry.gatech.edu/RibosomeGallery/; Jarasch 2011, see appendix p. 119 for ES assignment). ES27a is the longest and most flexible segment and can adopt two distinct conformations in yeast. It either points in the direction of the L1 stalk (L1 position) or towards the TE (exit position) (Beckmann et al., 2001). Due to its close vicinity to the TE, ES27a has been already suggested to act as a coordinator of exit site factors binding to the ribosome (Beckmann et al., 2001). Furthermore, the full ES27 is essential for cell function as the deletion of the entire ES27 is lethal in *T. thermophila* (Sweeney et al.,1994) and it was linked to support ribosome biogenesis as interaction partner for assembly factors (Bradatsch et al., 2012; Greber et al., 2012; Ramesh and Woolford, 2016; Kater

et al., 2017).

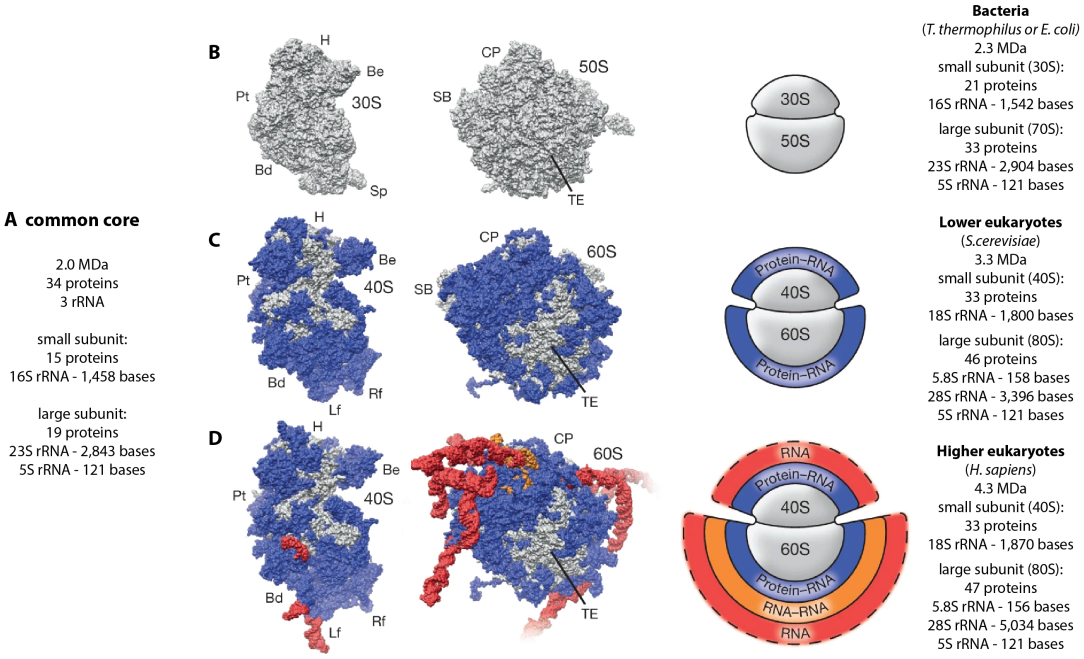

Figure 1.2: Ribosome composition and evolutional differences. Bacterial and eukaryotic ribosomes share a conserved core (**A**). In addition, each species comprises species-specific rRNA or protein extensions (**B-D**) increasing the overall mass of the ribosome. B/C/D from left to right: SSU; LSU; schematic representation indicating the increment of r-proteins and rRNA during evolution; detailed information about the ribosome composition. Be, beak; Bd, body; CP, central protuberance; H, head; Lf, left foot; Pt, platform; Rf, right foot. (Adjusted from Melnikov et al., 2012 and Anger et al., 2013)

1.2 Translation cycle

Translation is a highly regulated and dynamic process divided into four steps. Starting with initiation where the start codon (AUG) is recognized, subsequent elongation where the polypeptide chain is prolonged sequentially by subsequent addition of amino acids, followed by termination where the stop codon (UAG, UAA and UGA) is recognized and recycling by the release of the mRNA and splitting of the ribosome into its SUs at the very end. The translation process is a conserved mechanism and at each of the four stages, different factors associate with the ribosome catalyzing different reactions. (also summarized in Weisser and Ban, 2019).

Initiation. In prokaryotes, initiation starts with the mRNA bound to the SSU guided by the Shine-Dalgarno sequence in *E. coli* (SD, Shine and Dalgarno, 1974). The initiator tRNA, a specialized tRNA that is charged with a N-formylated methionine ($fMet - tRNA^{fMet}$), gets recruited to the SSU-mRNA complex by the interplay of three initiation factors (IF1-3). Joining of the LSU assembles the 70S ribosomes with the initiator tRNA located in the P-site. For prokaryotes as well as eukaryotic organelles (mitochondria and chloroplasts) the formyl group gets co-translationally removed by peptide deformylases (PDF) later on (Mazel et al., 1994).
Initiation in eukaryotes is more complex. Due to the different structure of the eukaryotic mRNA (m7cap and poly(A)-tail), initiation proceeds with significantly more factors than in prokaryotes and at least twelve factors are involved in initiation. In contrast to prokaryotes, the eukaryotic SSU scans along the mRNA from 5′ to 3′ in order to detect the start codon. Upon recognition, the initiator tRNA ($Met - tRNA_i$), gets anchored in the P-site. After the association of the 60S SU, the 80S ribosome is found in the P/P state and with an empty A-site and is ready to enter the elongation phase. (Jackson et al., 2010; Hinnebusch and Lorsch, 2012). Notably, the eukaryotic initiator tRNA does not harbor a formyl group and no PDF is needed to continue the synthesis of cytosolic proteins.

Since the start codon (AUG) also codes for methionine, most proteins start with a methionine at their N-terminus. This methionine is also called 'starter' or 'initiator' methionine (iMet).

Elongation. While initiation varies between pro- and eukaryotes, the following elongation process is basically conserved among the kingdoms of life (Rodnina and Wintermeyer, 2009) (fig. 1.3A).
The initiator tRNA with the bound starter methionine is present in the P-site. The next incoming aminoacyl-tRNA is delivered to the empty A-site with the help of elongation factor (EF) EF-Tu in prokaryotes or eEF1A in eukaryotes and is placed at its correct position via correct codon-anticodon pairing between tRNA and mRNA. The ribosome is in the so called PRE state (fig. 1.3B). After appropriate accommodation of the aminoacyl end of the tRNA into the PTC, the subsequent peptide bond formation elongates the nascent polypeptide chain by transferring the iMet (or the already existing NC) onto the new amino acid in the A-site (fig. 1.3A), leaving the tRNA in the

P-site deacylated. Upon peptide bond formation, the tRNA acceptor arm repositions with respect to the LSU, but the anticodon stems at the SSU stay in place. As tRNA movement is coupled with intersubunit rotations, this state is called the rotated state where tRNAs are in hybrid positions A/P or P/E (hybrid 1) (Agirrezabala et al., 2008; Frank and Agrawal, 2000). A short-lived hybrid state 2 intermediate with A/A and P/E tRNAs is also possible (fig. 1.3B) (Pan et al., 2007; Walker et al., 2008). Binding of the EF-G/eEF2 stabilizes the hybrid states and promotes the translocation of the deacylated tRNA by one codon from P- to E-site and the peptidyl-tRNA from A- to P-site. Followed by dissociation of EF-G/eEF2 the tRNAs are left in the canonical P/P and E/E states and with a vacant A-site and the ribosome has adopted the POST state (fig. 1.3B). From here the elongation cycle is repeated, resulting in a continuously growing NC that is synthesized from N- to C-terminus. The NC leaves the ribosome through the peptide exit tunnel in the 60S subunit, presenting the N-terminus first to the cytosol. Elongation is continued until the stop codon is reached and translation gets terminated.

Termination and recycling. When a stop codon (UAG, UAA and UGA) reaches the A-site, it cannot be decoded by a regular elongation tRNA. Release factors (RF) are necessary to recognize the stop codon, to hydrolyze the ester bond in the peptidyl-tRNA and to release the peptide chain (reviewed in Jackson et al., 2012). This is performed by RF1/RF2 and RF3 in prokaryotes and eRF1 and eRF3 in eukaryotes. Subsequent ribosome recycling is executed by the ribosome recycling factor (RRF) in prokaryotes or by ABCE1 in a coupled process with translation termination in eukaryotes (Peske et al., 2005; Pisarev et al., 2010; Shoemaker and Green, 2011; Becker et al., 2012; Heuer et al, 2017).

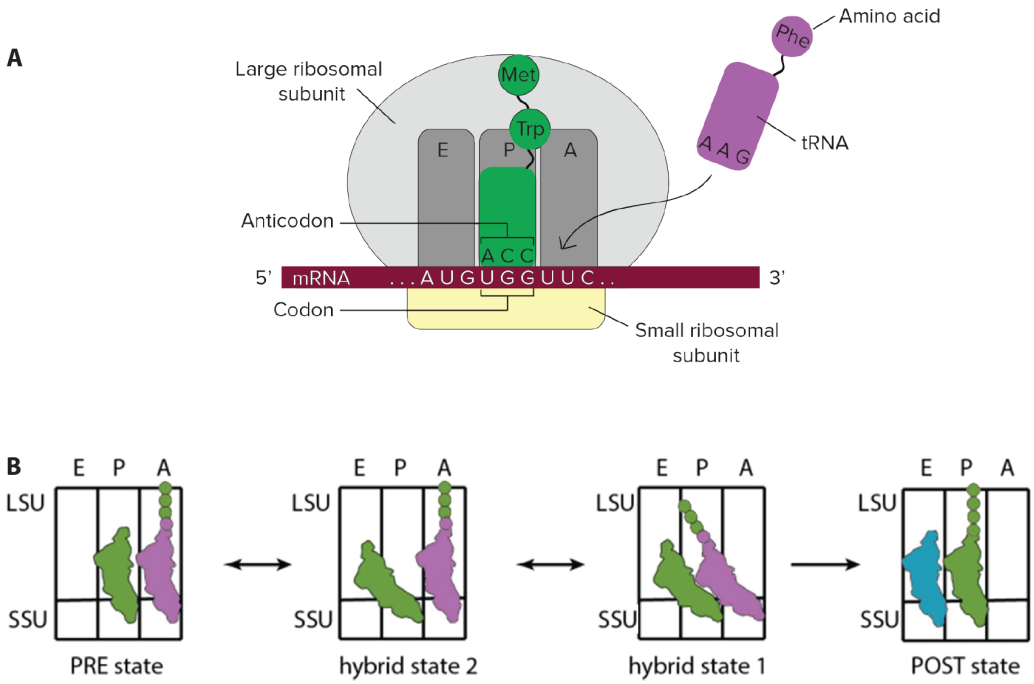

Figure 1.3: Schematic representation of translation elongation and corresponding tRNA states. The growing polypeptide chain is bound to the tRNA in the P-site (**A**). The new incoming amino acid loaded onto another tRNA is placed in the A-site via interaction of the mRNA codon with the tRNA anticodon resulting in A/A and P/P tRNA states (PRE translocation state). Upon peptide bond formation the NC is transferred onto the new aa in the A-site (**B**, left). After adopting hybrid states, translocation occurs ending up with the by one aa elongated NC in the P-site (POST translocation state, B right). The deacylated tRNA is moved to the E-site and the vacant A-site ready to accommodate the next aminoacyl-tRNA.
tRNA exit-site (E-site), peptidyl-tRNA binding site (P-site) and aminoacyl-tRNA binding site (A-site) are marked with E, P and A, respectively. P-site tRNA is labelled in green, A-site tRNA in purple and E-site tRNA in blue. PRE translocation state: A/A and P/P; hybrid 2: P/P moved to P/E; hybrid 1: A/A moved additionally to A/P; POST translocation state: P/P and E/E with the NC in P-site and a vacant A-site. Figure adapted from khanacademy (https://www.khanacademy.org/science/biology/gene-expression-central-dogma/translation-polypeptides/a/the-stages-of-translation) (A) and Matheisl, 2016 (B).

1.3 Ribosome exit site factors

The result of the translation cycle being repeated over and over is a growing nascent polypeptide chain that emerges from the ribosome through the ribosome peptide exit tunnel. It reaches the tunnel exit (TE) after synthesis of approximately 30 aa when stretched or approximately 60 aa when it adopts an α -helical conformation (Voss et al., 2006; Picking et al., 1992; Malkin and Rich, 1967).
Having left the exit tunnel means leaving the protective environment inside the ribosome and facing the very crowded environment of the cytosol (Zimmerman and Trach, 1991). In addition, the NC needs to be folded into its 3D structure to act as a fully functional protein. For that, some factors, also called ribosome-associated protein biogenesis factors (RPBs) or exit site factors, are binding at the TE to shield, fold or modify the NC. This binding hub for RPBs is mainly formed by rRNA (e.g. H24, H44, H59 and ESs) and in addition comprises the r-proteins uL22, uL23, uL24 and uL29 (fig. 1.4) (Kramer et al., 2009), where uL23 and uL29 are also referred to as universal adaptor site 1 (UAS1) (Halic and Beckmann, 2005). Some other proteins around the exit region are kingdom-specific proteins and only present in bacteria (bL17 and bL32) or eukaryotes (eL19, eL31, eL39) (fig. 1.4A). A second universal adaptor site (UAS2) was suggested to be maintained by uL22 and eL31 (Pech et al., 2010). Among the many exit site factors interacting with the NC or the TE are proteins assisting folding (chaperones), performing subcellular targeting (e.g. SRP) or are responsible for modifications of the newly synthesized polypeptide chain (methionine cleavage, acetylation) (fig. 1.4B). In the following, some of these factors present in eukaryotes are described in more detail.

1.3.1 Nascent Polypeptide-Associated Complex

The nascent polypeptide-associated complex (NAC) was originally identified as the first ribosome-associated factor that interacts with the NC (Wiedmann et al., 1994). It forms a stable heterodimeric complex consisting of the subunits α- and β-NAC and is conserved among eukaryotes (Wiedmann et al., 1994). Both SUs comprise a homologous NAC domain forming a β-sandwich-like structure with a hydrophobic core upon dimerization (Spreter et al. 2005; Liu et al. 2010; Wang et al. 2010). NAC is believed to play a role in co-translational protein folding as was proposed to have

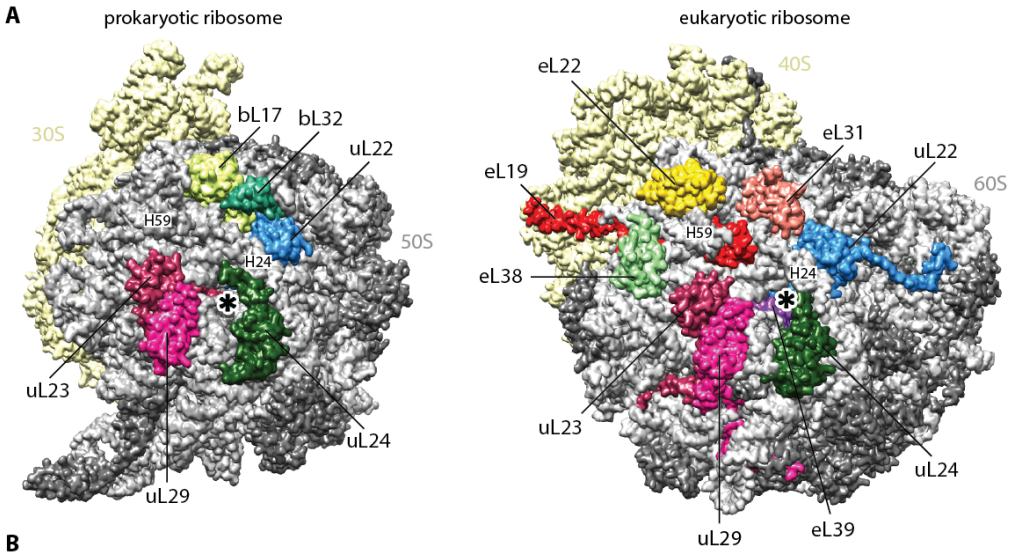

B

exit site factors	NC length	effect on NC	major ribosomal proteins involved	major ribosomal RNA involved
PDF	45-50 aa	deformulation of fMet	uL22	H24
MAP	40-45 aa	iMet cleavage	uL23/uL29; bL17	
NATs	~50 aa	acetylation of N-terminus	uL23/uL29	
NAC	~ 30 aa	chaperone-like	uL23/uL29, eL31, uL22	
RAC/Ssb	40-45 aa	chaperone	eL22, eL31; Ssb: uL29, eL19, eL39	H59, H24, ES12/h44
SRP	~30 aa	translocation/secretory pathway	uL23/uL29	H59, H24

Figure 1.4: Exit view of the ribosome and binding sites of exit site factors.
A, View of *E. coli* (left) and *S. cerevisiae* ribosome (right) focusing on the tunnel exit marked with an asterisk and specific exit site proteins highlighted. **B**, Exit site factors and their binding sites on the ribosome. The site adjacent to uL23/uL29 r-proteins is also referred to as universal adaptor site (UAS1). Adopted and modified from Giglione et al., 2015. References: PDF: Bingel-Erlenmeyer et al., 2008. Map: Sandikci et al., 2013; Bhakta et al., 2019, Wild et al., 2020, Fujii et al., 2018. NAT: Polevoda and Sherman 2003a; Gautschi et al., 2003; Polevoda et al., 2008. NAC: Wang et al., 1995; Pech et al., 2010; Gamerdinger et al., 2019; Lin et al., 2020; RAC: Peisker et al., 2008; Leidig et al., 2013; Zhang et al., 2017; Lee et al., 2016. SRP: Halic et al., 2004; Halic et al., 2006;, Becker et al., 2009. (extended version including data of this thesis, see appendix p. 120)

chaperones-like actvities (Bukau et al., 2000; Hartl and Hayer-Hartl, 2002; Rospert et al., 2002; Wegrzyn and Deuerling, 2005; Koplin et al., 2010).

NAC is equimolar expressed relative to ribosomes (Raue et al., 2007; Preissler and Deuerling, 2012) and both SUs interact with the NC (Wiedmann et al., 1994; Pech et al., 2010; Nyathi and Pool, 2015). However, only β-NAC has been shown to be critical for ribosome binding (Wegrzyn et al. 2006; Pech et al. 2010). Different cross-linking studies suggested NAC to form contacts to uL23 and uL29 (UAS1, Wegrzyn et al. 2006; Nyathi and Pool, 2015). However, it seems to maintain contacts to the opposite side of the TE to eL31 and uL22 (UAS2, Pech et al., 2010). This indicates a certain

degree of flexibility while NAC binds to the ribosome, but a structure of NAC on the ribosome has not been published at the start of this thesis. NAC is expected to bind to the ribosome when the NC has a length of about 30 aa (Wang et al., 1995).

While bound to the ribosome, NAC blocks SRP and Sec61 binding site and prevents unspecific interactions of the ribosome with the translocation machinery, thereby playing an important role in regulating protein transport (Möller et al., 1998; Forte et al., 2011; Zhang et al., 2012).

1.3.2 Ribosome-Associated Complex

The yeast ribosome-associated complex (RAC) is a chaperone consisting of a Hsp40 (Zuotin) and the Hsp70 homolog Ssz. Even though Hsp40-Hsp70 interactions are usually transient, in case of RAC they form a stable heterodimeric complex in yeast. As Ssz as a non-canonical Hsp70 is unable to hydrolyze ATP (Leidig et al., 2013), a catalytically active Hsp70 partner is needed for proper functioning of RAC. In yeast the additional Hsp70 partner of RAC is Ssb that, like RAC, also binds to ribosomes and facilitates the folding of aggregation prone, hydrophobic and intrinsically disordered NCs (Gautschi et al., 2002; Huang et al., 2005; Willmund et al., 2013). The deletion of RAC/Ssb in yeast causes severe growth defects and protein aggregation (Jaiswal et al., 2011, Willmund et al., 2013).

The ribosome-RAC interaction takes place on both SUs and specifically with the ribosomal proteins eL22 and eL31 close to the TE, as well as H59 on the LSU and ES12/h44 on the SSU (Peisker et al., 2008; Leidig et al., 2013; Zhang et al., 2014). In contrast, Ssb binds to eL39, uL29 and eL19 (Zhang et al., 2017; Zhand et al., 2020; Gumiero et al., 2016; Hanebuth et al., 2016). The entire RAC/SSb complex binds to the ribosome when the NC has a total length of about 40-50 residues (Gautschi et al., 2002; Hundley et al., 2002; Pfund et al., 1998).

1.3.3 Signal Recognition Particle

The universally conserved signal recognition particle (SRP) is involved in co-translational targeting of secretory and membrane proteins to the ER in eukaryotes. It recognizes a hydrophobic signal sequence at the N-terminus of the NC and delivers the ribosome to the ER by interacting with the SRP receptor (SR). The subsequent transfer

of the signal sequence to the protein conducting channel (PCC) Sec61 happens in a GTP dependent manner allowing the translocation through or insertion into the ER membrane (reviewed in Rapoport et al., 2017; Aviram and Schuldiner, 2017).

SRP is recruited to ribosomes at NC lengths of about 30 residues (Holtkamp et al., 2012; Bornemann et al., 2008) and both, SRP and the PCC are interacting with UAS1 (Halic et al., 2004; Pool et al., 2002; Becker et al., 2009). Therefore, they are sharing the same binding sites on the ribosome as NAC that was shown to act as a negative regulator in protein targeting (see NAC above).

1.3.4 Methionine aminopeptidases

Methionine aminopeptidases (MetAPs) are metalloproteases that cleave the starter methionine (iMet) from the N-terminus of the growing polypeptide chain in an irreversible process called N-terminal methionine excision (NME). The iMet is cleaved off when the penultimate residue of the NC is small and uncharged and has a radius of gyration < 1.2 Å. This is the case for Ala, Cys, Gly, Pro, Ser, Thr and Val (Sherman et al., 1985; Moerschell et al., 1990). NME is conserved form bacteria to higher eukaryotes and happens to up to 80% of proteins through all organisms (Meinnel et al., 1993). Additionally, in eukaryotic organelles and bacteria methionine deformylation by protein deformylases (PDFs) precedes the methionine cleavage (Solbiati et al., 1999). In general, NME is crucial for normal cell growth and it is a critical step during protein maturation (Giglione et al., 2004; Lowther and Matthews, 2000).

Regarding their molecular structure, all MetAPs contain a conserved 'pita bread' or aminopeptidase (AP) fold and share a conserved catalytic domain (Arfin et al., 1995; Li and Chang, 1995). The fold comprises a pseudo-2-fold symmetry (fig. 1.5) forming a center that allows two metal ions to bind (Lowther and Matthews, 2000). Moreover, MetAPs can be classified into different classes dependent on their specific motifs. Aminopeptidase type I (MetAP1/Map1) and II (MetAP2/Map2) are distinguished by a helical subdomain inserted within the C-terminal domain of type II MetAPs. In addition, subclassification into a and b describes the absence (prokaryotes) and presence (eukaryotes) of an N-terminal extension, respectively. Prokaryotes possess only one MetAP, interestingly type I in bacteria and type II in archaea (Keeling and Doolittle, 1996; Bradshaw and Yi, 2002). Since its deletion is lethal, this single isoform is essen-

tial in all prokaryotes (Chang et al., 1989). Eukaryotes as well as humans express two MetAP isoforms. In yeast, Map1 and Map2 are structurally similar, but share only little sequence homology (Lowther and Matthews, 2000; Datta, 2000). Notably, Map1 plays the major role in NME of the two isoforms (Giglione et al., 2004; Chen et al., 2002). Deletion of either Map1 or Map2 results in growth defects, whereas deletion of both MAP genes is lethal and shows the essential role of the removal of the initiator methionine from most proteins (Li and Chang, 1995). In addition, the importance of MetAPs for cell growth in yeast as well as bacteria make them a potential drug target to inhibit bacterial and fungal infections (Luo et al., 2003).

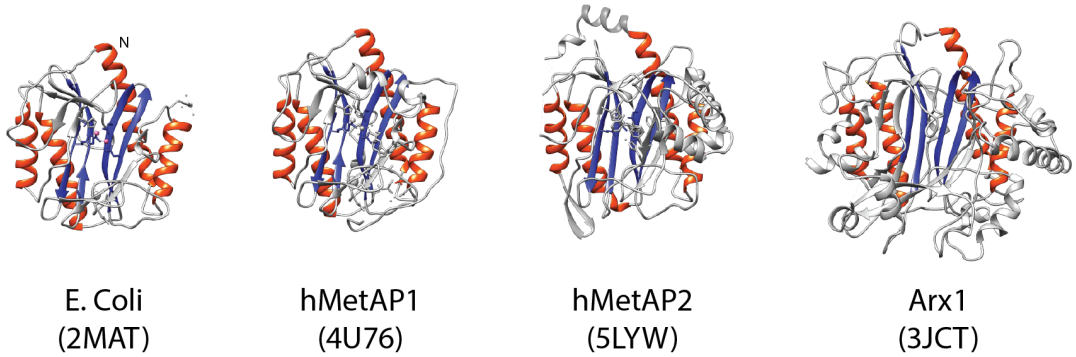

Figure 1.5: Conserved aminopeptidase (AP) fold. Typical 'pita bread' or aminopeptidase (AP) fold of E.coli Map type Ia (left) as the simplest model comprising a pseudo-2-fold symmetry of two α-helices (red) and two antiparallel β-strands (blue) in comparison with human MetAP1 and MetAP2, as well as yeast Arx1 harboring this MetAP-like fold. Notably, 90 aa and 110 aa of the N-terminus in hMetAP1 and hMetAP2 respectively, are missing in the structures. Bacterial Map and Arx1 structures are nearly complete. PDBs used are indicated. (adjusted from Lowther and Matthews, 2000 and Wild et al., 2020).

MetAPs process the very N-terminus of the NC and were shown to be associated directly with ribosomes. For yeast Map1, the N-terminal extension typical for type I aminopeptidases comprises two zinc finger domains. One harbors a Cys2-Cys2 zinc finger motif similar to those from the RING finger family (residues 22-40), the other comprises a Cys2-His2 motif similar to those found in RNA binding (residues 50-66) (Chang et al., 1990; Zuo et al., 1995). Since zinc-finger domains are in general involved in protein-protein and protein-nucleic acid interaction, this N-terminal region is assumed to play a role in ribosome binding (Vetro and Chang, 2002).
Map1 binding to the ribosome is largely independent of the NC and compared to bacterial Map, yeast Map1 shows no salt sensitivity that disrupts its binding to the

translation machinery (Sandikci et al., 2013; Nyathi and Pool, 2015). However, the binding site of yeast Map1 to the ribosome can only be estimated. Cross-linking studies suggested binding to UAS1 (Nyathi and Pool, 2015) that partially overlaps with the proposed binding of bacterial Map to uL23 and bL17 (Sandikci et al., 2013). Furthermore, the yeast 60S biogenesis factor Arx1 comprises the AP-fold (fig. 1.5) and interacts with ES27 as well as proteins at the TE additionally (Greber et al., 2012). A similar binding mode for yeast Map1 might be derived from this, but no structure of any eukaryotic MetAP on the translating ribosome is available. The required length of the NC for proper NME was estimated from bacteria to a total length of 40-45 aa (Sandikci et al., 2013; Ball and Kaesberg, 1973).

As already mentioned before, bacterial and yeast MetAP inhibitors are used as drug targets against pathogens (Luo et al., 2003). In humans, the second isoform, hMetAP2 is more extensively studied compared to hMetAP1. It displays higher concentration in tumor cells than in normal cells (Wu et al., 1993; Kanno et al., 2002) and hMetAP2-selective inhibitors have been used for cancer and autoimmune diseases treatment (Wang et al., 2003; Bernier et al., 2004). hMetAP2 seems to be more accessible to drugs as the pocket in its catalytic center comprises more space than in hMetAP1 (Addlagatta et al., 2015). Therefore, hMetAP2 was identified as the primary target of fumagillin that act as a potent inhibitor of angiogenesis (Sin et al., 1997). A derivative of fumagillin, TNP470, was already tested in preclinical and clinical trials to fight metastatic breast cancer, androgen-independent prostate cancer and acute leukemia amongst others (Kruger and Figg, 2000; Kudelka et al., 1997).

1.3.5 N-terminal acetyltransferases

These enzymes are described in more detail in the following chapters.

1.4 Protein Acetylation

Before a protein is fully functional it needs to go through different steps of maturation and modifications. Especially protein modifications exhibit wide spread functions and are dynamically regulated. They can occur co- or post-translationally, are reversible or irreversible and in general enlarge the pool of protein variants in a cheaper, faster and easier way instead of producing completely new proteins.

Most extensively studied examples for protein modifications are post-translational protein modifications (PTM) such as phosphorylation, methylation or ubiquitylation amongst others. Counterparts are proteases or enzymes that remove these modifications (e.g. phosphatases). Also combinations of different modifications are possible. Furthermore, PTMs are crucial for regulating biological functions and influence protein targeting, stability, folding and signaling (Lothrop et al., 2013; Audagnotto and Dal Peraro, 2017).

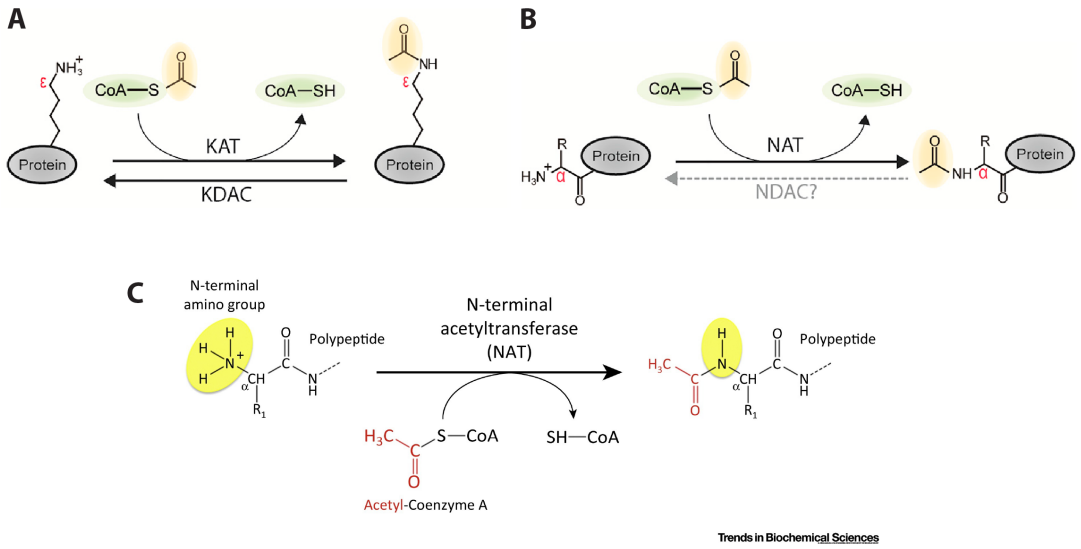

Figure 1.6: Mechanisms of protein acetylation. Schematic transfer of an acetyl group from acetyl-CoA **A**, onto the ϵ-amino group of lysine (N-ϵ-acetylation) by lysine acetyltransferases (KATs) with reverse process by lysine deacetylases (KDACs) or **B**, onto the α-amino group of proteins (N-α-acetylation) by N-terminal acetyl transferases (NATs), no enzyme for reverse reaction is known. **C**, Detailed view on N-α-acetylation. Figures adopted from Aksnes et al., 2019 and Aksnes et al., 2016.

One of the very wide spread protein modifications is the acetylation that can happen during or after protein synthesis. It is best known as post-translational histone modification, a reversible process also called ϵ-acetylation, that is carried out by histone or more general by lysine acetyltransferases or deacetylases (HATs/KATs or HDACs/KDACs respectively). In this process, an acetyl moiety gets transferred on the ϵ-amino group of lysines (fig. 1.6A). The whole process is evolutionary conserved, highly regulated and contributes to gene expression in eukaryotes, archaea and some bacteria (Menzies et al., 2016).

Apart from that, another kind of the very important acetylation occurs in the cell, the N-terminal acetylation (NTA) or N-α-acetylation. NTA is carried out by N-α-acetyltransferases where the gene is denoted as NAA and the protein as Naa. It was first discovered as a co-translational process, but later NTA was shown to occur also post-translationally (see chap. 1.5). Here, an acetyl-group gets transferred from acetyl-CoA onto the α-amino group at the very N-terminus of the nascent protein (fig. 1.6B, C). In contrast to ϵ-acetylation, NTA is an irreversible process as no 'NDACs' are know so far.

Although NTA is a very common and conserved modification in eukaryotes, the degree of acetylation differs between organisms. In humans and plants 80-90% of all soluble proteins are acetylated, in *D. melanogaster* 70-80%, and in *S. cerevisiae* 50-70% of all proteins carry an acetyl group at the N-terminus (Brown, 1970; Arnesen et al., 2009a; Bienvenut et al., 2012; Goetze et al., 2009; Van Damme et al., 2011a). Differences also occur in the acetylation state. Especially in yeast, substrates of the major NAT (NatA) are partially acetylated, meaning that the copies of the same protein were found in both, acetylated and unacetylated states. In contrast, the same substrates were found fully acetylated in humans (Arnesen et al., 2009a).

In contrast, prokaryotic proteins are only rarely acetylated, where the three transferases RimI, RimJ and RimL, acetylate specifically single ribosomal proteins (Yoshikawa et al., 1987, Tanaka et al., 1989; Jones and O'Connor, 2011). In archaea only 15% of the proteins carry this modification (Falb et al., 2006).

1.4.1 Effect of NTA

Adding an acetyl group to the N-terminus of the NC neutralizes the positive charge at the beginning of the growing polypeptide chain. It is expected to change its electrostatic properties and therefore may modify protein function (Allfrey et al., 1984; Ree et al., 2018). Moreover, NTA has been shown to lower the isoelectric point and affect a proteins electrophoretic mobility as well as increase the hydrophobicity of N-terminus (Polevoda et al., 1999; Asknes et al., 2016). These changes in biochemical properties seem to be fairly clear but the functional consequences are not well understood yet and were discussed contrarily.

At the beginning NTA was believed to protect proteins from degradation by blocking N-terminal ubiquitination (Jornvall, 1975; Hershko et al., 1984; Persson et al., 1985). In contrast, NTA was also found to generate specific degradation signals and therefore aiming for an opposite effect, also known as Ac/N-end in addition to the Arg/N-end rule pathway (Shemorry et al., 2013; Hwang et al., 2010; Varshavsky, 2011). As a consequence, it is difficult to make a general statement about the effect of NTA, but various studies show how this small modification influences a broad range of processes. It is involved in protein complex formation (Scott et al., 2011), subcellular localization (Forte et al., 2011) and protein targeting (Behnia et al., 2004; Setty et al., 2004) as well as sister chromatid cohesion and chromosome condensation (Hou et al., 2007; Williams et al., 2003; Pimenta-Marques et al., 2008). It affects protein-protein interactions and protein half-life (e.g. Aksnes et al., 2016) as well as drought stress and immune response in plants (Linster et al., 2015; Xu et al., 2015). In humans it impairs blood pressure regulation (Aksnes et al., 2015a) and certain NAT subunits are dysregulated in various cancers (Kalvik and Arnesen, 2013). Furthermore, the 2011 discovered X-linked Ogden Syndrome shows server developmental defects and early death of children having a Ser37Pro mutation in the catalytic SU of the major NAT, NatA (Rope et al., 2011). In addition, NATs function is related to neurodegenerative diseases via its involvement in protein aggregation and folding (Holmes et al., 2014; Weyer et al., 2017a; Arnesen et al., 2010; Bu et al., 2017).

1.5 Eukaryotic N-terminal Acetyltransferases

In total, eight different NAT enzymes (NatA-NatH) are know that carry out NTA in eukaryotes (fig. 1.7). They differ in their subunit composition and substrate specificity. Five of them are present in yeast, whereas multicellular eukaryotes additionally harbor NatF for membrane proteins and NatH for actin specific acetylation. In plants, NatG is responsible for NTA specifically in chloroplasts. The majority of NTA events takes place co-translationally in association with the ribosome (NatA-E) but post-translational action has been accounted for the later discovered NATs (NatF-H) (reviewed in Aksnes et al., 2019).

Each NAT is composed of one catalytic subunit (numbering refers as Naa10-80) and up to two larger auxiliary, also called ribosome binding subunits that are indicated

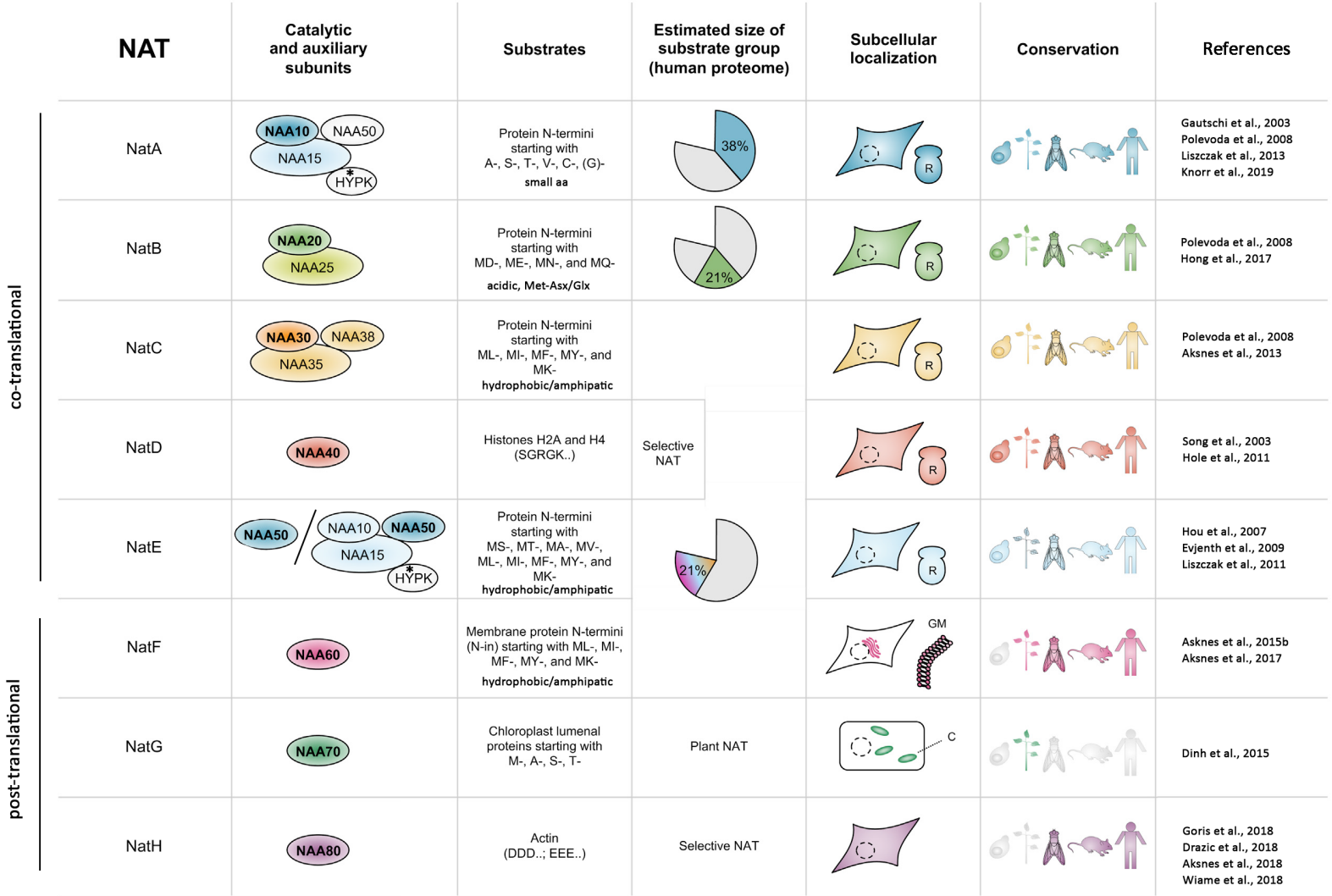

Figure 1.7: Overview of eukaryotic N-terminal acetyltransferases. The eight eukaryotic N-terminal acetyltransferases (NATs) (column 1) are characterized by their subunit composition (column 2), substrates (column 3), cellular localization (column 5) and conservation (column 6). Estimated size of the substrate group (column 4) with respect to the human proteome, key references are specified on the right. Catalytic SU are labeled with dark colors and lower numbers in complexes (Naa10-80), auxiliary SU are indicated in light colors if present. NatE can be present as monomer or in complex. *, HypK is not present in yeast. R, ribosome; GM, Golgi membrane; C, chloroplast. Adapted from Aksnes et al., 2019.

with higher numbers compared to their catalytic SUs (fig. 1.7). Usually, co-translational NATs are forming multisubunit complexes which have been shown to be associated with mono- as well as polyribosomes (Polevoda et al., 2008), whereas post-translational NATs as well as NatD are active as monomeric enzymes (Starheim et al., 2012; Aksnes et al., 2019). NatE can function as both, alone and in complex with the same SUs found in the NatA complex (Hou et al., 2007; Liszczak et al., 2011; Evjenth et al., 2009). The vast majority of acetylation is performed by NatA and B, whereas NatC, E and F acetylate to a minor extent. Originally, it was suggested by *in vitro* as well as *in vivo* studies that NATs perform acetylation on the NC when 20-50 aa residues emerge from the ribosome (Pestana and Pitot, 1975; Driessen et al., 1985) but a longer NC of around 80 aa has been suggested as well (Gautschi et al., 2003).
By which NAT a protein gets its modification is dependent on the first two amino acids.

1.5.1 NatA

If the penultimate residue of the NC is small and uncharged, an iMet cleavage precedes NTA (Frottin et al., 2006). Given a removed iMet and a NC exposing Ser, Ala, Thr, Val, Cys or Gly, these proteins are substrates for the major and best characterized NAT, NatA (Arnesen et al., 2005; Arnesen et al., 2009a; Polevoda et al., 1999). Among these substrates, however, differences in the acetylation state occur. Whereas Ser gets almost always acetylated, Gly N-termini are rarely modified in yeast and humans. In addition, for suboptimal substrates and in general for yeast NatA, partial acetylation is common (Arnesen et al., 2009a; Goetze et al., 2009; Van Damme et al., 2011a). Nevertheless, NatA is responsible for 40% of NatA mediated acetylation in humans (Arnesen et al., 2009a; Mullen et al., 1989; Polevoda et al., 1999; fig. 1.7).

The originally discovered NatA complex in yeast and humans comprised two subunits (Mullen et al., 1989; Arnesen et al., 2005). The large auxiliary or ribosome binding subunit Naa15 and the catalytic subunit Naa10 (Liszczak et al., 2013). Later on is has been shown that a third small subunit, Naa50, is physically associated with the NatA complex in yeast, human and fruit fly (Gautschi et al., 2003; Arnesen et al., 2006; Williams et al., 2003) but its function was not characterized yet. Naa50 has the same fold as the catalytic Naa10 as well as a homologous sequence but is inactive in yeast

as it lacks its acetylation activity (Gautschi et al., 2003; Deng et al., 2019; Arnesen et al., 2006). Nevertheless, it assembles with the other SUs to the heterotrimeric NatA complex in yeast where all SUs are present in equimolar amounts (Gautschi et al., 2003).

The auxiliary Naa15 cannot be active alone but it is required for efficient binding of the catalytic Naa10 to the ribosome (Gautschi et al., 2003). Therefore, Naa15 was suggested to play a role in positioning of NatA below the ribosomal TE (Polevoda et al., 2008). Furthermore, binding of NatA to the ribosome has been shown to be salt sensitive which might be explained by at least partially by electrostatic interactions (Gautschi et al., 2003; Magin et al., 2017). In addition, NatA was shown to cross-link to RNCs programmed with a non-NatA substrate and pellets with ribosomes where NC was released by puromycin treatment in binding assays (Gautschi et al., 2003). Therefore, NatA's interaction with the NC is not dependent on a specific aa sequence, meaning it can bind to non-substrate or non-programmed ribosomes as well.

Knockout of either Naa10 or Naa15 in yeast resulted in temperature-sensitive mutants, whereas ΔNaa50 yeast cells did not show an obvious phenotype. This led to the conclusion that NatA's biological function depends on Naa10 and Naa15 and Naa50 has just a supporting role (Gautschi et al., 2003). Triple deletion strains are not lethal in yeast and show the same temperature-sensitivity as in Naa15 or Naa10 deletion strains (Liszczak et al., 2013). Here, only co-overexpression of Naa15 and Naa10 could restore growth at higher temperatures (38°C). In addition, human Naa10 or Naa15 could complement for the corresponding yeast subunits in NatA deletion strains (Arnesen et al., 2009a).

NatA deletion is not lethal in yeast, but tremendous effects occur if NatA is not functioning in humans. One example is the already described Ogden syndrome (chap-1.4.1, Rope et al., 2011) in addition to other Naa10-related syndroms (Wu and Lyon, 2018). Furthermore, both subunits of NatA are overexpressed in several types of cancer (Kalvik and Arnesen, 2013).

1.5.2 NatB

NatB acetylates the starter methionine of proteins and carries out the second most frequent form of N-terminal acetylation. It modifies preferably acidic N-termini and serves substrates starting with Met-Glx and Met-Asx (MD-, ME-, MN-, MQ-) (Polevoda et al., 1999; Van Damme et al., 2012). It is responsible for about 20% of the human acetylome and acetylation occurs to nearly 100% for an affected protein in human and to 100% in yeast (Polevoda and Sherman, 2003a and 2003b; Arnesen et al., 2009a).

NatB subunits form a stable heterodimeric complex (Polevoda et al., 2003a and 2003b; Hong et al., 2017; Starheim et al., 2008). It is also able to bind ribosomes and similarly to NatA, the catalytic subunit Naa20 cannot bind to the ribosome without its auxiliary subunit Naa25 (Polevoda et al., 2008). In general, knockout strains of Naa20 and Naa25 show the most prominent phenotypes within the major NATs. This includes growth defects, suppressed cell motility and abnormal morphology as well as salt and temperature sensitivity (Polevoda et al., 2003a; Caesear et al., 2006; Yasuda et al., 2015). Human NatB can at least partially complement for the corresponding yeast NatB subunits and partially recover its Nt-acetylome (Van Damme et al., 2012).

In addition, NatB is important for cell cycle progression and Naa25 knockouts are missing visible actin cables (Hermann et al., 1997; Starheim et al., 2008/biochemJ). This destabilization of actin fibers goes back to the lack of acetylation of tropomyosin and actin that are both NatB substrates (Polevoda et al., 2003a; Singer and Shaw, 2003). Another important NatB substrate is α-Synuclein (α-Syn). It has an acetylated N-terminus and its aggregation is a hallmark for synucleinopathies such as the Parkinson's Disease. An unacetylated α-Syn shows for example a higher rate of pathology-causing aggregation. In contrast, the presence of the N-terminal acetyl-group deaccelerates the oligomerization process (Kang et al., 2018; Bu et al., 2017).

1.5.3 NatC-NatH

NatD is the second co-translational NAT where iMet removal is necessary and the second amino acid gets acetylated. It is highly specific for histones H2D and H4 and acetylates substrates starting with SGRGK- (Song et al., 2003; Hole et al., 2011). It consists of the catalytic subunit Naa40 solely and therefore is the only human co-

translational NAT that does not have an auxiliary ribosome binding subunit.

Nat C, E and F belong to the hydrophobic/amphipathic group and their substrates are partially overlapping. They all acetylate the methionine residue in N-termini starting with ML-, MI-, MF-, MY and MK-. In Addition, NatE also acetylates MS-, MT-, MA and MV- residues and all together they acetylate 20% of human proteins.

The heterotrimeric **NatC** complex comprises the catalytic subunit Naa30 and two auxiliary subunits, the large Naa35 and the smaller Naa38. Naa30 and Naa35 are analogues to the catalytic and auxiliary subunits in NatA and NatB (Polevoda and Sherman, 2001; Starheim et al., 2009/MolCellBiol). There is no structure available of NatC, but the subunit composition suggests a partially similar organization as the trimeric NatA complex.

NatE was originally identified as the catalytic subunit Naa50 that acetylates mainly hydrophobic N-termini of NCs retaining the iMet. It can act alone in humans but is also physically associated with Naa10 and Naa15 from NatA complex in yeast, human and *D. Melanogasta* (Gautschi et al., 2003; Arensen et al., 2006/Gene; Williams et al., 2003). Whereas in NatA Naa10 is the active catalytic subunit and iMet cleavage is necessary, in the trimeric NatE complex in higher eukaryotes Naa50 is the active catalytic subunit. It acetylates NatA-substrates keeping the iMet (MS/MT/MA/MV) as well as N-termini that are shared between NatC, E and F. (Liszczak et al., 2011; Evjenth et al., 2009). Please see hints to nomenclature below.

The NATs discovered more recently are acting post-translationally, are also more specialized NATs compared to the five above and consist of single catalytic subunits.

NatF is the catalytic Naa60 and present in multicellular eukaryotes but not in yeast. It has the same substrate specificity encountered for NatC and NatE (ML/MI/MF/MY/MK) but is specialized to acetylate transmembrane proteins (Van Damme et al., 2011a, Aksnes 2015b).

NatG is a plant specific NAT consisting of the catalytic Naa70. It is located in the chloroplast stroma and acetylates N-termini starting with M-, A-, S- and T- (Dinh et al., 2015).

NatH comprises the catalytic subunit Naa80 and is the only non-ribosome and non-

organelle associated NAT. It is present in the cytosol and acts selectively on the negatively charged actin N-terminus. Interestingly, actin is an example of a protein, on which different NATs are acting. First NatB acetylates the N-terminus of class I actins co-translationally. After the removal of the acetylated methionine by an unidentified aminopeptidase, NatH acetylates the exposed EEE- or DDD-N-terminal sequence post-translationally (Drazic et al., 2018; Goris et al., 2018; Berger et al., 1981; Redman and Rubenstein, 1981; Rubenstein and Martin, 1983). In case of class II actins, the part of the first acetylation might also be resumed by NatA (Wiame et al., 2018; Drazic et al., 2018).

1.5.4 A comment concerning NatA/NatE and general nomenclature

In literature the difference between NatA and NatE has never been clearly defined and its non-consistent use is still confusing.
NatE was originally discovered as a single subunit enzyme called Naa50 in humans having Nt-acetyltransferase activity, but acting mainly alone and not in complex with the ribosome (Hou et al., 2007). In contrast to substrates of NatA, NatE substrates start with an iMet on the N-terminus that is not cleaved (Evjenth et al., 2009; Van Damme et al., 2011b). Furthermore, however, Naa50 was also found as a part of the NatA complex in yeast, human and fruit fly, which was at first described as heterodimeric complex formed by Naa10 and Naa15 (Gautschi et al., 2003; Arnesen et al., 2006; Williams et al., 2003). In the trimeric NatA in yeast, the catalytic active Naa10 is responsible for the transfer of the acetyl group to the NC, whereas the associated Naa50 lacks acetyl transferase activity on iMet (Van Damme et al., 2015; Deng et al., 2019). Consequently, NatA can be defined as the complex having an active Naa10 and acetylating N-termini after removal of the iMet. On the other hand, NatE describes the trimeric complex having an active Naa50 and act on NCs retaining the iMet. Additionally, Naa50 has been shown to also perform ϵ-acetylation and it shows autoacetylation activity at lysine residues in human and fruit fly (Evjenth et al., 2009; Hou et al., 2007) that is not true for NatA (Magin et al., 2016).

Moreover, NAT nomenclature concerning the subunits were standardized after some confusion of different naming. The old and new names of NATs are shown in the appendix (p. 5). In this thesis the new NaaXX-nomenclature is used explicitly.

1.5.5 Non-catalytic role of NATs

The non-catalytic role of NATs will not be discussed here and is reviewed elsewhere (Aksnes et al., 2019).

1.6 Structural characterization of NAT subunits

1.6.1 Auxiliary subunits

Four NATs are harboring a large auxiliary subunit: NatA (Naa15), NatB (Naa25), NatC (Naa35) and NatE (also Naa15, if present as trimeric complex).

In 2013, the crystal structure of dimeric *S. pombe* NatA was solved (Liszczak et al., 2013). The structure revealed that Naa15 is arranged in 37 α-helices of which 26 are forming so-called tetratricopeptide repeat (TPR) motifs. A single TPR motif contains two antiparallel α-helices usually composed of 34 aa. TPRs are not specifically conserved in sequence, but in size, hydrophobicity and spacing of some aa within the motif (Lamb et al., 1995; Goebl and Yanagida, 1991). TPRs mostly appear in tandem arrays forming a right-handed helical spiral that builds up an amphipathic groove. They often function as a scaffold for protein-protein interactions but were also suggested to play a role in protein-DNA interactions (Goebl and Yanagida, 1991; Sikorski et al., 1991; Lamb et al., 1995; Blatch and Lassle, 1999) (fig. 1.8A, blue and yellow). Like other TPR-containing proteins, Naa15 forms a ring-like structure and encloses the catalytic subunit. The binding is maintained by hydrophobic interactions and hydrogen bonds at the interface of the two subunits (Liszczak et al., 2013). An overview of the TPRs within a secondary structure diagram of the yeast NatA auxiliary subunit is shown in the appendix (p. 5).

In addition to the described *S. pombe* structure, dimeric or trimeric NatA in complex with HypK from *C. thermophilum* and *H. sapiens* were published recently (Weyer et al., 2017a, Gottlieb and Marmorstein, 2018; Deng et al., 2020). Another crystal structure of yeast NatA is present in the PDB database (4XNH, fig. 1.8B) which was crystallized as the heterotrimeric complex harboring the additional Naa50 subunit and comprises a very similar architecture for Naa10 and Naa15 as *S. pombe* NatA (fig. 1.8A and B).

The NatB auxiliary subunit Naa25 shows a similar fold as NatA's Naa15. It contains

12 TPRs within the first 30 α-helices that are wrapping around its catalytic subunit in a similar way as in NatA (fig. 1.8C). The interaction is mediated also through hydrophobic interactions as well as several hydrogen bonds on the interface of the catalytic and auxiliary subunit (Hong et al., 2017).

There is no structure of NatC available, but it is very likely that Naa35 adopts a similar fold as the auxiliary subunits of NatA and NatB especially concerning the TRP motifs. Secondary structure analysis of yeast Naa35 showed a very similar α-helical pattern compared to Naa15 and Naa25, only disrupted by three small predicted β-sheet patches in between (Blatch and Lassle, 1999, appendix p. 5). This shows again the conservation in the secondary structure of the TPRs but not in the sequence.

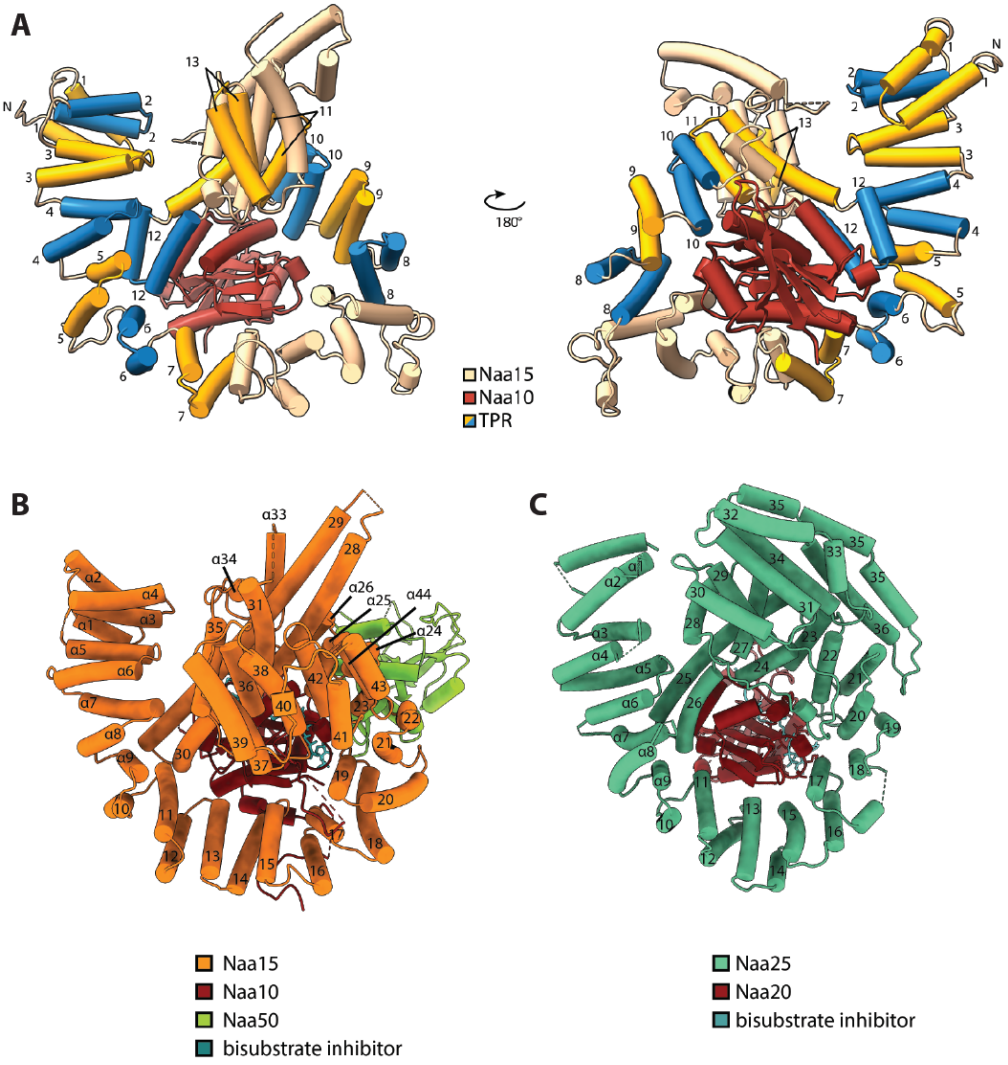

Figure 1.8: General architecture and TPR motifs in NATs. A, NatA from *S. pombe* (4KVM, Liszczak et al., 2013) with Naa15 shown in beige but with 13 TPR motifs indicated as tandem arrays in yellow and blue. Subunit composition of *S. cerevisiae* trimeric NatA complex from 4XNH (**B**) and dimeric NatB complex from *C. albicans* (5K18, Hong 2017) (**C**) both crystallized with a bisubstrate inhibitor (cyan). Catalytic SUs in red, auxiliary SU in orange or turquoise, additional Naa50 in yeast light green. α-helix labelling adjusted from Liszczak et al., 2013, or according to Hong et al., 2017 respectively. As bisubstrate acetyl-CoA was covalently linked to a 5 aa (CoA-SASEA, NatA) or 9 aa peptide (CoA-MDSEVAALVID, NatB), for inhibition acetyl-CoA was exchanged to a non-hydrolysable acetyl-CoA analog (acetonly-CoA) (Liszczak et al., 2013; Hong et al., 2017).

1.6.2 Catalytic subunits

Whereas not every NAT contains a ribosome binding subunit, all of them have at least one active catalytic SU. They all belong to a GNAT superfamily harboring the general GNAT fold (general control non-repressible 5 (GCN5)-related N-acetyltransferases) that is not restricted to NATs (Neuwald and Landsman, 1997). Therefore, the GNAT fold is present in many other transferase enzymes e.g. the already mentioned histone acetyltransferases (HAT) but also others such as aminoglycoside or serotonin acetyltransferases (reviewed in Vetting et al., 2005).

The NAT catalytic subunits comprise the highly conserved and central acetyl-CoA binding motif Q/RxxGxG/A, where x stands for any aa (Wolf et al., 1998). Variations of the aa composition in 'x' as well as the architecture around the CoA-binding motif might be responsible for the different substrate specificities among the NATs (Rathore et al., 2016). In addition, the V-shaped arrangement of the parallel β-sheets β4 and β5 plays an important role in acetyl-CoA accommodation and was shown to be the most rigid feature among all catalytic SUs (Dyda et al., 2000; Abboud et al., 2020) (fig. 1.9A, green and gold). Furthermore, this semi-open cavity senses the first 4-5 aa of the NC. In more detail, it is the α1-loop- α2 and the C-terminal β6-loop-β7 (fig I9A) that ensure substrate specificity (Liszczak et al., 2013; Liszczak et al., 2011).
The acetyl transfer itself happens through a nucleophilic attack of the deprotonated amino group of the substrate on the carbonyl carbon of acetyl-CoA (Ud-Din et al., 2016). The residues of the catalytic Naa10 mainly involved in the acetyl transfer are Leu22/24, Glu24/26, Tyr26/28 and Tyr139/181 in *S. pombe/S. cerevisiae* respectively (fig. 1.9B) that interact with the first two aa of the substrate via hydrogen bonds and van der Waals interactions (Liszczak et al., 2013).

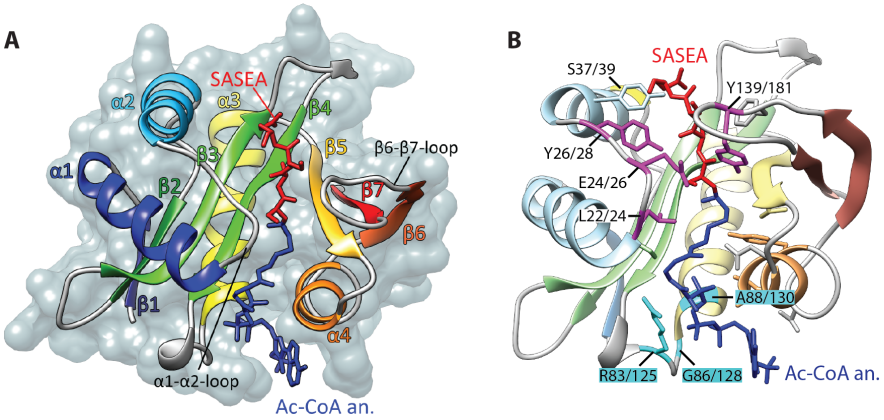

Figure 1.9: Architecture of the catalytic subunit of NatA. A, Structure of *S. pombe* Naa10 with secondary structure elements labelled and with the view on the bisubstrate inhibitor shown in red (NC) and dark blue (Ac-CoA analog). **B**, Similar view as in A, with important residues labeled. Catalytic center residues in magenta (Y26/28, E24/26, L22/24, Y139/181), acetyl-CoA binding motif in cyan (RxxGxxA). Amino acid numbers refer to *S. pombe* (and therefore human as well) first and then *S. cerevisiae* as second. The Ser37Pro (Ser39Pro in yeast) mutation causing the sever Ogden syndrome in human is labeled in yellow (Rope et al., 2011).

1.7 Aims of this thesis

The focus of this work was on the protein factors which are responsible for early co-translational processing of the NC. NME and NTA are very common and wide spread protein modifications that are performed mainly by Map1 and NatA and NatB respectively among eukaryotes. So far, these exit site factors have been only studied biochemically and structures of the protein complexes were only solved in isolation, but not in context with the ribosome (Lowther and Matthews, 2000; Polevoda et al., 2008; Gautschi et al., 2003; Liszczak et al., 2013; Hong et al., 2017). Thus the architecture of the co-translational protein modification machineries is largely unknown.

The goal of this thesis was to obtain complexes of translating ribosomes with the nascent chain processing enzymes Map1, NatA and NatB in yeast. Such stable complexes should be subjected to cryo-EM and single particle analysis (SPA) and structures should be biochemically validated.

To achieve this goal, two different approaches were chosen.
The first approach was a native pull out based a protocol published in 2007 (Oeffinger et al., 2007). In this quick purification protocol for ribonucleoprotein particles, harvested cells were rapidly frozen and grinded while cooling with liquid nitrogen. This prevents the damaging action of nucleases and proteases. Mild buffers were chosen for subsequent rapid thawing before the lysate was clarified. For affinity purification antibody-conjugated magnetic beads were used instead of antibody-conjugated resins. This allowed a fast and efficient purification in conditions that stabilize and enrich intact ribosome-bound complexes. The strains used for that approach harbored a TAP-tagged version of the protein of interest. Via the Protein A domain of the TAP-tag, the protein was bound to IgG-coupled magnetic beads, resulting in ribosomes co-purifying with the target protein after an elution with TEV protease. Subsequent cryo-EM analysis was used to visualize this complexes that were purified under native conditions.
The second approach was based on *in vitro* reconstitutions from purified components. Purified proteins were *in vitro* reconstituted with ribosome-nascent chain complexes (RNC) programmed with specific substrates. These were subjected to pelleting assays and mutational studies in order to validate the binding site of the factors to the ribosome obtained in the native structure. Furthermore, *in vitro* reconstitutions were also used for cryo-EM analysis and results were compared to the structure received from the native pull outs.

Obtained structures were then put in context with known structures and biochemical data about other exit site factors, such as chaperones or proteins involved in the targeting and translocation pathway. Collectively, this study was aiming for the understanding of the spatial and temporal organization of various nascent chain interacting factors assembling at the at the ribosomal tunnel exit.

2 Material and methods

2.1 DNA template generation

In order to generate ribosomes nascent chain complexes (RNC), ribosomes isolated from a cell-free translation extract in yeast were programmed with specific nascent polypeptides. For that, two constructs were designed for this thesis. First, the first 64 aa of the uL4 protein, a 60S ribosomal protein and well-known substrate of NatA (Gautschi et al., 2003) was used and its nucleotide sequence was modified in the way, that it contains a T7 promotor, a leader sequence and the start codon, followed by a octahistidine (His_8) for purification, a haemaglutinin (HA)-tag for western blot detection and a TEV cleavage site for tag removal. In addition, a ribosome stalling sequence from the upstream ORF of *gp48* in human cytomegalovirus (CMV) (Bhushan et al., 2010; Matheisl et al., 2015) was inserted C-terminally. Second, the first 88 aa of ABP1 (actin binding protein) were used for the second construct. It has been shown to be a good NatA substrate by unpublished selective ribosome profiling data supplied by Bernd Bukaus lab (Heidelberg) and was designed as a truncated version without a stop codon or any C-terminal stalling sequence. Both constructed were used for *in vitro* transcription into mRNA which was then used for *in vitro* translation to generate RNCs programmed with 86 aa or 88 aa of the uL4 or ABP1 construct respectively. Furthermore, both constructs are lacking the starter methionine and carried a serine at their N-terminus after TEV cleavage.

2.1.1 uL4 DNA template

DNA template for uL4-RNCs was amplified using pEX-A2 plasmid (appendix p. 128) containing a modified uL4-CMV fragment as template (tab. 1). Used primers were a NatA-uL4 forward primer (5'-GCAAGCTAATACGACTCACTATAGG-3') and NatA-uL4 reverse primer (5'-GAGCAAAAGCAGGTTTAAGGAGGA-3'). For PCR reaction, a 2x Phusion Flash High-Fidelity PCR Master Mix (Thermo Fisher) was used (tab. 2).

Table 1: Nucleotide sequence of uL4-DNA and corresponding protein sequence. 64 aa of the ribosomal protein uL4 were modified to a construct carrying a His_8-tag for purification, a haemaglutinin (HA)-tag for western blot detection, a TEV cleavage site and a CMV stalling sequence. The whole sequence was *in vitro* transcribed and afterwards *in vitro* translated into a NatA substrate of 86 aa length after TEV cleavage and tag removal.

T7 promotor	5′-TAATACGACTCACTATAGGG
leader	ACCAAACAAAACAAATAAAACAAAAAAAAA
start	ATG
His_8	CATCACCATCACCATCACCATCAC
HA	TACCCATACGATGTTCCAGATTACGCT
TEV site plus linker	GGATCCGATTACGACATCCCCACTACTGAGAAT CTTTATTTTCAG
64 aa of uL4	TCCCGTCCACAAGTTACTGTTCACTCTTTGACTGGT GAAGCTACTGCCAATGCCTTGCCATTGCCAGCTGTC TTCTCCGCTCCTATCCGTCCAGACATTGTCCACACT GTTTTCACCTCTGTGAACAAGAACAAGAGACAAGCT TACGCTGTTTCTGAAAAGGCTGGTCACCAAACCTCC GCTGAATCCTGG
CMV stalling sequence	ATGGAACCGCTGGTGCTGAGTGCGAAAAAACTGA GCAGCCTGCTGACCTGCAAATATATTCCTCCTTAA-3′

Total DNA sequence:
TAATACGACTCACTATAGGGACCAAACAAAACAAATAAAACAAAAAAAA
AATGCATCACCATCACCATCACCATCACTACCCATACGATGTTCCAGAT
TACGCTGGATCCGATTACGACATCCCCACTACTGAGAATCTTTATTTTC
AGTCCCGTCCACAAGTTACTGTTCACTCTTTGACTGGTGAAGCTACTGC
CAATGCCTTGCCATTGCCAGCTGTCTTCTCCGCTCCTATCCGTCCAGAC
ATTGTCCACACTGTTTTCACCTCTGTGAACAAGAACAAGAGACAAGCTT
ACGCTGTTTCTGAAAAGGCTGGTCACCAAACCTCCGCTGAATCCTGGAT
GGAACCGCTGGTGCTGAGTGCGAAAAAACTGAGCAGCCTGCTGACCTGC
AAATATATTCCTCCTTAA

Translated into:
MHHHHHHHHHYPYDVPDYAGSDYDIPTTENLYFQSRPQVTVHSLTGEATANALPLP
AVFSAPIRPDIVHTVFTSVNKNKRQAYAVSEKAGHQTSAESWMEPLVLSAKKLSS
LLTCKYIPP

Table 2: PCR set up for uL4 DNA amplification. PCR mix using 2x phusion master mix (Thermo Fisher) (left) and PCR program (right).

Pipetting scheme		PCR program		
Plasmid (20 ng/μl)	2.5 μl	98°C	20 sec	
Forward primer (10 pmol/μl)	2.5 μl	98°C	5 sec	
Reverse primer (10 pmol/μl)	2.25 μl	54°C	5 sec	30x
2x phusion master mix	25 μl	72°C	45 sec	
ddH_2O	17.5 μl	72°C	2 min	
Total volume	50 μl	15°C	∞	

2.1.2 ABP1 DNA template

After the removal of the starter methionine the unmodified ABP1 protein has an alanine at its N-terminus. As the cleavage by TEV protease always leaves a serine (or glycine) at the N-terminal position after cleavage (cleavage site: Glu X X Tyr X Gln | Gly or Ser), the alanine was exchanged to a serine in order to make a cleavage by TEV protease possible and to preserve the N-terminus as a NatA substrate. ABP1 was designed as a truncated construct, does not carry any stalling sequence and ends with a Pro at its C-terminus.

The DNA template for ABP1-RNCs was amplified using pEX-A128 plasmid (appendix p. 129) containing the adjusted ABP1 fragment as template (tab. 3). Used primers were a NatA-ABP1 forward primer (5'-AAGCTAATACGACTCACTATAGGG-3') as well as a NatA-ABP1 reverse primer (5'-AGGACACCAACCAATGATAATAATC-3'). For PCR reaction, a 2x Phusion Flash High-Fidelity PCR Master Mix (Thermo Fisher) was used (tab. 4).

Table 3: Nucleotide sequence of ABP1-DNA and corresponding protein sequence. 88 aa of ABP1 were modified to a construct carrying a His_8-tag for purification, a haemaglutinin (HA)-tag for western blot detection and a TEV cleavage site at its N-terminus. This truncated construct does not carry a stalling sequence and is having a proline at the C-terminus. The second aa is an alanine that was exchanged by a serine in order to provide a sufficient TEV cleavage site.

T7 promotor	5′-TAATACGACTCACTATAGGG
leader	ACCAAACAAAACAAATAAAACAAAAAAAAA
start	ATG
His_8	CATCACCATCACCATCACCATCAC
HA	TACCCATACGATGTTCCAGATTACGCT
TEV site plus linker	GGATCCGATTACGACATCCCCACTACTGAG AATCTTTATTTTCAG
88 aa of ABP1	**TCC**TTGGAACCTATTGATTATACTACTCACTCGAGAGAGA TCGACGCAGAGTACCTGAAGATTGTCAGAGGCTCCGATCC TGACACCACCTGGTTGATTATTTCACCCAATGCGAAAAAA GAATACGAACCTGAGTCTACCGGTTCCTCCTTTCACGATT TCTTGCAATTGTTTGATGAAACCAAGGTCCAGTACGGACT GGCACGTGTGTCCCCACCAGGGTCAGACGTTGAGAAGATT ATTATCATTGGTTGGTGT**CCT**-3′

Total DNA sequence:
TAATACGACTCACTATAGGGACCAAACAAAACAAATAAAACAAAAAAAA
AATGCATCACCATCACCATCACCATCACTACCCATACGATGTTCCAGAT
TACGCTGGATCCGATTACGACATCCCCACTACTGAGAATCTTTATTTTC
AGTCCTTGGAACCTATTGATTATACTACTCACTCGAGAGAGATCGACGC
AGAGTACCTGAAGATTGTCAGAGGCTCCGATCCTGACACCACCTGGTTG
ATTATTTCACCCAATGCGAAAAAAGAATACGAACCTGAGTCTACCGGTT
CCTCCTTTCACGATTTCTTGCAATTGTTTGATGAAACCAAGGTCCAGTA
CGGACTGGCACGTGTGTCCCCACCAGGGTCAGACGTTGAGAAGATTATT
ATCATTGGTTGGTGTCCT

Translated into:
MHHHHHHHHHYPYDVPDYAGSDYDIPTTENLYFQ**S**LEPIDYTTHSREIDAE
YLKIVRGSDPDTTWLIISPNAK KEYEPESTGSSFHDFLQLFDETK
VQYGLARVSPPGSDVEKIIIIGWC**P**

Table 4: PCR set up for ABP1 DNA amplification. PCR mix using 2x phusion master mix (Thermo Fisher) (left) and PCR program (right).

Pipetting scheme		PCR program		
Plasmid (20 ng/μl)	2.5 μl	98°C	15 sec	
Forward primer (10 pmol/μl)	2.5 μl	98°C	5 sec	
Reverse primer (10 pmol/μl)	2.25 μl	55°C	10 sec	30x
2x phusion master mix	25 μl	72°C	45 sec	
ddH_2O	17.5 μl	72°C	1 min	
Total volume	50 μl	15°C	∞	

All PCR products were purified using the PCR purification kit from Quiagen and DNA concentration was measured on a NanoDrop (Implen). Before they were used for *in vitro* transcription reactions, samples were loaded onto a 1% agarose gel for verification. Samples were incubated in a 1:10 ratio with 10x DNA loading dye (50% glycerol, 1 mM EDTA, 0.25% bromophenol blue, 0.25% xylene cyanol FF) and the gel was run in 1xTAE buffer (40 mM Tris, 20 mM acetic acid, 1 mM EDTA) at 120 V for 25 min. Bands were visualized by blue light excitation on Intas UV system.

2.2 *In vitro* transcription of uL4 and ABP1 mRNA

DNA templates from above were *in vitro* transcribed into capped mRNA using T7 mMESSAGE mMACHINE kit (Ambion) according to the manufacturers manual and using 1 μg of the corresponding purified PCR product for a 20 μl reaction. Incubation was for 1.5 h at 37°C and RNA was recovered by lithium chloride precipitation at -20°C o/n. The final product was resuspended in 30 μl nuclease-free water and its concentration determined at the NanoDrop (Implen).

2.3 *In vitro* translation and purification of uL4- and ABP1-RNC

Ribosome nascent chain complexes (RNCs) were obtained in a yeast ΔSki2 cell-free translation system using uL4 mRNA and ABP1 mRNA. Translation reactions were performed essentially as described before (Beckmann et al., 2001; Halic et al., 2004). If not stated different, all steps for the purification were carried out on ice.

1.2 ml *in vitro* translation reaction mix containing 48 μg uL4 or 68 μg ABP1 mRNA was incubated for 75 min at 17°C and stopped by adding 200 μg/ml cycloheximid.

The first purification step was managed by using the *Dynabeads*^{TM} His-Tag Isolation and Pulldown set (Thermo Fisher). 800 μl His-beads were equilibrated in 2 ml 250 buffer (50 mM Tris/HCl pH 7.0, 250 mM KOAc, 25 mM $Mg(OAc)_2$, 5 mM β-mercaptoethanol, 250 mM sucrose, 10 μg /ml cycloheximid, 0.1% Nikkol, 0.1% EDTA-free protease inhibitor cocktail pill (Roche), 0.1% RNase Inhibitor (SUPERase-In, 20U/μl (Thermo Fisher))) containing 10 μg/ml tRNA additionally. Beads were added to the *in vitro* translation reaction mix and incubated for 15 min at 4°C on a rotating wheel. Beads were harvested on a magnet, the flow through was collected and beads washed three times with 1 ml 250 buffer. Elution was performed for 5 min in 700 μl 250/350 buffer (250 buffer with 350 mM imidazole) at 4°C. The sample was split into two halves and each was loaded onto 400 μl high salt sucrose cushion (1 M sucrose, 50 mM Tris/HCl pH 7.0, 500 mM KOAc, 25 mM $Mg(OAc)_2$, 5 mM β-mercaptoethanol, 10 μg/ml cycloheximid, 0.1% Nikkol, 0.1% EDTA-free protease inhibitor cocktail pill (Roche)). Ribosomes were pelleted by centrifugation using a TLA 120.2 rotor (Beckman) for 45 min at 100,000 rpm and 4°C and resuspended in 30 μl 250 buffer on ice for 30 min while shaking. As RNCs are still containing the N-terminal His_8-HA-tag, they were treated with TEV protease in order to remove the tag. Therefore, the samples were pooled and diluted to a total volume of 1 ml with 250 buffer. Subsequently, 60 μl (uL4-RNCs) or 230 μl (ABP1-RNCs) of lab-made TEV protease were added. After incubation at RT for 45 min the mixture was spun through a 600 μl sucrose cushion in a TLA 100 rotor (Beckman) for 45 min at 100,000 rpm and 4°C. Afterwards, the pellet was resuspended in 30 μl grid buffer (20 mM Tris/HCl pH 7.0, 50 mM KOAc, 2.5 mM $Mg(OAc)_2$, 1 mM DTT, 125 mM Sucrose, 100 μg/mL Cycloheximide, 0.05% Nikkol) on ice while shaking for 30-45 min. The concentration of uL4- and ABP1-RNCs were measured photometrically where 0.1 $A_{260_{total}}$ correspond to 2 pmol 80S ribosomes.

For analyzing the samples on a 15% SDS-PAGE (chap. 2.6.2), they were heated in sample buffer to 65°C in order to preserve the peptidyl-tRNA bond.

2.4 Purification of non-programmed 80S ribosomes (np80S)

Ribosomes received from a yeast ΔSki2 cell-free translation system were treated under high salt and puromycin conditions as described before (Beckmann et al., 2001) in order to obtain ribosomes not programmed with any nascent chain (NC). 400 μl of the

cell-free translation extract were mixed with 400 μl 2x HP buffer (1mM puromycin, 1M KOAc, 40 mM HEPES pH 7.4, 50 mM $Mg(OAc)_2$, 2 mM DTT, 1 mM PMSF, 0.4 U/μl SUPERase-In) and loaded onto a 500 μl sucrose cushion (1 M sucrose, 20 mM HEPES pH 7.5, 500 mM KOAc, 25 mM $Mg(OAc)_2$, 1 mM DTT, 0.5 mM PMSF). Ribosomes were pelleted by centrifugation in a TLA 100.3 rotor (Beckman) for 1 h at 100,000 rpm and 4°C. The pellet was resuspenden in grid buffer (20 mM Tris/HCl pH 7.0, 50 mM KOAc, 2.5 mM $Mg(OAc)_2$, 1 mM DTT, 125 mM Sucrose, 100 μg/mL Cycloheximide, 0.05% Nikkol) and concentration was determined on a photometer.

2.5 RNase I treatment of ribosome nascent chain complexes (rtRNC)

For selective removal of eukaryotic specific expansion segments, RNCs or non-programmed ribosomes (np80S) were incubated with 40 U RNase I (Thermo Fisher) per 1 A_{260} unit of ribosomes for 45 min at 25°C. The reaction was stopped with 0.5 U SUPERase-In (Thermo Fisher) RNase inhibitor per 1 U of RNase I and the sample was placed on ice. The RNase I-treated RNCs are referred to as rtRNC.

2.6 Protein analysis

2.6.1 TCA precipitation

Samples for Polyacrylamide-Gel-Electrophoresis (PAGE) exceeding the volume of 20 μl to be loaded on a gel were precipitated with trichloroacetic acid (TCA) in order to concentrate the sample and decrease its volume. The sample was filled up to 1 ml with H_2O and subsequently 100 μl 0.15% Natrium-desoxycholate and 100 μl of 72% trichloroacetic acid (TCA) were added. After incubation on ice for 20 min, samples were pelleted in a table-top centrifuge at 14,000 rpm for 20 min at 4°C. The SN was sucked away and the pellet was washed with 1 ml ice cold (-20°C) acetone. A second round of centrifugation for 10 min was performed, the SN discarded and the sample dried with lid open under the hood at RT. The dried pellet was resuspended in 10 μl 1x SDS-sample buffer (prepared as 4xSB: 200 mM Tris/HCl pH 6.8, 8% (w/v)SDS, 40% (v/v) glycerol, 0.02% (w/v) bromophenol blue, 100 mM DTT).

2.6.2 Polyacrylamide-Gel-Electrophoresis (PAGE)

To separate proteins according to their molecular weight, Polyacrylamide-Gel-Electrophoresis (PAGE) was performed under denaturing conditions and using standard protocols (Laemmli, 1970).

Separation was either performed using 15% SDS-PAGE in 1x SDS running buffer (25 mM Tris, 192 mM glycine, 0.1% (w/v) SDS) or using Nu-PAGE gels (Life Technology) that preserve their neutral pH whilst running using 1x MES running buffer (50 mM MES, 50 mM tris base, 3.5 mM SDS, 1 mM EDTA acid free) or 1x MOPS running buffer (50 mM MOPS, 50 mM Tris base pH 7.7, 0.1% SDS, 1 mM EDTA). SDS-PAGE gels were run for 5 min at 180 V, followed by 55 min at 200 V. 4-12% Nu-PAGE gradient gels or 12% Nu-PAGE gels were run either in 1x MES running buffer or in 1x MOPS running buffer respectively for 40 min to 1 h at 180-200 V.

Denaturation of the samples in 1x SDS-sample buffer (prepared as 4xSB: 200 mM Tris/HCl pH 6.8, 8% (w/v) SDS, 40% (v/v) glycerol, 0.02% (w/v) bromophenol blue, 100 mM DTT) was performed for 10 min at 65°C to preserve peptidyl-tRNA in case of RNC samples or otherwise at 95°C for 5 min.

Gels were stained with SimplyBlue SafeStain (Thermo Fisher) according to the manual either directly or after western blot analysis to monitor transfer efficiency.

2.6.3 Semi-dry western blotting

Semi-dry western blot was used to analyze native TAP purification samples (chap. 2.9). After PAGE, proteins were transferred onto a PVDF membrane soaked in 100% methanol and pre-incubated in blotting buffer (20% (v/v) methanol, 48 mM Tris/HCl, 39 mM glycine, 0.037% (w/v) SDS). Blotting was performed for 1 h at a constant current of 150 mA (NatA) or 100 mA (Map). The membrane was stained for 1 min with Amido Black (0.1% (w/v) naphthol blue black, 7.5% (v/v) acetic acid, 20% (v/v) ethanol) on a shaker until clear bands were visible and destained afterwards in destaining solution (40% (v/v) ethanol, 10% (v/v) acetic acid) until a white background was obtained. To reduce unspecific binding, the membrane was incubated in 5% milk/1xTBS (20 mM Tris/HCl pH 7.6, 150 mM NaCl) for 30 min at RT or at 4°C o/n. After a short rinse with 1x TBS, the membrane was incubated with the first antibody (see below) for 1 h

at RT or at 4°C o/n, followed by three washing steps for 10 min each with 1x TBS. The horseradish peroxidase (HRP)-coupled secondary antibody was applied for 1 h at RT and the membrane was washed afterwards three times for 10 min each with 1x TBS-T (TBS with 0.1% (v/v) Tween).

The following antibodies were used:

- α-CAB (Thermo Fisher)
  - 1:5,000 in 5% milk/1xTBS for 1 h at RT or at 4°C o/n
  - Goat α-rabbit, 1:2,000 in 5% milk/1xTBS for 1 h at RT
- α-uL29 (polyclonal chicken antiserum, Davids Biotechnolgie)
  - 1:2,500 in 5% milk/1xTBS for 1 h at RT or at 4°C o/n
  - Rabbit α-chicken, 1:5,000 in 5% milk/1xTBS for 1h at RT
- α-HA probe (Santa Cruz)
  - 1:1,000 in 2% BSA for 1h at RT
  - Goat α-mouse, 1:5,000 in 5% milk/1xTBS for 1 h at RT

Protein signals were visualized using super signal ECL substrate (Thermo Fisher) on a AI600 imaging device (GE Healthcare).

2.7 Cloning, expression and protein purifications

2.7.1 Map1

Cloning of yeast Map1 was done by Birgitta Beatrix from our lab and Map1 was cloned as the full length version including a N-terminal propeptide sequence (Chang et al., 1992). In brief, MAP1 was obtained from *S. cerevisiae* genomic DNA using an upstream primer inserting a His_8-tag followed by a linker and a HRV 3C cleavage site. It was cloned into pET28a (appendix p. 131) using NcoI and EcoRI restriction sites.

Cells were harvested by centrifugation in a SCL6000 rotor (Sorvall) for 10 min at 4,500 rpm and 4°C. After washing with 1x PBS the pellet was finally resuspended

in cold lysis buffer (50 mM Tris pH 8.0, 500 mM NaCl, 1 mM PMSF, 1 EDTA-free protease inhibitor cocktail pill/50 ml (Roche)) and subjected to mechanical lysis using a Microfluidizer® (Microfluidics). Clarified lysate (SS34 (Sorvall), 15 min, 15,000 rpm, 4°C) was filtered and purified using a HisTrap HP column (GE Healthcare) equilibrated with HT-20 buffer (50 mM Tris pH 7.5, 500 mM NaCl, 20 mM imidazol, 10 mM β-mercaptoethanol). After elution with HRV 3C protease under high salt conditions, the main fractions were loaded onto a SP FF column (GE Healthcare) equilibrated with 20 mM HEPES at pH 7.0. Elution was performed by a linear salt gradient up to 1 M NaCl, the main fractions showing purified Map1 protein were pooled and the buffer was adjusted to 20 mM HEPES pH 7.5, 100 mM KOAc, 2.5 mM $Mg(OAc)_2$, 1 mM DTT, 0.5 mM PMSF, 10 μg/ml cycloheximide including a protease inhibitor cocktail tablet (Roche).

2.7.2 NatA

Cloning of the trimeric NatA complex was done by Birgitta Beatrix from our lab. In brief, NAA15 and NAA50 were obtained from *S. cerevisiae* genomic DNA. NAA15 was amplified using an upstream primer coding for a His_8-tag followed by a linker as well as a HRV 3C cleavage site and was cloned via NdeI and KpnI into MCS1 of pETDuet-1 (Novagen, appendix p. 130). NAA50 was cloned via NcoI and PstI into the MCS1 of pRSFDuet-1 (Novagen, appendix p. 130). For the catalytic SU, NAA10 was synthesized as a catalytic inactive mutant with an E26A mutation (Liszczak et al., 2013). It was ordered codon-optimized for *E. coli* at Eurofins Genomics (Ebersberg) and cloned via NdeI and XhoI into the MCS2 of pRSFDuet-1 already containing NAA50. After co-transformation of both plasmids into *E. coli* ER2566 cells, cultures were grown on LB medium and induced at 16°C o/n with 1 mM IPTG.

Harvesting and lysate preparation was done as described above (chap. 2.7.1). The HisTrap purification was also performed as described above but using HT buffer with 40 mM imidazole. After the elution with 500 mM imidazole, the two main fractions with NatA complex present were pooled, followed by a HRV 3C protease cleavage to remove the His-tag and was subsequently applied to size exclusion chromatography on a Superdex 200 column (GE Healthcare). Trimeric NatA complex eluted in a symmetric peak and was stored in GF buffer (20 mM Hepes pH 7.5, 200 mM KOAc,

10 mM $Mg(OAc)_2$, 1 mM DTT).

2.7.3 NatB

Cloning of the wildtype (wt) NatB complex was performed by Birgitta Beatrix from our lab. Shortly, the auxiliary SU Naa25 was obtained from *S. cerevisiae* genomic DNA using an upstream primer inserting a His_8-tag followed by a linker and a HRV 3C cleavage site. This construct was cloned into MCS1 of pRSFDuet-1 (Novagen, appendix p. 130) using NcoI and SacI restriction sites. The catalytic SU Naa20 was synthesized codon-optimized for *E. coli* (Eurofins Genomics) with the following mutations. E25A and H74A to obtain inactive mutants (Hong et al., 2017) and M36L to prevent an internal translation initiation. This modified Naa20 was cloned via NdeI and XhoI into MCS2 of the same plasmid. To overcome a disproportion of auxiliary to catalytic SU, Naa20 was cloned into pET21a (appendix p. 132) separately and was used for co-expression with the dimeric NatB construct. After transformation of both plasmids into *E. coli* BL21 cells, cultures were grown in LB medium and induction was performed with 1 mM IPTG at 16°C o/n.

Harvesting and lysate preparation was done as described above as well as HisTrap purification (chap. 2.7.1). After HisTrap purification NatB was either subjected to size exclusion chromatography on a Superdex 200 (GE Healthcare) and stored in 20 mM HEPES pH 8.0, 500 mM KOAc, 5 mM $Mg(OAc)_2$, 1 mM DTT; or it was loaded onto a PD10 column (GE Healthcare) to exchange the buffer to the same as above.

2.7.3.1 Site-directed mutagenesis

Based on an *in vitro* reconstituted structure of NatB with ABP1-RNC, four positively charged areas within the auxiliary SU that might responsible for NatB interaction with the ribosome were defined. A site-directed mutagenesis kit (New England BioLabs) was then used to introduce mutation in the DNA sequence by PCR. To that end, the plasmid used for Naa25 cloning above was amplified using primers carrying charge inversions were lysines or arginine were exchanged to glutamic acid (similar to Magin et al., 2017). Mutations were inserted in pairs and indicated as positive patches PP1-4, where PPall represents a plasmid with all four mutations at the same time (tab. 5). Site-directed mutagenesis was performed according to the manufacturers manual and

using the primers listed in tab 6. Expression and purification was performed in the same way as for the wildtype NatB.

Table 5: Mutations introduced in the auxiliary subunit of NatB. Mutation were intoduced via site-directed mutagegensis to the ribosome binding subunit Naa25 in *S. cerevisiae*. Mutations comprised charge inversions from lysine (K) or arginine (R) to glutamic acide (E) and are grouped into four positive patches (PP). PPall contains all mutations of all patches in the same plasmid.

Patch 1:	PP1	K723E, K725E
Patch 2:	PP2	K729E, K736E
Patch 3:	PP3	K747E, K751E
Patch 4:	PP4	K791E, R794E
PPall:	PP1-4	K723E, K725E, K729E, K736E, K747E, K751E, K791E, **R**794E

Table 6: Primer used for site-directed mutagenesis. Forward and reverse primer are listed for PP1-4. For PPall, mutations were introduced sequentially to PP2 by using PP3 and PP4 primer pairs. To introduce PP1 in addition, PPall fw and rev primer pairs were used.

	5′-3′ sequence	T_{anneal}
PP1 fw	GAGAATCGAAGATGAGGAAATTCAAAAAAAC	65°C
PP1 rev	TTCAAACTGTCTAGTGTTTTTAAGGTTGC	
PP2 fw	GAAATTCAAGAACTAATCAAAAACTCCCT CGAGAAGTTGAGGAG	68°C
PP2 rev	TTCAAACTGTCTAGTGTTTTTAAGGTTGC	
PP3 fw	TTCTGAAGCTTTAGTACAAGCATATG	57°C
PP3 rev	TAACCTTCAAATACATCATCGCAACAAC	
PP4 fw	GTAGAAAATTTATGAGAGCTCGGC	60°C
PP4 rev	ACTTTCTTGGATGCCTAGTAATGAATTTTTAATG	
PPall fw	TGAAGAAATTCAAGAACTAATCAAAAAC	57°C
PPall rev	TCTTCGATTCTCTTCAAACTGTCTAG	

2.8 Binding and competition assays

2.8.1 Binding assay of Map1 to 80S ribosomes

To characterize the binding situation of Map1 to ribosomes, Map1 was *in vitro* reconstituted with uL4-RNC or RNaseI-treated uL4-RNC (rtRNC) (chapters 2.3 and 2.5).

Binding reactions were performed using 2 pmol of ribosomes and a 30-fold molar excess of purified Map1 complex. The binding buffer was adjusted to a final concentration of 50 mM Tris pH 7.0, 150 mM KOAc and 2.5 mM $Mg(OAc)_2$. After preincubation of all components but ribosomes for 5 min on ice, the 2 pmol ribosomes were added and the sample was incubated for 15 min at RT. The reaction was loaded onto 600 μl sucrose cushion (750 mM sucrose, 20 mM HEPES pH 7.5, 150 mM KOAc, 2.5 mM $Mg(OAc)_2$, 1 mM DTT) and spun for 2.5 h in a SW55Ti rotor (Beckman) at 40,000 rpm and 4°C. The tubes were immediately frozen in liquid nitrogen and cut at 1/3 from the bottom. The upper 2/3 contained the supernatant (SN), whereas the lower 1/3 contained the pellet fraction (P). After TCA precipitation, Map1 binding to ribosomes was analyzed by SDS-PAGE. With successful binding both, bands representing ribosomal proteins and Map1, are visible in the pellet fraction after staining with SimplyBlue SafeStain (Thermo Fisher).

2.8.2 Binding assay of NatA to 80S ribosomes

Binding of NatA to ribosomes was explored by its *in vitro* reconstitution with uL4-RNC, rtRNCs or non-programmed 80S ribosomes (np80S) (chapters 2.3, 2.5 and 2.4). Two pmol of RNCs were incubated as described before (chap. 2.8.1) with a 10-fold molar excess of purified and inactive NatA complex. The binding buffer was specifically adjusted for NatA binding to a final concentration of 50 mM Tris pH 7.0, 150 mM KOAc, 1 mM acetyl-CoA and 5 mM $Mg(OAc)_2$. In addition, the sucrose cushions contained 5 mM $Mg(OAc)_2$ instead of 2.5 mM as for Map1 binding assays. After pelleting and SDS-PAGE analysis, protein bands were quantified with ImageJ (https://imagej.nih.gov/ij/). Quantified Naa15 bands were normalized against the ribosomal band at 50 kDa (appendix p. 134, asterisk). Each reaction was performed with four replicates. Error bars were calculated using the standard deviation from the mean.

2.8.3 Binding assay of NatB to 80S ribosomes

Binding assays were executed using wt NatB as well as mutated NatB (chap. 2.7.3) with uL4-RNC (chap. 2.3), RNaseI-treated uL4-RNCs (chap. 2.5), HA-RNCs (chap. 2.3), ABP1-RNCs (chap. 2.3) and non-programmed 80S ribosomes (np80S) (chap. 2.4).

The binding assays was performed described as before where 2 pmol RNCs or np80S were incubated with an 20-fold molar excess of the target protein (chap. 2.8.1). The binding buffer for NatB-ribosome interaction studies was adjusted to final concentrations of 50 mM Tris pH 7.5, 150 mM KOAc, 5 mM $Mg(OAc)_2$ and 1 mM acetyl-CoA. The sucrose cushion used for co-sedimentation of ribosome-bound NatB contained 750 mM sucrose, 20 mM HEPES pH 7.5, 150 mM KOAc, 5 mM $Mg(OAc)_2$, 1 mM DTT and 10 μg/ml cycloheximide. Similar to NatA binding behavior, NatB bound to all RNCs or ribosomes to the same extend, independent weather they carry a substrate or non-susbtrate or no NC. Therefore, the following binding assays with mutated NatB were performed using np80S in order to prevent any bias by a NC.

Binding assays with mutated NatB (PP1-4, PPall) were performed the same way as above but using an alternative centrifugation approach. After finishing the binding reaction, the sample was loaded onto a 100 μl sucrose cushion and spun for 1 h at 100,000 rpm and 4°C using a TLA 100 rotor (Beckman). The pellet was resuspended in 10 μl grid buffer (20 mM Tris/HCl pH 7.0, 50 mM KOAc, 2.5 mM $Mg(OAc)_2$, 1 mM DTT, 125 mM sucrose, 100 μg/ml cycloheximide, 0.05% Nikkol), the SN got TCA precipitated and samples were loaded on a 12% Nu-PAGE gel using MOPS running buffer.

2.8.4 Competition assay of Map1-TAP with NatA

To study the possibility of a concomitant binding of Map1 and NatA on the same 80S ribosomes, competition assays were performed. To 4 pmol of the final elution from Map1-TAP native pull out (chap. 2.9), recombinantly purified NatA was titrated with increasing concentration reaching a molar excess of 1:5 to 1:40. Incubation and centrifugation was performed as described above (chap. 2.8.1) and samples were loaded on a 12% Nu-PAGE gel. Subsequent western blot analysis using an α-CAB antibody reflects Map1 binding behavior dependent on the signal present in the pellet fraction or in the supernatant.

2.9 Native pull outs

A protocol for rapid affinity purification of ribonucleoprotein particles from cell lysates (Oeffinger et al., 2007) was used for native pull out purifications. Here, harvested cells were rapidly frozen and grinded while they were cooled with liquid nitrogen to prevent nucleases and proteases to be active. In addition, antibody-conjugated magnetic beads were used instead of sepharose. This allows a fast and efficient purification under conditions that stabilize and enrich intact ribosome-bound complexes. Based on this, the protocol was optimized to co-purify ribosomes with Map1 and NatA complexes.

2.9.1 Purification of native Map1-ribosome complexes

A native pull out was performed to trap Map1 on the translating 80S ribosome. To do that, Map1 was C-terminally tagged in *S. cerevisiae* using the tandem-affinity purification (TAP) tag. The tag comprises a Protein A domain (ProtA), a tobacco etch virus protease cleavage site (TEV) for elution and a calmodulin-binding domain (CaMBD) for an optional second purification step (fig. 2.1). The strain was ordered from Euroscarf (SC0000; MATa; ura3-52; leu2-3,112; YLR244c::TAP-KlURA3; accession number SC1694).

Figure 2.1: Tandem-affinity purification (TAP) tag composition for native ribosome-Map1 purification. CaMBD, calmodulin-binding domain; TEV, tobacco etch virus protease cleavage site; ProtA, protein A IgG binding domains.

If not stated different, the following steps were done on ice.

Yeast cultures were grown in YPD medium to 4.0 OD_{600} and 5 g of wet cells were resuspended in lysis buffer with low magnesium concentration (LB-2.5: 20 mM HEPES pH 7.5, 100 mM KOAc, 2.5 mM $Mg(OAc)_2$, 1 mM DTT, 0.5 mM PMSF, 10 μg/ml cycloheximide, protease inhibitor cocktail tablet (Roche)). Cell disruption was performed using a Freezer Mill (6970 EFM). The powder was resuspended in 15 ml LB-

2.5 and the lysate spun for 15 min at 4°C in an SS-34 rotor (Sorvall) at 15,000 rpm to clarify the lysate. The SN was loaded onto several 600 μl sucrose cushions (750 mM sucrose in LB-2.5) and centrifuged for 1 h at 100,000 rpm in a TLA 100.3 (Sorvall) at 4°C. The pellets were resuspended in LB-2.5 and pooled for subsequent TAP purification. 150 μl magnetic IgG-coupled Dynabeads M-270 Epoxy (Life Technologies) were equilibrated with 300 μl LB-2.5 containing 0.5% TritonX-100 (LB-2.5+T) twice and added to the pooled sample. The sample was incubated with the beads for 1 h at 4°C on a rotating wheel, harvested on a magnet and resuspended in 500 μl LB-2.5+T (sample: R). After three washing steps with 500 μl LB-2.5+T (sample: W1-3) and three washing steps with 500 μl LB-2.5 (sample: W4-6), ribosome-Map1 complexes were eluted in 120 μl LB-2.5 containing 70 units of Ac-TEV protease (Thermo Fisher) for 1 h at 20°C (sample: E). A concentration of 14 A_{260}/ml was measured on the NanoDrop (Implen). Due to sufficient purity of the sample, the second purification step using CaMBD was not necessary.

Samples were subsequently analyzed on a 12% Nu-PAGE gel (chap. 2.6.2). 0.1 $A_{260_{total}}$ of the elution was loaded on the gel as well as the same fractional amount of the other samples to monitor the purification process. If sample volume exceeded 20 μl, a TCA precipitation was performed (chap. 2.6.1). Samples were then further analyzes by western blot analysis (chap. 2.6.3).

2.9.2 Purification of native NatA-ribosome complexes

For the tandem affinity purification for native NatA-ribosome complexes, the ribosome binding SU of NatA (Naa15) was C-terminally tagged in *S. cerevisiae* using the tandem-affinity purification (TAP) tag as above (fig. 2.2). The Naa15-TAP tagged strain was ordered from Euroscarf (SC0000; MATa; ura3-52; leu2-3,112; YDL040c::TAP-KlURA3; accession number SC0765).

If not stated different, all following steps were carried out on ice.

Yeast cultures were grown to an OD_{600} of 4.0 in YPD medium, 7 g of wet cells were resuspended in lysis buffer (LB-10: 20 mM HEPES pH 7.5, 100 mM KOAc, 10 mM $Mg(OAc)_2$, 1 mM DTT, 0.5 mM PMSF, 10 μg/ml cycloheximide, protease inhibitor

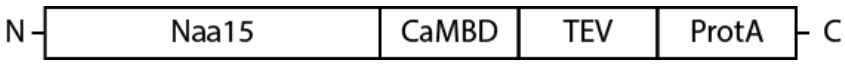

Figure 2.2: Tandem-affinity purification (TAP) tag composition for native ribosome-NatA purification. Naa15, NatA ribosome binding SU; CaMBD, calmodulin-binding domain; TEV, tobacco etch virus protease cleavage site; ProtA, protein A IgG binding domains.

cocktail tablet (Roche)) and disrupted utilizing a Freezer Mill (6970 EFM). The powder was resuspended in 20 ml LB-10 and the lysate clarified by centrifugation for 15 min at 4°C in an SS-34 rotor (Sorvall) at 15,000 rpm. 140 μl magnetic IgG-coupled Dynabeads M-270 Epoxy (Life Technologies) were washed with 250 μl lysis buffer containing 0.5% Triton (LB-10+T) twice and added to the lysate afterwards. Incubation was executed for 1 h at 4°C on a rotating wheel. Beads were harvested on a magnet and resuspended in 400 μl LB-10+T (sample: R). After six washing steps (3x with 500 μl LB-10+T, 3x with 500 μl LB-10; sample: W1-6), beads were incubated in 500 μl LB-10 containing 0.8 mM $CaCl_2$ (LB-10+Ca) for 10 min at 4°C on a rotating wheel (sample: Ca W1). In order to remove polyribosomes and to obtain a monosomal fraction, a subsequent S7 digestion was performed. For that, beads were incubated with 500 μl LB-10+Ca containing additional 11 U of S7 micrococcal nuclease (Roche) for 15 min at RT. The reaction was stopped by adding EGTA to a final concentration of 2 mM. The flow through was collected (sample: S7 FT), followed by three additional washing steps with 400 μl LB-10 (sample: S7 W1-3). NatA with its three subunits and all ribonucleoprotein particles were eluted in 140 μl LB-10 and 250 units of Ac-TEV protease (Thermo Fisher) over a duration of 1 h at 20°C on a rotating wheel (sample: E). Due to sufficient purity of the sample, the second purification step using CaMBD was not necessary. Native ribosome-NatA complexes eluted to an absorption of 5.8 A_{260}/ml.

0.1 $A_{260_{total}}$ of the elution was loaded on a 4-12% Nu-PAGE gel as well as the same fractional amount of the other samples to monitor the purification process. If sample volume exceeded 20 μl, a TCA precipitation was performed (chap. 2.6.1).

2.10 Sucrose density centrifugation

To study ribosome subunit composition in the elution of native pull outs or to obtain purified 80S RNCs, a polyribosome profile was recorded. Therefor, the sample was loaded onto a linear 10-40% sucrose gradient (20 mM HEPES pH 7.5, 100 mM KOAc, 10 mM $Mg(OAc)_2$, 1 mM DTT, 0.5 mM PMSF with 10% or 40% sucrose (w/v)) and spun in a SW40 rotor (Beckman) at 40,000 rpm for 2.5 h at 4°C. Gradients were collected from top to bottom (Gradient Station ip, BioComp) by monitoring the absorption profile at 254 nm (Econo UV Monitor, Bio-Rad).

2.11 Cryo-electron microscopy

2.11.1 Cryo-EM Analysis and model of the Map1-ribosome complex

Sample preparation

Four pmol of the freshly prepared samples from the native Map1-TAP pull out were adjusted to 40 μl total sample volume with LB-2.5 containing Nikkol to a final concentration of 0.05% (w/v). For cross-linking glutaraldehyde was added to a final concentration of 0.02% (w/v) and the sample was incubated for 15 min on ice. After a short spin of 5 min at 4°C and 14,000 rpm in a table top centrifuge (Eppendorf), 3.5 μl were applied to 2 nm precoated Quantinfoil R3/3 holey carbon support grids. Before sample application the grids were glow discharged for 30 sec at 0.3 mbar. Subsequent vitrification was performed by plunge freezing the grid into liquid ethane using Vitrobot Mark IV (FEI Company/Thermo Fisher) with an incubation time of 45 sec and blotting for 2-3 sec at 4°C and a humidity of 95%.

Data collection

Data were collected on a Titan Krios G3 (Thermo Fisher) assembled with a K2 direct detector (Gatan) at 300 keV using the semi-automated data acquisition software EPU (Thermo Fisher). 48 frames with a dose of 1.17 $e^-/Å^2$ per frame were collected in a defocus range of -0.5 to -3.2 μm. Magnification settings resulted in a pixel size of 1.059 Å/pixel. Frame alignment was executed with MotionCor2 (Zheng et al., 2017) and the estimation of the contrast transfer function (CTF) was performed with Gctf (Zhang, 2016).

Data processing

Micrographs were screened manually for ice quality and the resulting 8,358 micrographs were used for automated particle picking in Gautomatch (http://www.mrc-lmb.cam.ac.uk/kzhang/). After a two-dimensional (2D) classification in RELION 3.0 (Scheres, 2012; Kimanius et al., 2016) to discard non-ribosomal particles, in total 115,082 particles were subjected to an initial refinement round. Subsequent 3D classification into eight classes led to three classes only containing poorly resolved 80S ribosomes (7% with 8,234 particles, 1% with 1,226 particles, 0.01% with 149 particles) and one class showing the 60S subunit only (6%, 6,728 particles). The remaining four classes had good resolved 80S ribosomes all of which were programmed with tRNAs (mainly in A/A and P/P) and had the mobile expansion segment ES27a solely in the exit position. Besides, they already showed a small extra density between ES27a and the TE. One of this classes (12%, 13,804 particles) contains yeast eRF1 and ABCE1/Rli1 additionally. As individual processing of the four good resolved classes with focus on the expected Map1 binding site or on tRNA states did not lead to a clear shape or differences in the additional density below the TE, these four classes were merged for further processing (86%, 98,745 particles). A subsequent 3D classification using a binary soft mask enclosing ES27a and the region below the TE revealed one class (25%, 25,245 particles) that showed a well-shaped ES27a as well as a defined extra density where Map1 was expected. All other classes had either no good resolved ES27a or only showed fragmented densities at the expected Map1 position (24% with 23,499 particles, 28% with 27,590 particles, 23% with 22,411 particles). The good-resolved class was refined and subjected to another round of local 3D classification, this time with a mask covering only the tip of ES27a together with the Map1 position. The two resulting classes exhibited Map1 in two different conformations, either tightly connected to ES27a (47%, 11,938 particles) or with a looser connection to ES27a (53%, 13,307 particles). Both classes were CTF refined to an overall resolution of 3.9 Å and 3.8 Å according to the gold standard resolution criterion (FSC = 0.143) and comprising 10% or 12% of the total particle number after 2D classification respectively. Subsequent local resolution calculation were received using RELION.

Yeast Map1 model

As no structure of the yeast Map1 is available, a homology model was created us-

ing MODELLER (https://modbase.compbio.ucsf.edu/modweb/, Sali and Blundell, 1993). In order to place Map1 model into the electron density, this model was superimposed with Ebp1 structure (Wild et al., 2020; PDB 6SXO) that harbors a Map-like fold after docking of Ebp1 into the cryo-EM map. This was followed by a rigid-body fit of the Map1 model into the isolated densities.

Cryo-EM structures and models were displayed with Chimera (Pettersen et al., 2004) and ChimeraX (Goddard et al., 2018).

2.11.2 Cryo-EM Analysis and model of the NatA-ribosome complex

Sample preparation

Freshly prepared samples of the native Naa15-TAP pullout were adjusted to 5 A_{260}/ml and 3.5 μl were applied to 2 nm precoated Quantinfoil R3/3 holey carbon support grids as described above (chap. 2.11.1).

Data collection

Data collection was performed on a Titan Krios TEM (Thermo Fisher) equipped with a Falcon II direct detector at 300 keV under low-dose conditions of about 25 $e^-/Å^2$ for ten frames in total and a defocus range of -1.1 to -2.3 μm using the semi-automated software EM-TOOLS (TVIPS). Magnification settings resulted in a pixel size of 1.084 Å/ pixel. Original image stacks were summed and corrected for drift as well as beam-induced motion at the micrograph level using MotionCor2 (Zheng et al., 2017). Contrast transfer function (CTF) estimation and the resolution range of each micrograph were performed with Gctf (Zhang, 2016).

Data processing

After manual screening for ice quality and contaminations, 6,600 micrographs were used for automated particle picking in Gautomatch (http://www.mrc-lmb.cam.ac.uk/kzhang/). Non-ribosomal particles were discarded by 2D classification in RELION 2.1 (Scheres et al., 2012; Kimanius et al., 2016) beforehand, resulting in a data set with 262,507 particles. After an initial round of refinement, particles were first classified into eight classes. All of them showed ribosomes programmed with tRNAs, indicating that ribosomes bound to NatA were stalled during translation elongation. One class (38,597 particles) displayed the mobile expansion segment ES27a exclusively in

the L1 position, whereas four classes showed ES27a pointing to the TE (exit position). The remaining three classes either had low particle numbers or contained low resolution particles. The four classes with ES27a in the exit position showed an extra density below the TE which was not present in the class with ES27a in the L1 position. Therefore, these four classes were merged (183,282 particles, 70%) and further subsorted on tRNAs to obtain clean tRNA states. The majority of the particles contained tRNAs in A- and P-site as well as eIF5A in the E-site as described for native pull outs before (Schmidt et al., 2016a). These classes (100,625 particles, 55%) were joined and sorted for the presence of an extra density at the peptide exit site by a local classification using a soft mask. One of the three classes harboring one third of the classified particles showed the most prominent and best-defined density of NatA below the TE that could not be classified any further. This stable final NatA class containing 26,476 particles (equivalent to 10% of all particles) was refined to an average resolution of 3.4 Å according to the gold standard resolution criterion (FSC = 0.143).
Local resolution was obtained using RELION showing the core ribosome at a resolution < 4 Å. NatA exhibits a higher conformational heterogeneity as resolution ranges from 5 Å for parts close to the TE, to 12 Å at the tip of ES27a. Therefore, a local refinement was performed using a soft mask for NatA. This significantly improved local resolution for NatA density and led to an average resolution of 8 Å for most parts of the NatA map.

Molecular model of the NatA-ribosome complex

The model of the ribosome in the native NatA-ribosome complex was based on previous models of the yeast ribosome (PDB 5MC6 and PDB 5GAK, Schmidt et al., 2016b and 2016a respectively) which were initially fitted as rigid bodies in Chimera. ES27a was revised based on the model of the LSU rRNA uploaded as PDB 3IZF (Armache et al., 2010). Specifically, the tip of ES27a was redesigned using a structure of a CUUG-tetraloop (PDB 1RNG (Jucker and Pardi, 1995) as a template. ES7a was modeled based on PDB 5EM4 (Kater et al., 2017).
The three NatA SUs were rigid-body fitted in Chimeras using the crystal structure of *S. cerevisiae* trimeric NatA in complex with a bisubstrate (PDB 4XNH) with minor adjustments, such as the 'basic helix' (α33) that could be extended towards its ribosomal binding site, ES39a. To predict the number of aa between the TE and the catalytic

center of Naa10, the poly-Ala chain from 5MC6 was extended in COOT (Emsley et al., 2010) so that it reaches the catalytic center by the shortest route.

Cryo-EM structures and models were displayed with Chimera (Pettersen et al., 2004) and ChimeraX (Goddard et al., 2018).

2.11.3 Cryo-EM Analysis of RNase I-treated Ribosomes (rtRNCs)

Four pmol uL4-RNCs were treated with RNase I (chap. 2.5), applied to grids and 2,537 micrographs were collected as described above (chap. 2.11.2). RELION-3.0 (Scheres et al., 2012; Kimanius et al., 2016) 2D classification was used to discard non-ribosomal particles and the resulting 43,423 particles were refined against an 80S ribosome from *S. cerevisiae*. Already at the level of the first initial refinement the ribosomes were lacking density of large rRNA expansion segments, namely ES3, ES6 and ES 12 (SSU) and ES7, ES27 and ES39a (LSU). In addition, mobile rRNA such as h16 close to the mRNA exit or H76 from the L1 stalk of the large subunit were also missing. Particles were further subclassified into three classes of which one obtained higher resolution, containing 5,909 particles. This class was refined to a final resolution of 6.7 Å using three times binned particle images (pixel size: 3.252 Å). A control of non-treated RNCs were processed similarly. For comparison of both maps, a low-pass filter to 8 Å was applied to the maps and they are shown at the same contour level (3.7σ) (see chap. 3.1.3.1).

2.11.4 Cryo-EM analysis of the NatA-ABP1-RNC complex

Sample preparation

For cryo-EM samples and *in vitro* reconstitution, purified ABP1-RNCs were first loaded onto a 10-40% linear sucrose gradient (chap. 2.10), the 80S peak was collected and concentrated by centrifugation through a sucrose cushion (750 mM sucrose, 20 mM HEPES pH 7.5, 150 mM KOAc, 5 mM $Mg(OAc)_2$, 1 mM DTT) for 1 h at 100,000 rpm and 4°C in a TLA 110 rotor (Beckman). The pellet was resuspended in grid buffer (20 mM Tris/HCl pH 7.0, 50 mM KOAc, 2.5 mM $Mg(OAc)_2$, 1 mM DTT, 125 mM Sucrose, 100 μg/ml Cycloheximide, 0.05% Nikkol) and this gradient purified ABP1-RNCs were used for cryo-EM studies.

For *in vitro* reconstitution with NatA complex, the same binding condition used in

binding assays (chap. 2.8.3) but without the centrifugation step were chosen. That is 2 pmol RNCs, excess of trimeric NatA complex and acetyl-CoA to final concentration of 1 mM. The total reaction volume was 25 μl.

Freshly prepared samples were applied to 2 nm precoated Quantinfoil R3/3 holey carbon support grids and plunge frozen under the same condition used before with the same condition described above (chap. 2.11.2).

Data collection

Data were collected on a Titan Krios TEM (Thermo Fisher) equipped with a Falcon II direct detector at 300 keV to the same conditions described above (chap. 2.11.2).

Data processing

Micrographs were screened manually to reject those with bad ice quality or contaminations and those of good quality (13,828 micrographs) were used for automated particle picking in Gautomatch (http://www.mrc-lmb.cam.ac.uk/kzhang/). Non-ribosomal particles were separated in RELION 3.0 (Scheres et al., 2012; Kimanius et al., 2016) by 2D classification resulting in a clean dataset with 294,373 particles. After a first round of refinement a 3D classification into six classes was performed. Beside two low resolution classes comprising 6% (17,226 particles) and 5% (15,563 particles) from all particles, one class only showing 60S subunits (11%, 33,589 particles). The three other classes contained either ES27a in the L1 position (33%, 97,916 particles), ES27a in the exit position (38%, 110,353 particles) or ES27a as a mixture of both positions (7%, 19,726 particles). As known from the native NatA-ribosome structure (chap. 3.2.2), NatA binds to ribosomes only when ES27a adopts the exit position. In addition, an already prominent density for NatA was visible below the TE. Therefore, the class having ES27a solely in the exit position (110,353 particles) and with tRNAs in the P/P-state was used for a second classification round. A soft mask covering NatA region was applied and particles were classified into another six classes. One class contained only low resolution ribosomes (7%, 7,778 particles). Two of them exhibit NatA but missing either the connection to Naa50 (25%, 27,940 particles) or to ES39a (15%, 15,963 particles). Two classes had no NatA bound but had a small additional density near the TE instead, only differing in the positioning of ES27a (20%, 22,560 particles or 18%, 19,838 particles). The class comprising 16,274 particles (15%)

was the only one showing NatA in the same conformation as observed from native pull out (Knorr et al., 2019). This class could not be further classified. In order to reduce the movement of the SSU and to increase the resolution, the 40S SU was removed using the signal subtraction in RELION and the final class with 16,274 particles (equivalent to 5.5% of all particles) was refined to an overall resolution of 3.7 Å after CTF refinement according to the gold standard resolution criterion (FSC = 0.143).

2.11.5 Cryo-EM analysis and model of the ribosome-NatB complex

Sample preparation

To study the binding of NatB to the 80S ribosome, gradient purified ABP1-RNCs (chap. 2.3 and 2.10) were *in vitro* reconstituted with recombinantly purified inactive NatB complex to the same conditions as described above (chap. 2.8.3) but with 100 mM KOAc final concentration in the buffer and without the centrifugation step. In more detail, 2 pmol of ABP1-RNCs were incubated with a 20-times molar excess of wt NatB. The total reaction volume was 18 μl and Nikkol was added to a final concentration of 0.05% (w/v).

The freshly prepared sample was applied to 2 nm precoated Quantinfoil R3/3 holey carbon support grids and plunge frozen under the same condition used before (chap. 2.11.1).

Data processing

Data were collected on a Titan Krios TEM (Thermo Fisher) decorated with a Falcon II direct detector at 300 keV to the same conditions described above (chap. 2.11.2).

Data collection

A total amount of 8,986 micrographs were screened manually for ice quality and contaminations and used for automated particle picking in Gautomatch (http://www.mrc-lmb.cam.ac.uk/kzhang/). After a 2D classification in RELION 3.0 (Scheres et al., 2012; Kimanius et al., 2016) to eliminate non-ribosomal particles, 138,579 particles were subjected to an initial round of refinement and subsequently classified into eight classes. All classes were programmed with tRNAs in P/P state. Two classes either contained low resolution particles (7%, 9,823 particles) or only the 60S SU (4%, 5,271 particles) and were discarded. Two other classes had ES27a completely in the L1 position

(14%, 18,863 particles) or showing a mixture of ES27a in L1 and exit position (18%, 24,500 particles) and no clear extra density was visible. However, four classes displaying ES27a solely in the exit position as well as revealing an extra density below the TE. These classes were merged (85%, 80,119 particles) and subjected to a focused classification into two classes using a soft mask on the exit region. Here, 35,247 particles comprised a defined density within the masked area whereas the second class only showed noisy density at the tip of ES27a (44,872 particles). The crystal structure of NatB from *C. Albicans* (PDB 5K18, Hong et al., 2017) could already be fitted into the density of the good resolved class to assign NatB's subunits. This class was then further processed. A focused sorting on Naa20 was executed to obtain a balanced ratio between catalytic and auxiliary SU. The class where both SU were equally distributed (21,061 particles, corresponding to 15% of all particles) was CTF refined in RELION to an average resolution of 4.1 Å, showing a good resolved NatB in complex with the 80S ribosome (B1/primary binding site). As a supplementary processing step, this final class was subsorted using again a mask on the whole exit region. In both resulting classes, NatB was still in the same position as observed before. Surprisingly, in the higher occupied class (11,186 particles, 53%) another additional and shaped density behind the first NatB was visible. It is connected to ES27a and might be a secondary binding site for NatB (B2). As particle numbers decreased and coincide with lower resolution, a step backward was taken and the class with 35,247 particles were re-classified with a mask on the potential second binding site of NatB. Particles split into two almost equal classes showing either NatB in the already known B1 position (17,435 particles, 49%) or displaying a good resolved density for NatB in its potential second B2 position in addition to the regular B1 (17,812 particles, 51%). This last class, containing 13% of all particles from the beginning, was CTF refined to an overall resolution of 4.4 Å. All resolutions were obtained according to the gold standard resolution criterion (FSC = 0.143).

Local resolution was archived in RELION showing the core ribosome at a resolution < 4.4Å. In contrast, NatB is showing a resolution range starting at 5.5 Å for parts located closely to the TE and changing to above 12.5 Å at the very rim of NatB that is in great distance to the ribosome, as well as parts close to the flexible ES27a for B2 position.

Model building

The model of the ribosome was adapted from NatA-ribosome complex (chap. 2.11.2) but with appropriate adjustment of ES27a by rigid-body fitting into the density.

A homology model of NatB based on the crystal structure of *C. Albicans* NatB in complex with a bisubstrate inhibitor (PDB 5K18, Hong et al., 2017) was obtained by using MODELLER (https://modbase.compbio.ucsf.edu/modweb/, Sali and Blundell, 1993). This model was rigid-body fitted in chimera after minor adjustments, such as rearranging the C-terminal helices of Naa25. For length prediction of the NC between the TE and the catalytic Naa20 subunit, the poly-Ala chain from 5MC6 was extended in COOT (Emsley et al., 2010) accordingly.

3 Results

3.1 Map1 in complex with the 80S ribosome

Methionine aminopeptidase 1 (Map1) is the major enzyme removing the starter methionine in yeast. This important modification happens in up to 80% of proteins through all organisms. Therefore, one aim of this project was to determine the cryo-EM structure of this important enzyme in complex with the ribosome.

By performing a native pull out of the TAP-tagged Map1, endogenous Map1-ribosome complexes were purified directly from the cell lysate. After stabilizing the complexes by cross-linking with glutaraldehyde, they were subjected to cryo-EM and single particle analysis (SPA). Map1 binding to the ribosome was further characterized biochemically by performing *in vitro* binding assays.

3.1.1 Purification of native Map1-ribosome complexes

To obtain the structure of Map1 bound to translating ribosomes, a purification of Map1-ribosome complexes was performed using an adjusted protocol of a rapid affinity-purification to isolate intact ribosomes from cell lysate (Oeffinger et al., 2007; Schmidt et al., 2016a). For that purpose, a yeast strain with the C-terminally TAP-tagged Map1 was ordered (Euroscarf). After a spin of the cell lysate through a sucrose cushion for pelleting and subsequent resuspension, ribosomes were co-purified with Map1 via IgG-coupled magnetic beads interacting with the Protein A domain of the TAP-tag. The final TEV cleavage step resulted in co-elution of Map1, still harboring the calmodulin-binding domain (CaMBD), and ribosomal proteins. This process was monitored using the α-CAB antibody that detects the CaMBD (fig. 3.1A, B). A mass shift of about 20 kDa in the band corresponding to Map1 indicated the successful elution of Map1-ribosome complexes. The identity of Map1 and presence of ribosomal proteins was confirmed by mass spectrometry (Thomas Fröhlich, LMU Munich) (fig. 3.1C). The final sample at a concentration of 14 A_{260}/ml was used for subsequent cryo-EM analysis.

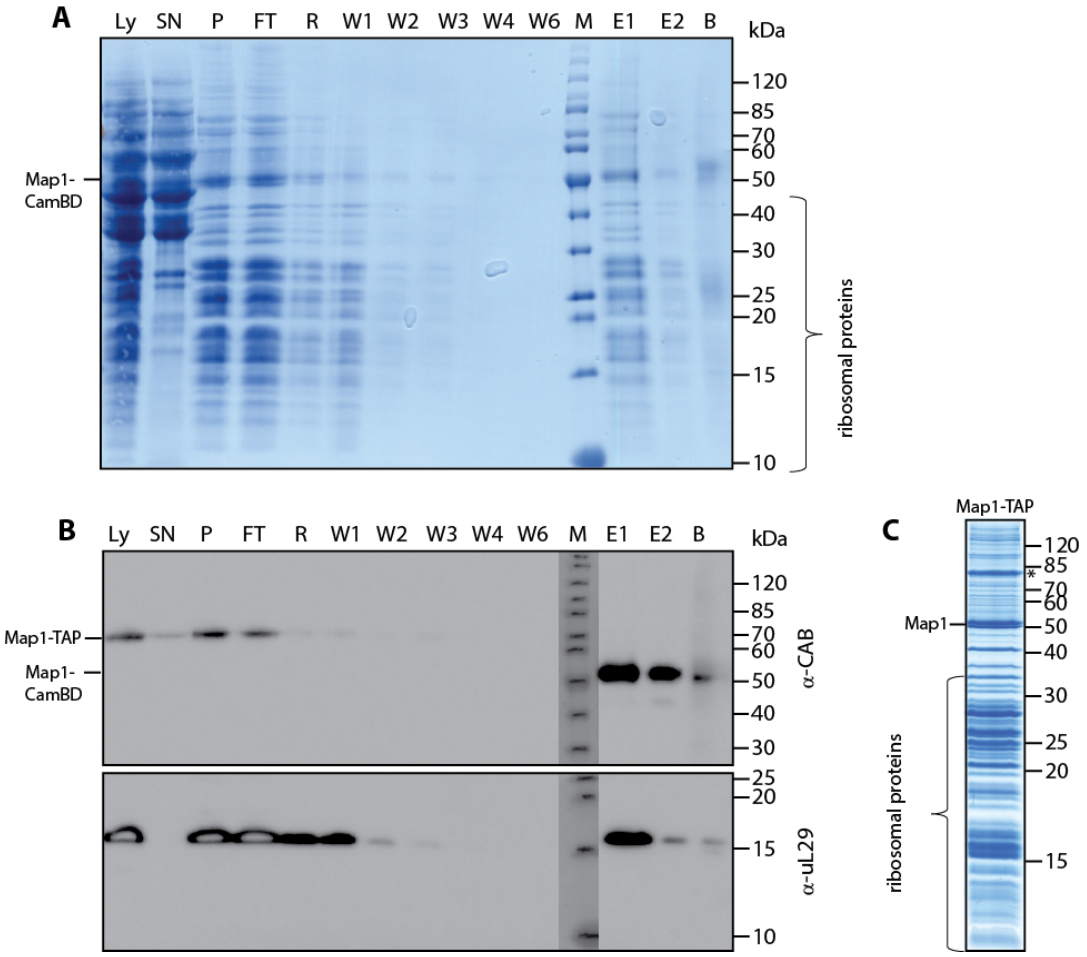

Figure 3.1: Affinity purification of native Map1-ribosome complexes. SDS-PAGE and Western Blot of the Map1-ribosome purification. **A**, Amido black stained PVDF membrane after the transfer from a 12% Nu-PAGE gel with aliquots from each purification step. **B**, Western Blot probed with an antibody against the CaMBD (α-CAB) that is still present after TEV cleavage. Cleavage is monitored as a shift of the α-CAB signal in the elution fraction. α-uL29 probes against the ribosomal protein uL29. **C**, 12% Nu-PAGE of the final elution of purified Map1-ribosome complexes. Ly, lysate; SN, supernatant; P, pellet; FT, flow through; R, resuspension; W, wash; E, elution; B, boiled beads. 0.1 A_{260} of E was loaded, for wash fractions 1/17 of the volume was loaded on the gel, for Ly, SN, P and FT 3 μl of the sample were loaded corresponding to 1/6,000 for L, 1/8,000 for SN and 1/1,000 for P and FT. TAP, tandem affinity purification tap; CaMBD, Calmodulin-binding domain, *, contamination from a viral protein.

3.1.2 Cryo-EM structure of the native Map1-ribosome complex

To characterize the binding of Map1 to translating yeast ribosomes, 4 pmol of a freshly prepared sample from Map1-TAP native pull out were cross-linked with 0.02% (w/v) glutaraldehyde and applied to holey carbon support grids for cryo-EM measurements on a Titan Krios G3 (Thermo Fisher) assembled with a K2 direct detector (Gatan) at 300 keV.

3.1.2.1 Data processing

After 2D classification in RELION to discard non-ribosomal particles, in total 115,082 particles were initially refined and subjected to the first round of 3D classification (fig. 3.2). Of the eight classes, half of them showed intact ribosomal particles, all predominantly in the pre-translocation state and programmed with tRNAs present in A- and P-sites. They all had ES27a fixed in the exit position without exception. These classes made up the majority of all particles (86%) and showed a fuzzy additional density close to the TE. After particle joining, a local classification using a binary soft mask covering ES27a as well as the region below the TE revealed one class with a well-defined ES27a and an additional globular non-ribosomal extra density that was assigned to Map1. These particles were subclassified further by applying a soft mask around the tip of ES27a and Map1. Two stable classes emerged from this step with almost the same amount of particles, showing the clear additional density for Map1 located between ES27a and the ribosome while adopting two different conformations. These final classes were CTF refined to an overall resolution of 3.9 Å or 3.8 Å for conformation 1 (Map1-80S-C1) or 2 (Map1-80S-C2) respectively. Local refinement of these maps with a mask on Map1 density did not improve the local resolution of Map1 in neither of the two conformations.

The average resolution for the two Map1 conformations is almost the same and indicating that the ribosome in both cases was refined to below 4 Å. Not surprisingly, the local resolution of Map1 bound to ES27 varies from 6.5 Å to beyond 12 Å, indicating a dynamic nature of Map1 when binding to the ribosome (fig. 3.3).

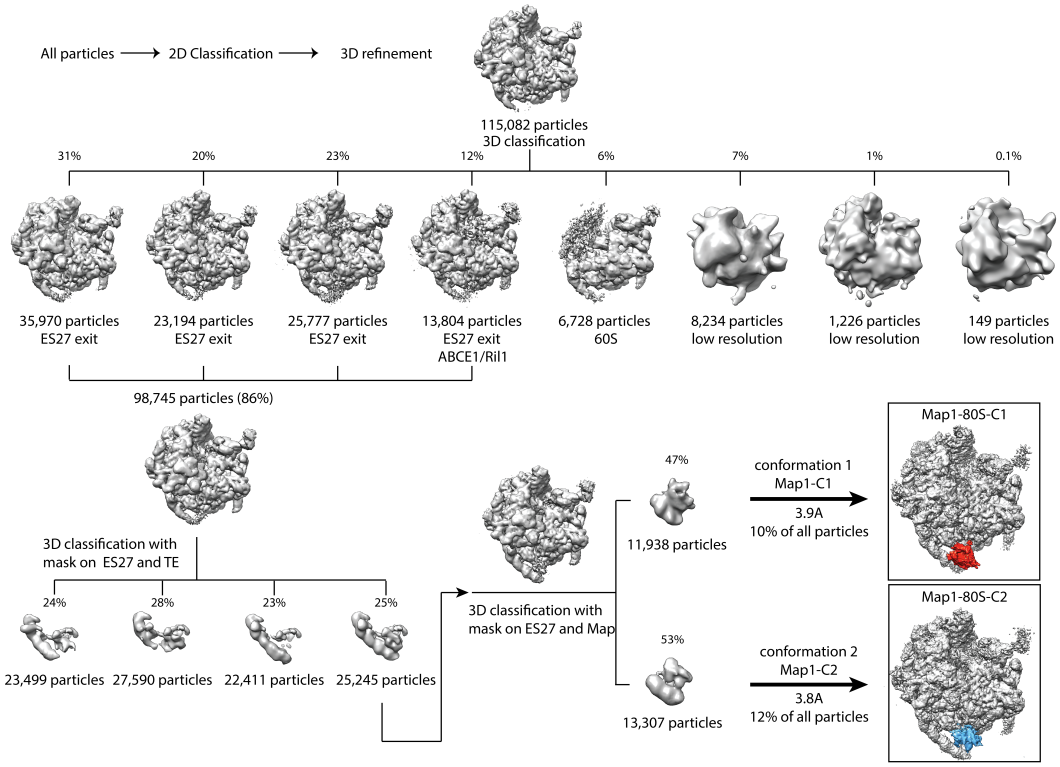

Figure 3.2: Classification scheme of the native Map1-ribosome complexes. Particles were picked with Gautomatch followed by RELION 2D classification to discard non-ribosomal particles. Subsequent refinement and 3D classification into eight classes resulted in four high resolution classes all showing ES27a explicitly in the exit position also accompanied with the most occupied classes. These classes, comprising 86% of all particles, were joined and subjected to a masked classification on ES27a and the region around the TE. One quarter of the particles formed a stable class with a defined ES27a and an additional density for Map1. This class was further subclassified applying a mask covering the tip of ES27a and the Map1 density. The resulting two stable classes showed Map1 in two conformations (red, blue), harboring 10% and 13% of all particles. Both classes were CTF refined to an overall resolution of 3.9 Å and 3.8 Å respectively. All maps are shown at the same contour level, percentages refer to the previous processing step.

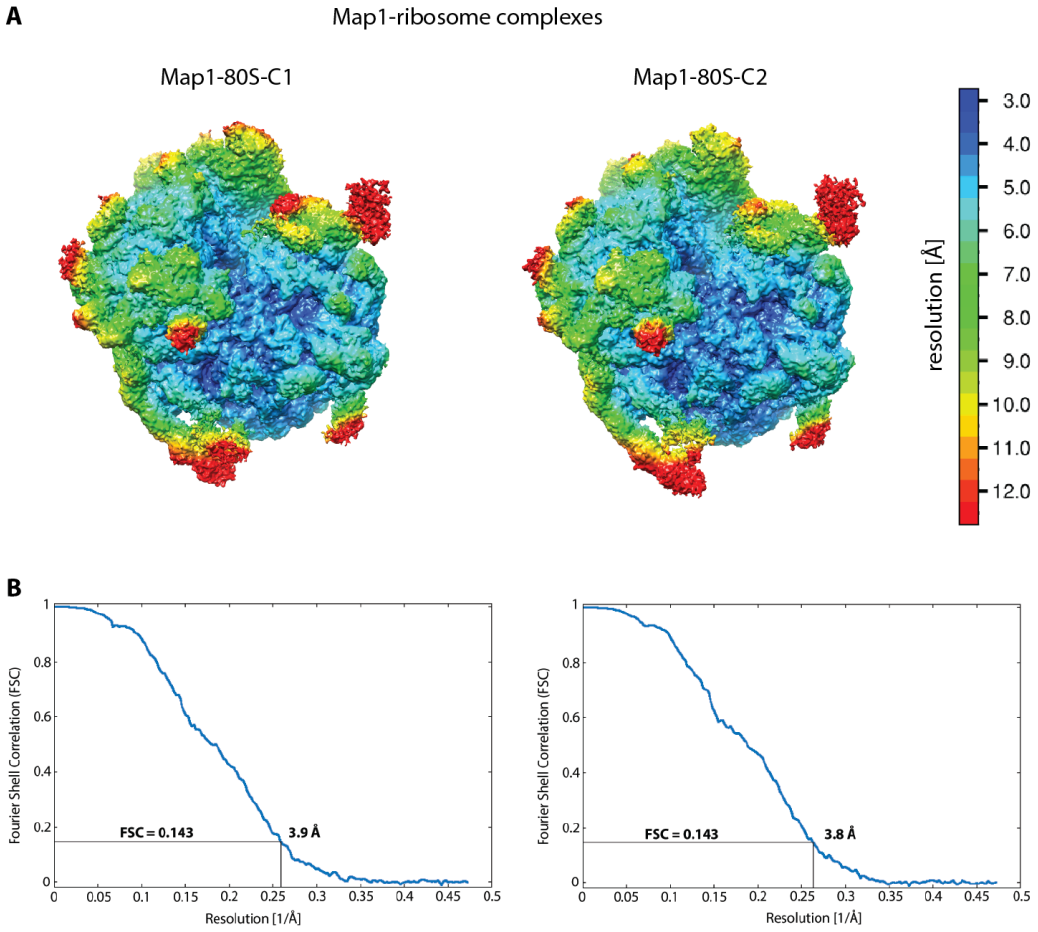

Figure 3.3: Local resolution and FSC curve of the two Map1 conformations obtained from Map1-ribosome complexes. A, Cryo-EM maps of 80S-Map1-C1 and 80S-Map1-C2 before post-processing and colored according to local resolution. The local resolution for Map1 varies from 6.5 to beyond 12 Å in both maps, indicating a high degree in flexibility. **B**, FSC curve of the maps displayed in A; the average resolution was calculated according to the gold standard.

3.1.2.2 Localization of Map1 on the 80S ribosome

Cryo-EM data processing of native Map1-TAP pull out allowed the overall positioning of Map1 on the yeast ribosome. Interestingly, the two conformations present (Map1-80S-C1 and Map1-80S-C2) shared the same binding sites at the ribosome, but to a different extent (fig. 3.4). In general, Map1 is positioned between the flexible expansion segment ES27a and the ribosomal TE, thereby contacting eL22 and the tip of the 18S rRNA helix H59 on the 60S SU (fig. 3.4A and B). A connection to the UAS1 (uL23 and uL29) is maintained only to a minor extent (fig. 3.4A, shown for Map1-C1). In addition, Map1 location was coupled with the position of ES27a. In more detail, ES27a was solely in the exit position, but adopting two sub-conformations. In Map1-C2 the tip of ES27a was placed below the TE, whereas it was moved backwards in Map1-C1 conformation (fig. 3.4B). As a consequence, Map1-C2 is located closer to the 60S SU but interferes with ES27a only on single contact sites (black arrows fig. 3.4A). In contrast, Map1-C1 has uninterrupted contact to ES27a with its bottom side and is located more centrally underneath the TE (fig. 3.4B).

In the absence of a yeast Map1 crystal structure, the sequence of Map1 was fed into MODELLER (Sali and Blundell, 1993). With this program a model was built based on the crystal structures of different human MetAPs. Notably, in the available structures the N-terminus could not be crystallized, leading to an model for *S. cerevisiae* where the first 80 N-terminal aa are lacking as well. Fitting of the obtained model into the electron density maps was guided by the structure of the ribosome-bound Map1 homolog ErbB3-binding protein 1 (Ebp1). Just like the already mentioned Arx1 (chap. 1.3.4), Ebp1 also contains the MetAP-like fold and was found in a similar position as Arx1 on the TE, interacting with ES27a as well (Wild et al., 2020; Wells et al., 2020; Greber et al., 2012). The very recently published human Ebp1-80S model was fitted into the Map1-80S density maps and superimposed with the Map1 homology model. For a final position, a rigid body fit of Map1 model into the separated densities was performed for each conformation. It is striking that in both Map1 conformations the model does not cover the whole electron density. Two extra densities (ED1 and ED2, fig. 3.4C) were observed. One protruding from ES27a to eL22 and H59 (ED1). The other one fuses directly with the emerging NC (ED2), but resolution is too low to assigned if the NC prolongs into the catalytic center of Map1 or ED2 extends into

the exit tunnel. Nevertheless, these extra densities might represent the missing zinc finger domains (around 80 aa) at Map1 N-terminus that are not present in the model but important for the proper functional alignment of Map1 on ribosomes (Vetro et al., 2002).

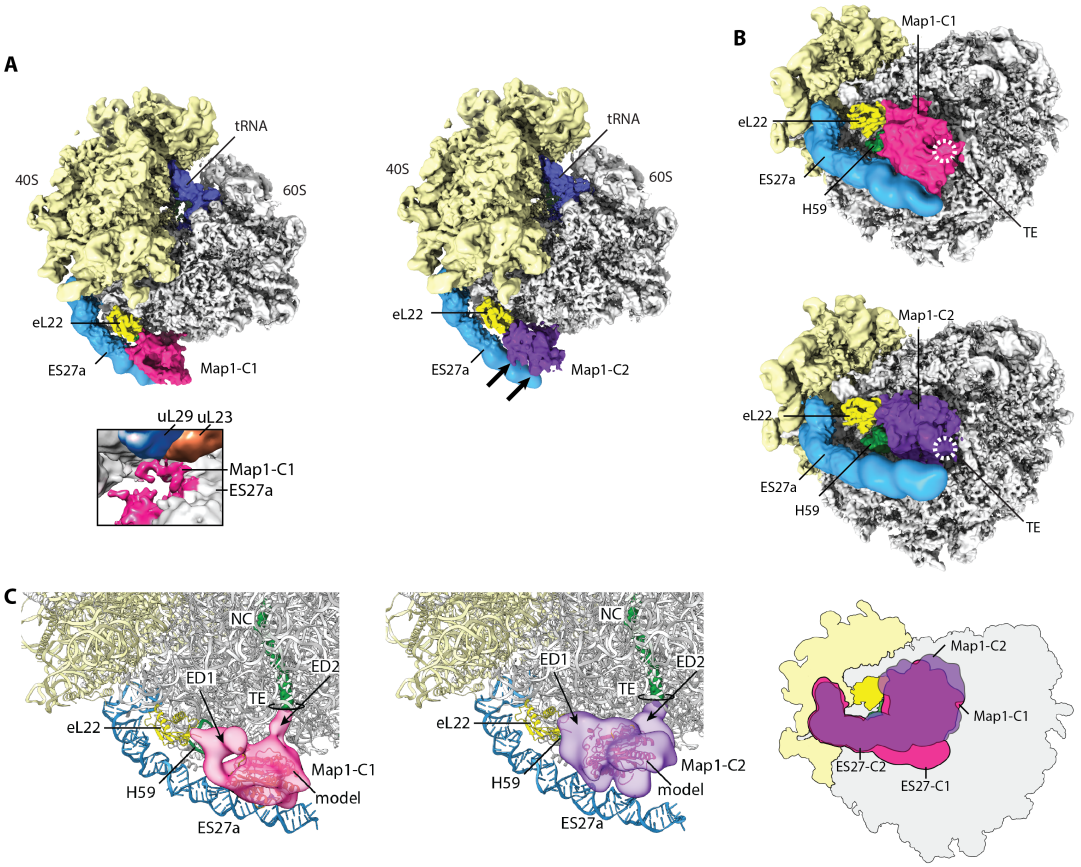

Figure 3.4: Cryo-EM structure of Map1-ribosome complexes. Cryo-EM structure of Map1 in complex with the 80S ribosome filtered according to local resolution. Isolated densities of Map1 in conformation 1 (Map1-80S-C1) or conformation 2 (Map1-80S-C2) were extracted after the final CTF refinement. **A**, Front view and **B**, bottom view on the peptide tunnel exit (TE, white dashed ring) as well as a schematic overlay of Map1-80S-C1 and Map1-80S-C2. Black arrows indicate the single contact sites of Map1-C2 to ES27a. **C**, Model of the 80S ribosome is shown in the front view with the isolated densities of the NC (green) as well as Map1-C1 (left) and Map1-C2 (right). A homology model (orange) for Map1, missing the first N-terminal 80 aa, was fitted into the Map1 density. Extra densities (ED1 and ED2) that were not covered by the Map1 model are indicated and may attribute for the N-terminal zinc-finger domains of Map1. ED1 fuses directly with the NC. Map1-C1: magenta, Map1-C2: purple, eL22: yellow, H59: green, 40S SU: light yellow, 60S SU: grey, tRNAs: dark blue, expansion segment ES27a: cyan, TE: tunnel exit. UAS1 shown in blue (uL29) and orange (uL23).

3.1.3 Contribution of ES27a in Map1-ribosome binding

3.1.3.1 Ribosomes without important expansion segments

The cryo-EM structure of Map1 bound to 80S ribosomes revealed a strong interaction of Map1 with the flexible ES27a. To verify this binding the contribution of expansion segments in ribosome binding should be analyzed. Expansion segments were suggested to play important roles in biogenesis (Greber et al., 2012; Bradatsch et al., 2012; Ramesh et al., 2016; Kater et al., 2017) or factor binding (Gomez Ramos et al., 2016; Beckmann et al., 2001; Knorr et al., 2019). Especially ES27 is essential in eukaryotic organisms. In fact, deletion of the entire ES27 is lethal and leads to defects in ribosome biogenesis (Sweeney et al., 1994; Jeeninga et al., 1997). Therefore, for a ribosome lacking ES27, a ES27 deletion strain could not be used. Instead, ESs need to be removed from fully functional ribosomes extracted from a healthy yeast strain. To that end, ribosomes were extracted from a ΔSki7 yeast strain and programmed with a NC comprising 64 aa of the ribosomal protein uL4 and a sequence coding for a CMV arrest peptide (termed uL4 ribosome nascent chain complexes, uL4-RNC, see chap. 2.1.1). At the N-terminus of the NC, a His- and HA-tag was inserted to monitor purification and to use it for detection respectively. A TEV protease step at the end cleaves the entire tag. To selectively remove ESs, uL4-RNCs were treated with RNase I (40U RNase I per 1 A_{260} unit of RNCs), an endoribonuclease that cleaves RNA strands. A cryo-EM structure of such RNAse I-treated RNCs (rtRNC) showed, that all ESs of the 40S (e.g. ES3, ES6) and the 60S (e.g. ES27a, ES39a, ES7a) as well as other protruding rRNA (h16 of the 40S or H76 connecting the L1 stalk of the 60S) were cleaved off (fig. 3.5A). Not affected were rRNA helices that are not extruding from the ribosome, such as H24 at the TE or H59 on the 60S SU, and ribosomal proteins stayed also intact as RNase I does not digests proteins.

In addition, digestion conditions were chosen in a way that RNCs still harbored an intact peptidyl-tRNA and therefore preserved the NC as tested by western blot analysis (fig. 3.5B). For that, uL4-RNCs that keep their tag were used in order to be detectable by α-HA, and were either directly used for western blot analysis or treated with RNase I first. The same intensity of the signal of the α-HA antibody detecting the peptidyl-tRNA in both samples shows that RNase I treatment only affects rRNA,

does not damage the peptidyl-tRNA and retains the NC.

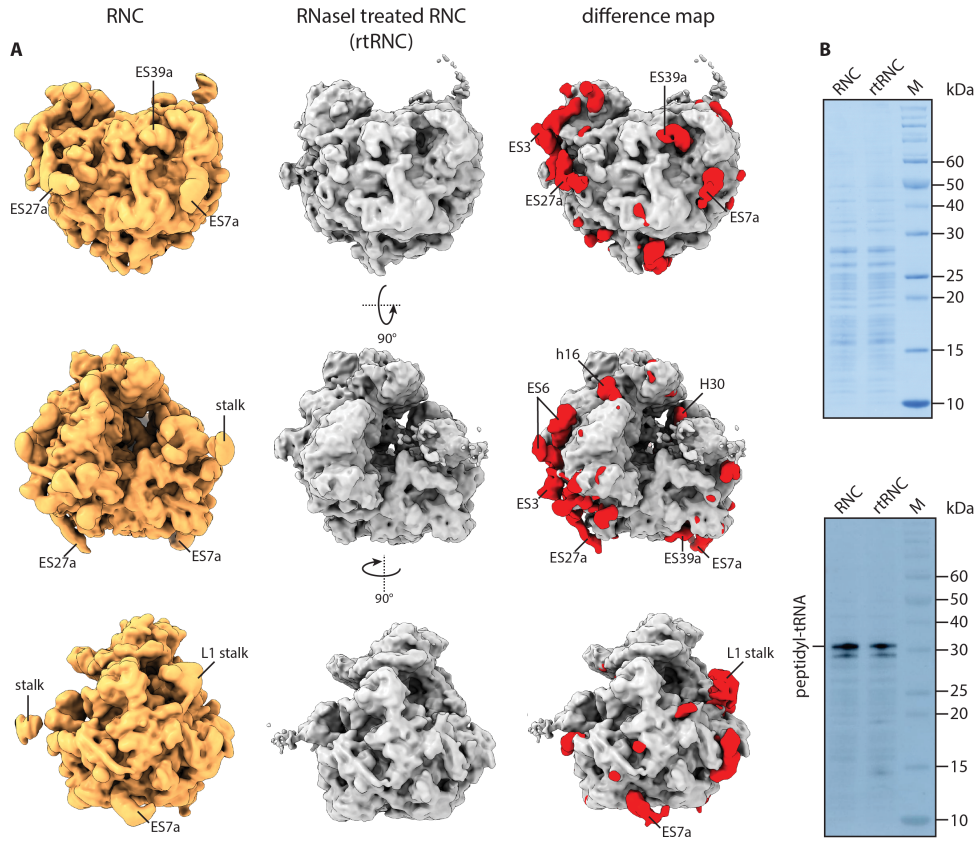

Figure 3.5: Cryo-EM structures and western blot of intact and RNase I-treated RNCs. **A**, Cryo-EM maps of untreated (RNC, orange) and RNase I-treated (rtRNC, gray) uL4-RNCs shown in the bottom, front and side view (row 1-3 respectively). Statistically significant differences between RNC and rtRNC are displayed in the right column as an overlay of a difference map between RNC and rtRNC (red) with the map of the rtRNCs (gray). Missing rRNA protrusions after the treatment are highlighted in red and comprise mainly expansion segments such as ES7a, ES27a and ES39a as well as the L1 stalk. Stalk, P1/P2 stalk. All maps were refined as three-times binned particles to a resolution of 6.7 Å, low-pass filtered to 8 Å and are shown at the same contour level (3.7σ). **B**, Amido black-stained PVDF membrane after the transfer of RNC and rtRNC separated on a 12% NuPAGE gel (top). Western blot of the same samples showing the signal of the α-HA antibody detecting peptidyl-tRNA (bottom). RNase I treatment does not affect the PTC and preserves the NC. An overlay of the membrane in A, with the antibody signal is shown.

3.1.3.2 Binding assays

Based on the results above, rtRNCs (RNase I-treated RNCs) were used to study the contribution of expansion segments in Map1-ribosome binding. rtRNC are lacking important ESs including ES27a, that was shown to be involved in Map1 binding to the ribosome (chap. 3.1.2.2). Therefore, binding assays were performed where recombinantly purified Map1 was incubated either with regular RNCs or rtRNCs (fig. 3.6). After pelleting these samples through a sucrose cushion, the presence of ribosomal bands as well as Map1 indicate binding. We could show that Map1 binds to regular RNCs in a stoichiometric manner (fig. 3.6, lane 4). However, the binding of Map1 to rtRNCs was not completely abolished, but decreased significantly compared to regular RNCs (fig. 3.6, lane 5). As the NC as well as proteins in general or H59 were not affected by RNaseI treatment (fig. 3.5A and B), this indicated a strong dependence of Map1 binding on the presence of ES27a.

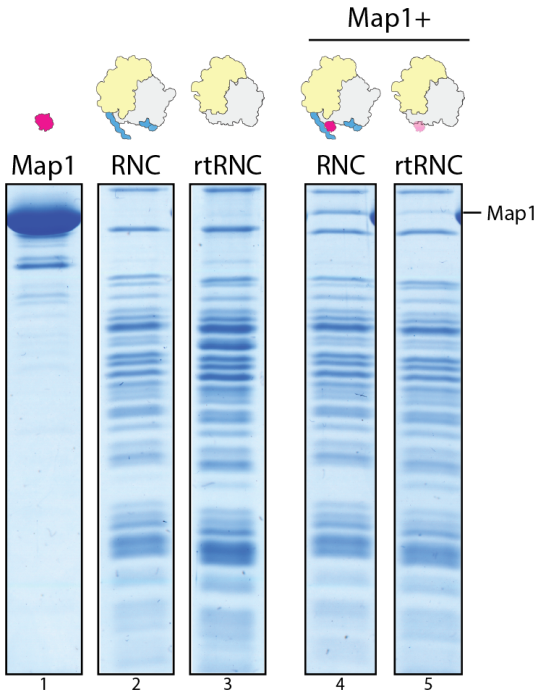

Figure 3.6: Contribution of ES27a to Map1-ribosome binding. 15% SDS-PAGE of recombinant Map1 (lane 1), uL4-RNCs (lane 2) and the same RNCs after RNaseI treatment (rtRNC, lane 3). Map1 co-sediments with RNC upon binding (lane 4). A significant decrease in binding was observed upon removal of expansion segments by RNaseI treatment (lane 5). For Map1 alone the supernatant (SN) fraction and for all other samples the pellet (P) fraction was loaded. For uncropped gel see appendix p. 133.

3.2 NatA in complex with the 80S ribosome

NatA is the most common and best characterized member of the NAT family and has the highest percentage of N-acetylated substrates. Thus, the aim was to obtain a cryo-EM structure of NatA bound to the ribosome. This was achieved by two approaches: native pull out and *in vitro* reconstitution.

For the native pull out a *S. cerevisiae* strain harboring a TAP-tagged Naa15 was used to purify endogenous NatA-ribosome complexes directly from cell lysates. For the *in vitro* approach ribosome nascent chain complexes (RNC) programmed with a defined substrate for NatA (ABP1) were reconstituted with recombinantly purified NatA complexes. In both cases, samples were subjected to cryo-EM and SPA. The obtained structures were subsequently biochemically verified using *in vitro* binding assays.

3.2.1 Purification of native NatA-ribosome complexes

To study NatA-ribosome interactions, the ribosome binding SU Naa15 was tagged in yeast with a C-terminal TAP-tag (Euroscarf). Purification of intact NatA-ribosome complexes was obtained by an adjusted protocol based on a rapid affinity-purification for ribonucleoprotein complexes as described and executed already before (Oeffinger et al., 2007 and chap 3.1.1). Again, the Protein A domain of the TAP-tag was bound to IgG coupled magnetic beads, resulting in ribosomes co-purifying with NatA complex after the elution with TEV protease. Subsequent analysis of the sample by a linear sucrose gradient centrifugation revealed a predominant portion of polyribosomes in the elution (fig. 3.7A). The presence of polyribosomes was confirmed by screening the sample on a Tecnai SPIRIT 120 keV microscope (Thermo Fisher), showing ribosomes organized in groups rather than being present as single 80S monosomes on the micrographs (fig. 3.7A). Furthermore, the NatA complex seemed to dissociate from the ribosomes upon gradient ultracentrifugation as determined by western blotting (data not shown). Moreover, NatA seemed not to be associated with every monosome or ribosome within a polyribosome group. As ribosomes without a bound NatA are also part of a polysome bundle, non-occupied ribosomes are eluted as well and therefore decreasing the occupancy with NatA as indicated by an initial cryo-EM measurement (data not shown). Nevertheless, NatA was initially bound to ribosomes and forming

a stable complex as NatA-ribosome complexes could be purified by a native pull out on Naa15.

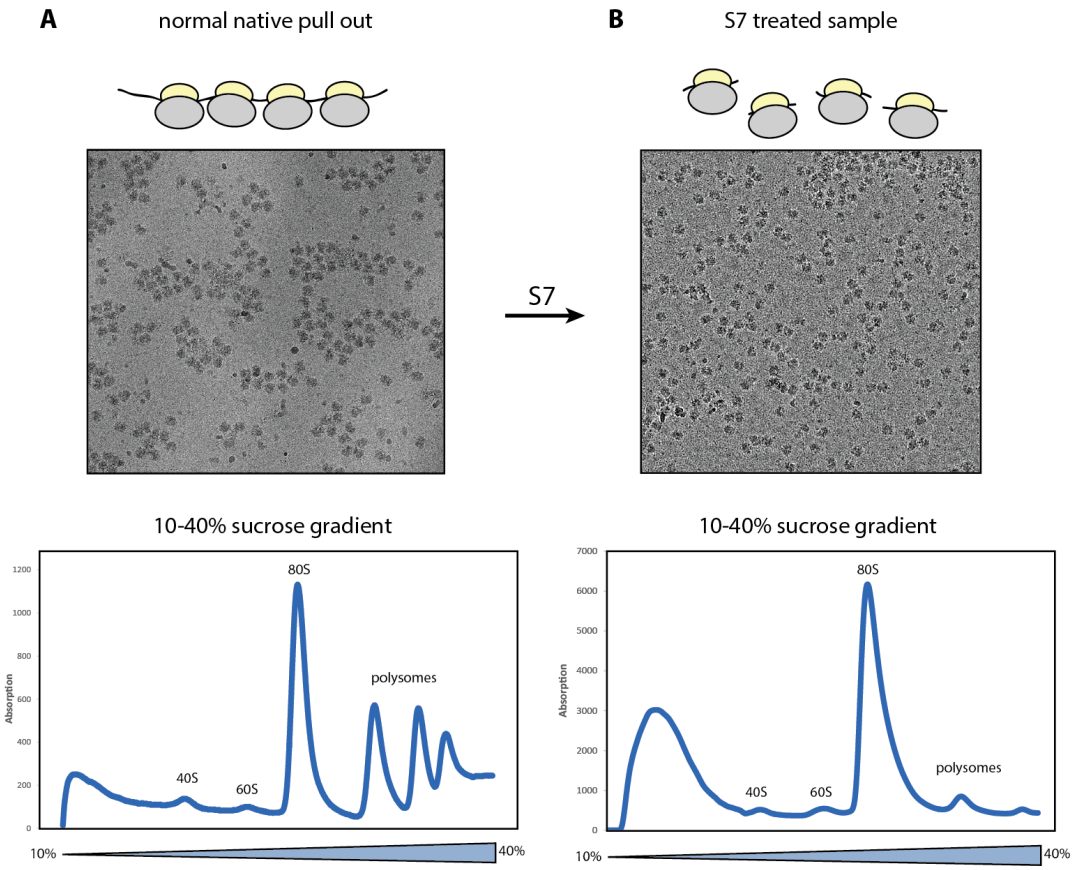

Figure 3.7: Micrographs and linear sucrose gradient profile showing the effect of S7 cleavage. Elution of the native pull out using TAP-tagged Naa15 showing purified ribosome-NatA complexes in a regular purification (**A**) and with additional S7 treatment (**B**). Micrographs from a low resolution Tecnai SPIRIT 120 keV microscope screening microscope (Thermo Fisher) as well as linear sucrose gradient centrifugation revealed a huge fraction of polyribosomes after the regular TAP-tag purification. The additional S7 cleavage included in the purification process cleaves the mRNA and leads to a monosomal fraction. This indicates an increased ratio between 80S monosome peak and polysome fractions in the sucrose gradient as well as single particles rather than groups of ribosomes visible on the micrographs.

To overcome the occupancy problem, an additional step was included during purification. A mild treatment with a nuclease should convert polyribosomes into monosomes without the need of a gradient centrifugation. Therefore, after initial incubation of the sample with magnetic beads and washing steps, a mild digestion with S7 nuclease directly on the beads was performed. S7 cleaves single stranded RNA

and therefore cuts apart polysomes connected via their mRNA (fig. 3.7B). In the flow through, after S7 cleavage, western blot analysis showed the presence of a signal only for a ribosomal protein, but not for Naa15-TAP (fig. 3.8A, B), confirming that non-NatA bound ribosomes were removed from the sample. The final TEV cleavage step resulted in co-elution of Naa15 (still carrying the CaMBD) with the other two NatA subunits (Naa10 and Naa50) and ribosomal proteins. This process was monitored by a mass shift of the band corresponding to Naa15 in the western blot using α-CAB (fig. 3.8A and B) and the identity of the proteins was confirmed by mass spectrometry (Thomas Fröhlich, LMU Munich) (fig. 3.8C). This is indicative of a successful purification of a complete and intact NatA-ribosome complex. Finally, the elution fraction was adjusted to 5 A_{260}/ml subjected to cryo-EM analysis.

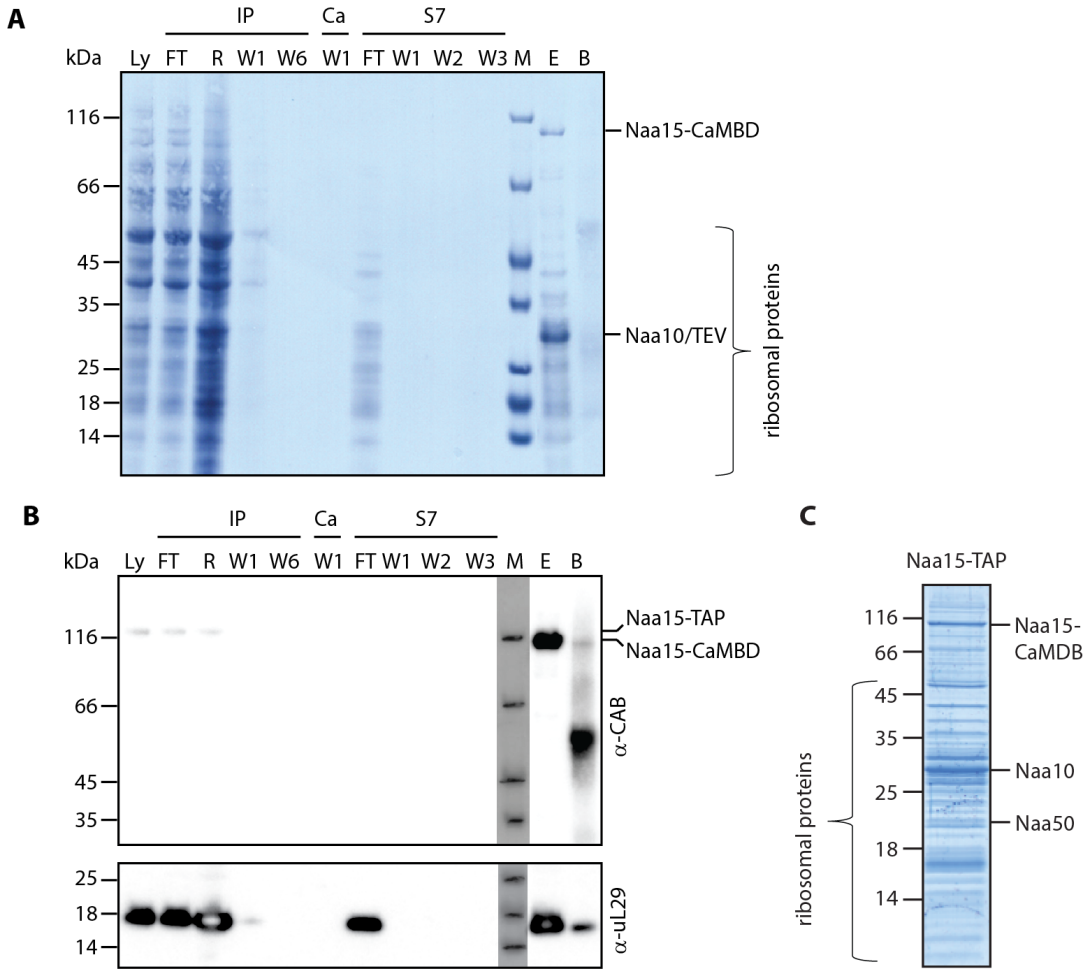

Figure 3.8: Affinity purification of native NatA-ribosome complexes. SDS-PAGE and western blot of the NatA-ribosome purification. **A**, Amido black-stained PVDF membrane after transfer from a 4-12% Nu-PAGE gel with aliquots from each purification step. **B**, Western blot probed with α-CAB against the ribosomal protein uL29. S7 nuclease treatment cleaves polyribosomes into monosomes and therefore (poly)ribosomes not associated with NatA complex get washed away. **C**, 15% SDS-PAGE of the final elution of purified NatA-ribosome complexes. Ly, lysate; FT, flow through; R, resuspension; W, wash; E, elution; B, boild beadsM IP, regular pull out samples; Ca, Ca^{2+} wash step to prepare for S7 cleavage; S7, S7 nuclease cleavage. 0.1 $A_{260_{total}}$ of the E was loaded, for Ly and FT 1/40,000 and for wash fractions 1/7 of the volume was loaded on the gel.

3.2.2 Cryo-EM structure of the native NatA-ribosome complex

In order to obtain a cryo-EM structure of NatA bound to the ribosome, a freshly prepared sample of the Naa15-TAP pull out was used at a concentration of 5 A_{260}/ml and applied to holey carbon support grids. Data were collected on a Titan Krios TEM (Thermo Fisher) equipped with a Falcon II direct detector at 300 keV.

3.2.2.1 Data processing

In total 262,507 particles remaining after 2D classification were initially refined and subjected to an initial 3D classification (fig. 3.9). In this first round, all classes displayed programmed ribosomes and showed expansion segment 27a (ES27a) either in its exit or L1 position. The most occupied classes in this data set had ES27a in the exit position and showed an additional density below the TE which was absent in the classes with ES27a in its L1 position. These classes were joined and subjected to further sorting on tRNA states. The majority of the classes were in the pre-translocation state, programmed with tRNAs in A- and P- site as well as eIF5A in the E-site (Schmidt et al., 2016a). The classes with the same A/A- and P/P-tRNA state were merged, followed by local classification applying a soft mask on the additional density at the TE. Two of the three classes showed only fragmented density for NatA revealing a rather flexible nature of the ribosome-NatA interaction. The most stable class, however, displayed a map with high occupancy of NatA and could not be sub-classified further. This final class, comprising 10% of all particles, was refined to an overall resolution of 3.4 Å, showing a well resolved ribosome but the local resolution for NatA ranged from 8 Å to beyond 12 Å (fig. 3.10A). This indicates once more the flexible nature of NatA on the ribosome. In order to improve the local resolution of NatA, a local refinement focusing on the NatA density only was performed. The overall resolution dropped to 4.8 Å and the ribosome resolution got worse, but the resolution of NatA itself improved to an average of 8 Å (fig. 3.10B). This made it possible to rigid body fit the crystals structure of the *S. cerevisiae* NatA including all three subunits (Naa10, Naa15 and Naa50; pdb 4XNH) into the density and with some minor adjustments a pseudo-atomic model of the ribosome-bound NatA complex was generated. Notably, the first 16 aa at Naa15 N-terminus are missing in the model (even less than in the crystal-structure) and are also not visible in the electron

density.

Furthermore, as ribosomes are programmed with A/A- and P/P-tRNAs and harboring eIF5A at the E-site (Schmidt et al., 2016b), this indicates that only translating ribosomes were associated with the NatA complex. This is supported by the fact, that only a very small portion of non-programmed ribosomes (0.4% of all 262,507 particles) are present in this data set.

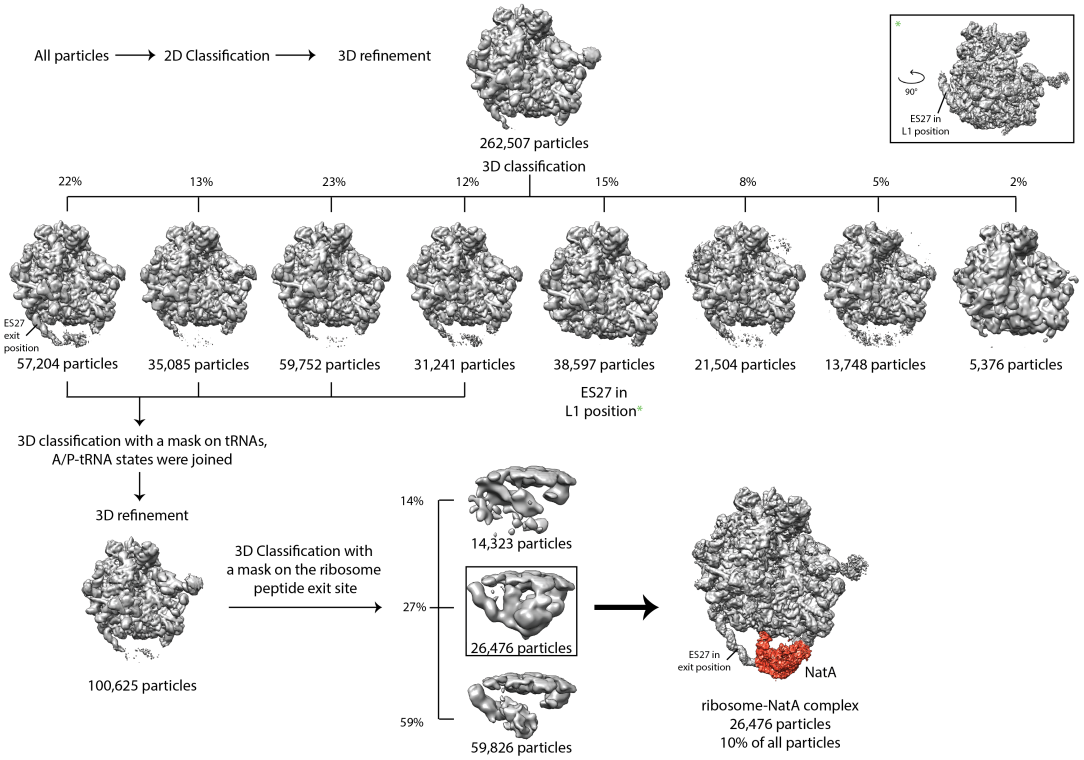

Figure 3.9: Classification scheme of the native NatA-ribosome complex. Particles were picked with Gautomatch and Relion 2D classification was used to discard non-ribosomal particles. Subsequent refinement and 3D classification into eight classes revealed ES27a in most of the classes in the exit position showing an additional density below the tunnel exit. Most prominent classes encompassing 70% of all particles, were joined and subjected to a masked classification on tRNAs. Particles containing tRNAs in the A/A- and P/P-site were merged (100,625 particles) and used for further local classification with a mask covering the exit region. Around one third of the particles formed a stable class with an additional density at the exit region representing NatA. This class, containing 10% of all particles from the beginning and was refined to an average resolution of 3.4 Å. All maps are shown at the same contour level.

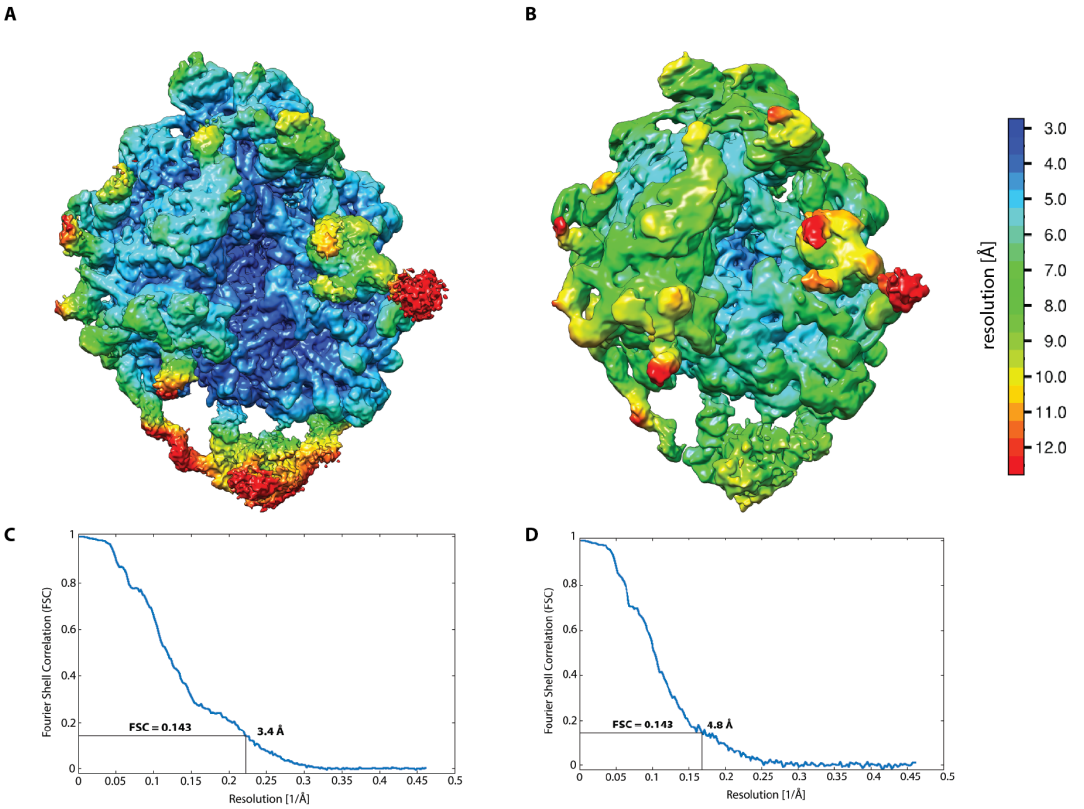

Figure 3.10: Local resolution and FSC curve of the NatA-ribosome complexes. The final map of the NatA-ribosome complex (fig. 3.9) was further improved by a focused refinement on NatA region. Maps after regular refinement (**A**) and masked refinement on NatA (**B**) are colored according to their local resolution. The overall resolution for the ribosome is below 4 Å, whereas NatA displays a higher degree of flexibility illustrated by a local resolution range of 7 to beyond 12 Å. After focused refinement the average resolution of the ribosome decreased to 4.8 Å but local resolution of NatA improved to an average of 8 Å. **C, D,** FSC curve of the maps displayed in A and B respectively.

3.2.2.2 Contacts sites of NatA to the ribosome

Cryo-EM analysis of a native Naa15-TAP pull out revealed that the trimeric NatA complex is positioned below and close to the ribosomal TE, exhibiting a similar architecture as the free NatA in a crystal structure (pdb 4XNH). In agreement with previously published biochemical data (Gautschi et al., 2003), Naa15 functions as the ribosome anchoring SU. It locates the catalytic SU underneath the TE whereby Naa10 itself does not contact the ribosome directly. The structure revealed the so far unknown function of Naa50 in yeast as being a second ribosome binding subunit contributing to the NatA-ribosome interaction (fig. 3.11).

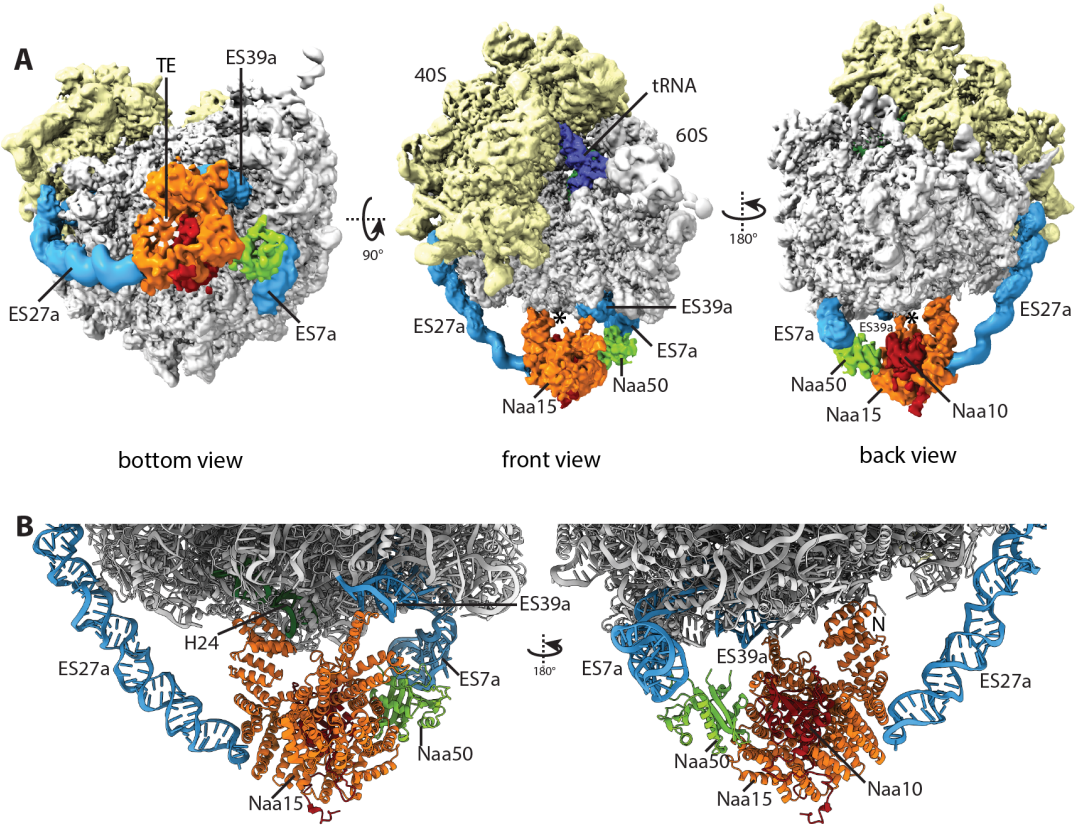

Figure 3.11: Cryo-EM structure and model of the NatA-ribosome complex. **A**, Cryo-EM structure of NatA in complex with a translating ribosome filtered according to local resolution. Isolated densities for NatA were extracted after focused refinement (Naa15: orange, Naa10: red, Naa50: green). Views are shown onto the peptide tunnel exit (TE, white dashed ring or black asterisk) (bottom view), rotated 90° horizontally (front view) and rotated 180° vertically (back view). 40S and 60S ribosomal SU are labelled in yellow or grey respectively, rRNA expansion segments (ES) are shown in cyan. **B**, Magnified view of the NatA-ribosome complex molecular model shown as in A, as front and back view.

In total, NatA maintains four contact sites with the ribosome, all of which contain rRNA. The first involves the interaction of Naa15 with H24 and H47 of the 28S rRNA (fig. 3.12A). Remarkably, in all other three contact sites eukaryotic specific rRNA expansion segments (ES) are involved. Naa15 interacts additionally with ES27a and ES39a, whereas Naa50 binds to ES7a (fig. 3.12B-D).

In more detail, the N-terminus of Naa15, specifically α2 of TPR1, contains five lysines (K37, 38, 41, 48, 49; fig. 3.12A) building electrostatic interactions with a pocket formed by H24 and H47. Ribosomal proteins uL22 and eL31 are in close proximity but no contacts to NatA were determined in the density map. The second interaction of Naa15 is accomplished on the tip of ES27a with involvement of α10 of TPR5 and α11 of TPR6, most likely by recognizing the minor groove and CUUG tetraloop of ES27a respectively (fig. 3.12B). The very flexible ES27a is usually observed at a very low resolution in structures. Here, ES27a is well-resolved completely until the tip as it gets stabilized by NatA binding. The third interaction of Naa15 is established at the shorter expansion segment ES39a. A previously characterized basic helix (α33) in *S. pombe* Naa15 has been shown to play a crucial role in ribosome binding (Magin et al., 2017). The *S. cerevisiae* equivalent harbors the same patch of lysines (K648-650; K652-653) interacting with rRNA helices H98 and H100 (C3154-U3157) and the major groove of H98-ES39a (fig. 3.12C). The fourth contact of NatA to the ribosome is exhibited by Naa50. The latter contacts TPRs 8 and 9 of Naa15 and bridges over to expansion segment ES7a (fig 3.12D) and therefore functions as a second ribosome binding subunit of the NatA complex. As this subunit has the lowest resolution among the three SU, its binding mode cannot be characterized in full detail, but the contact site may involve G450, G451 and G474 of ES7a and Ala83, Asn84 (within loop 2, fig. 3.12D) and His125 (within loop 1, fig. 3.12D) of Naa50, respectively.

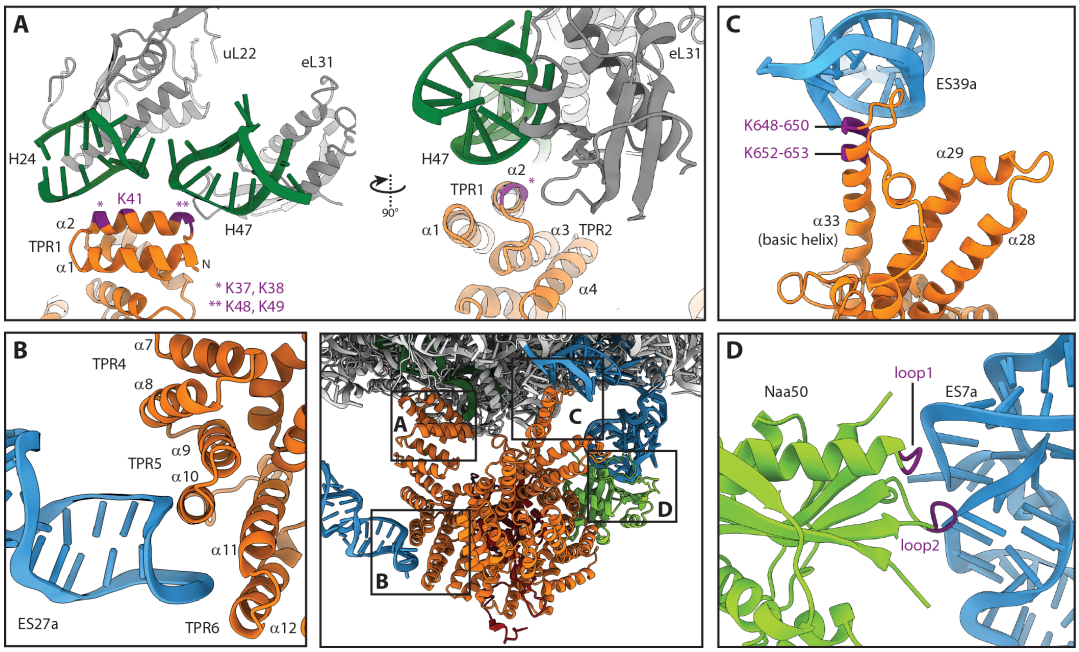

Figure 3.12: Molecular contact sites between NatA and the ribosome. Central panel as in fig. 3.11B (left) with contact sites indicated. Interactions of Naa15 N-terminus with H24 and H47 of 28S rRNA (**A**), Naa15 TPR5 and TPR6 with ES27a (**B**), basic helix (α33) of Naa15 with ES39a (**C**) and loop1 (aa 122-125) and loop2 (aa 81-84) of Naa50 with ES7a (**D**) are displayed. Lysines in A, and C, that were shown to contribute in binding are depicted in magenta (Magin et al., 2017).

In addition, two of the anchor points have also been described biochemically in co-sedimentation assays (Magin et al., 2017). Reverse charge mutations of lysines in both the Naa15 N-terminus and the already mentioned basic helix (α33) (Magin et al., 2017; Varland and Arnesen, 2018) showed a significant decrease in binding but did not abolish it completely. This can be now explained as interactions of Naa15 with H24, H47 and ES39a get disrupted, but the two additional binding sites to ES27a and ES7a still support binding of NatA to the ribosome.

A zoom into the contact sites of NatA-ribosome interaction with models fitted into the electron density as well as NatA model fitted into isolated densities are shown separately (fig. 3.13).

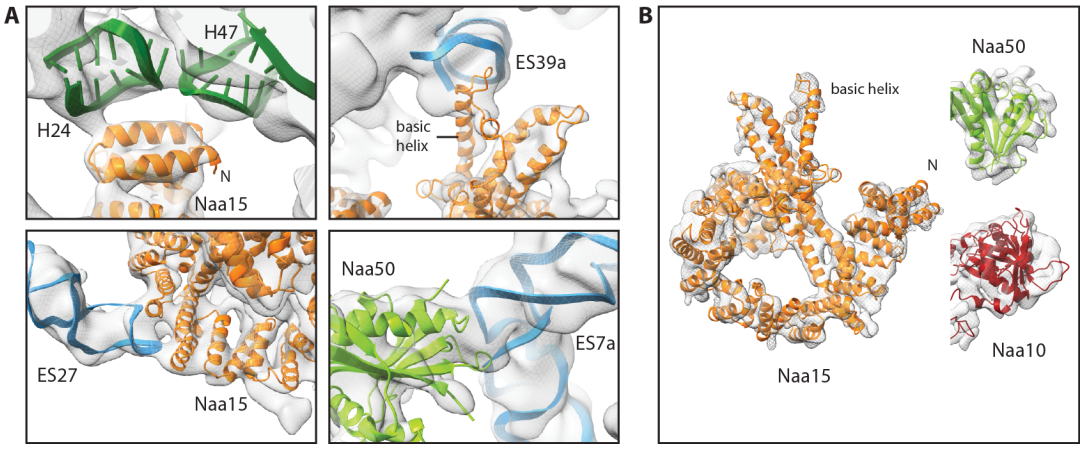

Figure 3.13: Fitting of NatA subunits into cryo-EM map and zoom into contact sites. A, Molecular contact sites displayed in similar views as shown in fig. R6 with models fitted into the electron density. **B**, Isolated densities of NatA shown after focused refinement on NatA with the model of NatA SUs fitted into the electron density.

3.2.2.3 Contribution of expansion segments to the ribosome-NatA interaction

Structural studies on the NatA-ribosome complex revealed surprisingly that only rRNA is involved in NatA binding. Two out of the four contact sites were already described biochemically to be important for NatA interaction with the ribosome (fig. 3.12A and C; Magin et al., 2017). In addition, three binding sites involved the eukaryotic expansion segments ES27a, ES7a and ES39a. To further confirm the contribution of these ES in ribosome-NatA interaction, *in vitro* binding assays were performed. First, recombinantly purified and catalytically inactive trimeric NatA complex (Naa10 (E26A); Liszczak et al., 2013) was incubated with ribosome nascent chain complexes (RNCs) carrying 64 aa of a well-characterized NatA substrate, the uL4 ribosomal protein, as nascent peptide (Gautschi et al., 2003). In addition, a C-terminal ribosome stalling sequence from upstream ORF of *gp48* in human cytomegalovirus (CMV) was used to obtain homogenously stalled RNCs (Bhushan et al., 2010; Matheisl et al., 2015). Second, RNCs lacking important ES (rtRNC), such as ES27a, ES7a and ES39a, were generated by a mild digestion of uL4-RNCs with RNase I that selectively cleaved off protruding rRNA as described in more detail in chap. 3.1.3.1. Digestion conditions were chosen in the way that RNCs still keeping an intact peptidyl-tRNA bond and therefore preserve the NC (chap 3.1.3.1).

Both, untreated and rtRNCs were used in binding studies with recombinant NatA in

near physiological buffer conditions (fig. 3.14A, lane 1-3). Since Naa15 SU is the best detectable band on a coomassie-stained gel, its intensity was read out by using ImageJ to examine NatA binding.

NatA binds to regular RNCs in a stoichiometric manner (fig. 3.14A, lane 4 and B upper part). However, RNase I treatment and the accompanied loss of important ES around the peptide exit region reduced NatA binding to these rtRNCs by about 80% (fig. 3.14C and B lower panel). This clearly indicated that expansion segments ES27a, ES7a and ES39a make a significant contribution to NatA-ribosome interaction. The remaining 20% of binding are likely due to the interaction of NatA with H24 and H47 that are still intact after RNase I treatment.

In conclusion, the biochemical data obtained from *in vitro* experiments largely confirmed the native NatA-ribosome structure, which showed NatA mainly anchored to the ribosome to ES. Hence, attributing a new role of ES in coordinating nascent chain modifying factors below the peptide exit tunnel.

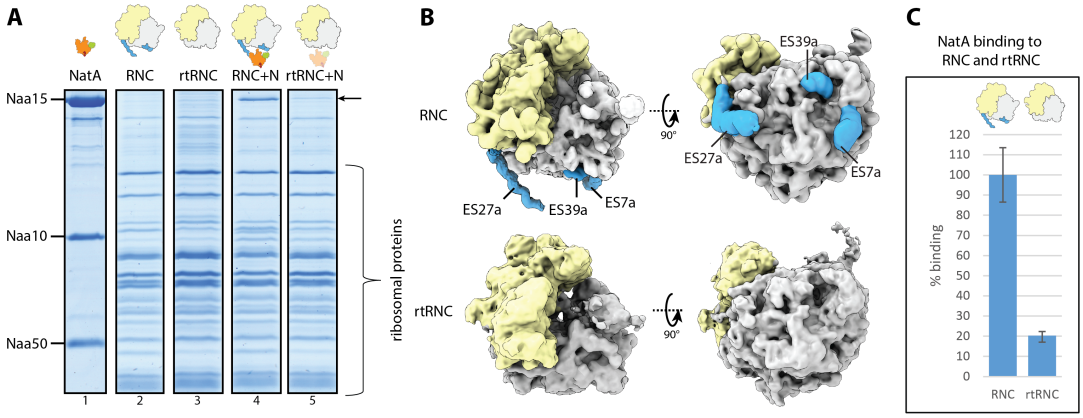

Figure 3.14: Contribution of ES27a, ES7a and ES39a to NatA-ribosome binding. A, 15% SDS-PAGE of recombinant trimeric NatA complex (lane 1), RNCs programmed with uL4 NC (lane 2) and the same RNCs after RNase I treatment (rtRNC, lane 3). Pellet fraction of NatA incubated with regular RNCs (lane 4) and with rtRNC (lane 5). **B**, Cryo-EM densities of purified uL4-RNCs (top, RNC) and the same RNCs with RNase I treatment (bottom, rtRNC). Eukaryotic specific expansion segments (ES) are labelled in cyan. **C**, Quantification of the binding situation with $N = 4$ independent samples for both RNCs and rtRNCs. Error bars were calculated using the standard deviation from the mean. For source data and full gels see appendix (p. 134).

3.2.3 Cryo-EM structure of the *in vitro* reconstituted NatA-ABP1-RNC complex

The structure obtained from the native ribosome-NatA pull out showed a clear binding of NatA to the ribosome via four contact sites. Nevertheless, NatA binds in a highly dynamic way especially because of its interaction with the flexible expansion segment ES27a. This flexibility may be explained by the fact that in native pull outs ribosomes are programmed with a variety of NCs, likely representing a mixture of various NatA substrates. Therefore, NatA may adopt many slightly different conformations below the TE to adjust its position for efficient acetylation and change its position dependent on the NC length and chemical property.

In order to improve the rigidity of the NatA-ribosome structure, a homogeneous population of RNCs carrying the same NC with a defined length was used. These RNCS were then used for *in vitro* reconstitutions with recombinant NatA as described before (chap. 2.3). As a substrate, the first 88 aa of actin binding protein 1 (ABP1) were chosen. The choice was based on yet unpublished selective ribosome profiling data analyzing NatA's proteome-wide binding sites in collaboration with the Bukau lab in Heidelberg. ABP1-RNCs were generated using truncated mRNA instead of mRNA coding for the CMV arrest peptide. *In vitro* reconstitution of NatA with ABP1-RNCs were performed at the same conditions as used in binding assays and subjected to cryo-EM analysis on a Titan Krios TEM (Thermo Fisher) equipped with a Falcon II direct detector at 300 keV.

3.2.3.1 Data processing

293,373 particles were used for an initial refinement after 2D classification and removal of non-ribosomal particles (fig. 3.15). Subsequent 3D classification into six classes revealed two highly occupied classes with either ES27a nearly completely in the L1 position or exclusively in the exit position, both showing tRNA in the P/P state. The class with ES27a in the exit position also comprised an additional well shaped density at the exit region for NatA. This class was subclassified by applying a soft mask on the exit region leading to one stable class (16,274 particles, 5.5% of all particles) showing an extra density located below the TE as observed in the native pull

out ('IP-like'). The other classes either showed no NatA or only fragmented density below the TE. Subsequent signal subtraction of the 40S SU of the IP-like class and a refinement running it only with local searches lead to an overall resolution of 3.7 Å after CTF refinement. In order to analyze if using a defined substrate instead of having a large mixture as present in the native sample led to a substantial gain in rigidity of the complex, local resolutions were calculated in RELION. Yet, local resolution distribution appeared similar to the one obtained for 'native' NatA (fig. 3.16, fig. 3.10), indicating that even with a single substrate NatA is still rather flexibly bound to the 60S subunit.

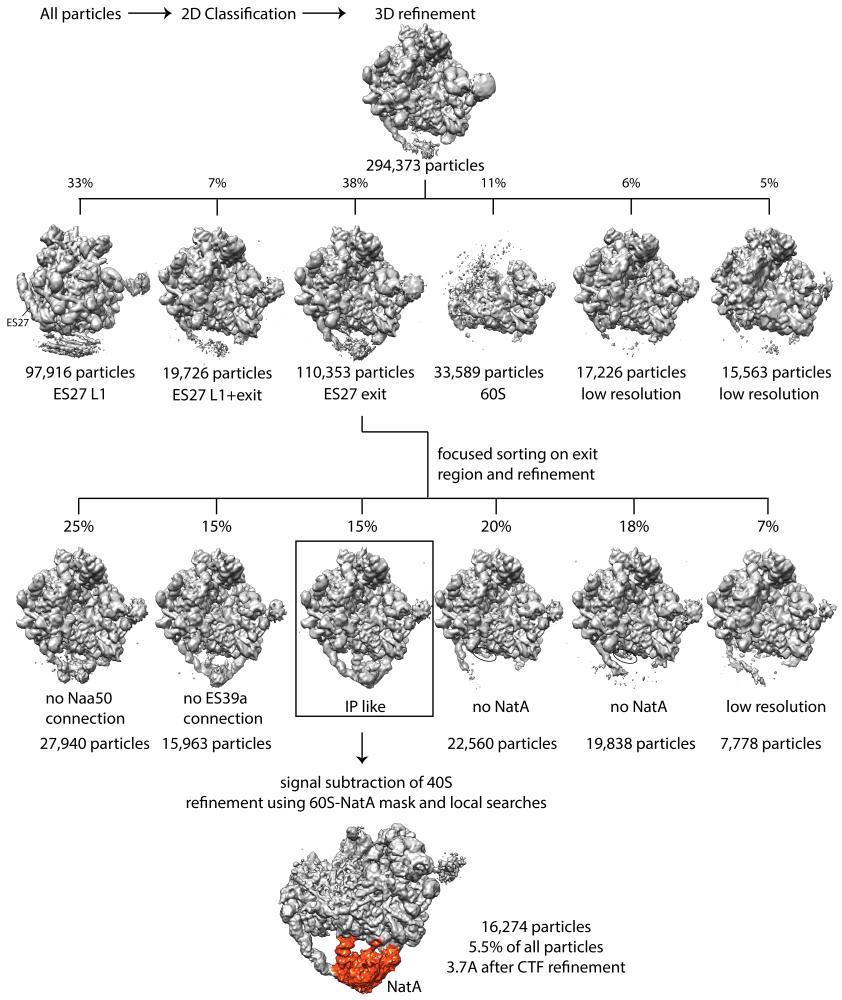

Figure 3.15: Classification scheme of NatA *in vitro* reconstituted with ABP1-RNCs. Particles were picked with Gautomatch and Relion 2D classification was used to discard non-ribosomal particles. Subsequent refinement and 3D classification into six classes revealed one class with ES27a in the exit position and a good shaped density below the TE for NatA (110,353 particles). This class was subjected to a masked 3D classification on the exit region, leading to a class showing NatA in the exact same position and conformation as observed in the native pull out (chap. 3.2.2). This map ('IP-like'), comprising 16,274 particles that corresponds to 5.5% of all particles after 2D classification, was used for a subsequent signal subtraction of the 40S subunit as well as a local refinement on the NatA region resulting in an overall resolution of 3.7 Å after CTF refinement. ES27 L1, in L1 position; ES27 exit, in exit position; IP like, same conformation as native pull out received by immunoprecipitation (chap 3.2.2).

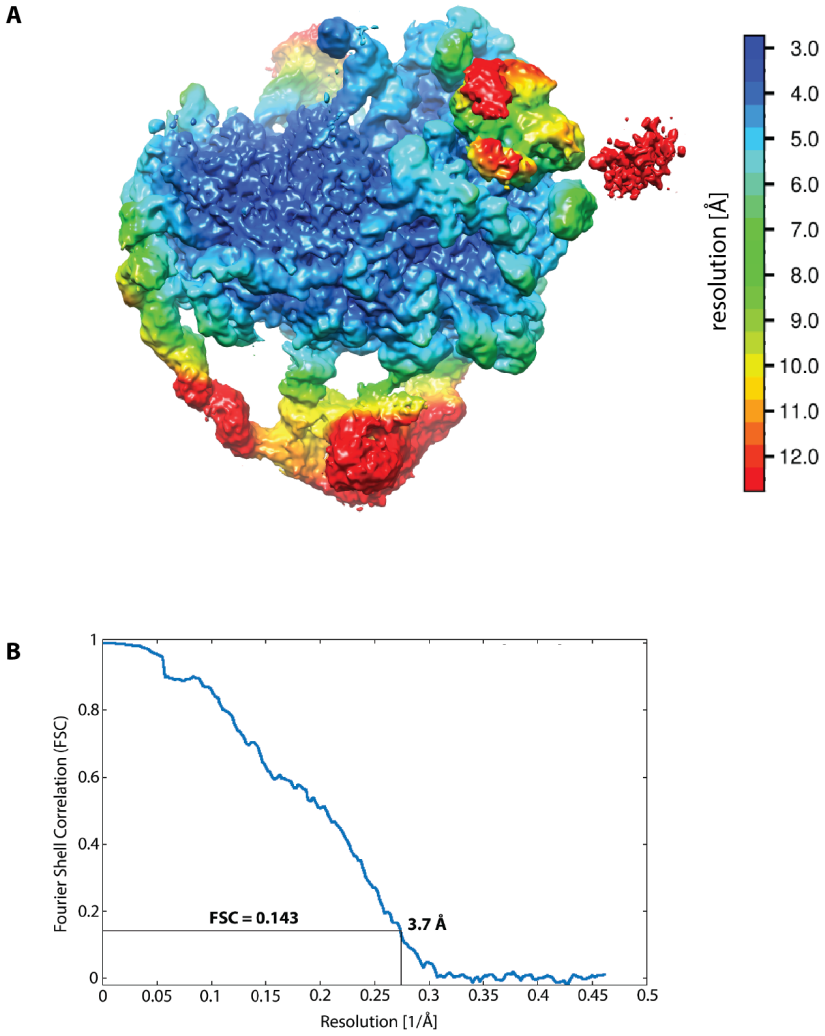

Figure 3.16: Local resolution and FSC curve of ABP1-RNC-NatA complexes. **A**, Local resolution of the final map of the ABP1-RNC-NatA complex after signal subtraction of the 40S SU in RELION and CTF refinement (fig 3.15. R10). The overall resolution of the core ribosome is below 4 Å, whereas NatA shows as before a higher degree of flexibility displayed by a local resolution range from 5 to above 12 Å. **B**, FSC curve of the maps shown in A. Resolution was calculated according to the gold standard.

3.2.3.2 Additional contact sites of NatA

The binding sites for NatA to the ribosome observed from native pull out data showed the positioning of NatA below the TE while interacting with three ESs (ES27a, ES7a and ES39a) as well as H24 at the TE. To counteract the broad mixture of NCs present in native pull outs, with ABP1-RNCs a defined substrate for NatA was provided and used for *in vitro* reconstitution and cryo-EM studies. Notably, the binding sites of NatA when bound to ABP1-RNCs are exactly the same as observed for the native structure. In addition, fitting the model of NatA obtained from the pull out into NatA density in ABP1-RNCs did not reveal any differences in the SU conformations (fig. 3.17). Therefore, the *in vitro* conditions reflect perfectly the native situation and conformation of NatA on the ribosome.

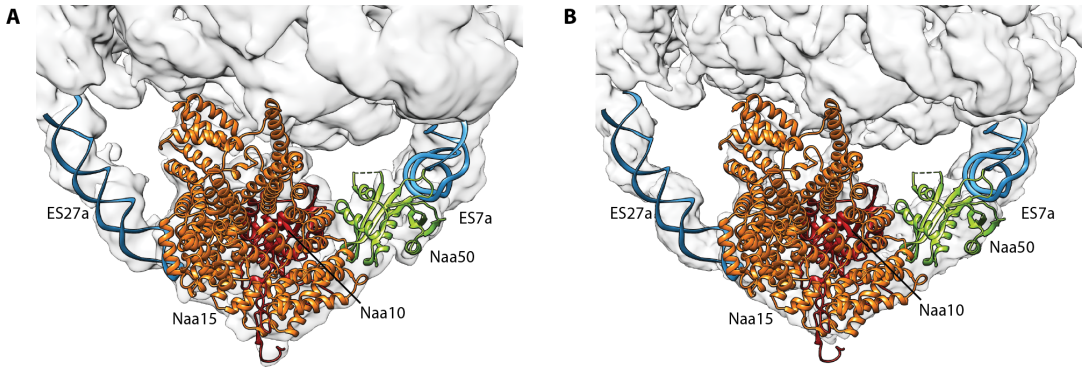

Figure 3.17: Comparison of NatA-ribosome complexes in native pull out and *in vitro* reconstitution. Zoom on NatA with model fitted into the density for the structure obtained by the native pull out of Naa15-TAP (**A**) and the *in vitro* reconstitution of NatA on ABP1-RNCs (**B**). Conformation and position of NatA in both cases is exactly the same. Map in A„ after local refinement on NatA, map in B after signal subtraction of the 40S SU and global refinement.

Nevertheless, the reconstituted sample exhibits two small additional densities compared to the native NatA-ribosome complex in the N-terminal region of the auxiliary SU. First, an extra density protruding from H59 on the 60S SU in the direction of Naa15's N-terminus has not been observed before (fig. 3.17A). It might be assigned to the missing 16 aa at the N-terminus of Naa15 that are not part of the model. According to its size it could bridge over to H59. Second, a prominent additional density appears close to the first TPRs of Naa15 and directly below the TE. In more detail, it is

connected to α1 close to the α1/α2-loop of TPR1 and α5 of TPR3 (fig. 3.18B1). As TPRs comprise a defined geometry and the fitted model is complete within that region, it is very likely that these additional density does not belong to the NatA complex. However, by protruding in the direction of the TE (fig. 3.18B2), this density might represent a fragment of the NC that is per se visible within the TE.

Even though NatA in the reconstitution exhibit nearly the same flexibility as NatA in the native pull out, a NC of a defined length seems to stabilize NatA binding within the regions close to the ribosome. The structure obtained from the reconstituted sample comprises the exact same binding sites for NatA to the ribosome, but in addition it provides more details on the Naa15 interaction with the ribosome.

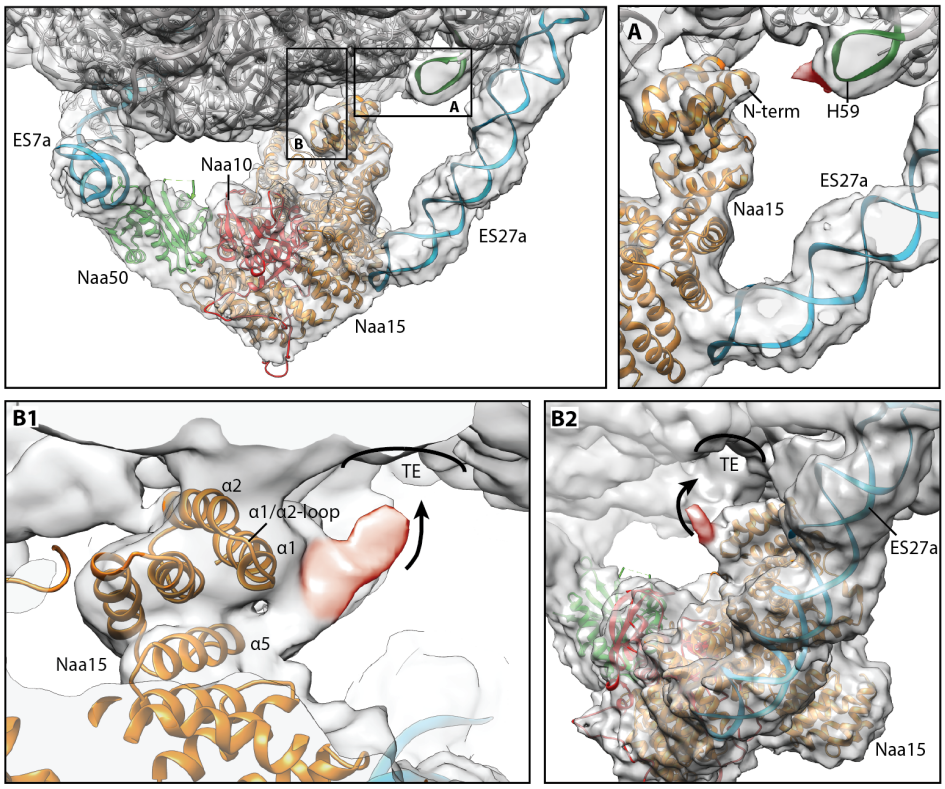

Figure 3.18: Additional densities present in the NatA-ABP1-RNC complexes. First panel shows the back view with additional binding sites indicated. **A**, Potential additional interaction site (red) appears between H59 and the missing 16 aa at the N-terminus of Naa15 occurring at lower contour levels. **B**, View rotated by about 60°with ES27 in the front (B2) or rotated additionally by 180° with view from ES7 (B1). Additional density (red) at the height of the first TPRs of Naa15 points into the TE and might belong to the NC.

3.2.4 Competition assay of Map1 and NatA

As iMet cleavage by methionine aminopeptidases needs to precede acetylation by NatA, the question arises if Map1 and NatA can bind concomitantly to the ribosome. To adress this question on a biochemical basis, competition assays were performed.

In order to simulate native conditions and having ribosomes carrying native Map1 substrates, the elution of Map1-TAP pull out (chap. 3.1.1) was used to incubate it with increasing amounts of recombinant NatA. After a spin through a sucrose cushion, supernatant (SN) and pellet (P) fraction were loaded on a gel and ribosome binding was monitored via α-CAB signal using western blot analysis (fig. 3.19). As the signal for Map1-CaMBD is present in the pellet fraction at all NatA concentrations and does not get diminished or pushed to the SN, NatA neither displaces nor disrupts Map1 binding to the ribosome. This suggests that both enzymes can bind at the same time (see discussion).

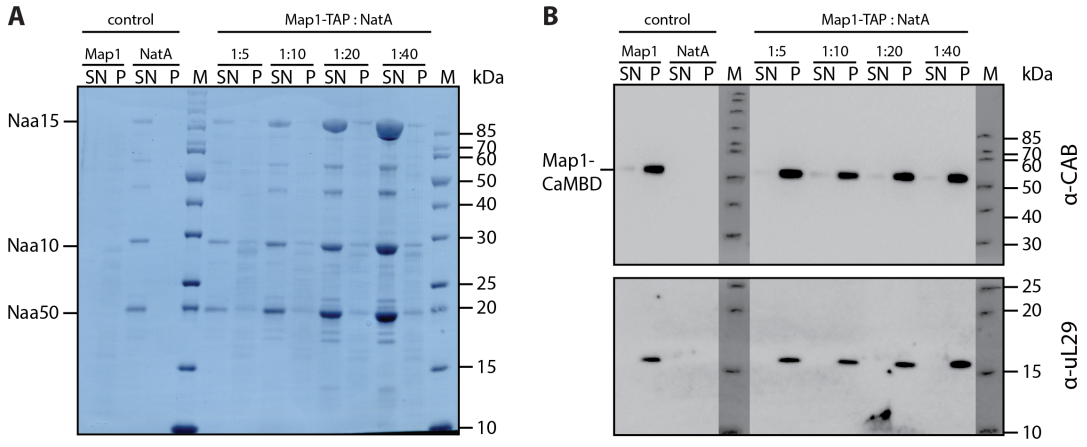

Figure 3.19: Competition assay of Map1-TAP with NatA. Four pmol of the native Map1-TAP elution fractions were incubated with increasing amounts of recombinant NatA protein and spun through a sucrose cushion. The ratio refers to the molar excess of NatA. **A**, Amido black-stained PVDF membrane after transfer of supernatant (SN) or pellet (P) fractions separated on a 12% Nu-PAGE gel. **B**, Western blot probed with α-CAB against Map1-CaMBD and α-uL29 against a ribosomal protein showing that NatA does not displace Map1 from ribosomes.

3.3 NatB in complex with the 80S ribosome

The second most common N-terminal acetyl-transferase is NatB which differs from NatA by a different SU composition as well as substrate recognition. NatB does not need the action of MetAPs because it acetylates the iMet directly when it is followed by Asx or Glx residues. The heterodimeric complex lacks a third SU analogous to NatA's Naa50, but its similar structural features analogous to those of Naa10 and Naa15 suggests a similar binding mode to the ribosome. To investigate NatB's binding behavior to ribosomes, its interaction was characterized by binding assays using different types of programmed ribosomes. This knowledge was used to continue with structural studies by performing an *in vitro* reconstitution of NatB on ABP1-RNCs followed by cryo-EM and SPA analysis and further verifications via mutagenesis studies.

3.3.1 *In vitro* characterization of NatB binding to 80S ribosomes

The binding of NatB to ribosomes was characterized using recombinantly purified NatB (fig. 3.20A) that was *in vitro* reconstituted with different types of programmed ribosomes. For RNCs carrying a substrate for NatB, uL4-RNCs were purified, but omitting the TEV cleavage step and therefore having a Met at the NC's N-terminus, resulting in a total length of 119 residues (termed substrate RNC/sRNC). As non-substrate RNCs (nsRNC) fully TEV-cleaved uL4-RNCs were used as they were utilized in NatA binding assays which start with a serine residue, comprising 86 aa in total. In addition, NatB was also bound to non-programmed 80S ribosomes (np80S) not carrying any NC. NatB was added in about 20-fold molar excess to 2 pmol of ribosomes and spun through a sucrose cushion (chap. 2.8.3). The pellet was resuspended and applied to SDS-PAGE. Bands representing NatB SUs in the pellet fraction together with ribosomal bands indicated binding. NatB exhibited binding to any kind of ribosomes, independent of the presence or type of the NC in a stoichiometric manner as identified by comparing the intensities of the best visible band representing Naa25 SU with the bands representing ribosomal proteins (fig. 3.20B).
Due to the overall similarity of its SUs, NatB was expected to bind in a similar way to ribosomes as NatA that includes interactions with eukaryotic specific expansion segments (ES). To investigate the involvement of ESs in NatB-ribosome binding, NatB was incubated with RNase I-treated uL4-RNCs lacking important ES (see chap 3.2.2.3).

The removal of ESs had an impact on NatB binding (fig. 3.20C) but to a lesser extent than for NatA. Therefore, NatB binding to ribosomes seems to be not as dependent on ESs than in the case of NatA. In fact, this suggests a different binding mode for NatB.

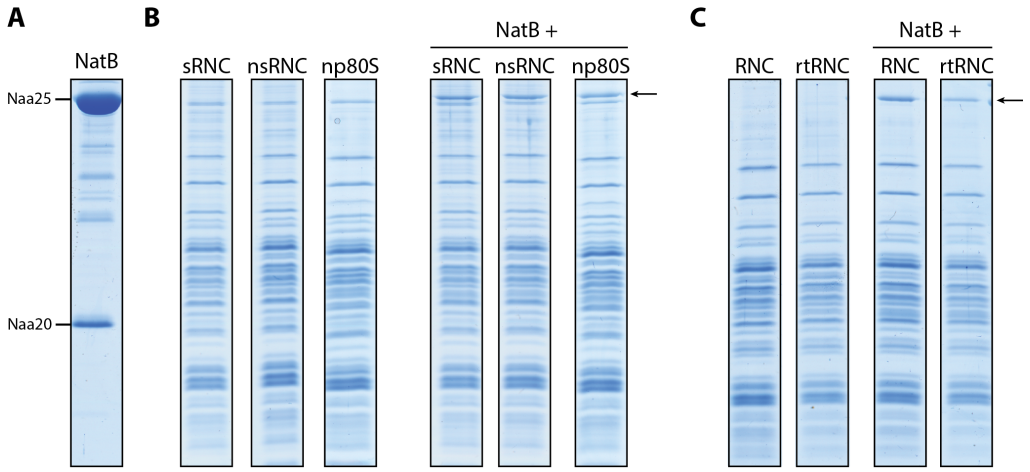

Figure 3.20: Binding Assays of NatB with differently programmed 80S ribosomes. 15% SDS-PAGE of recombinantly purified NatB (**A**) bound to substrate RNCs (sRNC), non-substrate RNCs (nsRNC), non-programmed 80S ribosomes (np80S) (**B**) and to RNase I-treated RNCs (rtRNCs) (**C**). For B and C pellet fractions are shown, indicating NatB binding to ribosomes independent of the composition of the NC in all cases. Only a partially decrease in binding was detected using rtRNCs that are lacking eukaryotic specific ES. sRNC, HA-uL4-RNC containing an N-terminal Met; snRNC, uL4-RNC starting with Ser; np80S, puromycin and high salt treated ribosomes not programmed with any NC; rtRNCs, RNase I-treated uL4-RNCs (cf. NatA). Binding was monitored by comparing Naa25 protein band (black arrow) that shows stoichiometric binding with ribosomal bands.

3.3.2 Cryo-EM analysis of the *in vitro* reconstituted NatB-ABP1-RNC complex

To investigate the position of NatB on a translating 80S ribosome, NatB was *in vitro* reconstituted on the well behaving and gradient purified ABP1-RNCs (chap. 2.3 , appendix p. 136). Two pmol ABP1-RNCs were incubated with a 20-times molar excess of NatB under native binding assay conditions and applied to cryo-EM measurements (chap. 2.8.3).

3.3.2.1 Data processing

Residual 138,576 particles after 2D classification were initially refined and subjected

to a first round of 3D classification (fig. 3.21). In four of the eight classes, ES27a was in the distinct exit position. This ES27a conformation previously resulted in a stable structure in the NatA-ribosome data set and therefore these classes were joined. Furthermore, they already showed an additional but unshaped density below the TE and were all programmed with tRNAs in P/P-state. After a focused sorting on the exit region using a soft binary mask, a class comprising 35,247 particles exhibited a defined density within the exit region. Already at this stage, the additional density could be assigned to NatB by fitting a crystal structure of NatB from *C. albicans* (PDB 5K18, Hong et al., 2017) into the electron density. However, differences in the intensity of the electron density of the two SU indicated a disproportion between catalytic and auxiliary SU. The catalytic SU seemed to be overrepresented and not in a 1:1 ratio with the auxiliary SU. Therefore, a further 3D classification with focus on the catalytic subunit was followed leading to a stable class with balanced ratio between the subunits. This final class, containing 21,061 particles (15% of all particles), was CTF refined in RELION to a final average resolution of 4.1 Å showing a clear density for NatB ('B1'/primary binding site). As an additional step, this final class was further subclassified using again a mask on the exit region. One class contained NatB in the regular B1 position. The other class showed an additional density between ES27a and B1, which was assigned as a secondary NatB ('B2'). To obtain a better resolution of NatB in B2 position and due to the limited number of particles, a step backwards was taken and the class with 35,247 particles was re-classified with a soft mask covering B2. Resulting classes showed either NatB in its regular B1 position or with B2 position in addition to the regular NatB binding site (fig. 3.21, purple). The latter comprised 17,812 particles (13% of all particles) and was CTF refined to an overall resolution of 4.4 Å.

The overall resolution of NatB in B1 position or with an additional NatB in B2 position shows the ribosome at a resolution below 4.1 or 4.4 Å, respectively (fig. 3.22). However, the local resolution of NatB ranges from 5 to below 12 Å, indicating the flexible nature of the ligand as already shown for NatA (chap. 3.2.2.1). Parts closer to the ribosome are less dynamic and better resolved, whereas peripheral regions of NatB or NatB in B2 position shows a higher flexibility. Especially B2 is associated with the highly flexible tip of ES27a (fig. 3.22A).

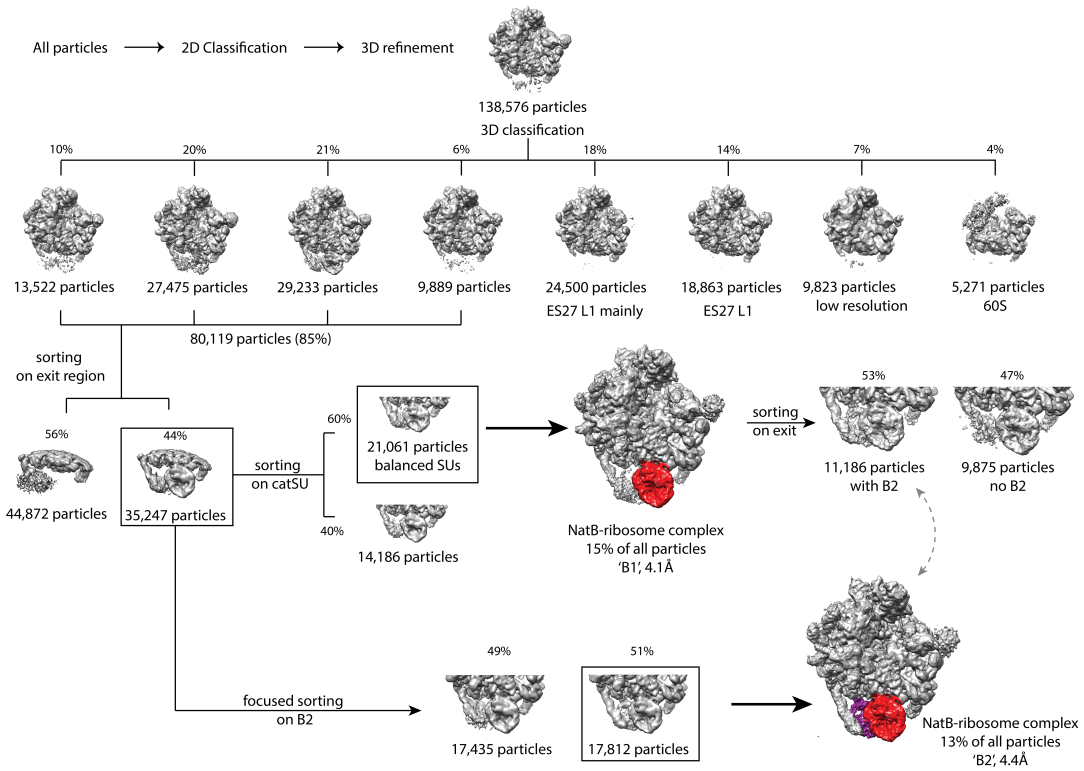

Figure 3.21: Classification scheme of NatB *in vitro* reconstituted with ABP1-RNCs. Particles were picked with Gautomatch and RELION 2D classification was used to discard non-ribosomal particles. Initial 3D classification into eight classes revealed four classes harboring tRNAs in P/P-state and with ES27a explicitly in the exit position. These classes were merged and subjected to a focused classification on the tunnel exit region using a soft binary mask, resulting in a class with a well-shaped additional density for NatB. Further classification with a mask applied to the catalytic subunit of NatB led to a stable class with balance ratio of NatB's catalytic and auxiliary subunit that was not in a 1:1 ratio before. This first final class contained 21,061 particles (15% of all particles) was subjected to CTF refinement in RELION yielding an average resolution of 4.1 Å ('B1', red). As an additional step, this class was subclassified performing a second focused classification on the exit region. One class contained NatB in the regular B1 position, the other class showed an additional and shaped density between ES27a and the primary NatB which was assigned as secondary NatB ('B2', purple). To obtain a better resolution of NatB in B2 position, a step backwards was taken and the class containing 35,247 particles was re-classified using a soft mask on B2 position. Resulting classes showed either NatB in its regular B1 position or with additional B2 position. The latter class was CTF refined to an overall resolution of 4.4 Å and contained 13% of all particles (17,812 in total).

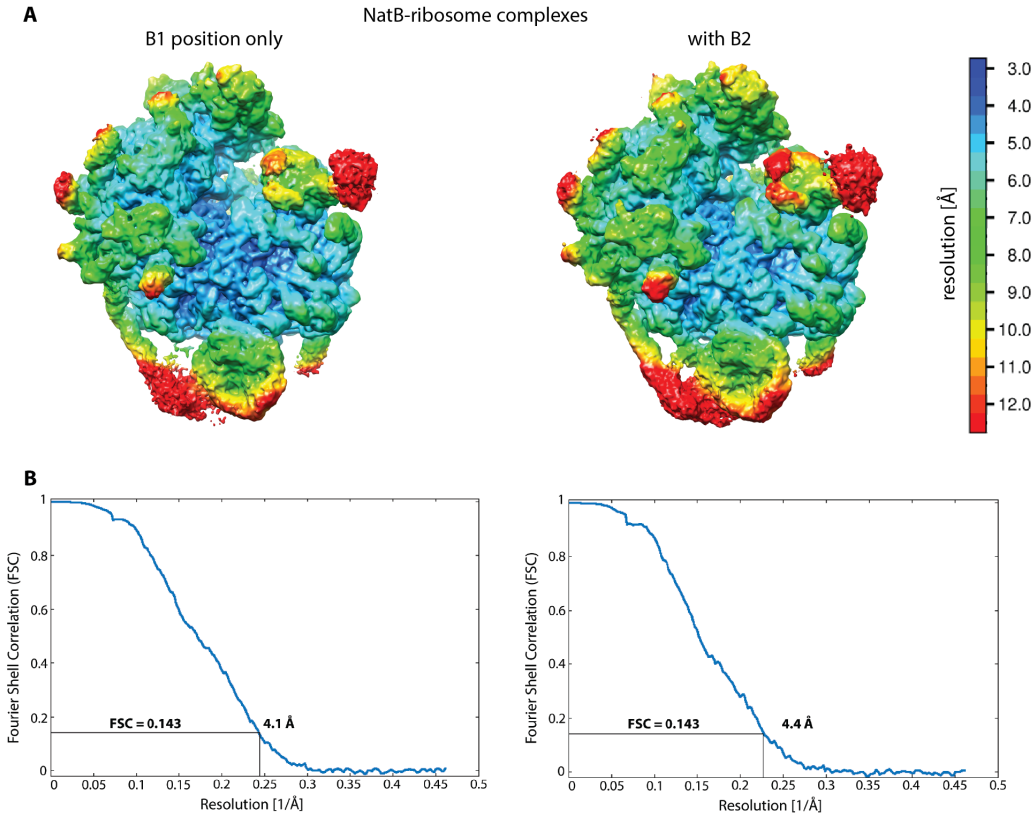

Figure 3.22: Local resolution and FSC curve of NatB-ribosome complexes. A, Local resolution of NatB-ribosome complexes with NatB in its regular B1 position only (left) and with an additional NatB in B2 position (right) with an average resolution of 4.1 and 4.4 Å respectively. Resolution range of 5 to beyond 12 Å for NatB indicates flexibility. **B**, FCS curves of the maps shown in A. The average resolution was calculated according to the gold standard.

3.3.2.2 Contact sites of NatB to the ribosome

Cryo-EM single particle analysis of *in vitro* reconstituted NatB on ABP1-RNCs revealed that NatB binds to the 60S SU and in the proximity of the TE. A homology model for yeast NatB on the basis of the crystal structure from *C. albicans* (Hong, et al., 2017) allowed the assignment of yeast NatB SU into the cryo-EM map. The disk-like Naa25 serves as a ribosome anchoring SU as suggested before (Polevoda et al., 2008) and positions Naa20 in a way, that the NC can access the catalytic center. The catalytic SU itself does not interact with the ribosome directly. Even if ES27a is in the exit position, well defined and visible until the tip, it does not interfere with NatB density (fig. 3.23).

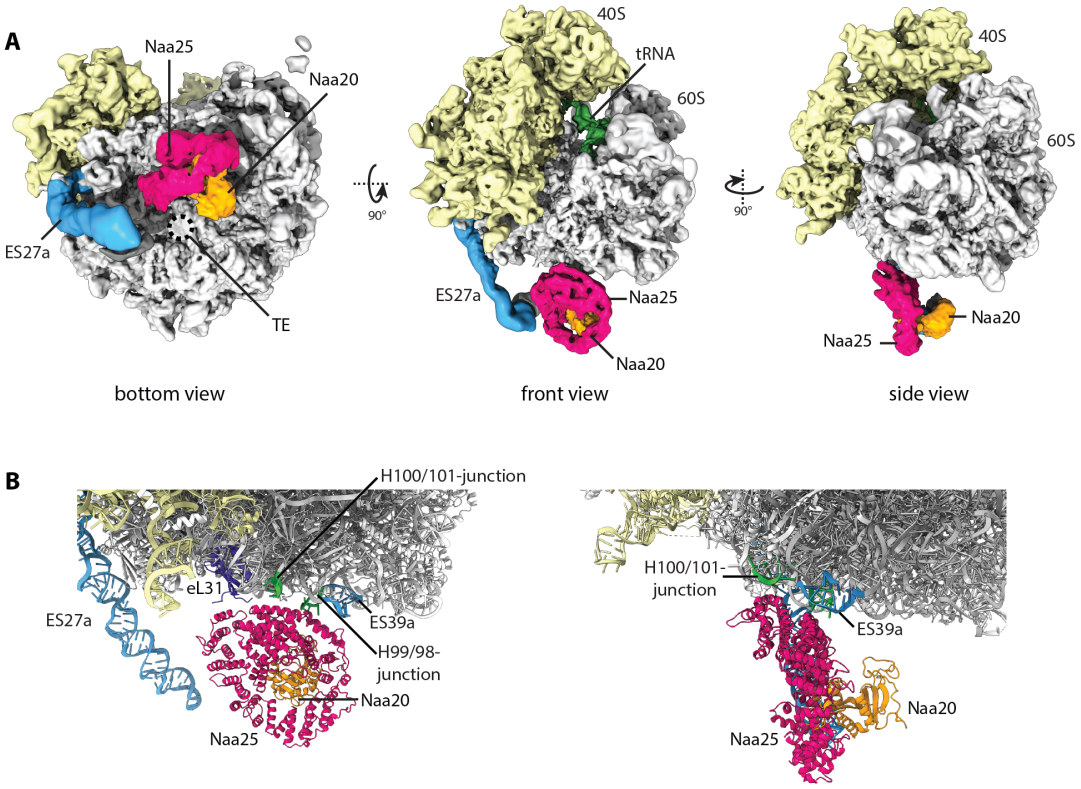

Figure 3.23: Cryo-EM structure and model of the NatB-ribosome complex. A, Cryo-EM structure of NatB (B1) in complex with translating 80S ribosomes filtered according to local resolution. Isolated densities of NatB were extracted after the final refinement step (Naa25: magenta, Naa20: orange). Views are shown on the peptide tunnel exit (TE, dashed ring) (bottom view), rotated 90° horizontally (front view) and rotated 90° vertically (side view). 40S and 60S ribosomal SUs are colored in yellow or grey respectively, rRNA expansion segments (ES) are shown in cyan. **B**, Enhanced view onto NatB-ribosome molecular model shown in front and side view as indicated in A. Ribosomal RNA involved in NatB binding is shown in green, ribosomal protein eL31 is labelled in dark blue.

NatB displayed two distinct interaction sites to the ribosome that mainly involved the C-terminus of the auxiliary subunit as well as ribosomal RNA (fig. 3.24). The strongest interaction was established between flipped-out bases at the junction of H100 and H101 of the 25S rRNA and α35 of Naa25 (fig. 3.24A). In more detail, U3317 and G3318 at the tip of H100/101-junction are presumably interacting with several positively charged aa within α35, where Lys736 is the closest to the rRNA tip. The second contact site is achieved by C3154 at the junction of H94 and H98 that builds a connection to Arg794 the third last aa at C-terminus of Naa25 (α36) (fig. 3.24B). Notably, the Naa25 C-terminus comprises several positively charged amino acids on its

surface that possibly further contribute to rRNA binding.
In the first two binding sites, only ribosomal RNA was involved. In addition to these main binding sites, a third contact site might occur between the Naa25 N-terminus that is close to the ribosomal protein eL31. This N-terminal part comprises TPRs that are generally involved in protein-protein interactions and might support binding to eL31, but the connection is only observed at lower contour levels.

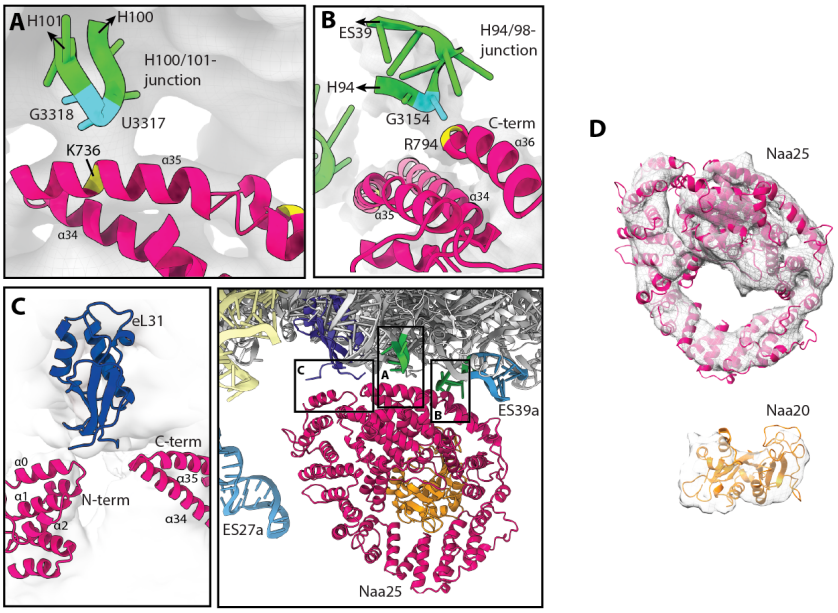

Figure 3.24: Contacts between NatB and the ribosome. The panel on bottom right shows the same view as the front view in fig. 3.23B with contact sites displayed. Interactions of a C-terminal helix of Naa25 (probably Lys736) with G3318 and U3317 within H100/101-junction (**A**), the Arg794 at the very C-terminus with G3154 within H94/98-junction (**B**) and the weaker interaction of Naa25 N-terminus and part of the C-terminus with eL31 (**C**) are shown. **D**, Isolated densities of NatB subunits after the final round of refinement shown in transparent with the model of Naa20 and Naa25 fitted into these densities.

3.3.2.3 Contribution of positive patches to NatB-ribosome binding

The binding of NatB to the ribosome seems to be maintained mainly by several positively charged aa located at the C-terminus of the auxiliary SU that interact with ribosomal RNA.

In order to test their contribution in ribosome binding, four positive patches (PP1-4) at the C-terminus of Naa25 were defined based on the structural insights above

(fig. 3.25A). All patches could be in principle involved in ribosome binding or are located close to the binding sites. Via charge inversion of Lys or Arg to Glu (similar to Magin et al., 2017) NatB double charge inversion mutants were created and bound to non-programmed 80S ribosomes to prevent any bias by a specific NC (fig. 3.25). Whereas mutations of single positive patches only had a minor impact on binding, NatB carrying mutations of all four patches (PPall) showed a more severe decrease in ribosome binding (fig. 3.25B). This indicated that the positive charges at the surface of the Naa25 C-terminus have a rather additive effect on ribosome binding.

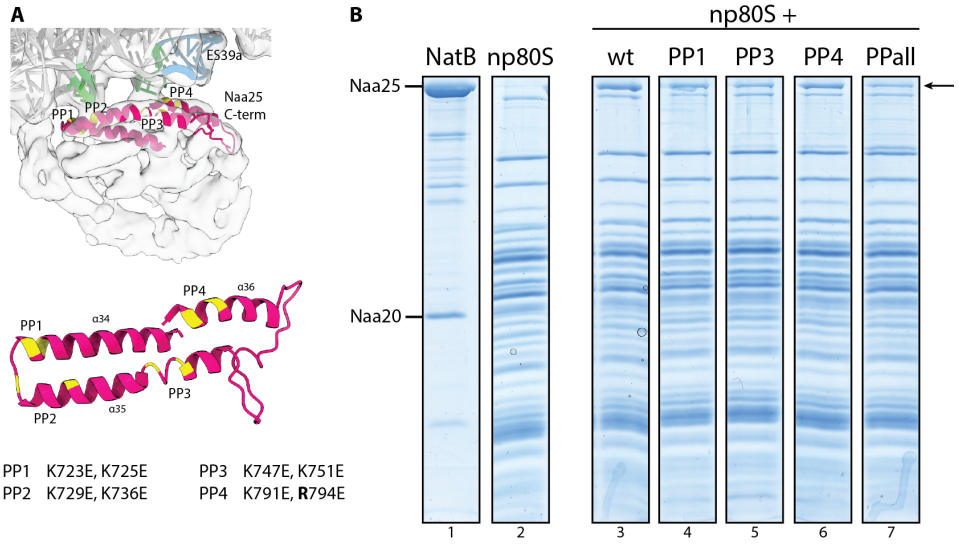

Figure 3.25: Contribution of Naa25's C-terminal positive patches to ribosome binding. **A**, Localization of the four positive patches (PP) at Naa25's C-terminus used for charge inversions shown within NatB density (top) or as top view (middle). Specific double charge inversions are indicated below (bottom) with the only mutation involving an Arg in bold. **B**, 15% SDS-PAGE of a binding assay using wt or mutant NatB complex and non-programmed idle 80S ribosomes (np80S). The supernatant fraction is shown for wt NatB (lane 1) and pellet fractions of the 80s ribosomes alone (lane 2) or incubated with NatB wt (lane 3), NatB with K723E and K725E (lane 4), NatB with K747E and K751E (lane 5), NatB with K791E and R794E (lane 6) and with NatB carrying mutations of all four positive charged patches (PPall, lane 7).

3.3.2.4 Characterization of the additional second NatB

During cryo-EM data processing an additional second binding site (B2) of NatB was encountered, located between ES27a, H59 and NatB in its primary B1 position (fig. 3.26). Connected to the flexible ES27a, it is less well resolved compared to B1. This only allowed a rigid body fit of NatB model into B2 density to estimate its orientation to the

ribosome. The C-terminus as well as the TPRs at the very N-terminus of Naa25(2) are interacting with the tip of ES27a. In addition, TPRs located more downstream of the N-terminus bind to the 60S SU of the ribosome by either interacting with H59 (α3-α6) or are in close proximity to H24 at the TE (α10). As a consequence, the catalytic SU of both NatB positions point to each other with both auxiliary subunits facing outside. Notably, the second Naa25 does not involve the same residues for ribosome binding as the primary Naa25, antagonizing the idea of unspecific binding. In addition, B2's interaction with ES27a might explain why ES27a is coordinated in the exit position in all observed classes.

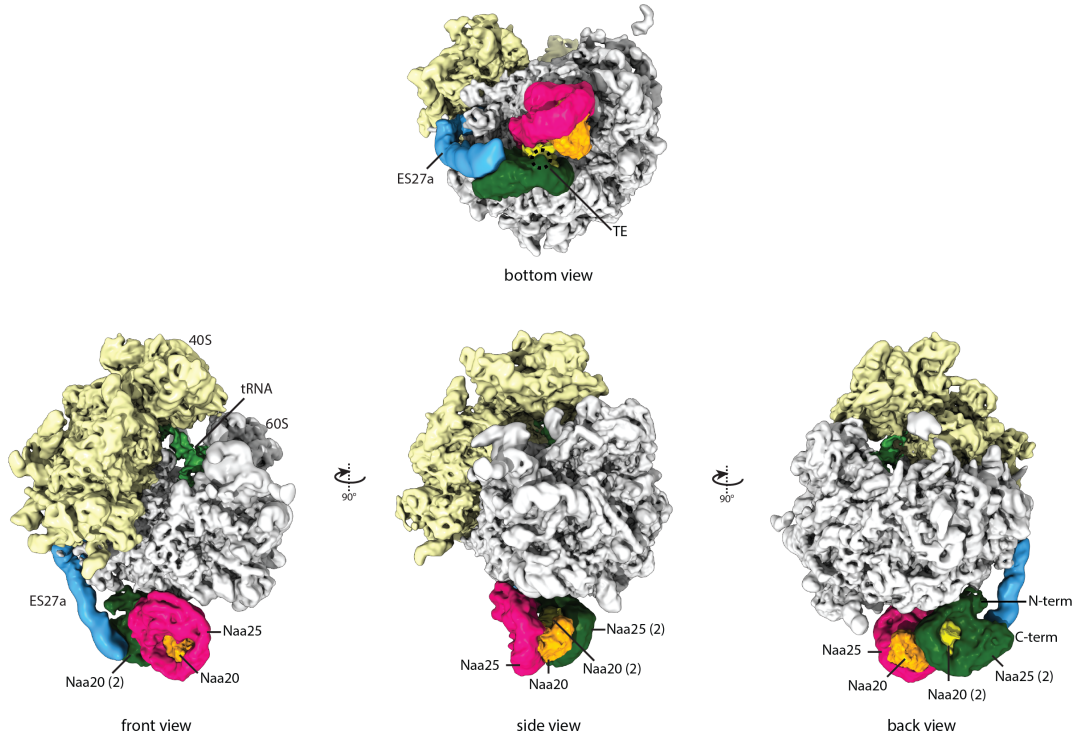

Figure 3.26: Cryo-EM structure of a potential additional NatB binding site. Cryo-EM structure of NatB in complex with translating 80S ribosomes with focused classification on NatB's potential secondary binding site. Maps are filtered according to local resolution. Isolated densities of NatB were extracted after the final refinement step (B1 position: Naa25 in magenta, Naa2 in orange; B2 position: Naa25(2) in green, Naa20(2) in yellow). Views are shown on the peptide tunnel exit (TE, dashed ring) (bottom view), rotated 90° horizontally (front view), rotated 90° vertically (side view) and rotated another 90° vertically (back view). 40S and 60S ribosomal SU are colored in yellow or grey respectively, rRNA expansion segments (ES) are shown in cyan.

4 Discussion

Ribosomes are the molecular machines synthesizing all proteins in the cell. During translation the nascent polypeptide chain (NC) moves from the peptidyl-transferase center through the exit tunnel to the tunnel exit (TE) site at the surface of the ribosome. As soon as the NC emerges from that site, it gets in touch with a variety of different factors. Here, the TE serves as a binding hub for a large number of proteins, so called exit site factors, that assist in co-translational folding, enzymatic processing or protein targeting. This includes chaperones, such as RAC or the chaperone-like NAC to support folding, the SRP/SR/Sec61 machinery for targeting and translocation, methionine aminopeptidases (MetAPs) to remove the starter methionine (iMet) from the NC and N-terminal acetyltransferases (NATs) that acetylate the N-terminus of the NC. For some exit factors, sequential processing of the NC is mandatory like iMet removal by MetAPs and subsequent acetylation by the major NAT, NatA. A cooperation between these two enzymes would make sense because two processing steps need to be coordinated. In case of NatB, another major NAT, methionine cleavage is not necessary and a coordination of these two enzymes would be incidental. Whereas for example co-translational targeting and translocation is quite well understood (Halic and Beckmann, 2005; Becker et al., 2009; Berndt et al., 2009; Voorhees and Hegde, 2016; Wild et al., 2019 amongst others), structural data for the early modifying enzymes are not yet available. Thus, solving the structure of a yeast MetAP and the two major NATs bound to the translating ribosome gives new insights into the interplay of these enzymes that are responsible for the most common early co-translational protein modifications. Furthermore, these data can be integrated into the scheme of exit site factors and extend our understanding of the coordination at the ribosomal exit site further.

4.1 Positioning of Map1 on the 80S ribosome

The structure of the major MetAP in yeast, Map1, in complex with the ribosome was obtained by a native pull out. Since the Map1-ribosome complexes turned out to be rather unstable and flexible for cryo-EM studies, they had to be cross-linked in order to determine their structure. However, the structure allowed for the first time the overall positioning of an eukaryotic MetAP below the exit tunnel. As expected, Map1 binds rather flexible to the 60S subunit and thereby mainly involves the mobile rRNA expansion segment ES27a, while additionally contacting the exit site via H59 and eL22. Contacts to the UAS1 (uL23 and uL29) are maintained only to a minor extent. From this rather flexible assembly, two main overall conformations of Map1 and ES27a could be enriched. While having the same contact sites at the ribosome, they distinguish in the position of ES27a as well as their number of contact points to the same. For both conformations the density showed the shape of the globular aminopeptidase (AP) domain with two protruding lobes, one of them showing a direct contact to the NC (chap. 3.1.2.2). Unfortunately, fitting of a model was not possible and thus the assignment of this density to Map1 is not ambiguous. Yet, for several reasons it is very likely that the observed density is indeed Map1.

The obstacle of Map1 being flexibly associated with the ribosome could be overcome by glutaraldehyde cross-linking. Despite the low local resolution, Map1 binding mode to ribosomes is similar to related enzymes that comprise the typical MetAP-like or AP fold, the structures of which were solved during the course of this thesis. Arx1 (associated with ribosomal export complex protein 1) is a yeast 60S biogenesis factor that shows sequence homology and structural similarity to MetAPs (fig 4.1A, 1.5) (Bradatsch et al., 2007; Greber et al., 2012; Greber et al., 2016). It is required for the export of pre-60S subunits from the nucleus into the cytosol (Bradatsch et al., 2007). *In vitro* cryo-EM structures showed that the AP fold accomplishes both, the binding to the ribosome and the interaction of Arx1 with the nucleoporins at the nuclear pore complex. In more detail, Arx1 interacts with ES27a as well as H59 and therefore shares the same binding sites to the ribosome as Map1. The binding of Arx1 to ES27a is maintained by two of the four α-helices within the AP fold. Furthermore, Arx1 maintains a strong connection to UAS1 which functions only as a minor binding site for Map1.

In contrast, Arx1 interacts with additional proteins at the TE (uL24 and eL19) (Greber et al., 2012).
Ebp1, ErbB3-binding protein 1, the human homolog of Arx1, has been shown to be associated with different rRNA species and is involved in cell proliferation and human cancer (Squatrito et al., 2004; Nguyen et al., 2018; Wells et al., 2020; Wild et al., 2020). It also comprises the MetAP-like fold, binds to the exit region by interacting with H59 and UAS1 and to ES27a with the same two helices of the AP fold as observed for Arx1. As Ebp1 has more similarities to the hMetAP2 isoform, the C-terminal insertion typical for type II MetAPs is building an additional contact to ES27a. Furthermore, another exit site protein is involved in ribosome-Ebp1 interaction as well (eL19) (Wild et al., 2020; Wells et al., 2020).

In conclusion, proteins harbouring the MetAP-like fold are likely primarily attached to the ribosome via their conserved globular AP domain to ES27a as also seen in our Map1-80S structures. In addition, H59 seems to function as a major contact for those proteins, whereas UAS1 serves either as minor (Map1) or prominent contact site (Arx1, Ebp1). Individual interactions characteristic for the protein itself are then established by protein-specific insertions or extensions (especially in the C-terminal region of Arx1 and Ebp1). Along those lines, the observed extra densities near H59 and TE in our Map1-80S reconstructions can be possibly attributed to the Map1-specific N-terminal zinc-fingers, which have been shown to play a role in ribosome association (Vetro et al., 2002).

During the course of this work, the Sengupta group published data on the *E. coli* Map (bMap) and its association with the ribosome (Bhakta et al., 2019). Two structure were obtained by *in vitro* reconstitutions of the bacterial Map alone and together with the peptide deformylase (PDF) to the 70S ribosome. Before bMap can cleave the iMet, PDFs need to remove the formyl group from the starter methionine. Even though these structures are at a resolution of about 10-15 Å, a comparison with our data showed that bMap in the Map/PDF sample matches perfectly the yeast Map1 position (fig. 4.1, right). bMap was described to interact with uL23 and H59 (Bhakta et al., 2019) in agreement with previous cross-linking studies where the binding was suggested between uL23 and bL17 (Sandikci et al., 2013). Furthermore, this binding site is in close proximity to H59. Notably, bMap adopts a different position if no other

factor is present. Its primary binding site was observed close to uL22, bL32 as well as H24 and H47. If this primary binding site is blocked by, for example PDF, bMap relocates to an alternative position at the TE. Bacterial ribosomes do not contain expansion segments, but this behaviour hints to a flexible nature of Map in bacterial as well.

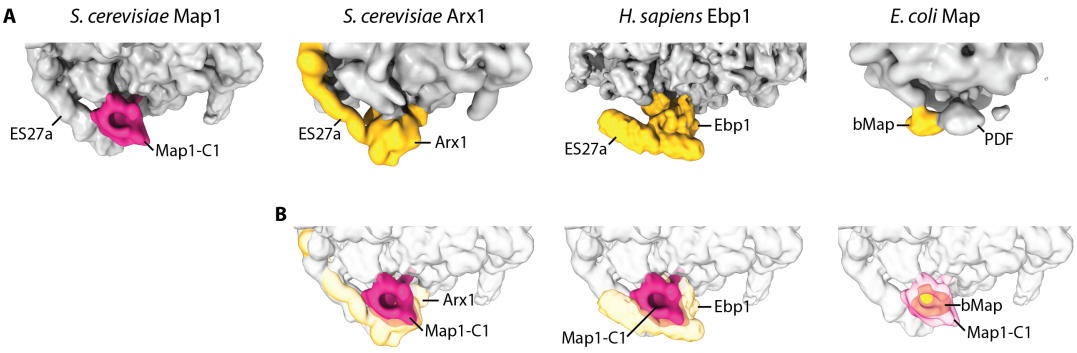

Figure 4.1: Comparison of yeast Map1 position with other MetAP-fold containing proteins on the ribosome. **A**, Yeast Map1-C1 (pink, left) followed by yeast Arx1, human Ebp1 and *E. coli* Map (bMap) that was reconstituted with the peptide deformylase (PDF) on the ribosome (left to right) labelled in yellow with ES27 if present. **B**, Overlay of Arx1, Ebp1 and bMap (yellow) with yeast Map1-C1 (pink). Gaussian filtered ribosomes were rigid body fitted in Chimera and densities of the factors isolated. Map1-C2 conformation would lead to a comparable result. EMDB: 6610 (Arx1), 10344 and 10609 (Ebp1), 9753 (*E. coli* Map).

Another study published recently shows the cryo-EM structure of *C. elegans* NAC in an *in vitro* reconstitution on the worm 60S ribosome (Gamerdinger et al., 2019). Interestingly, NAC density fuses with the NC similar to the yeast Map1 (fig. 4.2 left and middle). This is of special interest, as both exit factors belong to the early interactors with the NC and the question arises how they are coordinated.

The recent cryo-EM data confirmed previous cross-linking studies suggesting a binding of NAC to UAS1, therefore sensing the NC within the ribosomal peptide exit tunnel and guiding the growing NC to the cytosol (Gamerdinger et al., 2019; Wegrzyn et al. 2006; Nyathi and Pool, 2015). Even if not mentioned in the publication, NAC density bridges over to H59 but only forming a weak connection to the ribosome at this site (Gamerdinger et al., 2019; EMDB 4938). Furthermore, additional cross-linking studies suggested a concomitant binding of NAC and Map1 at UAS1 (Nyathi and Pool, 2015), but the comparison of the available structures show the opposite.

Map1 and NAC would clash into each other when superimposing the structures at the TE (fig. 4.2 right). Thus concomitant binding of these two factors can be excluded unless at least one of these factors changes its position as it was discussed for the bacterial Map above. This idea is supported by other cross-linking studies where NAC was also found to interact with eL31 and uL22 on the opposite site of the TE (termed UAS2, Pech et al., 2010), suggesting that in this case rather NAC then Map1 alters its position. Indeed, NAC was already observed relocated to a different position in the presence of the TTC5 protein, a tubulin-specific ribosome-associating factor (Lin et al., 2020). Having TTC5 bound, NAC was detected on the ribosome shifted into the direction of H24 and uL22 and away from UAS1. A putative N-terminal extension of the α-SU was observed and placed as Ala model between eL19 and eL22 (PDB 6T59, Lin et al., 2020). This would explain the cross-linking results of NAC to UAS2 (Pech et al., 2010; Zhang et al., 2012; Nyathi and Pool, 2015). In this alternative binding site NAC would still clash with Map1, but it shows the possibility of a general rearrangement and dynamic binding of NAC to ribosomes. Nevertheless, based on the structural data known so far, Map1 and NAC cannot simultaneously bind to the ribosome.

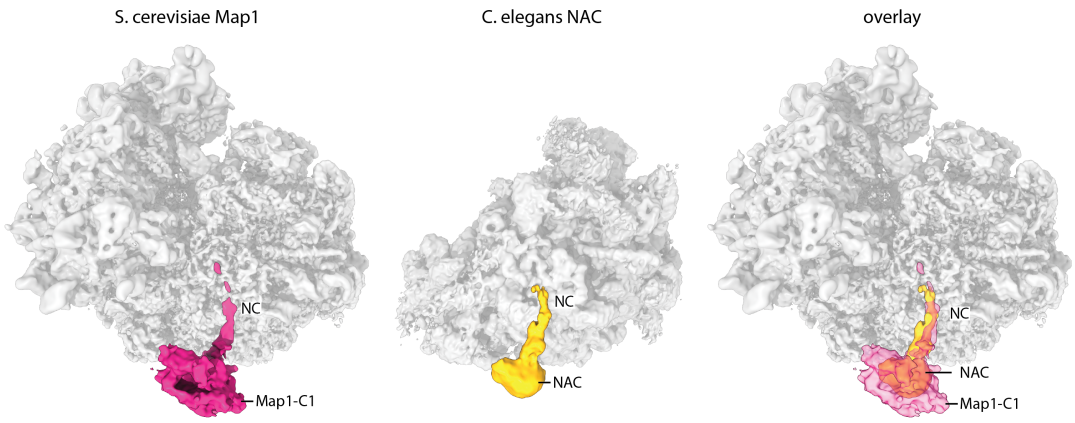

Figure 4.2: Comparison of Map1 and NAC binding to the ribosome. Isolated densities of yeast Map1-C1 (left) and *C. elegans* NAC (middle) with yeast 80S or *C. elegans* 60S in the background respectively. The overlay of both factors (right) with Map1 in transparent indicate that a concomitant binding is not possible. EMDB: 4938 (NAC, Gamerdinger et al., 2019).

4.2 Binding of NatA on the 80S ribosome and comparison with Map1

NatA acts on the ribosome after MetAPs has cleaved the iMet, in case the new N-terminus exposes a small aa in the second position. This suggests a sequential action of the two enzymes on the NC, but binding to the ribosome might be a different question. To investigate if Map1 and NatA compete or cooperate on processing NatA substrates, we first determined the cryo-EM structure of NatA-ribosome complexes and subsequently compared them to our Map1-ribosome structure.

Like Map1-ribosome complexes, NatA-80S complexes were also successfully obtained via the native pullout approach. Here, however, no cross-linking was necessary to maintain the intact complex, indicating that the NatA-ribosome assembly is comparably more stable.
Indeed, the sample from the native pull out revealed four stable anchor points of NatA on the 80S ribosome in yeast. Contrary to previous studies suggesting NatA binding to UAS1 (uL23 and uL29) as observed by analyzing different TAP-tagged yeast strains (Polevoda et al., 2008), ribosome binding is exclusively established via rRNA. Moreover, three of the four sites involved eukaryotic specific expansion segments and their triangular arrangement positions the trimeric NatA complex directly below the TE. A model for the trimeric *S. cerevisiae* NatA complex based on a crystal structure of the free NatA (PDB 4XNH) was rigid-body fitted into the electron density without the need of a rearrangement of the SUs. In addition, the model could be improved especially at the ribosome binding sites. Therefore, our data show that NatA's two auxiliary SUs (Naa15 and Naa50) on the ribosome create a position of the catalytic Naa10 in a way that it faces the ribosomal TE at a distance of about 50 Å. Considering the distance from the 3'-CCA end of the tRNA to the TE, a minimum length of 50 aa in total or 20 aa from the TE would be required to reach the catalytic center of NatA on a direct way (fig. 4.3). This is in the upper range of the 25-55 aa of the NC for N-terminal acetylation suggested earlier by *in vitro* studies (Polevoda and Sherman, 2003a). Furthermore, the minimum length of 50 aa is in agreement with the required minimal length of 40-45 aa for the iMet removal estimated in bacteria as it precedes NTA by NatA (Sandikci et al., 2013; Ball and Kaseberg, 1973).

Naa50, with so far unknown function, comprises like Naa10 the GNAT fold for acety-

lation activity. In humans and fruit fly, Naa50 can act either alone or in complex with Naa10 and Naa15 (see introduction) and has acetylation activity against NCs retaining the iMet (Evjenth et al., 2009; Hou et al., 2007; Van Damme et al., 2015; Williams et al., 2003). In the yeast trimeric NatA-ribosome complex, Naa50 is located 85 Å away from the TE. For this distance a NC length of about 70 aa would be needed to reach Naa50's catalytic center and is therefore located significantly further away than Naa10. In addition, Naa50 in yeast is inactive as it lacks the acetyl-CoA binding motif (Gautschi et al., 2003; Deng et al., 2019; Van Damme et al., 2015; Arnesen et al., 2006) and therefore has presumably only a stabilizing role of trimeric NatA to the ribosome. In conclusion, Naa50 serves as an additional ribosome binding SU but not as active catalytic SU in yeast.

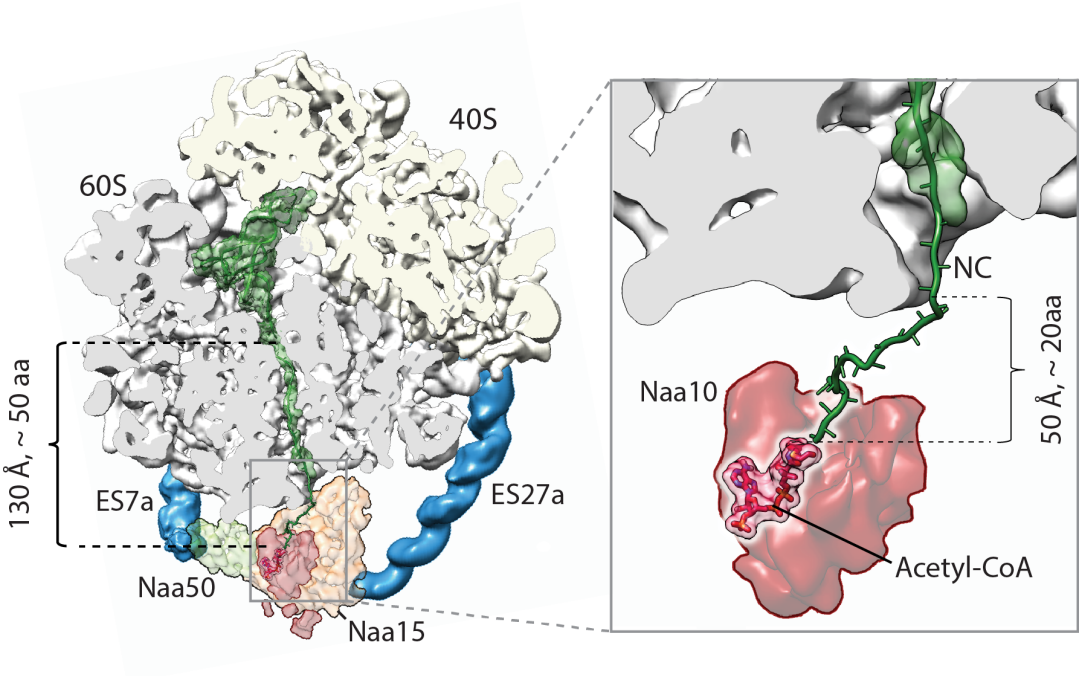

Figure 4.3: Minimum length of the NC required for acetylation by NatA. Cut view focusing on the NC and catalytic center of NatA. A minimum length of the NC, shown as Ala model, of 50 aa in total, or 20 aa from the TE is necessary to reach the catalytic center directly. Peptidyl-tRNA: green, Naa10: red, Naa15: orange, Naa50: light green, ES27a: cyan, 40S: yellow, 60S: gray.

The native pull out which was used to purify intact NatA-ribosome complexes included an additional S7 digestion step for NatA enrichment. This led to a well resolved structure explaining NatA's interaction with the ribosome. A disadvantage of this approach is the presence of ribosomes programmed with a broad mixture of NCs that comprise different lengths and aa compositions. Especially the binding to the very flexible ES27a allows NatA to adopt slightly different conformations and varying its position to perfectly 'catch' different NCs for acetylation. These minimal movements might be the reason for a still low local resolution of the NatA complex compared to the overall 80S ribosome (chap. 3.2.2). To overcome the flexibility of NatA on the ribosome determined in native pull out data, ABP1-RNCs carrying a NC of a defined aa composition were incubated with an inactive NatA mutant and subjected to cryo-EM analysis. Data processing revealed that the binding mode of NatA in the *in vitro* reconstituted sample is exactly the same as in the native pull out and reflects perfectly the native situation and conformation of NatA on the ribosome. Despite overall similarities, some minor but interesting differences between these structures were observed. On the one hand, the hitherto invisible N-terminus of the auxiliary Naa15 seems to be better visible now. On the other hand, an extra density near the N-terminal TPRs of Naa15 are very likely to originate from the NC. This is interesting because conceptually it could have an impact on NatA function. TPRs are in general protein-protein mediating entities (reviewed in Zeytuni and Zarivach, 2012) and here they could act as a guide for the NC towards the catalytic center (fig. 4.4). This was already suggested before by several studies performing protein sequence analyses and predicting TPRs within Naa15, as well as the other auxiliary SUs of the major NATs (Naa25 of NatB and Naa35 of NatC) (Polevoda and Sherman, 2003b). Contrary to other *in vitro* studies suggesting a NC length of 25-55 aa (Polevoda and Sherman, 2003a), an unusual long length of the NCs of 80-100 aa for NatA processing was also observed by cross-linking experiments (Gautschi et al., 2003). Observing longer NCs may indicate a 'guiding' of the NC along the TPRs (fig. 4.4) and a later acetylation event. In addition, we can even speculate on NatA as being not only a processing enzyme but also as kind of a holdase, the may even assist in folding in a chaperone-like manner.

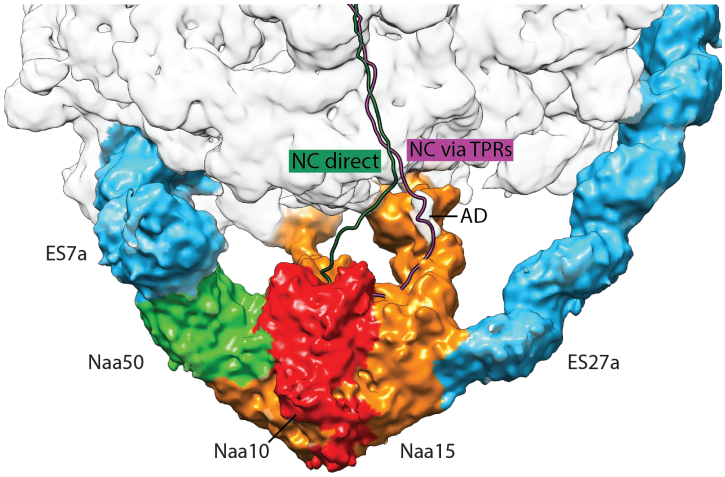

Figure 4.4: Possible routes of the NC into the catalytic center of NatA. Additional density (AD) in the structure of NatA reconstituted on RNCs programmed with 88 aa of ABP1 suggests a guiding of the NC along Naa15's TPR repeats (purple) instead of entering the catalytic center directly (dark green). Densities are colored according to NatA model obtained from native pull out with Naa10 in red, Naa15 in orange and Naa50 in light green. ES are labelled in cyan. Additional density within Naa15 that points towards the TE is left in gray. The model of the original NC (dark green) was revised using COOT.

Map1-NatA interplay

To assess if Map1 and NatA act in concert or sequentially, both obtained structures were superimposed. Map1-C1 could in principle bind to the ribosome with NatA at the same time. If shown in the front view, Map1 is located adjacent to NatA with only having a minor overlap with the Naa15 N-terminus (fig. 4.5A). In contrast, however, Map1-C2 would clash with the N-terminal TPRs of NatA's auxiliary SU (fig. 4.5B). Notably, both exit factors extensively engage with ES27a and interestingly ES27a is in clearly distinguishable positions when bound to either factor. This structural analysis suggests two possible scenarios for the Map1-NatA interplay.

The first is sequential binding of Map1 and NatA that is dictated by the position of ES27a (fig. 4.5C). Starting with Map1-C1 that might be responsible for the positioning of ES27a in its exit position. Here, Map1 is tightly bound to ES27a, H59 and eL22. During the transition from C1 to C2 conformation, ES27a shifts by about 12° closer towards the position found in the NatA-80S complex. This might lead to a weakening of ES27a interactions with Map1, which is yet still connected to the ribosome via eL22 and H59 (Map1-C2). Upon binding of NatA, ES27a could move further for about 19°,

which could lead to the final dissociation of Map1. In total, ES27a shifts by about 30° from Map1-C1 to NatA position, guiding the exit factor binding by its distinct positions.

However, our structure does not exclude concomitant binding, if the intrinsic flexibility of Map1 is taken into account. As shown for bacteria, Map is able to in principle adopt alternative binding site as soon as another exit factor (PDF in bacteria) blocks its primary binding site (Bhakta et al., 2019). Having another enzyme present, e.g. NatA, might relocate Map1 on the yeast ribosome as well. This is supported by our biochemical data, where NatA was not able to replace Map1 in a competition assay (fig. 3.19). This leads to the second scenario and a handover model for the NC: as NatA interacts with H24 while Map1 binds on the other side of the TE and already interacts with the NC, Map1 could transfer the NC after NME to NatA. In turn, NatA guides the NC along its TPRs into the catalytic center. In addition, having both enzymes bound around the TE at the same time, an even more protective environment for the NC is created during modification and prevents other exit factors to interfere.

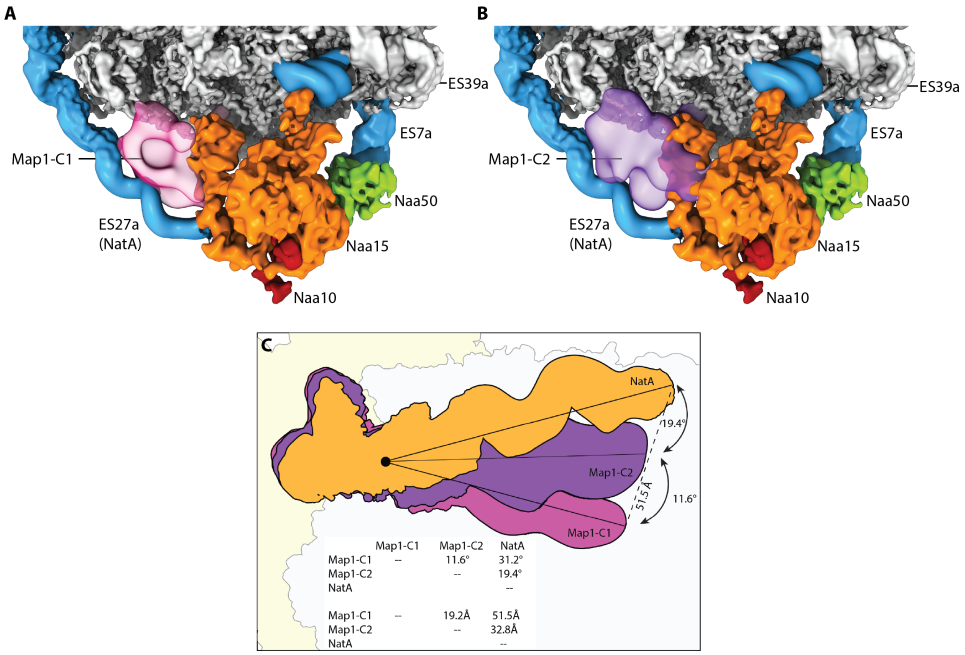

Figure 4.5: Possible concomitant binding of Map1 and NatA on the 80S ribosome. Overlay of Map1-C1 (**A**) or Map1-C2 (**B**) with NatA-ribosome complexes with Map1 shown in transparent. Naa15 in orange, Naa10 in red and Naa50 in green. **C**, View on ES27a conformations in Map1-C1-, Map1-C2- and NatA-ribosome complexes (pink, purple and orange respectively). Angles and distances are indicated in the table below.

4.3 Binding of NatB on the 80S ribosome and comparison with Map1 and NatA

One of the aims of this work was to study the interplay of the factors responsible for early processing of the NC. For Map1 and NatA a sequential modification of the NC, namely first NME then NTA, is known. NatB, the second most common NAT, also acetylates many proteins, but in contrasts to NatA it acetylates the iMet directly. Nevertheless, both might need to scan the ribosome for sufficient substrate. Therefore, the question arises how Map1 and NatB are coordinated as they do not need each other's action for NC modifications and how the two pathways (Map1/NatA) and NatB can exclude or integrate each other.

For the NatB-ribosome structure determination, the logic choice would be a native pull out again, also tagging the auxiliary SU that has been suggested to be involved in ribosome binding (Polevoda et al., 2008). Unfortunately, a C-terminal TAP tagged version of Naa25 is not available in the strain collection at Euroscarf, indicating already that the C-terminus might play an important role in the NatB function. Inserting a different tag C- or N-terminally as well as internally did not lead to a successful co-purification of ribosomes with the NatB complex. However, an *in vitro* reconstitution of NatA on specifically programmed RNCs showed that the *in vitro* approach mimics the native situation very well (chap. 3.2.3). Therefore, the same experiment was performed with NatB.

Surprisingly, the *in vitro* reconstitution of a catalytically inactive NatB on ABP1-RNCs revealed a complete different binding mode of NatB on the ribosome compared to NatA, even though the similarities in the architecture of the auxiliary SUs might have indicated the opposite.
The dimeric NatB complex sits offside the exit tunnel and establishes only two major contacts to the ribosomes, in contrast to NatA that maintains four. However, similar to NatA, these contacts again only involve rRNA and are established by positively charged patches at the C-terminus of the auxiliary SU. Noticeably, NatB binding does not involve any ESs. Another part of the C-terminus as well as TPRs at the N-terminus of Naa25 might be involved in a weaker binding to eL31, but this connection was only observed at lower contour levels. Notably, the close vicinity of Naa25's N- and

C-terminus to the ribosome may explain, why N- and C-terminal tagging of Naa25 in yeast was not successful.

The NatB-ribosome structure revealed, that only the auxiliary Naa25 SU forms contacts to the ribosome as proposed before by deletion studies (Polevoda et al., 2008). As observed in the crystal structure of *C. albicans*, Naa25 wraps around the catalytic Naa20. This structure could be rigid-body fitted basically in the same conformation as observed in the crystal structure, indicating that major structural rearrangements are not required to bind the ribosome. Like in the case of NatA, the catalytic SU Naa20 does not contact the ribosome. Naa25 positions it such, that the catalytic center points towards the TE at a distance of about 65 Å. Also taking the distance from the PTC to the TE into account, the polypeptide chain would need a minimum length of about 55 aa in total, or 25 aa from the TE to reach the catalytic center on a direct way (fig. 4.6). The minimal length of the NC for NatA and NatB is therefore in a similar range (50 and 55 aa total), even though NatB most likely requires longer NC than NatA.

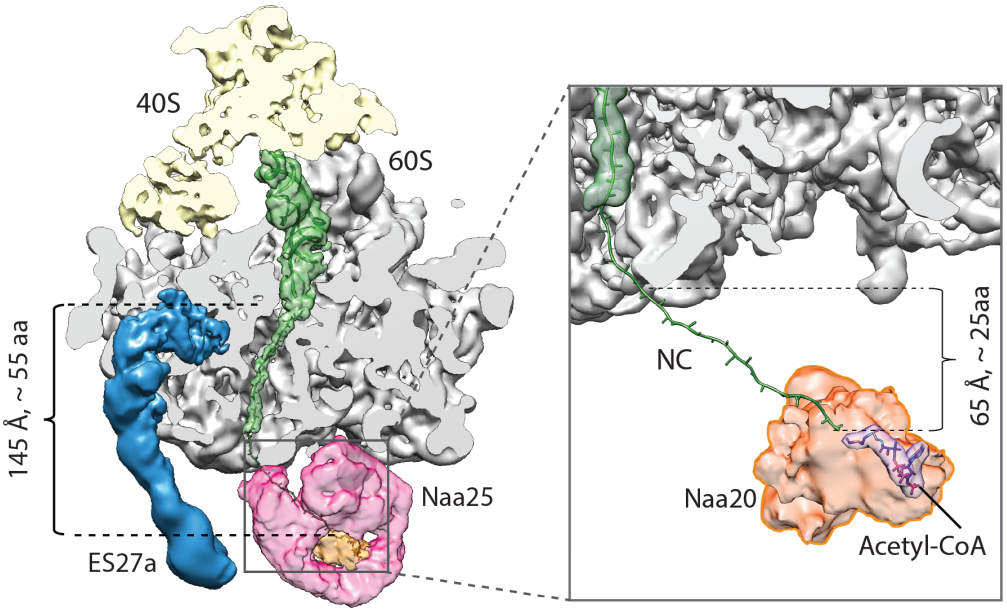

Figure 4.6: Minimum length of the NC required for acetylation by NatB. Cut view focusing on the NC and catalytic center of NatB. A minimum length of the NC (shown as Ala model) of 55aa in total, or 25aa from the TE is necessary to reach the catalytic center directly. Peptidyl-tRNA: green, Naa20: orange, Naa25: magenta, ES27a: cyan, 40S: yellow, 60S: gray.

To make comparisons easier, NatB auxiliary SU Naa25 will be shown in teal and NatB catalytic SU in pink from now on.

The interplay of NatB with other factors

Even though NatB is located more distant from the TE, NatA and NatB are overlapping to a large extent, indicating that both cannot bind at the same time without a tremendous rearrangement (fig. 4.7). This is rather unlikely, as they acetylate different substrates and there is no biochemical need for concomitant binding after substrate recognition. In contrast, Map1 and NatB do not clash when both are bound to the ribosome, but this would leave Map1 unemployed at the TE as NatB substrates get not modified by MetAPs.

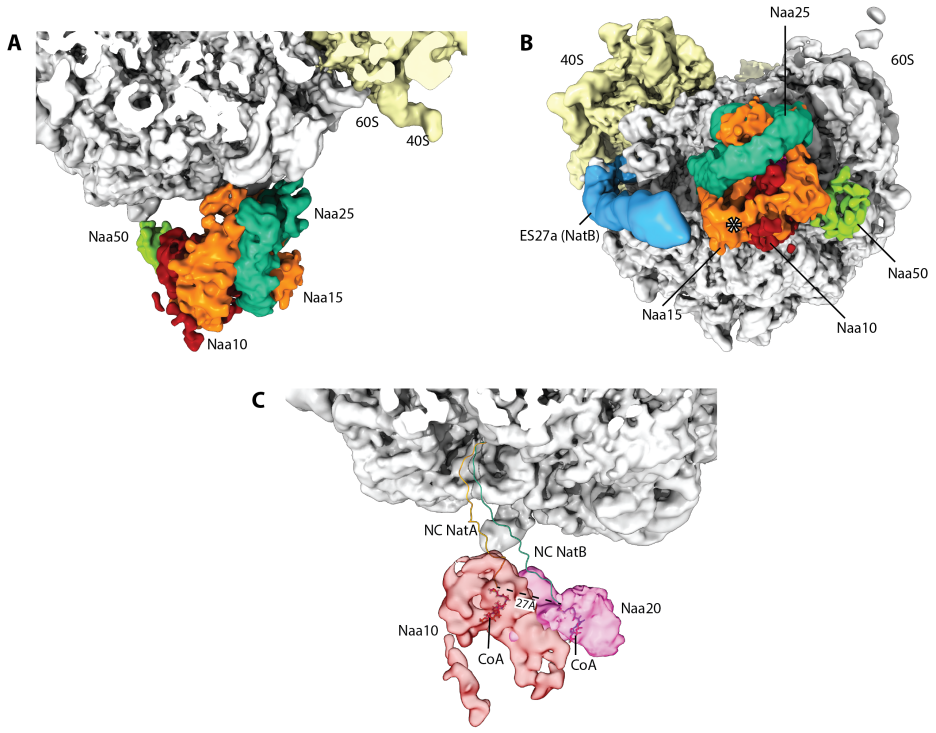

Figure 4.7: Comparison of NatA and NatB binding to the ribosome. **A**, Side view from ES27a direction showing NatB (Naa25 teal, Naa20 hidden) on the ribosome overlaid with NatA (Naa10 red, Naa15 orange, Naa50 green). Concomitant binding of both ligands is not possible as the auxiliary SUs are overlapping to a large extent. **B**, bottom view focusing the TE (asterisk) of the same composition as in A. **C**, View as in A, showing the catalytic SUs only (Naa10 red, Naa20 pink) with the model of a minimum NC length (yellow and teal respectively) that is required to reach the catalytic centers. Naa20 and Naa25 catalytic centers have a distance of about 27 Å where NatB is located farer away from the TE. The minimal length of the NC is 50 aa for NatA and 55 aa for NatB. CoA, acetyl-CoA.

Furthermore, ES27a is in a NatB specific exit positon, but in contrast to NatA or Map1 this ES is not required for anchoring NatB to the ribosome. These issues might be

explained by the second NatB (B2) that was observed in the data in addition to NatB in its primary B1 position (fig. 4.8A), but the binding of B2 needs to be evaluated carefully. Since NatB is reconstituted with a high molar excess, the second NatB might indeed only be an *in vitro* artefact and due to unspecific rRNA binding. However, there are several arguments that speak against this.

First, a pelleting assay of NatB with RNCs lacking important ES only showed a minor effect on NatB binding compared to the same experiment with NatA and Map1. As only B2 loses its interaction partner ES27a, the effect is not as severe because B1 binding is not affected and therefor not the whole binding of NatB to ribosomes abolished. This shows, that even after pelleting both NatB proteins are stably associated with the ribosome.

Structurally, B2 is inversely oriented with respect to the first NatB and its auxiliary SU interacts with ES27a. Therefore, B2 might locate ES27a in its distinct NatB exit position. Furthermore, in this arrangement B2 blocks the entire binding site below the TE not only for Map1 but also for any other exit site factor (fig. 4.8A). This would exclude an accidentally or unnecessary binding of other factors to non-suitable substrates. In addition, B2 shields the NC. In contrast to NatA that contacts H24, neither of the NatB proteins maintain a direct connection to the TE. Shielding the area below the TE by B2 creates a protective environment for the NC to find unhindered its way to the catalytic center. Notably, in both cases the TPRs of the one NatB are in close proximity of the catalytic center of the other NatB. Therefore they might support each other in guiding of the NC similar to the guiding in ABP1-NatA complexes.

However, the side where the NC enters the catalytic center of B2 is pointing away from the TE. The NC would need to leave the protected environment below the TE in the direction of ES27a and making a detour to reach into the catalytic center of B2. Therefore, the unfavorably located catalytic center of B2 argues against an executing role of the secondary NatB and it might perform a more stabilizing role for B1. Furthermore, B1 exists on the ribosome without B2, but not the other way round. This leads to the assumption that NatB in the primary position is likely responsible for acetylation. However, exit factors tend to occupy alternative binding sites if the primary is blocked. This might be another possible scenario for B2 and B1 respectively.

In conclusion, the secondary NatB seems not be an artefact of the *in vitro* set up but its final role still needs to be determined.

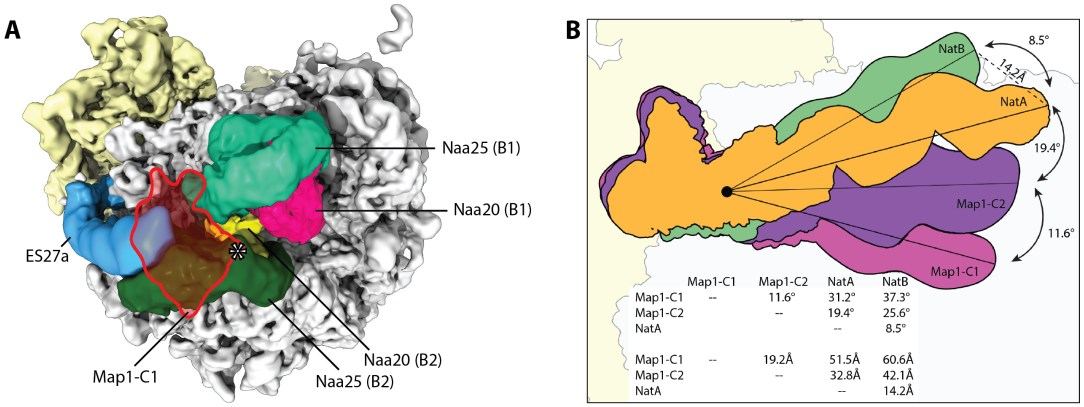

Figure 4.8: Possible blocking of the tunnel exit by a second NatB and sub-conformations of ES27a. A, Bottom view focusing on the TE (asterisk) of NatB-ribosome complexes where a second NatB (B2) is bound. NatB is shown in B1 position (auxiliary SU in teal, catalytic in pink) and in B2 position (auxiliary SU in green, catalytic in yellow), overlaid with Map1 shown as contour. **B**, Schematic overview about the positions of ES27a present in Map1 (pink and purple), NatA (orange) and NatB (green) maps with angles and distances indicated in the table below.

Possible role of ES27a as a mediator

The overall question that should be answered is the interplay of different exit site factors at the ribosomal TE. In context of NatB this question refers to the interplay of Map1, NatA and NatB. Strikingly, all three enzymes exhibit ES27a in its exit position but in each case in a specific way. This is interesting since the ribosome may be able to discriminate different exit factors based on its ES27a position.

Assuming ES27a when NatA is bound as the reference position, ES27a moves in the direction of the TE for Map1 binding but away from the TE in the opposite direction for NatB (fig. 4.8B). The shifted position of ES27a when NatB is bound enlarges the distance even more to 40 or 60 Å when Map1-C2 or Map1-C1 is bound respectively. This might be a way of the ribosome to exclude concomitant binding of Map1 and NatB.

Furthermore, NatA and NatB somehow need to check if 'their' substrate comes out of the ribosome, but without the need of concomitant binding (fig. 4.7A and B). In

an eventual screening process ES27a might function as a mediator being in a more TE-near position for the Map1/NatA pathway. Here, substrate sensing might be performed by Map1 first as it is more abundant in the cell than NATs. If Map1 recognizes its substrate, ES27a is positioned properly and allows NatA to join after iMet removal. If there is no iMet to cleave as the NC is not a substrate for Map1, Map1 would leave the TE, ES27a is not trapped in a specific subconformation and might help NatB to associate. Of course, a direct proof for this is still missing.

4.4 Coordination of exit site factors at the ribosomal tunnel exit

With the structures obtained in this thesis and discussed above, the interplay of different exit site factors including chaperones (NAC/RAC), modifying (Map1, NatA, NatB) and targeting enzymes (SRP/Sec61) can be now discussed in more detail.

In general, they all form contacts to the ribosome via electrostatic interactions to the negatively charged ribosomal RNA. Positively charged patches are present in NAC (Wegrzyn et al. 2006; Pech et al. 2010; Shen et al., 2019), NatA (Magin et al., 2017; Weyer et al., 2017a; Knorr et al., 2019), NatB (chap. 3.3.2.3), Map (Sandikci et al., 2013 for bacteria), RAC/SSb (Leidig et al. 2013; Zhang et al. 2014; Gumiero et al. 2016; Lee et al. 2016, Weyer et al., 2017b) and SRP (Becker et al., 2017). Furthermore, all discussed exit factors are binding to the ribosome independent of the NC, either by binding to non-translating vacant ribosomes (Map1, SRP, Ssb), binding to non-substrate ribosomes, meaning to ribosomes carrying any NC (NAC) or both is true for (NatA, NatB) (Map1: Nyathi and Pool, 2015; SRP: Powers and Walter, 1996; Ssb: Hanebuth et al., 2016; NAC: del Alamo et al., 2011; NatA: Gautschi et al., 2003; Knorr et al., 2019; NatB: chap. 3.3.1).

Even if it seems that all exit factors can bind at any time to the ribosome independently of the NC, it is obvious that not all factors can sit on empty ribosomes and wait for the NC to test for the presence of the correct substrate to work on. Alone for steric reasons this is not possible. Furthermore, a study where the copy number and occupancy of different exit site factors was determined and compared for empty ribosomes and randomly translating ribosomes (tab. 7, Raue et al., 2007) support this finding. It showed lower abundance of SRP and modifying enzymes (NatA, Map1, Map2) com-

pared to chaperones such as RAC or the chaperone-like NAC (Koplin et al., 2010, Kirstein-Miles et al., 2013). Chaperones exhibit high copy numbers in the cell (Finka et al., 2013) as they support folding of many proteins they tend to stay longer on the ribosome. In contrast, transient interactions are shown for bacterial Map (Sandikci et al., 2013) and are also expected for NATs (Dörfel and Lyon, 2015). This suggests the idea of a dynamic cycling of different exit factors including re-localization to alternative binding sites (Map1 chap. 3.1.2.2; NAC, Gamerdinger et al., 2019; Lin et al., 2020), a flexible nature and high on and off rates at the TE.

In this context, ES27a was suggested to function as a global coordinator of such events by possibly delivering exit site factors to the ribosome (Beckmann et al., 2001). Recent studies and this thesis are in agreement with this prediction. Contrary to deletion studies showing the absence of the entire expansion segment ES27 being lethal (Sweeney et al., 1994), it has been uncovered that deleting only the flexible part of ES27, namely ES27a, is not lethal in yeast (Fujii et al., 2018; Shankar et al., 2020). Notably, a ES27a deletion strain does not even show any growth phenotype under normal conditions (Shankar et al., 2020). However, two studies investigated independently that N-terminal processing of the NC is influenced upon ES27a deletion in yeast (Fujii et al.,2018; Shankar et al., 2020). In more detail, Map1, Map2, NatA and NatB were all shown to be less associated with ribosome ΔES27a strains based on quantitative MS and additional polysome mRNA-Seq analysis (Fujii et al.,2018; Shankar et al., 2020). That ES27a deletion strains showed a de-enrichment of Map1 on ribosomes is in agreement with our *in vitro* study indicating a significant decrease of Map1 binding when ES27a was removed by an RNase I treatment (chap. 3.6). This highlights again that our *in vitro* approach matches with the published *in vivo* data. It is not surprising that in the same studies NatA is downregulated together with Map1 as these processes are dependent on each other. NatA binding is also dependent on the presence ES27a but also additionally on ES39a and ES7a (chap. 3.2.2.2), but it would lack substrates when the iMet is not removed because of improper Map1 association with the ribosome. Furthermore, the absence of ES27a coincides with an increase of mRNAs encoding for proteins involved in folding and targeting, e.g. specific chaperones or ER proteins and an increased protein aggregation tendency (Shankar et al., 2020). In the light of the results of this thesis, this makes sense, as NME and NTA

are wide spread protein modifications that are impeded by the removal of ES27a.

In conclusion, the idea of ES27a being responsible for factor recruitment to the ribosome is emphasized with this new data and this work proves first evidence for this hypothesis on a structural basis. It shows how three early exit site factors, Map1, NatA and NatB are coordinated below the tunnel exit by ES27a that adopt distinct sub-conformations dependent on the factor bound (fig. 4.8B). Notably, ES27a moves almost 40° between its extreme positions showing for the first time its high mobility within the general exit position. However, it remains to be clarified whether ES27a delivers the factors actively to the TE or whether the position of ES27a only passively correlates with the position of the factors.

Table 7: Ribosome occupancy and concentration of exit site factors. Molecules per cell as well as the occupancy to non-translating and randomly translating ribosomes were determined in a logarithmically growing yeast cell culture measured as his-tagged proteins by quantitative immunoblotting (Raue et al., 2007). For comparison, the copy number of exit factors measured by quantitative mass-spectrometry are shown in the right column (Kulak et al., 2014). EGD2 and EGD1 are coding for α- and β-NAC SUs; for SRP, the core component of the signal recognition particle SRP68 was used; for NatA copy numbers for all three subunits are shown separately. n.d., not detected.

	Molecules/cell	non-translating ribosomes	Randomly translating ribosomes	Molecules/cell according to Kulak et al., 2014
ribosomal particles	310,000			
NAC	400,000	88%	89%	208,442 (EGD2)/ 135,399 (EGD1)
Ssb1/2	280,000	15%	30%	17,606/356,434
RAC	90,000	19%	35%	45,188 (Zuo)/ 59,449 (Ssz)
Map1	20,000	2%	4%	22,474
SRP	8,000	n.d.	1%	8,622 (SRP68)
NatA	7,500	2%	4%	6,445 (Naa15)/ 3,740 (Naa10)/ 9,455 (Nasa50)
Map2	6,000	1%	2%	5,248

Taking everything together, a unifying model of the possible coordination of exit factors binding around TE can be described now on a structural basis (fig. 4.9).

First, the earliest interacting factor NAC (Wiedemann et al., 1994) binds to the ribosome. For subsequent acetylation by NatA, NAC needs to dissociate to free the space for Map1 at the TE. Hereby, Map1 coincides with ES27a in its exit position. Dependent on its conformation, Map1 can either stay on the ribosome once NatA binds, or a sequential binding of Map1 and NatA is orchestrated by ES27a. Upon NatA binding, ES27a rearranges into its NatA position to provide a triangular arrangement of three expansion segments for a dynamic association of NatA with the ribosome. It seems that there is a competition between the Map1/NatA pathway and SPR and RAC in accessing the TE. Concomitant binding of both factors with NatA is not possible for steric reasons. The secretory pathway by SRP and Sec61 would exclude acetylation by NATs on a structural basis as these factor would clash at the TE. In addition *in vivo* and *in vitro* experiments of acetylated and non-acetylated N-termini used to monitor ER targeting showed that N-terminal processing inhibits translocation into the ER and therefore anti-correlates protein targeting with NTA (Forte et al., 2011). Furthermore, N-terminal processing in general should be a fast event. In yeast, translation speed is at about 10 aa per second (Boven and Gullov, 1979). Assuming an average protein size of 467 aa (Harrison et al., 2003), the majority of proteins get synthesized in less than a minute, meaning that N-terminal modifications need to be completed before. Therefore, it is likely, that chaperones such as RAC or other Hsp70-like proteins are binding after NatA dissociated to support further protein maturation and folding.

On the other hand, NAC and SRP or Sec61 cannot bind at the same time. It has been shown that NAC prevents unspecific association of Sec61 and mistargeting and therefore regulates co-translational protein transport to the ER (Gamerdinger et al. 2015, Möller et al., 1998). Having NAC bound as the earliest interactor it would need to leave upon SRP binding. As rebinding of NAC seems to be possible later on (Zhang et al., 2012; Nyathi and Pool, 2015), a dynamic binding and re-localization of NAC fits to the concept of flexibility of most of the exit factors.

Cross-linking studies with NAC and the chaperone RAC suggest simultaneous binding (Nyathi and Pool, 2015) that could be confirmed on a structural basis (Gamerdinger

et al., 2019; Zhang et al., 2014; fig. 4.9).

Based on the structures presented here, NatB (as B1) and NAC do not share the same binding sites and would be able to bind concomitantly. NAC could in principle stay on the ribosome after NatB joined and might support folding, guiding of the NC or shielding the NC from unwanted cytosolic interactions. Exactly like NatA, NatB would need to leave the ribosome before RAC can associate and also negatively affect SRP-dependent targeting (Forte et al., 2011). The potential second NatB binding site would block the entire TE and exclude any other factor to bind at the same time when the both NatB proteins are present (fig. 4.9, table).

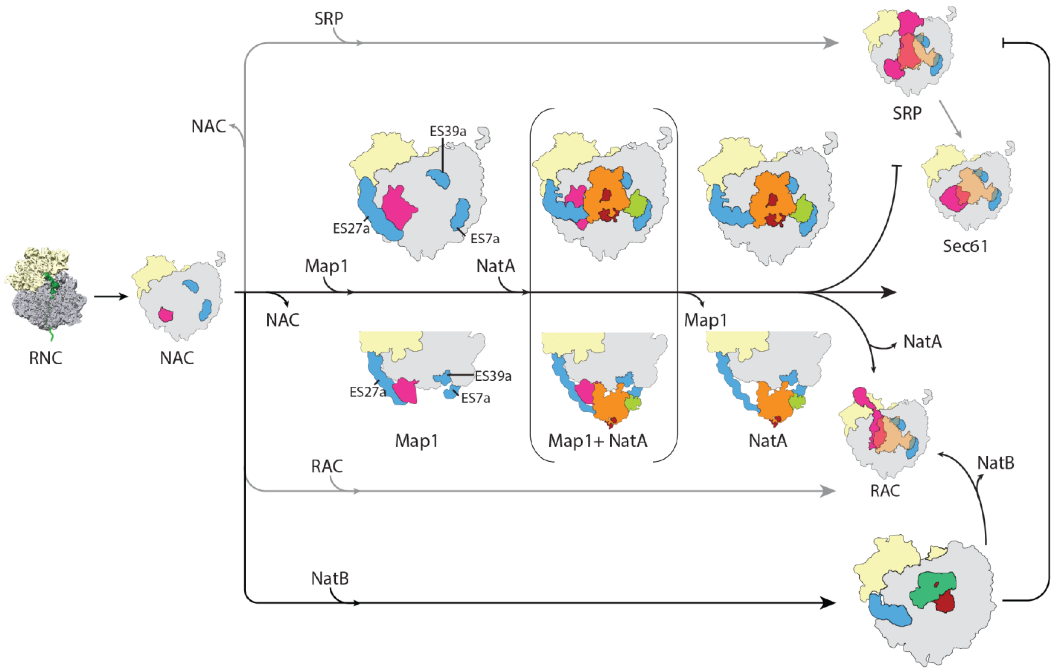

	NAC	NAC_{alt}	Map	NatA	NatB	$NatB_{B2}$	RAC	SRP
NAC	-	-	X	V	V	X	V	X
NAC_{alt}	-	-	X	P	P	X	P	X
Map	X	X	-	P	P	X	X	X
NatA	V	P	P	-	X	X	X	X
NatB	V	P	P	X	-	-	X	X
$NatB_{B2}$	X	X	X	X	-	-	X	X
RAC	V	P	X	X	X	X	-	P
SRP	X	X	X	X	X	X	P	-

Figure 4.9: The interplay of different exit site factors. Schematic representation of NAC, Map1, NatA, NatB, RAC, SRP and Sec61 bound to the translating 80S ribosome in the front or bottom view and in comparison with NatA and NatB binding sites (top). For NAC the primary binding site is shown, Map1 is shown in Map1-C1 conformation. EMDB used for comparisons: 1651 (Sec61), 2844 (SRP), 6105 (RAC), 0202 (NatA).
A matrix (bottom) shows all possible combinations indicating if simultaneous binding is possible (V), not possible (X) or partially possible (P, only minimal overlap, binding is possible assuming flexibility of ligands). NAC_{alt}, alternative binding found in context with TTC5 protein (EMDB 10380, Lin et al., 2020); $NatB_{B2}$, having the potential second NatB bound in addition (chap. 3.3.2.4).

5 Conclusion and outlook

Protein synthesis happens on the ribosome where the growing polypeptide chain emerges through the ribosome peptide exit tunnel into the cytosol. During this phase multiple protein factors bind either to the area surrounding the TE and/or interact with the NC directly. They are all associated with the ribosome and support folding (chaperones such as RAC or the chaperone-like NAC), perform N-terminal processing of the NC (Map1, NatA, NatB) or act as targeting factors to the ER (SRP/Sec61). This thesis gives a more detailed insight into the spatial and temporal coordination of these exit factors in yeast.

The focus of this work was on the early interactors which are responsible for early processing of the NC. iMet excision by methionine aminopeptidases and N-terminal acetylation belong to the most abundant co-translational protein modifications and start to happen at the stage when the NC has an approximate length of 40-55 aa and has left the ribosomal peptide exit tunnel.

The binding of these modifying enzymes and other exit site factors to the ribosome can be summarized under the keyword of flexibility. Map1, NatA and NatB have in common that the very mobile ES27a is placed in its exit position. Map1 and NatA both directly bind to ES27a, which turns out to be a crucial interaction partner for ribosome binding. NatB interacts only with ES27a when a second NatB protein is present. Depended on the enzyme bound, ES27a adopts defined sub-conformations and seems to serve as the coordinator of these factors. In total, it moves by about 40° starting from its first Map1 position over to its NatA and then NatB position. It is likely, that this regulates factor binding to the TE. For example, ES27a in NatB position is too far away to be bound by Map1. This would exclude Map1 binding for NME that is not necessary for NatB acetylation. In addition, different exit factors have been shown to adjust their binding position if other factors are present or their primary binding site is blocked (chap. 4.1; Bhakta et al., 2019; Gamerdinger et al., 2019; Lin et al., 2020). The interaction of the early exit factors with the mobile ES27a might allow them to change their position further and supports the idea of a general flexible

binding and a dynamic cycling of exit factors at the TE. Furthermore, for interactions of NATs with the ribosome, unexpectedly mainly rRNA is involved in binding. Here, electrostatic interactions of the auxiliary subunits with the ribosome support a flexible and transient binding mode.

Coming back to the spatial and temporal orchestration of exit site factors, three pathways can be defined. The chaperone pathway via RAC, a separate targeting pathway (SRP/Sec61) and another pathway for NTA via Map1/NatA or NatB alone. A sequential handover is only possible for NTA and RAC. SRP and NTA pathway exclude each other on a biochemical as well as structural basis. In contrast, the chaperone-like NAC seems to fulfill its task as the earliest interactor and might precede all other pathways. The question if Map1 and NatA bind simultaneously or sequentially did not lead to a final answer. Furthermore, if NatB binds as a single NatB or as a dimer could not be answered. More research would need to be done to finalize the interplay of exit factors whilst considering their flexibility.

In case of Map1, the structure on the ribosome was obtained via a native pull out but the sample needed to get cross-linked in order to stabilize Map1 on the ribosome. Here, additional structural studies in combination with NatA and NatB might give further insights into the coordination of these factors and their possible concomitant binding. Especially the position of ES27a that might be able to engage an intermediate position to the defined ones found in this studies, would be interesting and would contribute to the understating of flexible binding.
For NatB a subsequent step would be to get the ribosome binding SU tagged for a native pull out and to answer the question about the potential second binding site of NatB and if one or two NatB proteins are associated with the ribosome *in vivo*. The challenge will be to find the right tag on an appropriate position to co-purify both NatB SUs with the ribosome as Naa25 C-terminus for sure and N-terminus likely is involved in ribosome binding.
In general, further studies on a structural as well as biochemical basis would get additional insights about simultaneous binding and interactions of more exit factors, including possible rebinding as proposed for NAC (Zhang et al., 2012). Suitable substrates would be needed for *in vitro* studies that complies with the different requirements of diverse factors. In addition, ribosome profiling data would supplement

these results.
Moreover, continuing work on higher eukaryotes or especially humans to study NTA on a structural basis, might help to fight against diseases that are linked to a malfunction or misregulation of NATs. However, the human system is more complex and for example expansion segments are way longer than in yeast. The expected even greater flexibility of ESs and binding factors will be challenging for structural studies.

In summary, structure and localization of Map1, NatA and NatB gives a new starting point to study co-translational exit site factor coordination in yeast and the interplay at the TE further. In addition, it provides the basis for additional research that can be extended to the human system where especially NTA is linked to various types of diseases and cancer.

Appendix

Secondary structure of the 28S rRNA of *S. cerevisiae*

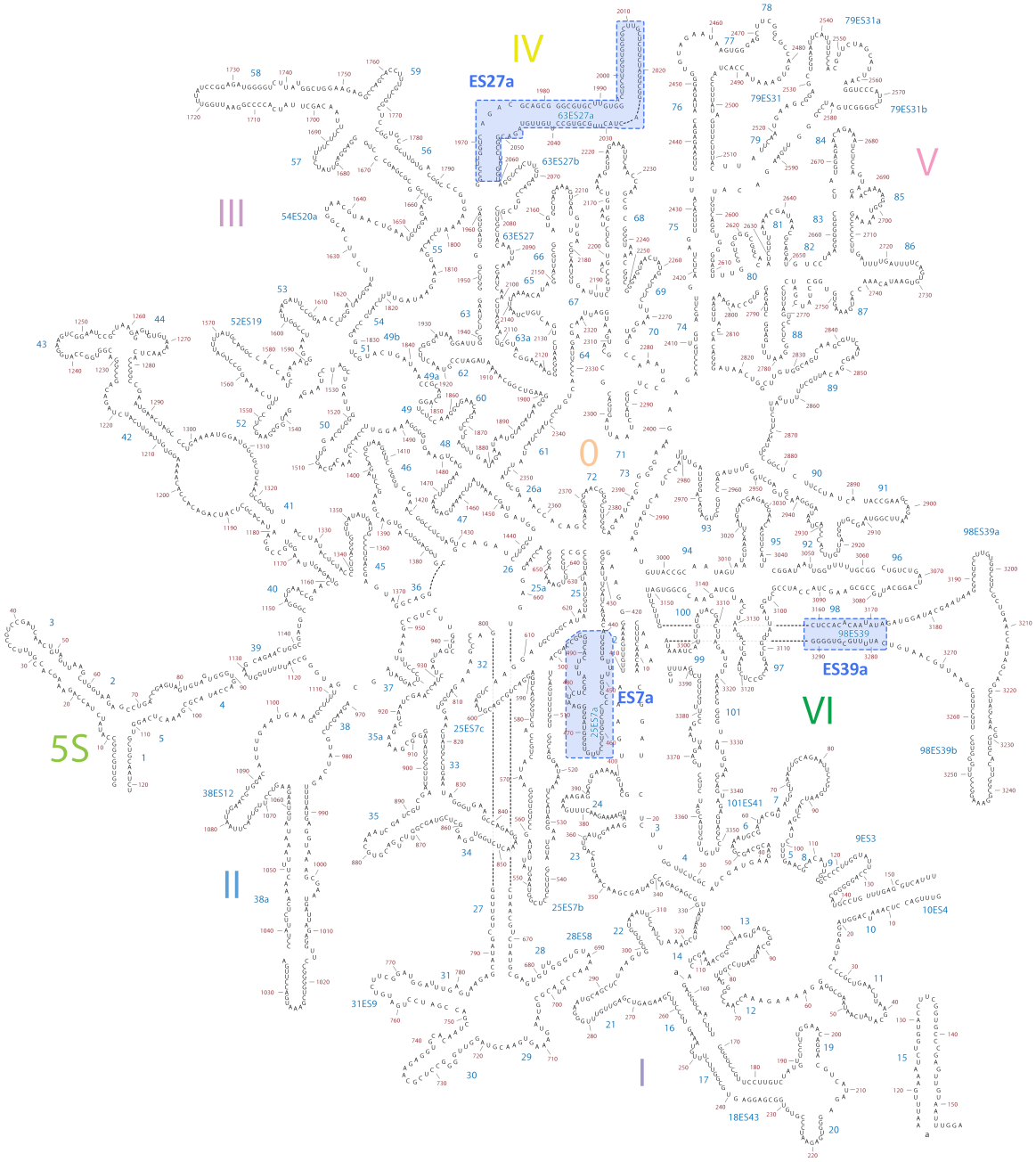

Expansion segments ES7a, ES27a and ES39a are labeled in blue. Adopted form http://apollo.chemistry.gatech.edu/RibosomeGallery/.

Exit site factors and their binding sites to the ribosome (extended)

Figure is on the next page. Exit view of the ribosome and binding sites of exit site factors, extended by the results of this thesis (Knorr et al., 2019 for NatA), otherwise according to p. 9.

A

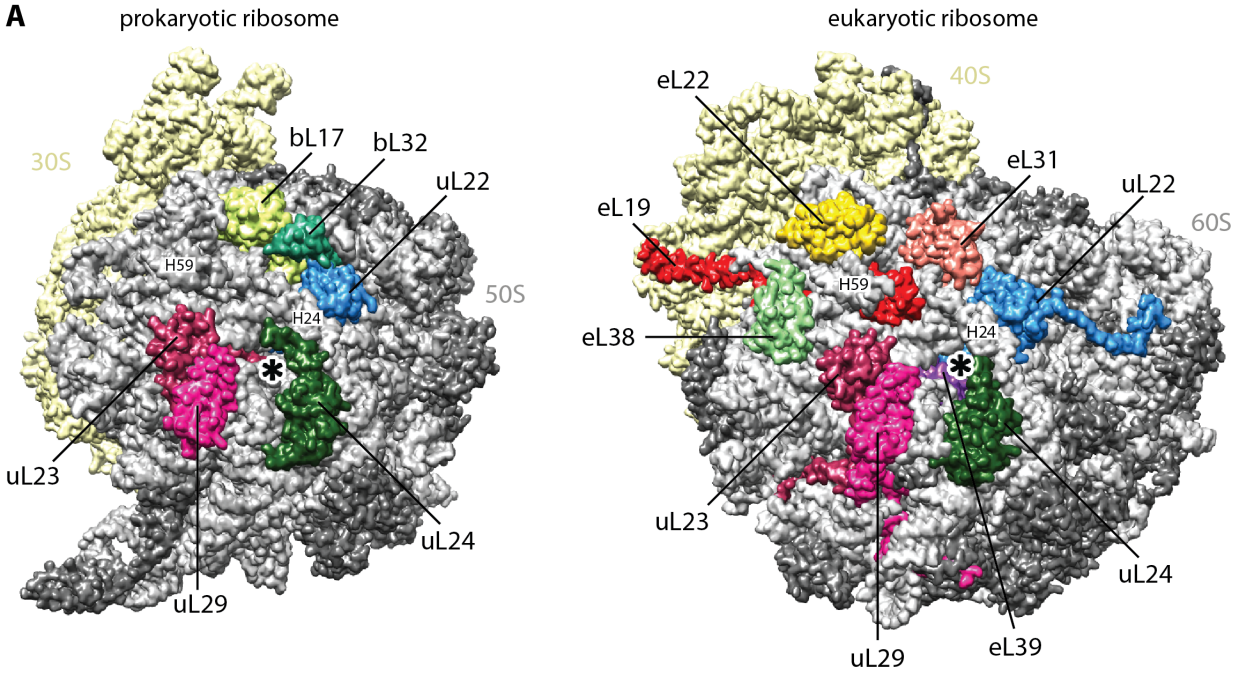

B

exit site factors	NC length	effect on NC	major ribosomal proteins involved	major ribosomal RNA involved
PDF	45-50 aa	deformulation of fMet	uL22, bL32	H24
MAP	40-45 aa	iMet cleavage	uL23/uL29, uL22/eL31, eL19, bL32, bL17	H59, ES27
NatA	> 50 aa	acetylation of N-terminus	--	H24, ES7a, ES27a, ES39a
NatB	> 55 aa	acetylation of N-terminus	eL31	H94/98, H100/101
NAC	~ 30 aa	chaperone-like	uL23/uL29; eL31, uL22; eL39, eL19	H59
RAC/Ssb	40-45 aa	chaperone	eL22, eL31; Ssb: uL29, eL19, eL39	H59, H24, es12/h44
SRP	~30 aa	translocation/secretory pathway	uL23/uL29	H59, H24

Nomenclature of N-terminal acetyltransferases

Table showing the new nomenclature and alternative names for NATs with the uniprot accession number indicated. Adopted from Polevoda et al., 2009.

NAT	Primary name	Synonyme	Yeast (uniprot)	Human (uniprot)
NatA	Naa10	Ard1p; TE2	P07347	P41227
	Naa11	Ard2p	-	Q9BSU3
	Naa15	Nat1p; NARG1; NATH; TBDN	P12945	Q9BXJ9
	Naa16	Nat2p; NARG1L	-	Q6N069
NatB	Naa20	Nat3p; hNat5p	Q06504	P61599
	Naa25	Mdm20p; p120	Q12387	Q14CX7
NatC	Naa30	Mak3p; hNat12p	Q03503	Q147X3
	Naa35	Mak10p; hEGAP	Q02197	Q5VZE5
	Naa38	Mak31p; hLsm8p	P23059	O95777
NatD	Naa40	Nat4p; hNat11p	Q04751	Q86UY6
NatE	Naa50	Nat5p; hNat13p; San	Q08689	Q9GZZ1
NatF	Naa60	Hat4, Nat15	-	Q9H7X0
NatG	Naa70	AtNaa70	-	-
NatH	Naa80	Fus2, Nat6	-	Q93015

TPRs and secondary structure diagram for Naa15

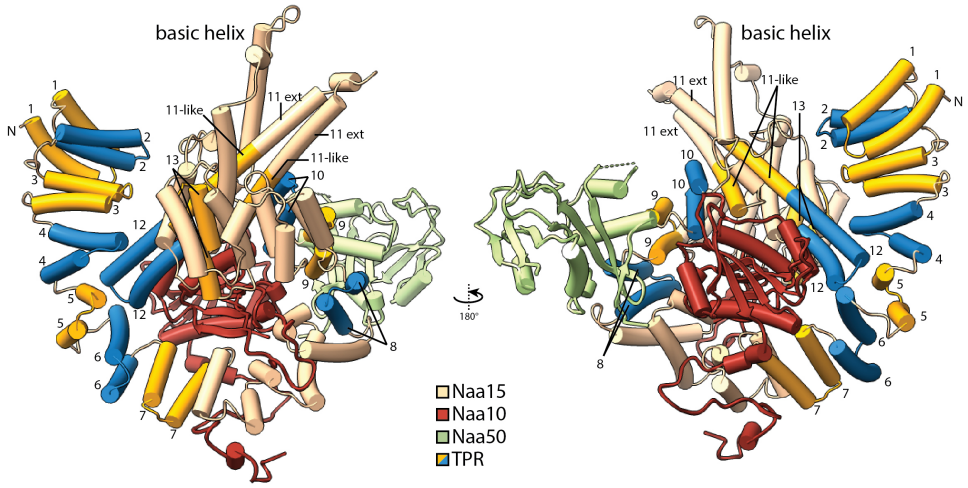

Overview of the ribosome-bound NatA structure. *S. cerevisiae* Naa15 is shown in beige, except for the 13 TPR motifs displayed alternating in yellow and blue and numbered according to Liscszak et al. 2013 (PDB 4KVM). TPR 11 is not a canonical TPR; instead, it shows extended α-helices and is therefore labeled with 11-like and 11 ext for extended. Naa10 is shown in red and Naa50 is shown in green.

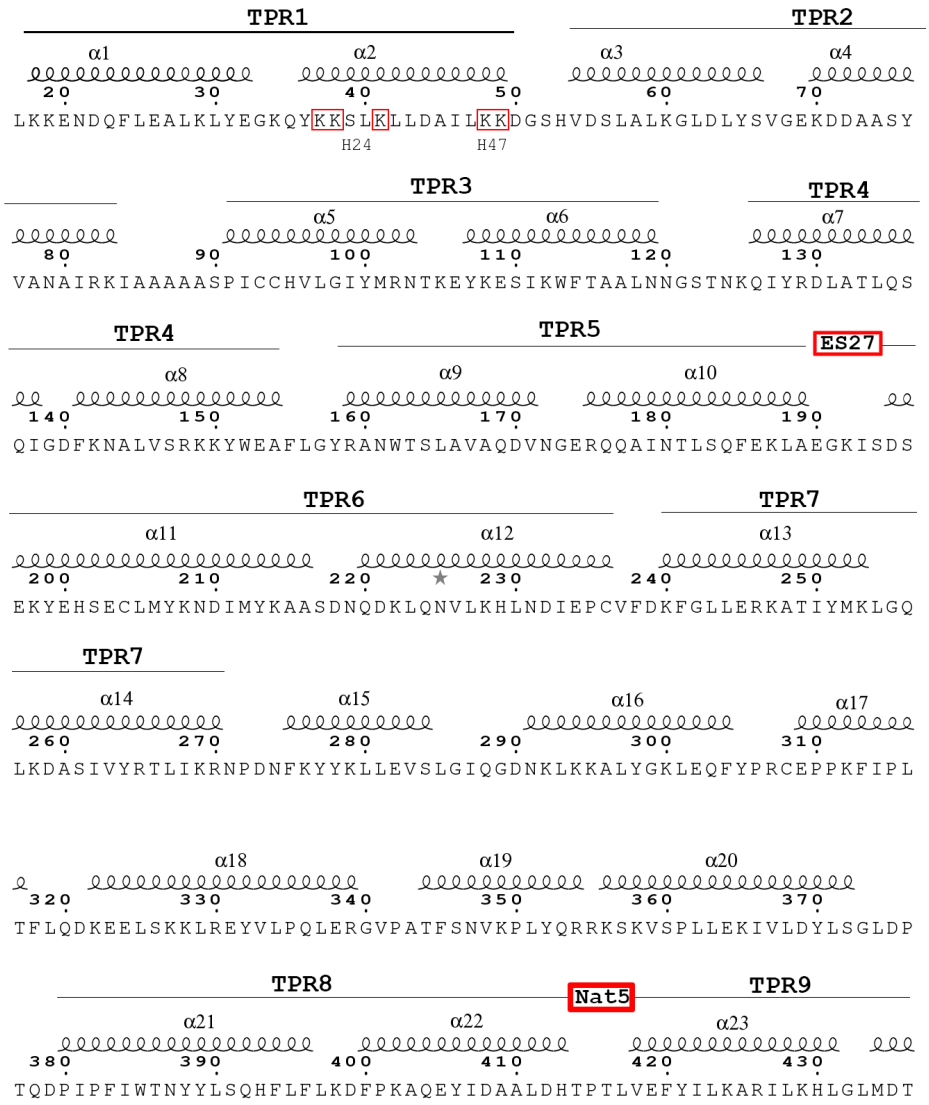
TPR1
TPR2
α1
α2
α3
α4
20
30
40
50
60
70
LKKENDQFLEALKLYEGKQYKKSLKLLDAILKKDGSHVDSLALKGLDLYSVGEKDDAASY
H24
H47
TPR3
TPR4
α5
α6
α7
80
90
100
110
120
130
VANAIRKIAAAAASPICCHVLGIYMRNTKEYKESIKWFTAALNNGSTNKQIYRDLATLQS
TPR4
TPR5
ES27
α8
α9
α10
140
150
160
170
180
190
QIGDFKNALVSRKKYWEAFLGYRANWTSLAVAQDVNGERQQAINTLSQFEKLAEGKISDS
TPR6
TPR7
α11
α12
α13
200
210
220
230
240
250
EKYEHSECLMYKNDIMYKAASDNQDKLQNVLKHLNDIEPCVFDKFGLLERKATIYMKLGQ
TPR7
α14
α15
α16
α17
260
270
280
290
300
310
LKDASIVYRTLIKRNPDNFKYYKLLEVSLGIQGDNKLKKALYGKLEQFYPRCEPPKFIPL
α18
α19
α20
320
330
340
350
360
370
TFLQDKEELSKKLREYVLPQLERGVPATFSNVKPLYQRRKSKVSPLLEKIVLDYLSGLDP
TPR8
Nat5
TPR9
α21
α22
α23
380
390
400
410
420
430
TQDPIPFIWTNYYLSQHFLFLKDFPKAQEYIDAALDHTPTLVEFYILKARILKHLGLMDT

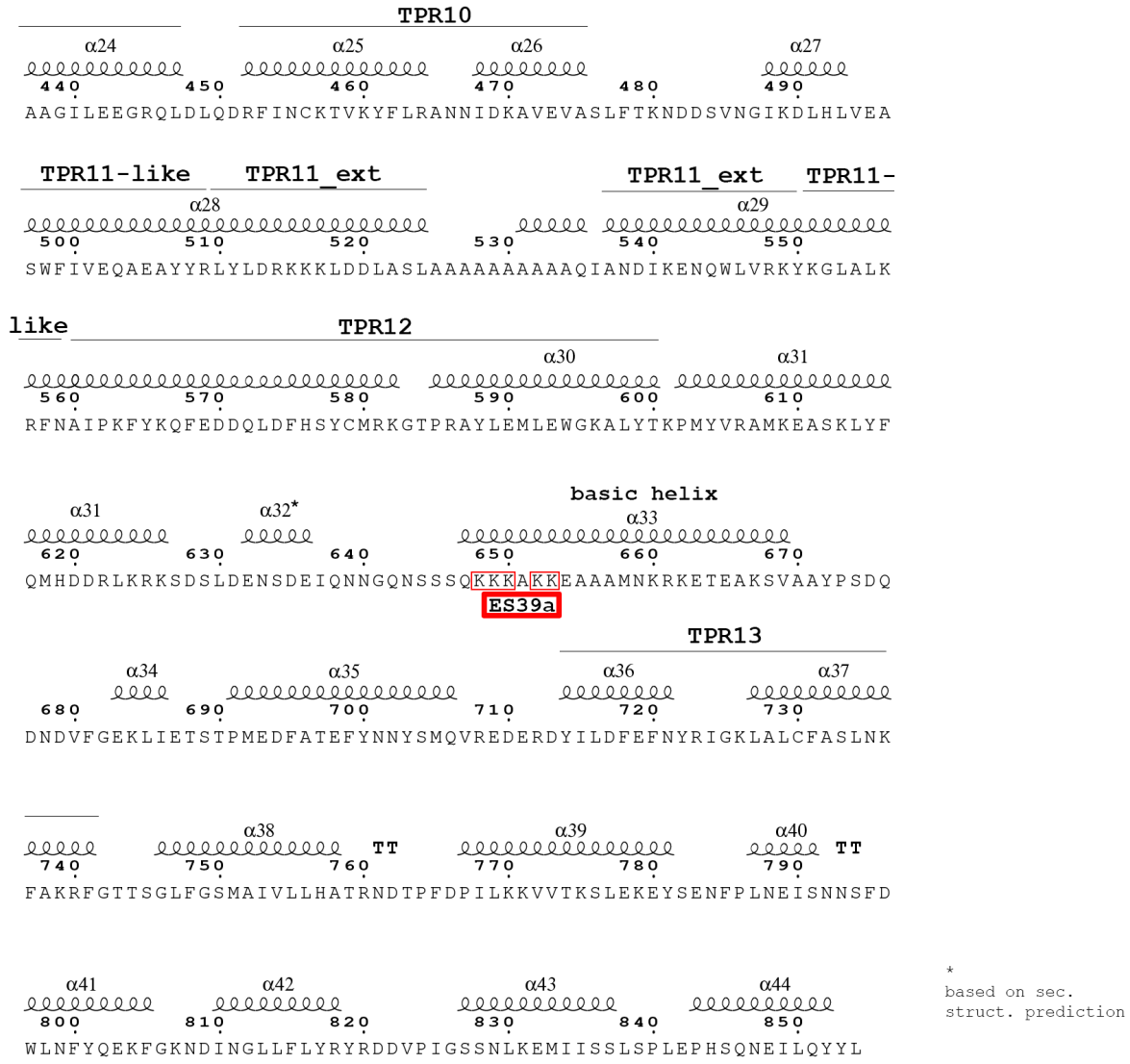

Secondary structure diagram for Naa15. TPR motifs anre indicated and numbered. Interaction sites of Naa15 with ES27a, ES39a and Naa50 are shown as red boxes.

Secondary structure alignment of NatA, NatB and NatC auxiliary subunits

Results colour-coded for secondary structure

The current colourscheme of the alignment is for **secondary structure type**.

The 3-state (H, E C) secondary structure for each sequence is represented by a colour. If a sequence in the alignment has no colours assigned, this means that either there is no DSSP information available (if this was requested), or that no prediction was possible for that sequence (if this was requested).
The colour assignments are:

HELIX (H) STRAND (E) You have selected to perform secondary structure prediction using **DSSP** (Kabsch and Sander, 1983) and **PSIPRED** (Jones, 1999).

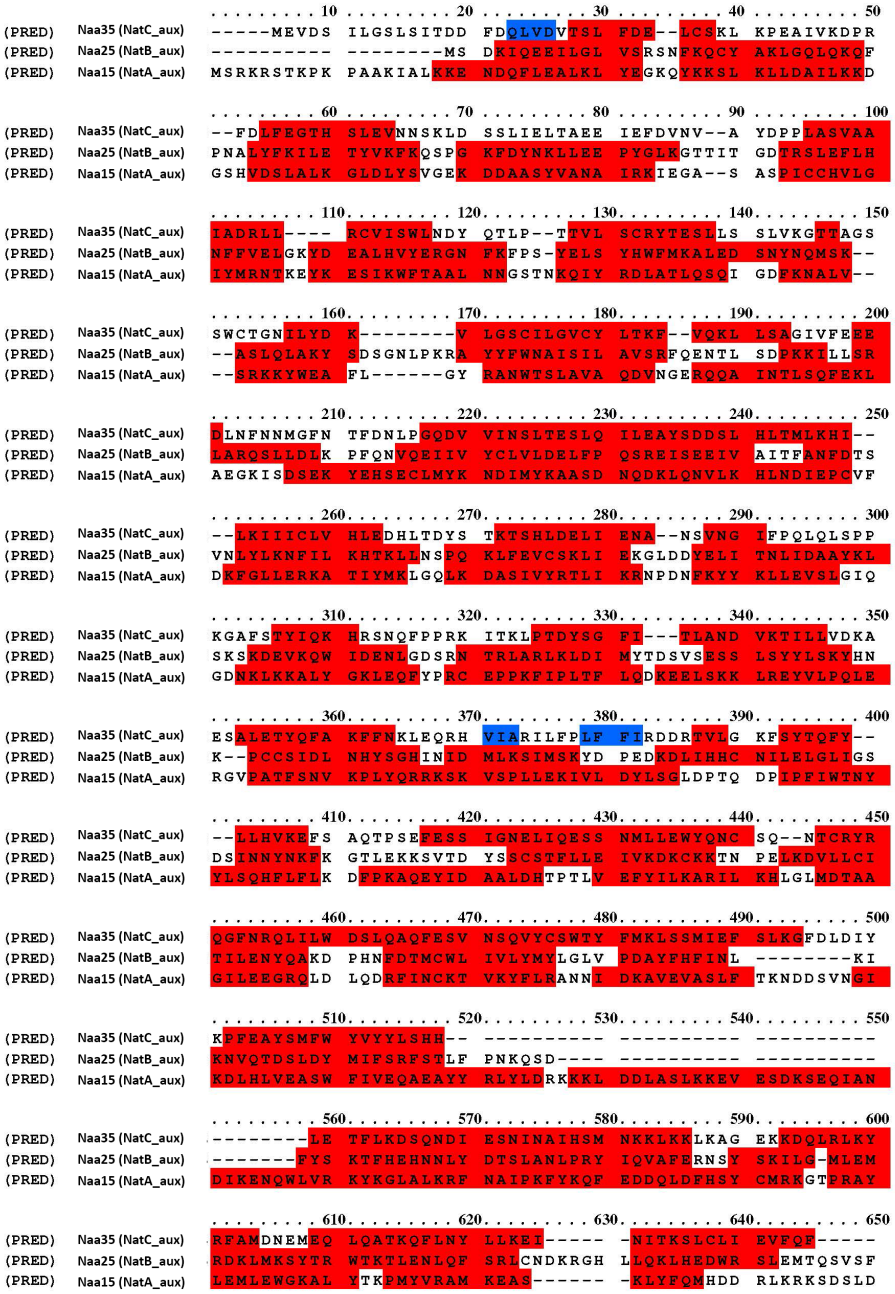

Secondary structure alignment of NatA, NatB and NatC auxiliary subunits. Naa15 (NatA), Naa25 (NatB) and Naa35 (NatC) were alinged using praline (http://www.ibi.vu.nl/programs/pralinewww/) and alignedment was colored according to secondary structure elements.

Plasmid maps

pEX-A2

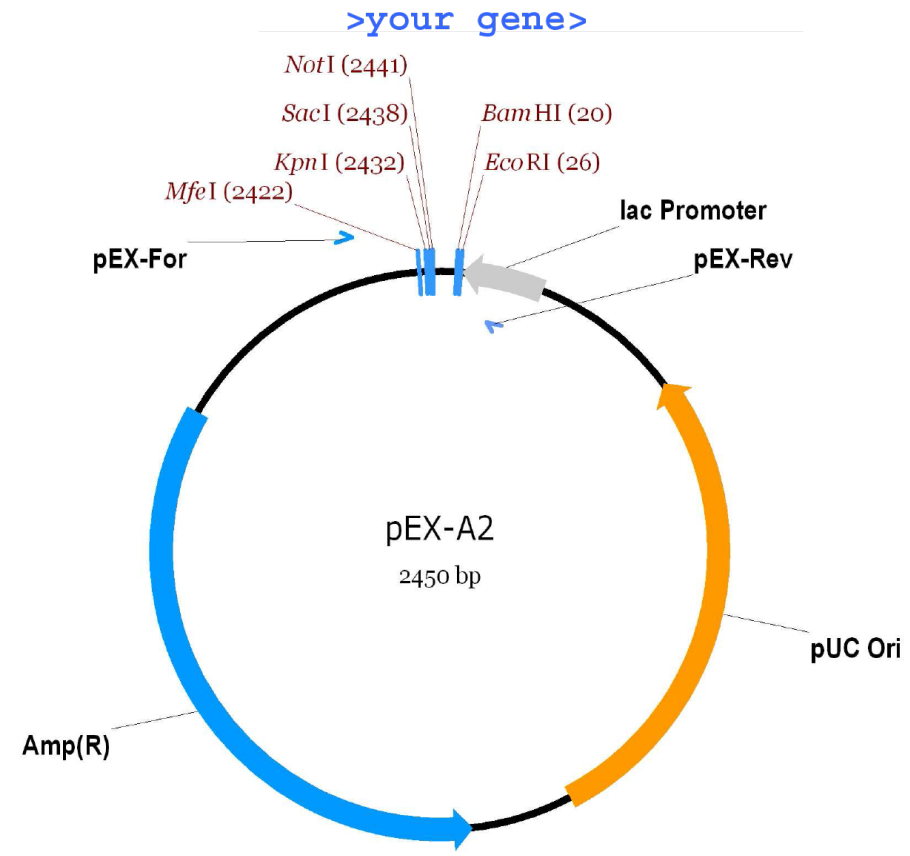

MCS: GGAGCAGACAAGCCCGTCAGGGCGCGTCAGCGGGTGTTGGCGGGTGTCGGGGC TGGCTTAACTATGCGGCATCAGAGCAGATTGTACTGAGAGTGCACcaattgGG TAC-CgagctcGCGGCCGCAAGC>your_gene>ACCTGCTTTTGCTCGCTTgg atccGAATTC-CTGTGTGAAATTGTTATCCGCTCACAATTCCACACAACATACG AGCCGGAAG-CATAAAGTGTAAAGCCTG

pEX-A128

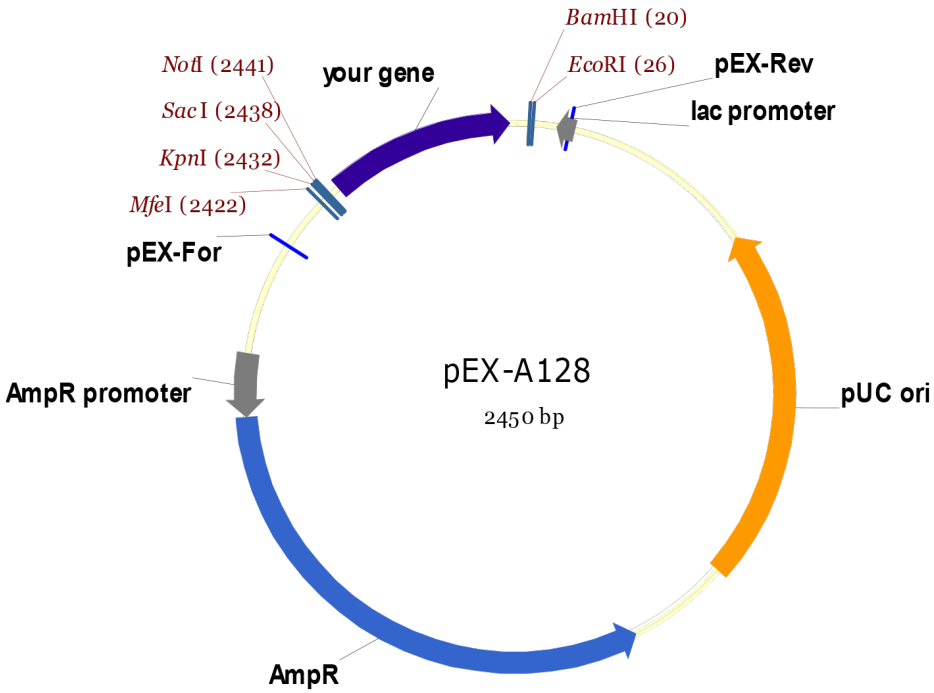

GGAGCAGACAAGCCCGTCAGGGCGCGTCAGCGGGTGTTGGCGGGTGTCG GGGCTG-GCTTAACTATGCGGCATCAGAGCAGATTGTACTGAGAGAAAGG caattgGGTAC-CgagctcGCGGCCGCAAGC>your_gene>ACCTGCTT TTGCTCGCTTGGATCCgaattcAAAG-GTGAAATTGTTATCCGCTCACAA TTCCACACAACATACGAGCCGGAAGCATAAAGT-GTAAAGCCTG

pETDuet-1

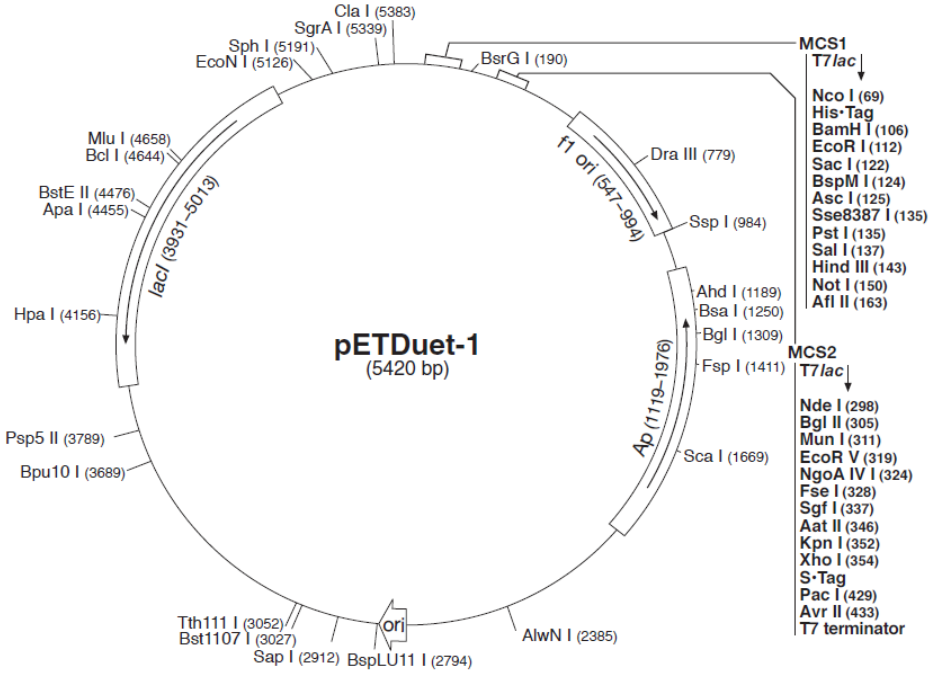

pRSFDuet-1

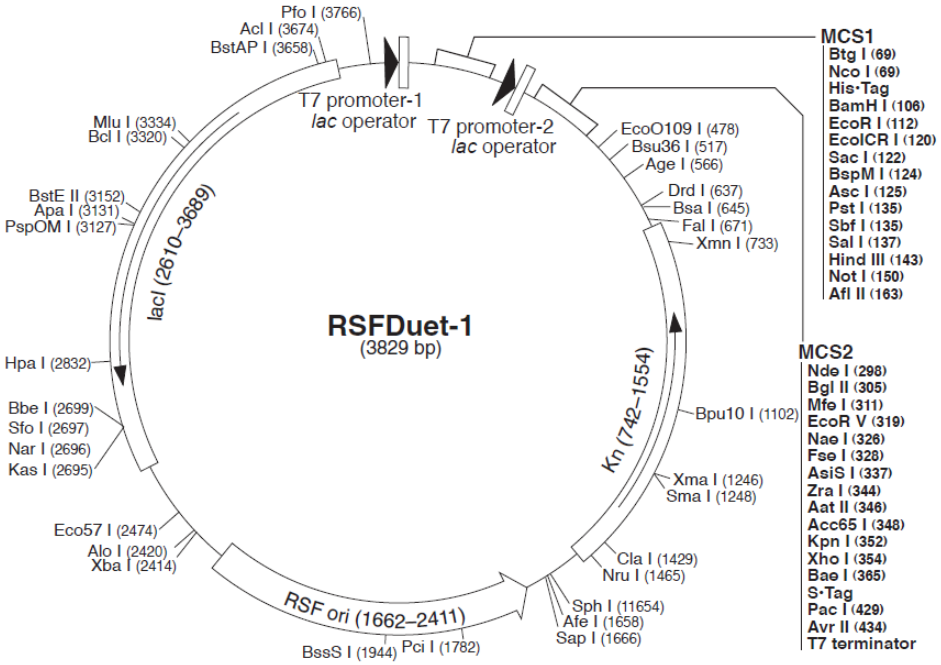

pET28a

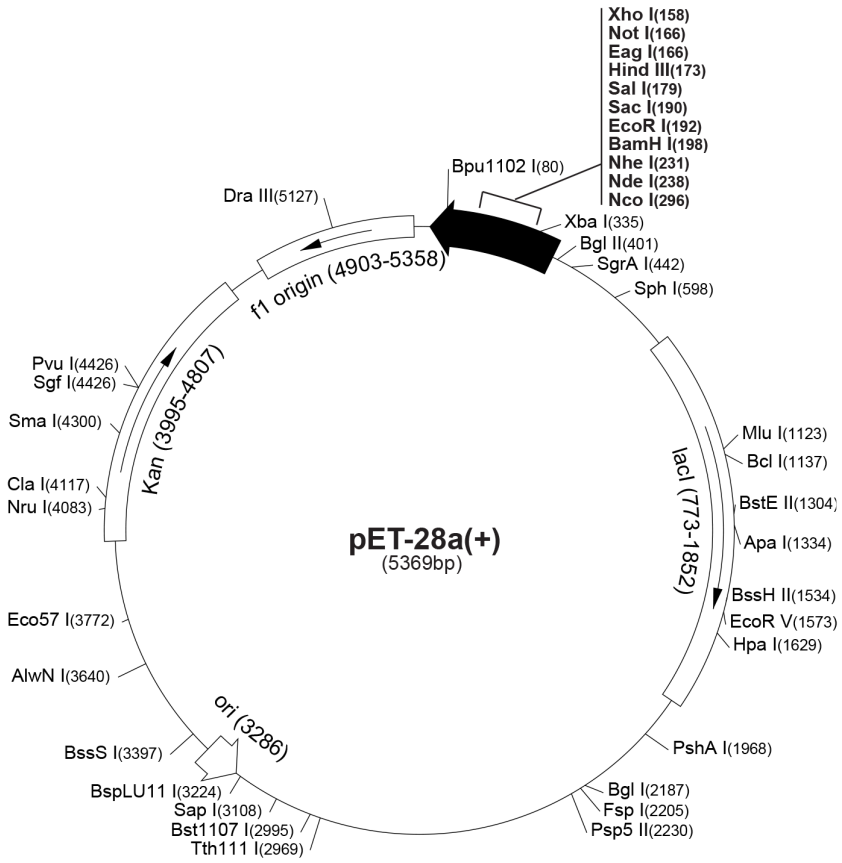
Xho I(158)
Not I(166)
Eag I(166)
Hind III(173)
Sal I(179)
Sac I(190)
EcoR I(192)
BamH I(198)
Nhe I(231)
Nde I(238)
Nco I(296)
Bpu1102 I(80)
Xba I(335)
Bgl II(401)
SgrA I(442)
Sph I(598)
Mlu I(1123)
Bcl I(1137)
BstE II(1304)
Apa I(1334)
BssH II(1534)
EcoR V(1573)
Hpa I(1629)
PshA I(1968)
Bgl I(2187)
Fsp I(2205)
Psp5 II(2230)
Tth111 I(2969)
Bst1107 I(2995)
Sap I(3108)
BspLU11 I(3224)
BssS I(3397)
AlwN I(3640)
Eco57 I(3772)
Nru I(4083)
Cla I(4117)
Sma I(4300)
Sgf I(4426)
Pvu I(4426)
Dra III(5127)
f1 origin (4903-5358)
Kan (3995-4807)
lacI (773-1852)
ori (3286)
pET-28a(+)
(5369bp)

pET21a

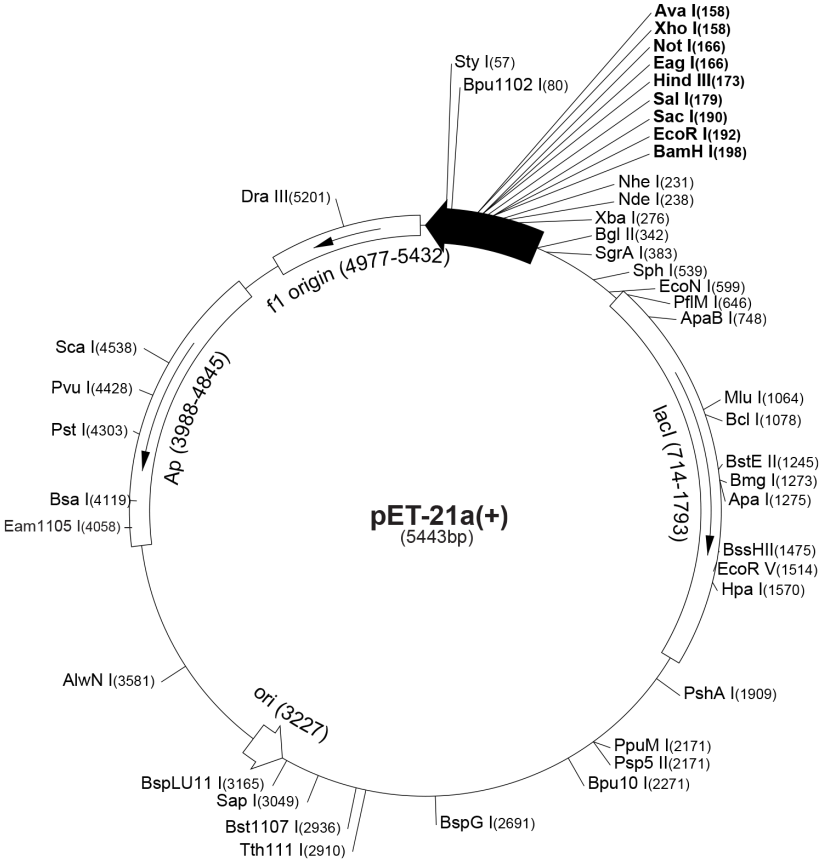
Ava I(158)
Xho I(158)
Not I(166)
Eag I(166)
Hind III(173)
Sal I(179)
Sac I(190)
EcoR I(192)
BamH I(198)
Sty I(57)
Bpu1102 I(80)
Nhe I(231)
Nde I(238)
Xba I(276)
Bgl II(342)
SgrA I(383)
Sph I(539)
EcoN I(599)
PflM I(646)
ApaB I(748)
Dra III(5201)
f1 origin (4977-5432)
Sca I(4538)
Pvu I(4428)
Pst I(4303)
Ap (3988-4845)
Bsa I(4119)
Eam1105 I(4058)
pET-21a(+)
(5443bp)
lacI (714-1793)
Mlu I(1064)
Bcl I(1078)
BstE II(1245)
Bmg I(1273)
Apa I(1275)
BssHII(1475)
EcoR V(1514)
Hpa I(1570)
PshA I(1909)
PpuM I(2171)
Psp5 II(2171)
Bpu10 I(2271)
BspG I(2691)
AlwN I(3581)
ori (3227)
BspLU11 I(3165)
Sap I(3049)
Bst1107 I(2936)
Tth111 I(2910)

Uncropped gels

Map1 binding assays

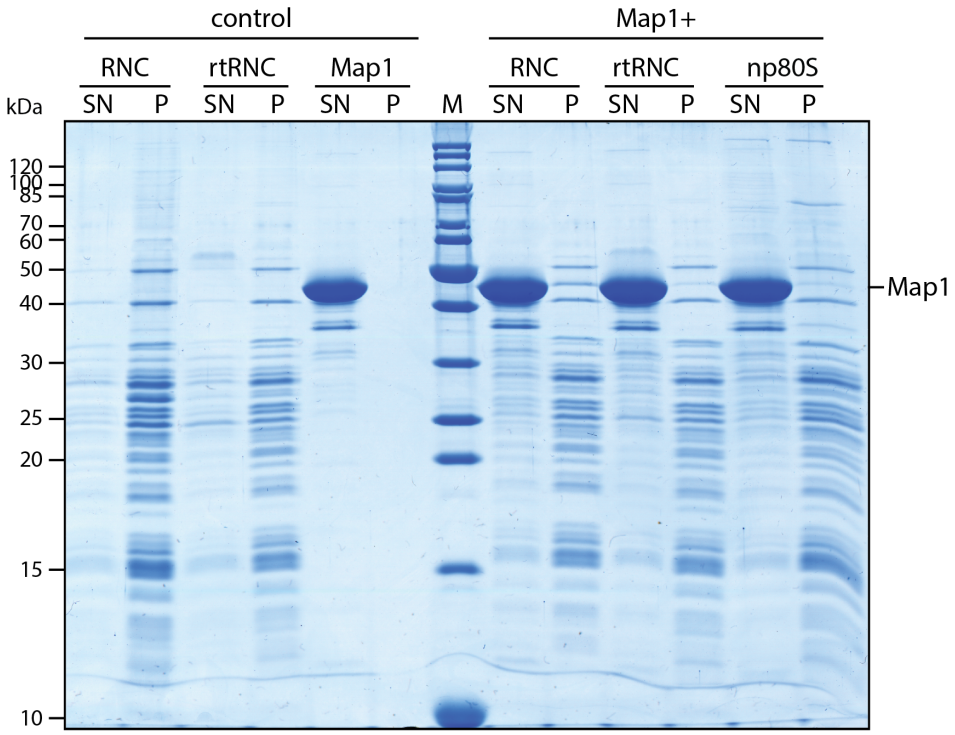

Binding assay of Map1 with RNase I-treated RNCs. 15%SDS-PAGE after an *in vitro* binding assay showing the supernatant (SN) and pellet (P) fractions of RNCs or RNase I-treated RNCs (rtRNC) incubated with recombinant Map1. See fig. 3.6, page 65.

NatA binding assays with rtRNC

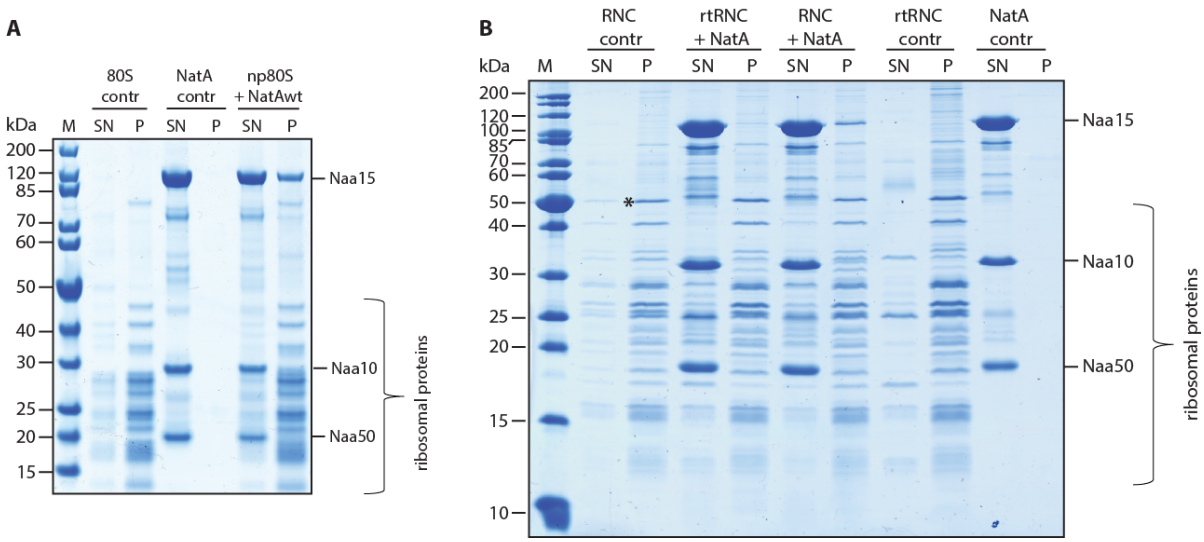

Binding assay of NatA with empyt and RNase I-treated RNCs. **A**, 4–12% Nu-PAGE gel after an *in vitro* binding assay showing the supernatant (SN) and pellet (P) fractions of either empty 80S ribosomes or NatA or 80S ribosomes incubated with recombinant NatA, indicating NatA binding to empty ribosomes independently of an emerging nascent chain. **B**, 15% SDS–PAGE with supernatant and pellet fractions of a representative binding assay using either uL4-RNCs (RNC) or RNase I–treated uL4-RNCs (rtRNC). A representative ribosomal band used for normalization is marked with an asterisk. See fig. 3.14, page 78.

NatB binding assays

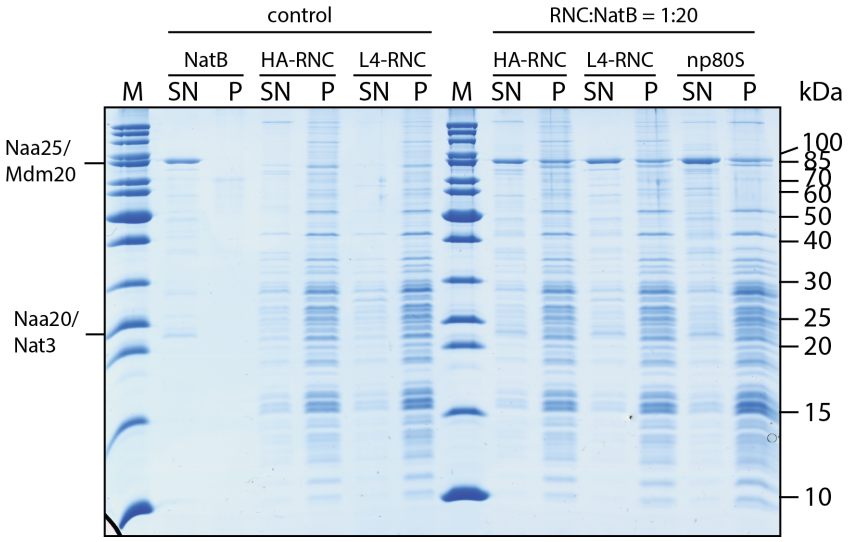

Binding assay of NatB with substrate, non-substrate and non-programmed RNC. 15% SDS-PAGE after an *in vitro* binding assay showing the supernatant (SN) and pellet (P) fractions of substrate RNCs (HA-RNC), non-substrate RNCs (L4RNC) or non-programmed 80S (np80S) incubated with recombinant NatB complex. See fig. 3.20, page 87.

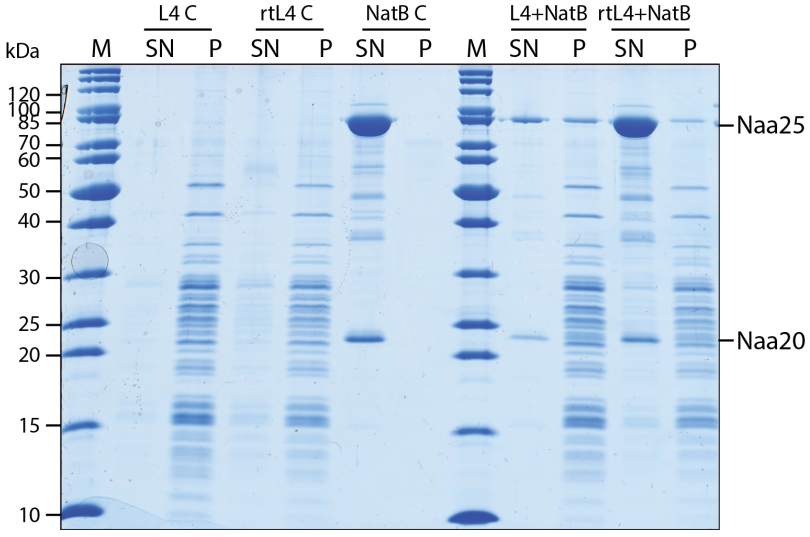

Binding assay of NatB with RNase I-treated RNC. 15% SDS-PAGE after an *in vitro* binding assay showing the supernatant (SN) and pellet (P) fractions of RNC (L4) or RNase I–treated uL4-RNCs (rtRNC) incubated with recombinant NatB. See fig. 3.20, page 87.

NatB binding to ABP1-RNC

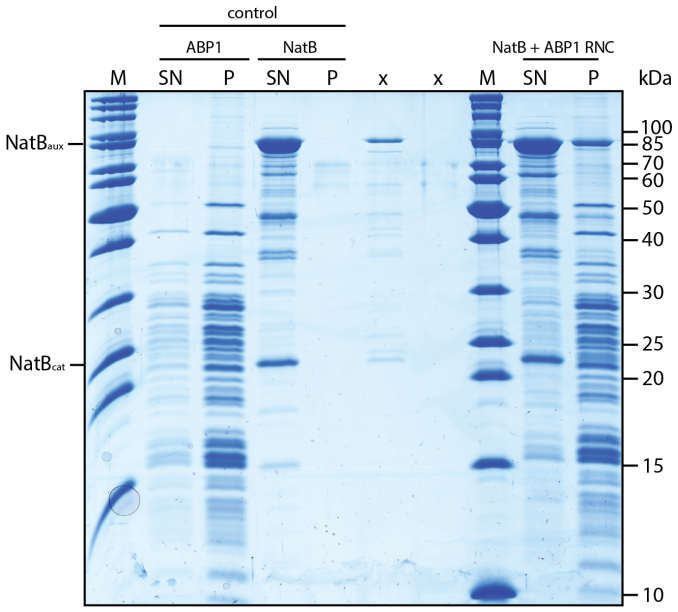

Binding assay of NatB with ABP1-RNC. 15% SDS-PAGE after an *in vitro* binding assay showing the supernatant (SN) and pellet (P) fractions of ABP1-RNC incubated with recombinant NatB. See fig. 3.21, page 89.

Wildtype and mutant NatB binding assays

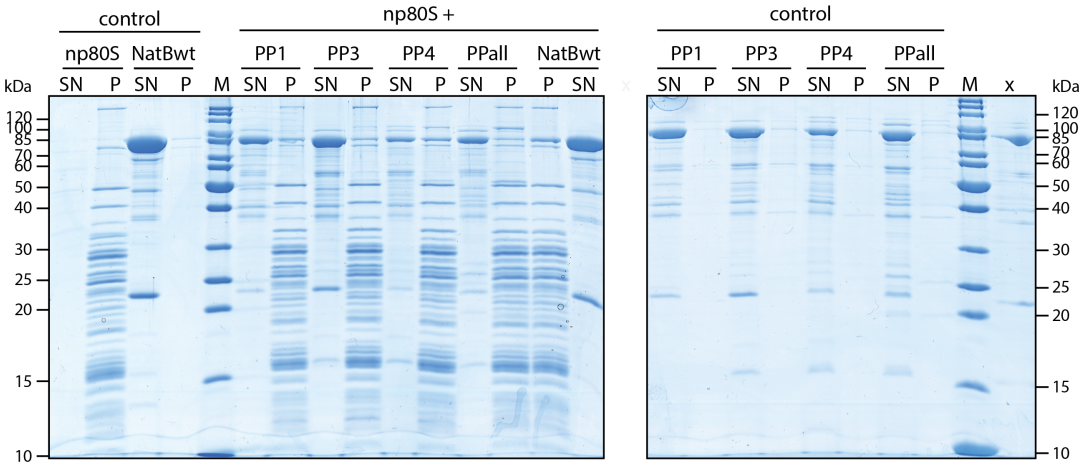

Binding assay of wt NatB with NatB mutans carrying charge inversions. 15% SDS-PAGE of a binding assay using wt or mutant NatB complex and nonprogrammed idle 80S ribosomes (np80S). Mutations were inserted as double charge inversions indicated as positive patches (PP) according to fig. 3.25, page 93.

NAT structures determined to date

NAT	Subunits	Species	Co-crystallized with	PDB	Publication
ssNAT	ssNAT	*S. solfataricus*	Acetyl-CoA	2X7B	Liszczak and Marmorstein (2013)
NatA	Naa10	*S. pombe*	Acetyl-CoA	4KVX	Liszczak et al. (2013)
	Naa10 Naa15		Acetyl-CoA	4KVO	
			Bisubstrate inhibitor	4KVM	
	Naa10 Naa15	*S. cerevisiae*	Apo	4HNY	Neubauer (2012)
			ppGpp	4HNX	
			IP_6	4HNW	
	Naa10 Naa15 HYPK	*C. thermophilum*	CoA[a]	5NNR	Weyer et al. (2017)
			Carboxymethyl CoA	5NNP	
	Naa10 Naa15	*H. sapiens*	acetyl-CoA[a]	6C9M	Gottlieb and Marmorstein (2018)
	Naa10 Naa15 HYPK			6C95	
NatB	Naa20 Naa25	*C. albicans*	CoA MES	5K04	Hong et al. (2017)
			Bisubstrate inhibitor	5K18	
NatD	Naa40	*H. sapiens*	Acetyl-CoA	4U9V	Magin et al. (2015)
			CoA H2A/H4 peptide	4U9W	
		S. pombe	Acetyl-CoA	4UA3	
NatE	Naa50	*H. sapiens*	CoA peptide	3TFY	Liszczak et al. (2011)
			CoA acetylated peptide	4X5K	N/A
			CoA	2PSW	N/A
			Acetyl-CoA	2OB0	
	Naa10 Naa15 Naa50	*S. cerevisiae*	ppGpp Bisubstrate inhibitor	4XPD	Neubauer (2012)
			Bisubstrate inhibitor[a] IP_6	6O07	Deng et al. (2019)
NatF	Naa60	*H. sapiens*	CoA	5ICW	Stove et al. (2016)
			Bisubstrate inhibitor	5ICV	
			CoA	5HH0	Chen et al. (2016)
	$Naa60_{F34A}$			5HH1	
	Naa60		Acetyl-CoA	5HGZ	
NatH	Naa80	*H. sapiens*	Acetyl-CoA	5WJD	Goris et al. (2018)
			Bisubstrate inhibitor	5WJE	

[a]Denotes that density for the corresponding added co-factor was not observed.

NAT structures determined to date. Table of x-ray structures from Gottlieb L, Marmorstein R. Biochemical and structural analysis of N-terminal acetyltransferases. Methods Enzymol. 2019; 626:271-299 (doi:10.1016/bs.mie.2019.07.016). Neubauer (2012) refers to PDB 4XNH in addition. The x-ray structure of the NatC complex got published in 2020 after the submission of this thesie by Grunwald S, Hopf LVM, Bock-Bierbaum T, Lally CCM, Spahn CMT, Daumke O. Divergent architecture of the heterotrimeric NatC complex explains N-terminal acetylation of cognate substrates. Nat Commun. 2020;11(1):5506. doi:10.1038/s41467-020-19321-8. Therefore, it is only NatG of which a x-ray structure is still missing.

List of Abbreviations

μg	Microgram
μl	Microliter
μM	Micromolar
2D	Two-dimensional
3D	Three-dimensional
Å (unit)	Ångstroem
A. thaliana	*Arabidopsis thaliana*
aa	Amino acid
aa-tRNA	Aminoacyl-tRNA
ac-CoA	Acetyl-CoA
AP fold	Aminopeptidase fold
A-site	Aminoacyl-site
ATP	Adenosine triphosphate
C albicans	*Candida albicans*
C. elegans	*Caenorhabditis elegans*
CMV	Cytomegalovirus
cryo-EM	Cryo-electron microscopy
C-terminal	Carboxyterminal
D. melanogaster	*Drosophila melanogaster*
DC	Decoding center
DNA	Deoxyribonucleic acid
DTT	1,4-dithiothreitol
E. coli	*Escherichia coli*
ECL	Electro chemiluminescence
eEF	Eukaryotic elongation factor
EF	Elongation factor
EGTA	Ethylene glycol tetraacetic acid
EDTA	Ethylenediaminetetraacetic acid

eIF	Eukaryotic initiation factor
EMDB	Electron Microscopy Data Bank
ER	Endoplasmic reticulum
ES	Expansion segment
E-site	Exit-site
FSC	Fourier shell correlation
GNAT	General control non-repressible 5 (GCN5)-related N-acetyltransferases
GTP	Guanosine triphosphate
H. sapiens	*Homo sapiens*
HA	Hemagglutinin
HAT	Histone acetyltransferase
HDAC	Histone deacetylase
HRP	Horseradish peroxidase
IF	Initiation factor
IPTG	isopropyl-beta-D-thiogalactoside
KAT	Lysine acetyltransferase
kDa	Kilodalton
KDAC	Lysine deacetylase
LB	Lysogeny broth
LSU	Large ribosomal subunit
MDa	Megadalton
MES	2-(N-morpholino)ethanesulfonic acid
mg	Milligram
mM	Millimolar
MOPS	3-(N-morpholino)propanesulfonic acid
mRNA	Messenger RNA
MW	Molecular weight
NAC	Nascent polypeptide-associated complex
NAT	N-terminal acetyltransferase
NC	Nascent chain
NME	N-terminal methionine excision

NTA	N-terminal acetylation
N-terminal	Aminoterminal
o/n	Over night
OD	Optical density
ORF	Open reading frame
P	Pellet
PAGE	Polyacrylamide gel electrophoresis
PBS	Phosphate-buffered saline
PCC	Protein conducting channel
PCR	Polymerase chain reaction
PDB	Protein data bank
PMSF	Phenylmethylsulfonyl fluoride
P-site	Peptidyl-site
PTC	Peptidyl transferase center
PVDF	Polydivinylfluoride
RAC	Ribosome-Associated Complex
RF	Release factor
RNC	Ribosome nascent chain complexes
RNC	Ribosome-nascent chain complex
rpm	Revolutions per minute
r-proteins	Ribosomal proteins
rRNA	Ribosomal RNA
RT	Room temperature
S (unit)	Svedberg unit
S. cerevisiae	*Saccharomyces cerevisiae*
S. pombe	*Schizosaccharomyces pombe*
SD	Shine-Dalgarno
SDS	Sodium dodecyl sulfate
SN	Supernatant
SPA	Single particle analysis
SRP	Signal recognition particle
SSU	Small ribosomal subunit

T. thermophile	*Tetrahymena thermophile*
TAP	Tandem affinity purification
TCA	Trichloroacetic acid
TE	Tunnel exit
TPR	Tetratricopeptide repeat
Tris	Tris(hydroxymethyl)aminomethane
tRNA	Transfer RNA
U	units
wt	Wild type
YPD	Yeast extract peptone dextrose

References

ABBOUD, A., BEDOUCHA, P., BYSKA, J., ARNESEN, T., AND REUTER, N. Dynamics-function relationship in the catalytic domains of N-terminal acetyltransferases. *Comput Struct Biotechnol J 18* (2020), 532–547.

ADDLAGATTA, A., HU, X., LIU, J. O., AND MATTHEWS, B. W. Structural basis for the functional differences between type i and type ii human methionine aminopeptidases. *Biochemistry 44*, 45 (2005), 14741–9.

AGIRREZABALA, X., LEI, J., BRUNELLE, J. L., ORTIZ-MEOZ, R. F., GREEN, R., AND FRANK, J. Visualization of the hybrid state of trna binding promoted by spontaneous ratcheting of the ribosome. *Mol Cell 32*, 2 (2008), 190–7.

AKSNES, H., DRAZIC, A., AND ARNESEN, T. (Hyper)tension release by N-terminal acetylation. *Trends Biochem Sci 40*, 8 (2015a), 422–4.

AKSNES, H., DRAZIC, A., MARIE, M., AND ARNESEN, T. First Things First: Vital Protein Marks by N-Terminal Acetyltransferases. *Trends Biochem Sci 41*, 9 (2016), 746–760.

AKSNES, H., GORIS, M., STROMLAND, O., DRAZIC, A., WAHEED, Q., REUTER, N., AND ARNESEN, T. Molecular determinants of the N-terminal acetyltransferase Naa60 anchoring to the Golgi membrane. *J Biol Chem 292*, 16 (2017), 6821–6837.

AKSNES, H., MARIE, M., ARNESEN, T., AND DRAZIC, A. Actin polymerization and cell motility are affected by NAA80-mediated posttranslational N-terminal acetylation of actin. *Commun Integr Biol 11*, 4 (2018), e1526572.

AKSNES, H., OSBERG, C., AND ARNESEN, T. N-terminal acetylation by NatC is not a general determinant for substrate subcellular localization in Saccharomyces cerevisiae. *PLoS One 8*, 4 (2013), e61012.

AKSNES, H., REE, R., AND ARNESEN, T. Co-translational, Post-translational, and Non-catalytic Roles of N-Terminal Acetyltransferases. *Mol Cell 73*, 6 (2019), 1097–1114.

AKSNES, H., VAN DAMME, P., GORIS, M., STARHEIM, K. K., MARIE, M., STOVE, S. I., HOEL, C., KALVIK, T. V., HOLE, K., GLOMNES, N., FURNES, C., LJOSTVEIT, S., ZIEGLER, M., NIERE, M., GEVAERT, K., AND ARNESEN, T. An organellar nalpha-acetyltransferase, naa60, acetylates cytosolic N termini of transmembrane proteins and maintains Golgi integrity. *Cell Rep 10*, 8 (2015b), 1362–74.

ALLFREY, V. G., DI PAOLA, E. A., AND STERNER, R. Protein side-chain acetylations. *Methods Enzymol 107* (1984), 224–40.

ANGER, A. M., ARMACHE, J. P., BERNINGHAUSEN, O., HABECK, M., SUBKLEWE, M., WILSON, D. N., AND BECKMANN, R. Structures of the human and Drosophila 80S ribosome. *Nature 497*, 7447 (2013), 80–5.

ARFIN, S. M., KENDALL, R. L., HALL, L., WEAVER, L. H., STEWART, A. E., MATTHEWS, B. W., AND BRADSHAW, R. A. Eukaryotic methionyl aminopeptidases: two classes of cobalt-dependent enzymes. *Proc Natl Acad Sci U S A 92*, 17 (1995), 7714–8.

ARMACHE, J. P., JARASCH, A., ANGER, A. M., VILLA, E., BECKER, T., BHUSHAN, S., JOSSINET, F., HABECK, M., DINDAR, G., FRANCKENBERG, S., MARQUEZ, V., MIELKE, T., THOMM, M., BERNINGHAUSEN, O., BEATRIX, B., SODING, J., WESTHOF, E., WILSON, D. N., AND BECKMANN, R. Cryo-EM structure and rRNA model of a translating eukaryotic 80S ribosome at 5.5Å resolution. *Proc Natl Acad Sci U S A 107*, 46 (2010), 19748–53.

ARNESEN, T., ANDERSON, D., BALDERSHEIM, C., LANOTTE, M., VARHAUG, J. E., AND LILLEHAUG, J. R. Identification and characterization of the human ARD1-NATH protein acetyltransferase complex. *Biochem J 386*, Pt 3 (2005), 433–43.

ARNESEN, T., ANDERSON, D., TORSVIK, J., HALSETH, H. B., VARHAUG, J. E., AND LILLEHAUG, J. R. Cloning and characterization of hNAT5/hSAN: an evolutionarily conserved component of the NatA protein N-alpha-acetyltransferase complex. *Gene 371*, 2 (2006), 291–5.

ARNESEN, T., GROMYKO, D., KAGABO, D., BETTS, M. J., STARHEIM, K. K., VARHAUG, J. E., ANDERSON, D., AND LILLEHAUG, J. R. A novel human NatA Nalpha-terminal acetyltransferase complex: hNaa16p-hNaa10p (hNat2-hArd1). *BMC Biochem 10* (2009b), 15.

ARNESEN, T., STARHEIM, K. K., VAN DAMME, P., EVJENTH, R., DINH, H., BETTS, M. J., RYNINGEN, A., VANDEKERCKHOVE, J., GEVAERT, K., AND ANDERSON, D. The chaperone-like protein HYPK acts together with NatA in cotranslational N-terminal acetylation and prevention of Huntingtin aggregation. *Mol Cell Biol 30*, 8 (2010), 1898–909.

ARNESEN, T., VAN DAMME, P., POLEVODA, B., HELSENS, K., EVJENTH, R., COLAERT, N., VARHAUG, J. E., VANDEKERCKHOVE, J., LILLEHAUG, J. R., SHERMAN, F., AND GEVAERT, K. Proteomics analyses reveal the evolutionary conservation and divergence of N-terminal acetyltransferases from yeast and humans. *Proc Natl Acad Sci U S A 106*, 20 (2009a), 8157–62.

AUDAGNOTTO, M., AND DAL PERARO, M. Protein post-translational modifications: In silico prediction tools and molecular modeling. *Comput Struct Biotechnol J 15* (2017), 307–319.

AVIRAM, N., AND SCHULDINER, M. Targeting and translocation of proteins to the endoplasmic reticulum at a glance. *J Cell Sci 130*, 24 (2017), 4079–4085.

BALL, L. A., AND KAESBERG, P. Cleavage of the N-terminal formylmethionine residue from a bacteriophage coat protein in vitro. *J Mol Biol 79*, 3 (1973), 531–7.

BECKER, M. M., LAPOUGE, K., SEGNITZ, B., WILD, K., AND SINNING, I. Structures of human SRP72 complexes provide insights into SRP RNA remodeling and ribosome interaction. *Nucleic Acids Res 45*, 1 (2017), 470–481.

BECKER, T., BHUSHAN, S., JARASCH, A., ARMACHE, J. P., FUNES, S., JOSSINET, F., GUMBART, J., MIELKE, T., BERNINGHAUSEN, O., SCHULTEN, K., WESTHOF, E., GILMORE, R., MANDON, E. C., AND BECKMANN, R. Structure of monomeric yeast and mammalian Sec61 complexes interacting with the translating ribosome. *Science 326*, 5958 (2009), 1369–73.

BECKER, T., FRANCKENBERG, S., WICKLES, S., SHOEMAKER, C. J., ANGER, A. M., ARMACHE, J. P., SIEBER, H., UNGEWICKELL, C., BERNINGHAUSEN, O., DABERKOW, I., KARCHER, A., THOMM, M., HOPFNER, K. P., GREEN, R., AND BECKMANN, R. Structural basis of highly conserved ribosome recycling in eukaryotes and archaea. *Nature 482*, 7386 (2012), 501–6.

BECKMANN, R., SPAHN, C. M., ESWAR, N., HELMERS, J., PENCZEK, P. A., SALI, A., FRANK, J., AND BLOBEL, G. Architecture of the protein-conducting channel associated with the translating 80s ribosome. *Cell 107*, 3 (2001), 361–72.

BEHNIA, R., PANIC, B., WHYTE, J. R., AND MUNRO, S. Targeting of the Arf-like GTPase Arl3p to the Golgi requires N-terminal acetylation and the membrane protein Sys1p. *Nat Cell Biol 6*, 5 (2004), 405–13.

BERG, P., AND OFFENGAND, E. J. An Enzymatic Mechanism for Linking Amino Acids to RNA. *Proc Natl Acad Sci U S A 44*, 2 (1958), 78–86.

BERGER, E. M., COX, G., WEBER, L., AND KENNEY, J. S. Actin acetylation in Drosophila tissue culture cells. *Biochem Genet 19*, 3-4 (1981), 321–31.

BERNDT, U., OELLERER, S., ZHANG, Y., JOHNSON, A. E., AND ROSPERT, S. A signal-anchor sequence stimulates signal recognition particle binding to ribosomes from inside the exit tunnel. *Proc Natl Acad Sci U S A 106*, 5 (2009), 1398–403.

BERNIER, S. G., LAZARUS, D. D., CLARK, E., DOYLE, B., LABENSKI, M. T., THOMPSON, C. D., WESTLIN, W. F., AND HANNIG, G. A methionine aminopeptidase-2 inhibitor, PPI-2458, for the treatment of rheumatoid arthritis. *Proc Natl Acad Sci U S A 101*, 29 (2004), 10768–73.

BHAKTA, S., AKBAR, S., AND SENGUPTA, J. Cryo-EM Structures Reveal Relocalization of MetAP in the Presence of Other Protein Biogenesis Factors at the Ribosomal

Tunnel Exit. *J Mol Biol 431*, 7 (2019), 1426–1439.

BHUSHAN, S., MEYER, H., STAROSTA, A. L., BECKER, T., MIELKE, T., BERNINGHAUSEN, O., SATTLER, M., WILSON, D. N., AND BECKMANN, R. Structural basis for translational stalling by human cytomegalovirus and fungal arginine attenuator peptide. *Mol Cell 40*, 1 (2010), 138–46.

BIENVENUT, W. V., SUMPTON, D., MARTINEZ, A., LILLA, S., ESPAGNE, C., MEINNEL, T., AND GIGLIONE, C. Comparative large scale characterization of plant versus mammal proteins reveals similar and idiosyncratic n-alpha-acetylation features. *Mol Cell Proteomics 11*, 6 (2012), M111 015131.

BINGEL-ERLENMEYER, R., KOHLER, R., KRAMER, G., SANDIKCI, A., ANTOLIC, S., MAIER, T., SCHAFFITZEL, C., WIEDMANN, B., BUKAU, B., AND BAN, N. A peptide deformylase-ribosome complex reveals mechanism of nascent chain processing. *Nature 452*, 7183 (2008), 108–11.

BLATCH, G. L., AND LASSLE, M. The tetratricopeptide repeat: a structural motif mediating protein-protein interactions. *Bioessays 21*, 11 (1999), 932–9.

BONVEN, B., AND GULLOV, K. Peptide chain elongation rate and ribosomal activity in Saccharomyces cerevisiae as a function of the growth rate. *Mol Gen Genet 170*, 2 (1979), 225–30.

BORNEMANN, T., JOCKEL, J., RODNINA, M. V., AND WINTERMEYER, W. Signal sequence-independent membrane targeting of ribosomes containing short nascent peptides within the exit tunnel. *Nat Struct Mol Biol 15*, 5 (2008), 494–9.

BRADATSCH, B., LEIDIG, C., GRANNEMAN, S., GNADIG, M., TOLLERVEY, D., BOTTCHER, B., BECKMANN, R., AND HURT, E. Structure of the pre-60S ribosomal subunit with nuclear export factor Arx1 bound at the exit tunnel. *Nat Struct Mol Biol 19*, 12 (2012), 1234–41.

BRADSHAW, R. A., AND YI, E. Methionine aminopeptidases and angiogenesis. *Essays Biochem 38* (2002), 65–78.

BROWN, J. L. The N-terminal region of soluble proteins from procaryotes and eucaryotes. *Biochim Biophys Acta 221*, 3 (1970), 480–8.

BU, B., TONG, X., LI, D., HU, Y., HE, W., ZHAO, C., HU, R., LI, X., SHAO, Y., LIU, C., ZHAO, Q., JI, B., AND DIAO, J. N-Terminal Acetylation Preserves alpha-Synuclein from Oligomerization by Blocking Intermolecular Hydrogen Bonds. *ACS Chem Neurosci 8*, 10 (2017), 2145–2151.

BUKAU, B., DEUERLING, E., PFUND, C., AND CRAIG, E. A. Getting newly synthesized proteins into shape. *Cell 101*, 2 (2000), 119–22.

CAESAR, R., WARRINGER, J., AND BLOMBERG, A. Physiological importance and identification of novel targets for the N-terminal acetyltransferase NatB. *Eukaryot Cell 5*, 2 (2006), 368–78.

CHANG, S. Y., MCGARY, E. C., AND CHANG, S. Methionine aminopeptidase gene of Escherichia coli is essential for cell growth. *J Bacteriol 171*, 7 (1989), 4071–2.

CHANG, Y. H., TEICHERT, U., AND SMITH, J. A. Purification and characterization of a methionine aminopeptidase from saccharomyces cerevisiae. *J Biol Chem 265*, 32 (1990), 19892–7.

CHANG, Y. H., TEICHERT, U., AND SMITH, J. A. Molecular cloning, sequencing, deletion, and overexpression of a methionine aminopeptidase gene from Saccharomyces cerevisiae. *J Biol Chem 267*, 12 (1992), 8007–11.

CHEN, S., VETRO, J. A., AND CHANG, Y. H. The specificity in vivo of two distinct methionine aminopeptidases in saccharomyces cerevisiae. *Arch Biochem Biophys 398*, 1 (2002), 87–93.

CRICK, F. Central dogma of molecular biology. *Nature 227*, 5258 (1970), 561–3.

CRICK, F. H., BARNETT, L., BRENNER, S., AND WATTS-TOBIN, R. J. General nature of the genetic code for proteins. *Nature 192* (1961), 1227–32.

DATTA, B. MAPs and POEP of the roads from prokaryotic to eukaryotic kingdoms. *Biochimie 82*, 2 (2000), 95–107.

DEL ALAMO, M., HOGAN, D. J., PECHMANN, S., ALBANESE, V., BROWN, P. O., AND FRYDMAN, J. Defining the specificity of cotranslationally acting chaperones by systematic analysis of mRNAs associated with ribosome-nascent chain complexes. *PLoS Biol 9*, 7 (2011), e1001100.

DENG, S., MAGIN, R. S., WEI, X., PAN, B., PETERSSON, E. J., AND MARMORSTEIN, R. Structure and Mechanism of Acetylation by the N-Terminal Dual Enzyme NatA/Naa50 Complex. *Structure 27*, 7 (2019), 1057–1070 e4.

DENG, S., MCTIERNAN, N., WEI, X., ARNESEN, T., AND MARMORSTEIN, R. Molecular basis for N-terminal acetylation by human NatE and its modulation by HYPK. *Nat Commun 11*, 1 (2020), 818.

DINH, T. V., BIENVENUT, W. V., LINSTER, E., FELDMAN-SALIT, A., JUNG, V. A., MEINNEL, T., HELL, R., GIGLIONE, C., AND WIRTZ, M. Molecular identification and functional characterization of the first Nalpha-acetyltransferase in plastids by global acetylome profiling. *Proteomics 15*, 14 (2015), 2426–35.

DRAZIC, A., AKSNES, H., MARIE, M., BOCZKOWSKA, M., VARLAND, S., TIMMERMAN, E., FOYN, H., GLOMNES, N., REBOWSKI, G., IMPENS, F., GEVAERT, K., DOMINGUEZ, R., AND ARNESEN, T. NAA80 is actin's N-terminal acetyltransferase and regulates cytoskeleton assembly and cell motility. *Proc Natl Acad Sci U S A 115*, 17 (2018), 4399–4404.

DÖRFEL, M. J., AND LYON, G. J. The biological functions of Naa10 - From amino-terminal acetylation to human disease. *Gene 567*, 2 (2015), 103–31.

DRIESSEN, H. P., DE JONG, W. W., TESSER, G. I., AND BLOEMENDAL, H. The mechanism of N-terminal acetylation of proteins. *CRC Crit Rev Biochem 18*, 4 (1985), 281–325.

DYDA, F., KLEIN, D. C., AND HICKMAN, A. B. GCN5-related N-acetyltransferases: a structural overview. *Annu Rev Biophys Biomol Struct 29* (2000), 81–103.

EMSLEY, P., LOHKAMP, B., SCOTT, W. G., AND COWTAN, K. Features and development of Coot. *Acta Crystallogr D Biol Crystallogr 66*, Pt 4 (2010), 486–501.

EVJENTH, R., HOLE, K., KARLSEN, O. A., ZIEGLER, M., ARNESEN, T., AND LILLEHAUG, J. R. Human Naa50p (Nat5/San) displays both protein N alpha- and N epsilon-acetyltransferase activity. *J Biol Chem 284*, 45 (2009), 31122–9.

FALB, M., AIVALIOTIS, M., GARCIA-RIZO, C., BISLE, B., TEBBE, A., KLEIN, C., KONSTANTINIDIS, K., SIEDLER, F., PFEIFFER, F., AND OESTERHELT, D. Archaeal N-

terminal protein maturation commonly involves N-terminal acetylation: a large-scale proteomics survey. *J Mol Biol 362*, 5 (2006), 915–24.

FERBITZ, L., MAIER, T., PATZELT, H., BUKAU, B., DEUERLING, E., AND BAN, N. Trigger factor in complex with the ribosome forms a molecular cradle for nascent proteins. *Nature 431*, 7008 (2004), 590–6.

FINKA, A., AND GOLOUBINOFF, P. Proteomic data from human cell cultures refine mechanisms of chaperone-mediated protein homeostasis. *Cell Stress Chaperones 18*, 5 (2013), 591–605.

FORTE, G. M., POOL, M. R., AND STIRLING, C. J. N-terminal acetylation inhibits protein targeting to the endoplasmic reticulum. *PLoS Biol 9*, 5 (2011), e1001073.

FRANK, J., AND AGRAWAL, R. K. A ratchet-like inter-subunit reorganization of the ribosome during translocation. *Nature 406*, 6793 (2000), 318–22.

FROTTIN, F., MARTINEZ, A., PEYNOT, P., MITRA, S., HOLZ, R. C., GIGLIONE, C., AND MEINNEL, T. The proteomics of N-terminal methionine cleavage. *Mol Cell Proteomics 5*, 12 (2006), 2336–49.

FUJII, K., SUSANTO, T. T., SAURABH, S., AND BARNA, M. Decoding the Function of Expansion Segments in Ribosomes. *Mol Cell 72*, 6 (2018), 1013–1020 e6.

GAMERDINGER, M., HANEBUTH, M. A., FRICKEY, T., AND DEUERLING, E. The principle of antagonism ensures protein targeting specificity at the endoplasmic reticulum. *Science 348*, 6231 (2015), 201–7.

GAMERDINGER, M., KOBAYASHI, K., WALLISCH, A., KREFT, S. G., SAILER, C., SCHLOMER, R., SACHS, N., JOMAA, A., STENGEL, F., BAN, N., AND DEUERLING, E. Early Scanning of Nascent Polypeptides inside the Ribosomal Tunnel by NAC. *Mol Cell 75*, 5 (2019), 996–1006 e8.

GAUTSCHI, M., JUST, S., MUN, A., ROSS, S., RUCKNAGEL, P., DUBAQUIE, Y., EHRENHOFER-MURRAY, A., AND ROSPERT, S. The yeast N(alpha)-acetyltransferase NatA is quantitatively anchored to the ribosome and interacts with nascent polypeptides. *Mol Cell Biol 23*, 20 (2003), 7403–14.

GAUTSCHI, M., MUN, A., ROSS, S., AND ROSPERT, S. A functional chaperone triad on the yeast ribosome. *Proc Natl Acad Sci U S A 99*, 7 (2002), 4209–14.

GERBI, S. A. The evolution of eukaryotic ribosomal DNA. *Biosystems 19*, 4 (1986), 247–58.

GERBI, S. A. Expansion segment: regions of variable size that interrupt the universal core secondary structure of ribosomal RNA. *R.A. Zimmermann, A.E. Dahlberg (Eds.), Ribosomal RNA: Structure, Evolution, Processing, and Function in Protein Synthesis, CRC Press, New York (1996)* (1996), 71–87.

GIGLIONE, C., BOULAROT, A., AND MEINNEL, T. Protein N-terminal methionine excision. *Cell Mol Life Sci 61*, 12 (2004), 1455–74.

GIGLIONE, C., FIEULAINE, S., AND MEINNEL, T. N-terminal protein modifications: Bringing back into play the ribosome. *Biochimie 114* (2015), 134–46.

GÓMEZ RAMOS, L. M., SMEEKENS, J. M., KOVACS, N. A., BOWMAN, J. C., WARTELL, R. M., WU, R., AND WILLIAMS, L. D. Yeast rRNA Expansion Segments: Folding and Function. *J Mol Biol 428*, 20 (2016), 4048–4059.

GODDARD, T. D., HUANG, C. C., MENG, E. C., PETTERSEN, E. F., COUCH, G. S., MORRIS, J. H., AND FERRIN, T. E. UCSF ChimeraX: Meeting modern challenges in visualization and analysis. *Protein Sci 27*, 1 (2018), 14–25.

GOEBL, M., AND YANAGIDA, M. The TPR snap helix: a novel protein repeat motif from mitosis to transcription. *Trends Biochem Sci 16*, 5 (1991), 173–7.

GOETZE, S., QELI, E., MOSIMANN, C., STAES, A., GERRITS, B., ROSCHITZKI, B., MOHANTY, S., NIEDERER, E. M., LACZKO, E., TIMMERMAN, E., LANGE, V., HAFEN, E., AEBERSOLD, R., VANDEKERCKHOVE, J., BASLER, K., AHRENS, C. H., GEVAERT, K., AND BRUNNER, E. Identification and functional characterization of N-terminally acetylated proteins in Drosophila melanogaster. *PLoS Biol 7*, 11 (2009), e1000236.

GORIS, M., MAGIN, R. S., FOYN, H., MYKLEBUST, L. M., VARLAND, S., REE, R., DRAZIC, A., BHAMBRA, P., STOVE, S. I., BAUMANN, M., HAUG, B. E., MARMORSTEIN, R., AND ARNESEN, T. Structural determinants and cellular environ-

ment define processed actin as the sole substrate of the N-terminal acetyltransferase NAA80. *Proc Natl Acad Sci U S A 115*, 17 (2018), 4405–4410.

GOTTLIEB, L., AND MARMORSTEIN, R. Structure of Human NatA and Its Regulation by the Huntingtin Interacting Protein HYPK. *Structure 26*, 7 (2018), 925–935 e8.

GREBER, B. J., BOEHRINGER, D., MONTELLESE, C., AND BAN, N. Cryo-EM structures of Arx1 and maturation factors Rei1 and Jjj1 bound to the 60S ribosomal subunit. *Nat Struct Mol Biol 19*, 12 (2012), 1228–33.

GREBER, B. J., GERHARDY, S., LEITNER, A., LEIBUNDGUT, M., SALEM, M., BOEHRINGER, D., LEULLIOT, N., AEBERSOLD, R., PANSE, V. G., AND BAN, N. Insertion of the Biogenesis Factor Rei1 Probes the Ribosomal Tunnel during 60S Maturation. *Cell 164*, 1-2 (2016), 91–102.

GUMIERO, A., CONZ, C., GESE, G. V., ZHANG, Y., WEYER, F. A., LAPOUGE, K., KAPPES, J., VON PLEHWE, U., SCHERMANN, G., FITZKE, E., WOLFLE, T., FISCHER, T., ROSPERT, S., AND SINNING, I. Interaction of the cotranslational Hsp70 Ssb with ribosomal proteins and rRNA depends on its lid domain. *Nat Commun 7* (2016), 13563.

HALIC, M., BECKER, T., POOL, M. R., SPAHN, C. M., GRASSUCCI, R. A., FRANK, J., AND BECKMANN, R. Structure of the signal recognition particle interacting with the elongation-arrested ribosome. *Nature 427*, 6977 (2004), 808–14.

HALIC, M., AND BECKMANN, R. The signal recognition particle and its interactions during protein targeting. *Curr Opin Struct Biol 15*, 1 (2005), 116–25.

HALIC, M., GARTMANN, M., SCHLENKER, O., MIELKE, T., POOL, M. R., SINNING, I., AND BECKMANN, R. Signal recognition particle receptor exposes the ribosomal translocon binding site. *Science 312*, 5774 (2006), 745–7.

HANEBUTH, M. A., KITYK, R., FRIES, S. J., JAIN, A., KRIEL, A., ALBANESE, V., FRICKEY, T., PETER, C., MAYER, M. P., FRYDMAN, J., AND DEUERLING, E. Multivalent contacts of the Hsp70 Ssb contribute to its architecture on ribosomes and nascent chain interaction. *Nat Commun 7* (2016), 13695.

HARRISON, P. M., MILBURN, D., ZHANG, Z., BERTONE, P., AND GERSTEIN, M. Identification of pseudogenes in the Drosophila melanogaster genome. *Nucleic Acids Res*

31, 3 (2003), 1033–7.

HARTL, F. U., AND HAYER-HARTL, M. Molecular chaperones in the cytosol: from nascent chain to folded protein. *Science 295*, 5561 (2002), 1852–8.

HASHEM, Y., DES GEORGES, A., DHOTE, V., LANGLOIS, R., LIAO, H. Y., GRASSUCCI, R. A., HELLEN, C. U., PESTOVA, T. V., AND FRANK, J. Structure of the mammalian ribosomal 43S preinitiation complex bound to the scanning factor DHX29. *Cell 153*, 5 (2013), 1108–19.

HERMANN, G. J., KING, E. J., AND SHAW, J. M. The yeast gene, MDM20, is necessary for mitochondrial inheritance and organization of the actin cytoskeleton. *J Cell Biol 137*, 1 (1997), 141–53.

HERSHKO, A., HELLER, H., EYTAN, E., KAKLIJ, G., AND ROSE, I. A. Role of the alpha-amino group of protein in ubiquitin-mediated protein breakdown. *Proc Natl Acad Sci U S A 81*, 22 (1984), 7021–5.

HEUER, A., GEROVAC, M., SCHMIDT, C., TROWITZSCH, S., PREIS, A., KOTTER, P., BERNINGHAUSEN, O., BECKER, T., BECKMANN, R., AND TAMPE, R. Structure of the 40S-ABCE1 post-splitting complex in ribosome recycling and translation initiation. *Nat Struct Mol Biol 24*, 5 (2017), 453–460.

HINNEBUSCH, A. G., AND LORSCH, J. R. The mechanism of eukaryotic translation initiation: new insights and challenges. *Cold Spring Harb Perspect Biol 4*, 10 (2012).

HOLE, K., VAN DAMME, P., DALVA, M., AKSNES, H., GLOMNES, N., VARHAUG, J. E., LILLEHAUG, J. R., GEVAERT, K., AND ARNESEN, T. The human N-alpha-acetyltransferase 40 (hNaa40p/hNatD) is conserved from yeast and N-terminally acetylates histones H2A and H4. *PLoS One 6*, 9 (2011), e24713.

HOLMES, W. M., MANNAKEE, B. K., GUTENKUNST, R. N., AND SERIO, T. R. Loss of amino-terminal acetylation suppresses a prion phenotype by modulating global protein folding. *Nat Commun 5* (2014), 4383.

HOLTKAMP, W., LEE, S., BORNEMANN, T., SENYUSHKINA, T., RODNINA, M. V., AND WINTERMEYER, W. Dynamic switch of the signal recognition particle from scanning to targeting. *Nat Struct Mol Biol 19*, 12 (2012), 1332–7.

HONG, H., CAI, Y., ZHANG, S., DING, H., WANG, H., AND HAN, A. Molecular Basis of Substrate Specific Acetylation by N-Terminal Acetyltransferase NatB. *Structure 25*, 4 (2017), 641–649 e3.

HOU, F., CHU, C. W., KONG, X., YOKOMORI, K., AND ZOU, H. The acetyltransferase activity of San stabilizes the mitotic cohesin at the centromeres in a shugoshin-independent manner. *J Cell Biol 177*, 4 (2007), 587–97.

HUANG, P., GAUTSCHI, M., WALTER, W., ROSPERT, S., AND CRAIG, E. A. The Hsp70 Ssz1 modulates the function of the ribosome-associated J-protein Zuo1. *Nat Struct Mol Biol 12*, 6 (2005), 497–504.

HUNDLEY, H., EISENMAN, H., WALTER, W., EVANS, T., HOTOKEZAKA, Y., WIEDMANN, M., AND CRAIG, E. The in vivo function of the ribosome-associated Hsp70, Ssz1, does not require its putative peptide-binding domain. *Proc Natl Acad Sci U S A 99*, 7 (2002), 4203–8.

HWANG, C. S., SHEMORRY, A., AND VARSHAVSKY, A. N-terminal acetylation of cellular proteins creates specific degradation signals. *Science 327*, 5968 (2010), 973–7.

JACKSON, R. J., HELLEN, C. U., AND PESTOVA, T. V. The mechanism of eukaryotic translation initiation and principles of its regulation. *Nat Rev Mol Cell Biol 11*, 2 (2010), 113–27.

JACKSON, R. J., HELLEN, C. U., AND PESTOVA, T. V. Termination and post-termination events in eukaryotic translation. *Adv Protein Chem Struct Biol 86* (2012), 45–93.

JAISWAL, H., CONZ, C., OTTO, H., WOLFLE, T., FITZKE, E., MAYER, M. P., AND ROSPERT, S. The chaperone network connected to human ribosome-associated complex. *Mol Cell Biol 31*, 6 (2011), 1160–73.

JARASCH, A. *3D modeling of ribosomal RNA using cryo-electron microscopy density maps*. PhD thesis, Ludwig-Maximilians-Universität München, May 2011. http://nbn-resolving.de/urn:nbn:de:bvb:19-131016, p. 66.

JEENINGA, R. E., VAN DELFT, Y., DE GRAAFF-VINCENT, M., DIRKS-MULDER, A., VENEMA, J., AND RAUE, H. A. Variable regions V13 and V3 of Saccharomyces cere-

visiae contain structural features essential for normal biogenesis and stability of 5.8S and 25S rRNA. *RNA 3*, 5 (1997), 476–88.

JENNER, L., MELNIKOV, S., GARREAU DE LOUBRESSE, N., BEN-SHEM, A., ISKAKOVA, M., URZHUMTSEV, A., MESKAUSKAS, A., DINMAN, J., YUSUPOVA, G., AND YUSUPOV, M. Crystal structure of the 80S yeast ribosome. *Curr Opin Struct Biol 22*, 6 (2012), 759–67.

JONES, J. D., AND O'CONNOR, C. D. Protein acetylation in prokaryotes. *Proteomics 11*, 15 (2011), 3012–22.

JORNVALL, H. Acetylation of Protein N-terminal amino groups structural observations on alpha-amino acetylated proteins. *J Theor Biol 55*, 1 (1975), 1–12.

JUCKER, F. M., AND PARDI, A. Solution structure of the CUUG hairpin loop: a novel RNA tetraloop motif. *Biochemistry 34*, 44 (1995), 14416–27.

KALVIK, T. V., AND ARNESEN, T. Protein N-terminal acetyltransferases in cancer. *Oncogene 32*, 3 (2013), 269–76.

KANG, J., CHUN, Y. S., HUH, J., AND PARK, J. W. FIH permits NAA10 to catalyze the oxygen-dependent lysyl-acetylation of HIF-1alpha. *Redox Biol 19* (2018), 364–374.

KANNO, T., ENDO, H., TAKEUCHI, K., MORISHITA, Y., FUKAYAMA, M., AND MORI, S. High expression of methionine aminopeptidase type 2 in germinal center B cells and their neoplastic counterparts. *Lab Invest 82*, 7 (2002), 893–901.

KATER, L., THOMS, M., BARRIO-GARCIA, C., CHENG, J., ISMAIL, S., AHMED, Y. L., BANGE, G., KRESSLER, D., BERNINGHAUSEN, O., SINNING, I., HURT, E., AND BECKMANN, R. Visualizing the Assembly Pathway of Nucleolar Pre-60S Ribosomes. *Cell 171*, 7 (2017), 1599–1610 e14.

KEELING, P. J., AND DOOLITTLE, W. F. Methionine aminopeptidase-1: the MAP of the mitochondrion? *Trends Biochem Sci 21*, 8 (1996), 285–6.

KIMANIUS, D., FORSBERG, B. O., SCHERES, S. H., AND LINDAHL, E. Accelerated cryo-EM structure determination with parallelisation using GPUs in RELION-2. *Elife 5* (2016).

KIRSTEIN-MILES, J., SCIOR, A., DEUERLING, E., AND MORIMOTO, R. I. The nascent polypeptide-associated complex is a key regulator of proteostasis. *EMBO J 32*, 10 (2013), 1451–68.

KNORR, A. G., SCHMIDT, C., TESINA, P., BERNINGHAUSEN, O., BECKER, T., BEATRIX, B., AND BECKMANN, R. Ribosome-NatA architecture reveals that rRNA expansion segments coordinate N-terminal acetylation. *Nat Struct Mol Biol 26*, 1 (2019), 35–39.

KOPLIN, A., PREISSLER, S., ILINA, Y., KOCH, M., SCIOR, A., ERHARDT, M., AND DEUERLING, E. A dual function for chaperones SSB-RAC and the NAC nascent polypeptide-associated complex on ribosomes. *J Cell Biol 189*, 1 (2010), 57–68.

KRAMER, G., BOEHRINGER, D., BAN, N., AND BUKAU, B. The ribosome as a platform for co-translational processing, folding and targeting of newly synthesized proteins. *Nat Struct Mol Biol 16*, 6 (2009), 589–97.

KRAMER, G., RAUCH, T., RIST, W., VORDERWULBECKE, S., PATZELT, H., SCHULZE-SPECKING, A., BAN, N., DEUERLING, E., AND BUKAU, B. L23 protein functions as a chaperone docking site on the ribosome. *Nature 419*, 6903 (2002), 171–4.

KRUGER, E. A., AND FIGG, W. D. TNP-470: an angiogenesis inhibitor in clinical development for cancer. *Expert Opin Investig Drugs 9*, 6 (2000), 1383–96.

KUDELKA, A. P., LEVY, T., VERSCHRAEGEN, C. F., EDWARDS, C. L., PIAMSOMBOON, S., TERMRUNGRUANGLERT, W., FREEDMAN, R. S., KAPLAN, A. L., KIEBACK, D. G., MEYERS, C. A., JAECKLE, K. A., LOYER, E., STEGER, M., MANTE, R., MAVLIGIT, G., KILLIAN, A., TANG, R. A., GUTTERMAN, J. U., AND KAVANAGH, J. J. A phase I study of TNP-470 administered to patients with advanced squamous cell cancer of the cervix. *Clin Cancer Res 3*, 9 (1997), 1501–5.

KULAK, N. A., PICHLER, G., PARON, I., NAGARAJ, N., AND MANN, M. Minimal, encapsulated proteomic-sample processing applied to copy-number estimation in eukaryotic cells. *Nat Methods 11*, 3 (2014), 319–24.

LAEMMLI, U. K. Cleavage of structural proteins during the assembly of the head of bacteriophage T4. *Nature 227*, 5259 (1970), 680–5.

LAMB, J. R., TUGENDREICH, S., AND HIETER, P. Tetratrico peptide repeat interactions: to TPR or not to TPR? *Trends Biochem Sci 20*, 7 (1995), 257–9.

LECOMPTE, O., RIPP, R., THIERRY, J. C., MORAS, D., AND POCH, O. Comparative analysis of ribosomal proteins in complete genomes: an example of reductive evolution at the domain scale. *Nucleic Acids Res 30*, 24 (2002), 5382–90.

LEE, K., SHARMA, R., SHRESTHA, O. K., BINGMAN, C. A., AND CRAIG, E. A. Dual interaction of the Hsp70 J-protein cochaperone Zuotin with the 40S and 60S ribosomal subunits. *Nat Struct Mol Biol 23*, 11 (2016), 1003–1010.

LEIDIG, C., BANGE, G., KOPP, J., AMLACHER, S., ARAVIND, A., WICKLES, S., WITTE, G., HURT, E., BECKMANN, R., AND SINNING, I. Structural characterization of a eukaryotic chaperone–the ribosome-associated complex. *Nat Struct Mol Biol 20*, 1 (2013), 23–8.

LI, X., AND CHANG, Y. H. Amino-terminal protein processing in Saccharomyces cerevisiae is an essential function that requires two distinct methionine aminopeptidases. *Proc Natl Acad Sci U S A 92*, 26 (1995), 12357–61.

LIN, Z., GASIC, I., CHANDRASEKARAN, V., PETERS, N., SHAO, S., MITCHISON, T. J., AND HEGDE, R. S. TTC5 mediates autoregulation of tubulin via mRNA degradation. *Science 367*, 6473 (2020), 100–104.

LINSTER, E., STEPHAN, I., BIENVENUT, W. V., MAPLE-GRODEM, J., MYKLEBUST, L. M., HUBER, M., REICHELT, M., STICHT, C., MOLLER, S. G., MEINNEL, T., ARNESEN, T., GIGLIONE, C., HELL, R., AND WIRTZ, M. Downregulation of N-terminal acetylation triggers ABA-mediated drought responses in Arabidopsis. *Nat Commun 6* (2015), 7640.

LISZCZAK, G., ARNESEN, T., AND MARMORSTEIN, R. Structure of a ternary Naa50p (NAT5/SAN) N-terminal acetyltransferase complex reveals the molecular basis for substrate-specific acetylation. *J Biol Chem 286*, 42 (2011), 37002–10.

LISZCZAK, G., GOLDBERG, J. M., FOYN, H., PETERSSON, E. J., ARNESEN, T., AND MARMORSTEIN, R. Molecular basis for N-terminal acetylation by the heterodimeric NatA complex. *Nat Struct Mol Biol 20*, 9 (2013), 1098–105.

LIU, Y., HU, Y., LI, X., NIU, L., AND TENG, M. The crystal structure of the human nascent polypeptide-associated complex domain reveals a nucleic acid-binding region on the NACA subunit. *Biochemistry 49*, 13 (2010), 2890–6.

LOTHROP, A. P., TORRES, M. P., AND FUCHS, S. M. Deciphering post-translational modification codes. *FEBS Lett 587*, 8 (2013), 1247–57.

LOWTHER, W. T., AND MATTHEWS, B. W. Structure and function of the methionine aminopeptidases. *Biochim Biophys Acta 1477*, 1-2 (2000), 157–67.

LUO, Q. L., LI, J. Y., LIU, Z. Y., CHEN, L. L., LI, J., QIAN, Z., SHEN, Q., LI, Y., LUSHINGTON, G. H., YE, Q. Z., AND NAN, F. J. Discovery and structural modification of inhibitors of methionine aminopeptidases from Escherichia coli and Saccharomyces cerevisiae. *J Med Chem 46*, 13 (2003), 2631–40.

MAGIN, R. S., DENG, S., ZHANG, H., COOPERMAN, B., AND MARMORSTEIN, R. Probing the interaction between NatA and the ribosome for co-translational protein acetylation. *PLoS One 12*, 10 (2017), e0186278.

MAGIN, R. S., MARCH, Z. M., AND MARMORSTEIN, R. The N-terminal Acetyltransferase Naa10/ARD1 Does Not Acetylate Lysine Residues. *J Biol Chem 291*, 10 (2016), 5270–7.

MALKIN, L. I., AND RICH, A. Partial resistance of nascent polypeptide chains to proteolytic digestion due to ribosomal shielding. *J Mol Biol 26*, 2 (1967), 329–46.

MATHEISL, S. *High-resolution structure of the human translation termination complex*. PhD thesis, Ludwig-Maximilians-Universität München, Aug. 2016. http://nbn-resolving.de/urn:nbn:de:bvb:19-197693, p. 23.

MATHEISL, S., BERNINGHAUSEN, O., BECKER, T., AND BECKMANN, R. Structure of a human translation termination complex. *Nucleic Acids Res 43*, 18 (2015), 8615–26.

MAZEL, D., POCHET, S., AND MARLIERE, P. Genetic characterization of polypeptide deformylase, a distinctive enzyme of eubacterial translation. *EMBO J 13*, 4 (1994), 914–23.

MEINNEL, T., MECHULAM, Y., AND BLANQUET, S. Methionine as translation start signal: a review of the enzymes of the pathway in Escherichia coli. *Biochimie 75*, 12 (1993), 1061–75.

MELNIKOV, S., BEN-SHEM, A., GARREAU DE LOUBRESSE, N., JENNER, L., YUSUPOVA, G., AND YUSUPOV, M. One core, two shells: bacterial and eukaryotic ribosomes. *Nat Struct Mol Biol 19*, 6 (2012), 560–7.

MENZIES, K. J., ZHANG, H., KATSYUBA, E., AND AUWERX, J. Protein acetylation in metabolism - metabolites and cofactors. *Nat Rev Endocrinol 12*, 1 (2016), 43–60.

MOERSCHELL, R. P., HOSOKAWA, Y., TSUNASAWA, S., AND SHERMAN, F. The specificities of yeast methionine aminopeptidase and acetylation of amino-terminal methionine in vivo. Processing of altered iso-1-cytochromes c created by oligonucleotide transformation. *J Biol Chem 265*, 32 (1990), 19638–43.

MOLLER, I., JUNG, M., BEATRIX, B., LEVY, R., KREIBICH, G., ZIMMERMANN, R., WIEDMANN, M., AND LAURING, B. A general mechanism for regulation of access to the translocon: competition for a membrane attachment site on ribosomes. *Proc Natl Acad Sci U S A 95*, 23 (1998), 13425–30.

MULLEN, J. R., KAYNE, P. S., MOERSCHELL, R. P., TSUNASAWA, S., GRIBSKOV, M., COLAVITO-SHEPANSKI, M., GRUNSTEIN, M., SHERMAN, F., AND STERNGLANZ, R. Identification and characterization of genes and mutants for an N-terminal acetyltransferase from yeast. *EMBO J 8*, 7 (1989), 2067–75.

NEUWALD, A. F., AND LANDSMAN, D. GCN5-related histone N-acetyltransferases belong to a diverse superfamily that includes the yeast SPT10 protein. *Trends Biochem Sci 22*, 5 (1997), 154–5.

NGUYEN, D. Q., HOANG, D. H., NGUYEN VO, T. T., HUYNH, V., GHODA, L., MARCUCCI, G., AND NGUYEN, L. X. T. The role of ErbB3 binding protein 1 in cancer: Friend or foe? *J Cell Physiol 233*, 12 (2018), 9110–9120.

NYATHI, Y., AND POOL, M. R. Analysis of the interplay of protein biogenesis factors at the ribosome exit site reveals new role for NAC. *J Cell Biol 210*, 2 (2015), 287–301.

OEFFINGER, M., WEI, K. E., ROGERS, R., DEGRASSE, J. A., CHAIT, B. T., AITCHISON, J. D., AND ROUT, M. P. Comprehensive analysis of diverse ribonucleoprotein complexes. *Nat Methods 4*, 11 (2007), 951–6.

PAN, D., KIRILLOV, S. V., AND COOPERMAN, B. S. Kinetically competent intermediates in the translocation step of protein synthesis. *Mol Cell 25*, 4 (2007), 519–29.

PECH, M., SPRETER, T., BECKMANN, R., AND BEATRIX, B. Dual binding mode of the nascent polypeptide-associated complex reveals a novel universal adapter site on the ribosome. *J Biol Chem 285*, 25 (2010), 19679–87.

PEISKER, K., BRAUN, D., WOLFLE, T., HENTSCHEL, J., FUNFSCHILLING, U., FISCHER, G., SICKMANN, A., AND ROSPERT, S. Ribosome-associated complex binds to ribosomes in close proximity of Rpl31 at the exit of the polypeptide tunnel in yeast. *Mol Biol Cell 19*, 12 (2008), 5279–88.

PERSSON, B., FLINTA, C., VON HEIJNE, G., AND JORNVALL, H. Structures of N-terminally acetylated proteins. *Eur J Biochem 152*, 3 (1985), 523–7.

PESKE, F., RODNINA, M. V., AND WINTERMEYER, W. Sequence of steps in ribosome recycling as defined by kinetic analysis. *Mol Cell 18*, 4 (2005), 403–12.

PESTANA, A., AND PITOT, H. C. Acetylation of nascent polypeptide chains on rat liver polyribosomes in vivo and in vitro. *Biochemistry 14*, 7 (1975), 1404–12.

PETTERSEN, E. F., GODDARD, T. D., HUANG, C. C., COUCH, G. S., GREENBLATT, D. M., MENG, E. C., AND FERRIN, T. E. UCSF Chimera–a visualization system for exploratory research and analysis. *J Comput Chem 25*, 13 (2004), 1605–12.

PFUND, C., LOPEZ-HOYO, N., ZIEGELHOFFER, T., SCHILKE, B. A., LOPEZ-BUESA, P., WALTER, W. A., WIEDMANN, M., AND CRAIG, E. A. The molecular chaperone Ssb from Saccharomyces cerevisiae is a component of the ribosome-nascent chain complex. *EMBO J 17*, 14 (1998), 3981–9.

PICKING, W. D., PICKING, W. L., ODOM, O. W., AND HARDESTY, B. Fluorescence characterization of the environment encountered by nascent polyalanine and polyserine as they exit Escherichia coli ribosomes during translation. *Biochemistry 31*, 8 (1992), 2368–75.

PIMENTA-MARQUES, A., TOSTOES, R., MARTY, T., BARBOSA, V., LEHMANN, R., AND MARTINHO, R. G. Differential requirements of a mitotic acetyltransferase in somatic and germ line cells. *Dev Biol 323*, 2 (2008), 197–206.

PISAREV, A. V., SKABKIN, M. A., PISAREVA, V. P., SKABKINA, O. V., RAKOTONDRAFARA, A. M., HENTZE, M. W., HELLEN, C. U., AND PESTOVA, T. V. The role of ABCE1 in eukaryotic posttermination ribosomal recycling. *Mol Cell 37*, 2 (2010), 196–210.

POLEVODA, B., ARNESEN, T., AND SHERMAN, F. A synopsis of eukaryotic Nalpha-terminal acetyltransferases: nomenclature, subunits and substrates. *BMC Proc 3 Suppl 6* (2009), S2.

POLEVODA, B., BROWN, S., CARDILLO, T. S., RIGBY, S., AND SHERMAN, F. Yeast N(alpha)-terminal acetyltransferases are associated with ribosomes. *J Cell Biochem 103*, 2 (2008), 492–508.

POLEVODA, B., CARDILLO, T. S., DOYLE, T. C., BEDI, G. S., AND SHERMAN, F. Nat3p and Mdm20p are required for function of yeast NatB Nalpha-terminal acetyltransferase and of actin and tropomyosin. *J Biol Chem 278*, 33 (2003), 30686–97.

POLEVODA, B., NORBECK, J., TAKAKURA, H., BLOMBERG, A., AND SHERMAN, F. Identification and specificities of N-terminal acetyltransferases from Saccharomyces cerevisiae. *EMBO J 18*, 21 (1999), 6155–68.

POLEVODA, B., AND SHERMAN, F. NatC Nalpha-terminal acetyltransferase of yeast contains three subunits, Mak3p, Mak10p, and Mak31p. *J Biol Chem 276*, 23 (2001), 20154–9.

POLEVODA, B., AND SHERMAN, F. N-terminal acetyltransferases and sequence requirements for N-terminal acetylation of eukaryotic proteins. *J Mol Biol 325*, 4 (2003a), 595–622.

POLEVODA, B., AND SHERMAN, F. Composition and function of the eukaryotic N-terminal acetyltransferase subunits. *Biochem Biophys Res Commun 308*, 1 (2003b), 1–11.

POOL, M. R., STUMM, J., FULGA, T. A., SINNING, I., AND DOBBERSTEIN, B. Distinct modes of signal recognition particle interaction with the ribosome. *Science 297*, 5585

(2002), 1345–8.

POWERS, T., AND WALTER, P. The nascent polypeptide-associated complex modulates interactions between the signal recognition particle and the ribosome. *Curr Biol 6*, 3 (1996), 331–8.

PREISSLER, S., AND DEUERLING, E. Ribosome-associated chaperones as key players in proteostasis. *Trends Biochem Sci 37*, 7 (2012), 274–83.

RAMESH, M., AND WOOLFORD, J. L., J. Eukaryote-specific rRNA expansion segments function in ribosome biogenesis. *RNA 22*, 8 (2016), 1153–62.

RAPOPORT, T. A., LI, L., AND PARK, E. Structural and Mechanistic Insights into Protein Translocation. *Annu Rev Cell Dev Biol 33* (2017), 369–390.

RATHORE, O. S., FAUSTINO, A., PRUDENCIO, P., VAN DAMME, P., COX, C. J., AND MARTINHO, R. G. Absence of N-terminal acetyltransferase diversification during evolution of eukaryotic organisms. *Sci Rep 6* (2016), 21304.

RAUE, U., OELLERER, S., AND ROSPERT, S. Association of protein biogenesis factors at the yeast ribosomal tunnel exit is affected by the translational status and nascent polypeptide sequence. *J Biol Chem 282*, 11 (2007), 7809–16.

REDMAN, K., AND RUBENSTEIN, P. A. NH2-terminal processing of Dictyostelium discoideum actin in vitro. *J Biol Chem 256*, 24 (1981), 13226–9.

REE, R., VARLAND, S., AND ARNESEN, T. Spotlight on protein N-terminal acetylation. *Exp Mol Med 50*, 7 (2018), 1–13.

RODNINA, M. V., AND WINTERMEYER, W. Recent mechanistic insights into eukaryotic ribosomes. *Curr Opin Cell Biol 21*, 3 (2009), 435–43.

ROPE, A. F., WANG, K., EVJENTH, R., XING, J., JOHNSTON, J. J., SWENSEN, J. J., JOHNSON, W. E., MOORE, B., HUFF, C. D., BIRD, L. M., CAREY, J. C., OPITZ, J. M., STEVENS, C. A., JIANG, T., SCHANK, C., FAIN, H. D., ROBISON, R., DALLEY, B., CHIN, S., SOUTH, S. T., PYSHER, T. J., JORDE, L. B., HAKONARSON, H., LILLEHAUG, J. R., BIESECKER, L. G., YANDELL, M., ARNESEN, T., AND LYON, G. J. Using VAAST to identify an X-linked disorder resulting in lethality in male infants due to N-terminal acetyltransferase deficiency. *Am J Hum Genet 89*, 1 (2011), 28–43.

ROSPERT, S., DUBAQUIE, Y., AND GAUTSCHI, M. Nascent-polypeptide-associated complex. *Cell Mol Life Sci 59*, 10 (2002), 1632–9.

RUBENSTEIN, P. A., AND MARTIN, D. J. NH2-terminal processing of Drosophila melanogaster actin. Sequential removal of two amino acids. *J Biol Chem 258*, 18 (1983), 11354–60.

SALAH UD-DIN, A. I., TIKHOMIROVA, A., AND ROUJEINIKOVA, A. Structure and Functional Diversity of GCN5-Related N-Acetyltransferases (GNAT). *Int J Mol Sci 17*, 7 (2016).

SALI, A., AND BLUNDELL, T. L. Comparative protein modelling by satisfaction of spatial restraints. *J Mol Biol 234*, 3 (1993), 779–815.

SANDIKCI, A., GLOGE, F., MARTINEZ, M., MAYER, M. P., WADE, R., BUKAU, B., AND KRAMER, G. Dynamic enzyme docking to the ribosome coordinates N-terminal processing with polypeptide folding. *Nat Struct Mol Biol 20*, 7 (2013), 843–50.

SCHERES, S. H. RELION: implementation of a Bayesian approach to cryo-EM structure determination. *J Struct Biol 180*, 3 (2012), 519–30.

SCHMIDT, C., BECKER, T., HEUER, A., BRAUNGER, K., SHANMUGANATHAN, V., PECH, M., BERNINGHAUSEN, O., WILSON, D. N., AND BECKMANN, R. Structure of the hypusinylated eukaryotic translation factor eIF-5A bound to the ribosome. *Nucleic Acids Res 44*, 4 (2016b), 1944–51.

SCHMIDT, C., KOWALINSKI, E., SHANMUGANATHAN, V., DEFENOUILLERE, Q., BRAUNGER, K., HEUER, A., PECH, M., NAMANE, A., BERNINGHAUSEN, O., FROMONT-RACINE, M., JACQUIER, A., CONTI, E., BECKER, T., AND BECKMANN, R. The cryo-EM structure of a ribosome-Ski2-Ski3-Ski8 helicase complex. *Science 354*, 6318 (2016a), 1431–1433.

SCOTT, D. C., MONDA, J. K., BENNETT, E. J., HARPER, J. W., AND SCHULMAN, B. A. N-terminal acetylation acts as an avidity enhancer within an interconnected multiprotein complex. *Science 334*, 6056 (2011), 674–8.

SETTY, S. R., STROCHLIC, T. I., TONG, A. H., BOONE, C., AND BURD, C. G. Golgi targeting of ARF-like GTPase Arl3p requires its Nalpha-acetylation and the integral

membrane protein Sys1p. *Nat Cell Biol 6*, 5 (2004), 414–9.

SHANKAR, V., RAUSCHER, R., REUTHER, J., GHARIB, W. H., KOCH, M., AND POLACEK, N. rRNA expansion segment 27Lb modulates the factor recruitment capacity of the yeast ribosome and shapes the proteome. *Nucleic Acids Res 48*, 6 (2020), 3244–3256.

SHEMORRY, A., HWANG, C. S., AND VARSHAVSKY, A. Control of protein quality and stoichiometries by N-terminal acetylation and the N-end rule pathway. *Mol Cell 50*, 4 (2013), 540–51.

SHEN, K., GAMERDINGER, M., CHAN, R., GENSE, K., MARTIN, E. M., SACHS, N., KNIGHT, P. D., SCHLOMER, R., CALABRESE, A. N., STEWART, K. L., LEIENDECKER, L., BAGHEL, A., RADFORD, S. E., FRYDMAN, J., AND DEUERLING, E. Dual Role of Ribosome-Binding Domain of NAC as a Potent Suppressor of Protein Aggregation and Aging-Related Proteinopathies. *Mol Cell 74*, 4 (2019), 729–741 e7.

SHERMAN, F., STEWART, J. W., AND TSUNASAWA, S. Methionine or not methionine at the beginning of a protein. *Bioessays 3*, 1 (1985), 27–31.

SHINE, J., AND DALGARNO, L. The 3'-terminal sequence of Escherichia coli 16S ribosomal RNA: complementarity to nonsense triplets and ribosome binding sites. *Proc Natl Acad Sci U S A 71*, 4 (1974), 1342–6.

SHOEMAKER, C. J., AND GREEN, R. Kinetic analysis reveals the ordered coupling of translation termination and ribosome recycling in yeast. *Proc Natl Acad Sci U S A 108*, 51 (2011), E1392–8.

SIKORSKI, R. S., MICHAUD, W. A., WOOTTON, J. C., BOGUSKI, M. S., CONNELLY, C., AND HIETER, P. TPR proteins as essential components of the yeast cell cycle. *Cold Spring Harb Symp Quant Biol 56* (1991), 663–73.

SIN, N., MENG, L., WANG, M. Q., WEN, J. J., BORNMANN, W. G., AND CREWS, C. M. The anti-angiogenic agent fumagillin covalently binds and inhibits the methionine aminopeptidase, MetAP-2. *Proc Natl Acad Sci U S A 94*, 12 (1997), 6099–103.

SINGER, J. M., AND SHAW, J. M. Mdm20 protein functions with Nat3 protein to acetylate Tpm1 protein and regulate tropomyosin-actin interactions in budding yeast.

Proc Natl Acad Sci U S A 100, 13 (2003), 7644–9.

SOLBIATI, J., CHAPMAN-SMITH, A., MILLER, J. L., MILLER, C. G., AND CRONAN, J. E., J. Processing of the N termini of nascent polypeptide chains requires deformylation prior to methionine removal. *J Mol Biol 290*, 3 (1999), 607–14.

SONG, O. K., WANG, X., WATERBORG, J. H., AND STERNGLANZ, R. An Nalpha-acetyltransferase responsible for acetylation of the N-terminal residues of histones H4 and H2A. *J Biol Chem 278*, 40 (2003), 38109–12.

SPRETER, T., PECH, M., AND BEATRIX, B. The crystal structure of archaeal nascent polypeptide-associated complex (NAC) reveals a unique fold and the presence of a ubiquitin-associated domain. *J Biol Chem 280*, 16 (2005), 15849–54.

SQUATRITO, M., MANCINO, M., DONZELLI, M., ARECES, L. B., AND DRAETTA, G. F. EBP1 is a nucleolar growth-regulating protein that is part of pre-ribosomal ribonucleoprotein complexes. *Oncogene 23*, 25 (2004), 4454–65.

STARHEIM, K. K., ARNESEN, T., GROMYKO, D., RYNINGEN, A., VARHAUG, J. E., AND LILLEHAUG, J. R. Identification of the human N(alpha)-acetyltransferase complex B (hNatB): a complex important for cell-cycle progression. *Biochem J 415*, 2 (2008), 325–31.

STARHEIM, K. K., GEVAERT, K., AND ARNESEN, T. Protein N-terminal acetyltransferases: when the start matters. *Trends Biochem Sci 37*, 4 (2012), 152–61.

STARHEIM, K. K., GROMYKO, D., EVJENTH, R., RYNINGEN, A., VARHAUG, J. E., LILLEHAUG, J. R., AND ARNESEN, T. Knockdown of human N alpha-terminal acetyltransferase complex C leads to p53-dependent apoptosis and aberrant human Arl8b localization. *Mol Cell Biol 29*, 13 (2009), 3569–81.

SWEENEY, R., CHEN, L., AND YAO, M. C. An rRNA variable region has an evolutionarily conserved essential role despite sequence divergence. *Mol Cell Biol 14*, 6 (1994), 4203–15.

TANAKA, S., MATSUSHITA, Y., YOSHIKAWA, A., AND ISONO, K. Cloning and molecular characterization of the gene rimL which encodes an enzyme acetylating ribosomal protein L12 of Escherichia coli K12. *Mol Gen Genet 217*, 2-3 (1989), 289–93.

TAYLOR, M. M., GLASGOW, J. E., AND STORCK, R. Sedimentation coefficients of RNA from 70S and 80S ribosomes. *Proc Natl Acad Sci U S A 57*, 1 (1967), 164–9.

VAN DAMME, P., EVJENTH, R., FOYN, H., DEMEYER, K., DE BOCK, P. J., LILLEHAUG, J. R., VANDEKERCKHOVE, J., ARNESEN, T., AND GEVAERT, K. Proteome-derived peptide libraries allow detailed analysis of the substrate specificities of N(alpha)-acetyltransferases and point to hNaa10p as the post-translational actin N(alpha)-acetyltransferase. *Mol Cell Proteomics 10*, 5 (2011b), M110 004580.

VAN DAMME, P., HOLE, K., GEVAERT, K., AND ARNESEN, T. N-terminal acetylome analysis reveals the specificity of Naa50 (Nat5) and suggests a kinetic competition between N-terminal acetyltransferases and methionine aminopeptidases. *Proteomics 15*, 14 (2015), 2436–46.

VAN DAMME, P., HOLE, K., PIMENTA-MARQUES, A., HELSENS, K., VANDEKERCKHOVE, J., MARTINHO, R. G., GEVAERT, K., AND ARNESEN, T. NatF contributes to an evolutionary shift in protein N-terminal acetylation and is important for normal chromosome segregation. *PLoS Genet 7*, 7 (2011a), e1002169.

VAN DAMME, P., LASA, M., POLEVODA, B., GAZQUEZ, C., ELOSEGUI-ARTOLA, A., KIM, D. S., DE JUAN-PARDO, E., DEMEYER, K., HOLE, K., LARREA, E., TIMMERMAN, E., PRIETO, J., ARNESEN, T., SHERMAN, F., GEVAERT, K., AND ALDABE, R. N-terminal acetylome analyses and functional insights of the N-terminal acetyltransferase NatB. *Proc Natl Acad Sci U S A 109*, 31 (2012), 12449–54.

VARLAND, S., AND ARNESEN, T. Investigating the functionality of a ribosome-binding mutant of NAA15 using Saccharomyces cerevisiae. *BMC Res Notes 11*, 1 (2018), 404.

VARSHAVSKY, A. The N-end rule pathway and regulation by proteolysis. *Protein Sci 20*, 8 (2011), 1298–345.

VETRO, J. A., AND CHANG, Y. H. Yeast methionine aminopeptidase type 1 is ribosome-associated and requires its N-terminal zinc finger domain for normal function in vivo. *J Cell Biochem 85*, 4 (2002), 678–88.

VETTING, M. W., LP, S. D. C., YU, M., HEGDE, S. S., MAGNET, S., RODERICK, S. L., AND BLANCHARD, J. S. Structure and functions of the GNAT superfamily of acetyltransferases. *Arch Biochem Biophys 433*, 1 (2005), 212–26.

VOORHEES, R. M., AND HEGDE, R. S. Structure of the Sec61 channel opened by a signal sequence. *Science 351*, 6268 (2016), 88–91.

VOSS, N. R., GERSTEIN, M., STEITZ, T. A., AND MOORE, P. B. The geometry of the ribosomal polypeptide exit tunnel. *J Mol Biol 360*, 4 (2006), 893–906.

WALKER, S. E., SHOJI, S., PAN, D., COOPERMAN, B. S., AND FREDRICK, K. Role of hybrid tRNA-binding states in ribosomal translocation. *Proc Natl Acad Sci U S A 105*, 27 (2008), 9192–7.

WANG, J., SHEPPARD, G. S., LOU, P., KAWAI, M., BAMAUNG, N., ERICKSON, S. A., TUCKER-GARCIA, L., PARK, C., BOUSKA, J., WANG, Y. C., FROST, D., TAPANG, P., ALBERT, D. H., MORGAN, S. J., MOROWITZ, M., SHUSTERMAN, S., MARIS, J. M., LESNIEWSKI, R., AND HENKIN, J. Tumor suppression by a rationally designed reversible inhibitor of methionine aminopeptidase-2. *Cancer Res 63*, 22 (2003), 7861–9.

WANG, L., ZHANG, W., WANG, L., ZHANG, X. C., LI, X., AND RAO, Z. Crystal structures of NAC domains of human nascent polypeptide-associated complex (NAC) and its alphaNAC subunit. *Protein Cell 1*, 4 (2010), 406–416.

WANG, S., SAKAI, H., AND WIEDMANN, M. NAC covers ribosome-associated nascent chains thereby forming a protective environment for regions of nascent chains just emerging from the peptidyl transferase center. *J Cell Biol 130*, 3 (1995), 519–28.

WEGRZYN, R. D., AND DEUERLING, E. Molecular guardians for newborn proteins: ribosome-associated chaperones and their role in protein folding. *Cell Mol Life Sci 62*, 23 (2005), 2727–38.

WEGRZYN, R. D., HOFMANN, D., MERZ, F., NIKOLAY, R., RAUCH, T., GRAF, C., AND DEUERLING, E. A conserved motif is prerequisite for the interaction of NAC with ribosomal protein L23 and nascent chains. *J Biol Chem 281*, 5 (2006), 2847–57.

WEISSER, M., AND BAN, N. Extensions, Extra Factors, and Extreme Complexity: Ribosomal Structures Provide Insights into Eukaryotic Translation. *Cold Spring Harb*

Perspect Biol 11, 9 (2019).

WELLS, J. N., BUSCHAUER, R., MACKENS-KIANI, T., BEST, K., KRATZAT, H., BERNINGHAUSEN, O., BECKER, T., GILBERT, W., CHENG, J., AND BECKMANN, R. Structure and function of yeast Lso2 and human CCDC124 bound to hibernating ribosomes. *PLoS Biol 18*, 7 (2020), e3000780.

WEYER, F. A., GUMIERO, A., GESE, G. V., LAPOUGE, K., AND SINNING, I. Structural insights into a unique Hsp70-Hsp40 interaction in the eukaryotic ribosome-associated complex. *Nat Struct Mol Biol 24*, 2 (2017b), 144–151.

WEYER, F. A., GUMIERO, A., LAPOUGE, K., BANGE, G., KOPP, J., AND SINNING, I. Structural basis of HypK regulating N-terminal acetylation by the NatA complex. *Nat Commun 8* (2017a), 15726.

WIAME, E., TAHAY, G., TYTECA, D., VERTOMMEN, D., STROOBANT, V., BOMMER, G. T., AND VAN SCHAFTINGEN, E. NAT6 acetylates the N-terminus of different forms of actin. *FEBS J 285*, 17 (2018), 3299–3316.

WIEDMANN, B., SAKAI, H., DAVIS, T. A., AND WIEDMANN, M. A protein complex required for signal-sequence-specific sorting and translocation. *Nature 370*, 6489 (1994), 434–40.

WILD, K., ALEKSIC, M., LAPOUGE, K., JUAIRE, K. D., FLEMMING, D., PFEFFER, S., AND SINNING, I. MetAP-like Ebp1 occupies the human ribosomal tunnel exit and recruits flexible rRNA expansion segments. *Nat Commun 11*, 1 (2020), 776.

WILD, K., BECKER, M. M. M., KEMPF, G., AND SINNING, I. Structure, dynamics and interactions of large srp variants. *Biol Chem 401*, 1 (2019), 63–80.

WILLIAMS, B. C., GARRETT-ENGELE, C. M., LI, Z., WILLIAMS, E. V., ROSENMAN, E. D., AND GOLDBERG, M. L. Two putative acetyltransferases, san and deco, are required for establishing sister chromatid cohesion in Drosophila. *Curr Biol 13*, 23 (2003), 2025–36.

WILLMUND, F., DEL ALAMO, M., PECHMANN, S., CHEN, T., ALBANESE, V., DAMMER, E. B., PENG, J., AND FRYDMAN, J. The cotranslational function of

ribosome-associated Hsp70 in eukaryotic protein homeostasis. *Cell 152*, 1-2 (2013), 196–209.

WOLF, E., VASSILEV, A., MAKINO, Y., SALI, A., NAKATANI, Y., AND BURLEY, S. K. Crystal structure of a GCN5-related N-acetyltransferase: Serratia marcescens aminoglycoside 3-N-acetyltransferase. *Cell 94*, 4 (1998), 439–49.

WU, S., GUPTA, S., CHATTERJEE, N., HILEMAN, R. E., KINZY, T. G., DENSLOW, N. D., MERRICK, W. C., CHAKRABARTI, D., OSTERMAN, J. C., AND GUPTA, N. K. Cloning and characterization of complementary DNA encoding the eukaryotic initiation factor 2-associated 67-kDa protein (p67). *J Biol Chem 268*, 15 (1993), 10796–801.

WU, Y., AND LYON, G. J. NAA10-related syndrome. *Exp Mol Med 50*, 7 (2018), 1–10.

XU, F., HUANG, Y., LI, L., GANNON, P., LINSTER, E., HUBER, M., KAPOS, P., BIENVENUT, W., POLEVODA, B., MEINNEL, T., HELL, R., GIGLIONE, C., ZHANG, Y., WIRTZ, M., CHEN, S., AND LI, X. Two N-terminal acetyltransferases antagonistically regulate the stability of a nod-like receptor in Arabidopsis. *Plant Cell 27*, 5 (2015), 1547–62.

YAMAMOTO, H., COLLIER, M., LOERKE, J., ISMER, J., SCHMIDT, A., HILAL, T., SPRINK, T., YAMAMOTO, K., MIELKE, T., BURGER, J., SHAIKH, T. R., DABROWSKI, M., HILDEBRAND, P. W., SCHEERER, P., AND SPAHN, C. M. Molecular architecture of the ribosome-bound Hepatitis C Virus internal ribosomal entry site RNA. *EMBO J 34*, 24 (2015), 3042–58.

YASUDA, K., TAKAHASHI, M., AND MORI, N. Mdm20 Modulates Actin Remodeling through the mTORC2 Pathway via Its Effect on Rictor Expression. *PLoS One 10*, 11 (2015), e0142943.

YOSHIKAWA, A., ISONO, S., SHEBACK, A., AND ISONO, K. Cloning and nucleotide sequencing of the genes rimI and rimJ which encode enzymes acetylating ribosomal proteins S18 and S5 of Escherichia coli K12. *Mol Gen Genet 209*, 3 (1987), 481–8.

ZEYTUNI, N., AND ZARIVACH, R. Structural and functional discussion of the tetratrico-peptide repeat, a protein interaction module. *Structure 20*, 3 (2012), 397–405.

ZHANG, K. Gctf: Real-time CTF determination and correction. *J Struct Biol 193*, 1 (2016), 1–12.

ZHANG, Y., BERNDT, U., GOLZ, H., TAIS, A., OELLERER, S., WOLFLE, T., FITZKE, E., AND ROSPERT, S. NAC functions as a modulator of SRP during the early steps of protein targeting to the endoplasmic reticulum. *Mol Biol Cell 23*, 16 (2012), 3027–40.

ZHANG, Y., MA, C., YUAN, Y., ZHU, J., LI, N., CHEN, C., WU, S., YU, L., LEI, J., AND GAO, N. Structural basis for interaction of a cotranslational chaperone with the eukaryotic ribosome. *Nat Struct Mol Biol 21*, 12 (2014), 1042–6.

ZHANG, Y., SINNING, I., AND ROSPERT, S. Two chaperones locked in an embrace: structure and function of the ribosome-associated complex RAC. *Nat Struct Mol Biol 24*, 8 (2017), 611–619.

ZHANG, Y., VALENTIN GESE, G., CONZ, C., LAPOUGE, K., KOPP, J., WOLFLE, T., ROSPERT, S., AND SINNING, I. The ribosome-associated complex RAC serves in a relay that directs nascent chains to Ssb. *Nat Commun 11*, 1 (2020), 1504.

ZHENG, S. Q., PALOVCAK, E., ARMACHE, J. P., VERBA, K. A., CHENG, Y., AND AGARD, D. A. MotionCor2: anisotropic correction of beam-induced motion for improved cryo-electron microscopy. *Nat Methods 14*, 4 (2017), 331–332.

ZIMMERMAN, S. B., AND TRACH, S. O. Estimation of macromolecule concentrations and excluded volume effects for the cytoplasm of Escherichia coli. *J Mol Biol 222*, 3 (1991), 599–620.

ZUO, S., GUO, Q., LING, C., AND CHANG, Y. H. Evidence that two zinc fingers in the methionine aminopeptidase from Saccharomyces cerevisiae are important for normal growth. *Mol Gen Genet 246*, 2 (1995), 247–53.

Acknowledgements

That's it, this is the end. Not only the end of my thesis, also the end of my life as a PhD student in the Beckmann lab. And of course I wouldn't have made it so far without some very important people around me.

First of all I want to thank Roland Beckmann for having me in the lab already as a masters student and offering me to continue as a PhD and QBM student. By providing a great scientific environment and an own cryo-EM facility I really enjoyed working here the whole time. Even though the NatA project looked promising after my master thesis, it turned out to be quite challenging to trap and enrich a 'wobbly ligand' on the ribosome. I really have to say THANK YOU for not giving up my project which made me at the end to an expert in flexible ligands and leading unexpectedly to two additional structures - just as wobbly as NatA.

In that turn, also many thanks to Birgitta Beatrix and Thomas Becker who were supervising me already during my master thesis and were constantly part of my projects. I don't know what I would have done without you!!

Otto Berninghausen and the cryo-queens, Susi Rieder and Charlotte Ungewickel – thank you so much for showing me your world, teaching me in vitrobotting and microscope handling. Some of the things I never wanted to miss.

I am really grateful for the office crew, starting with Andre Heuer and continuing with Lukas Kater and Michael Ameismeier, keeping our processing pipline and everything else running. Special thanks to Michi in addition for a 24/7 WhatsApp support for whatever processing issue ;-)

As an indispensable part of the lab – Heidi Sieber, Joanna Musial and Andrea Gilmozzi, thank you being supportive all the time and keeping the lab in shape. Thank you Heidi being a perfect 'neighbor' and Joanna for your support and really good work in cloning and purifications of my wobbly ligands. You saved me a lot of time! And I really enjoyed working with all of you.

We started a collaboration with the Bukau lab in Heidelberg exchanging structural against ribosome profiling data. Thanks to you guys for very good conversations about the whole exit ligand family. Based on your data we were able to improve our structures and led Wibke Rüdiger into our lab, who joined for a practical and did amazing work within a quite short period of time.

Thanks to QBM for supporting me the whole time, the many possibilities for continuing education and the great people I got to know here over the time. I am really curious where you guys end up after your PhD.
In addition, I want to thank everyone in the Beckmann group, for being in this group, for amazing cake afternoons, really creative ideas and the best Christmas parties ever. I want to highlight Vivek Shanmuganatan, Ting Su and Jen Wells I really enjoyed working with and I had a great time with you not only on conferences and retreats!

Aside from work, many many thanks to my family and friends who have been supportive all the time. Thank you for taking part in my journey to my PhD and thank you for being part of my life - it would be a complete different world without you.